Controlled Cellular Uptake of Elastin-Like Polypeptide Diblock Copolymers for

Thermally Targeted Drug Delivery

by

Sarah Reagan MacEwan

Department of Biomedical Engineering
Duke University

Date:_____

Approved:

_____
Ashutosh Chilkoti, Supervisor

_____
Mark Dewhirst

_____
Charles Gersbach

_____
David Katz

_____
Michael Zalutsky

Dissertation submitted in partial fulfillment of
the requirements for the degree of Doctor
of Philosophy in the Department of
Biomedical Engineering in the Graduate School
of Duke University

2014

ABSTRACT

Controlled Cellular Uptake of Elastin-Like Polypeptide Diblock Copolymers for Thermally Targeted Drug Delivery

by

Sarah Reagan MacEwan

Department of Biomedical Engineering
Duke University

Date:_____

Approved:

_____
Ashutosh Chilkoti, Supervisor

_____
Mark Dewhirst

_____
Charles Gersbach

_____
David Katz

_____
Michael Zalutsky

An abstract of a dissertation submitted in partial fulfillment of the requirements for the degree of Doctor of Philosophy in the Department of Biomedical Engineering in the Graduate School of Duke University

2014

Abstract

Targeted drug delivery to solid tumors aims to increase the accumulation of drug at the site of disease while limiting accumulation in healthy tissues. Thus, targeted delivery serves to enhance therapeutic efficacy while minimizing off-target side effects. Targeting drug to the site of disease is especially important for many current anti-cancer therapeutics whose cytotoxic effects are not exclusive to cancer cells. Drug carriers can improve tumor targeting of drug cargo by either passive or active mechanisms. Passive targeting of drug carriers occurs by the enhanced permeability and retention effect, whereby long circulating drug carriers can accumulate in the tumor by extravasation from the tumor's leaky vasculature and be retained in the tumor due to the lack of an organized tumor lymphatic system. Alternatively, active targeting can improve drug delivery to the tumor by means of functionalizing a drug carrier such that it interacts specifically with the tumor tissue. Traditionally, actively targeted drug carriers rely on intrinsic features of the tumor such as upregulated cell receptors, overexpressed extracellular enzymes, or depressed tissue pH. These intrinsic targets, however, are heterogeneous across cancer classes and between patients with a single tumor type. Therefore traditional active targeting cannot be applied to a breadth of cancers or patients without prior knowledge of the cancer phenotype.

Active targeting can alternatively be achieved by an extrinsic trigger, independent of the characteristics of the tumor. This approach could thereby achieve targeted drug delivery in a breadth of tumor types and cancer patients. This dissertation describes one such approach that exploits cell-penetrating peptides (CPPs) to achieve receptor-independent and non-specific uptake in a variety of cancer cells. The function of this non-specific CPP is controlled by an extrinsic trigger by means of the modulation of its local interfacial density with temperature-triggered micelle assembly. Elastin-like polypeptide diblock copolymers (ELP_{BC}s) were used as the drug carrier platform, as their lower critical solution temperature phase transition behavior permits their controlled self-assembly from unimer to micelle in response to a thermal stimulus. CPP-ELP_{BC}s were recombinantly synthesized in *E. coli* with CPP-functionalization at their hydrophilic terminus, such that temperature-triggered micelle assembly would result in the decoration of CPP on the micelle corona. The CPP-ELP_{BC} design was carefully optimized to permit micelle self-assembly in response to the clinically relevant trigger of mild hyperthermia.

Temperature-triggered micelle assembly of CPP-ELP_{BC}s achieved controlled cellular uptake *in vitro* by means of their CPP density modulation, such that cellular uptake was minimized at physiologic temperature and was greatly enhanced at conditions of mild hyperthermia. This effect was achieved in multiple cell lines, albeit with variable magnitude. Controlled uptake of the CPP-ELP_{BC} carrier could control the

intracellular delivery of appended drug cargo. This controlled intracellular delivery was translated to controlled therapeutic effect when the CPP-ELP$_{BC}$ was genetically appended to a proapoptotic peptide drug cargo. These drug-loaded CPP-ELP$_{BC}$s achieved controlled cytotoxicity in cancer cells, whereby significant cell death was induced at conditions of mild hyperthermia, but cells at physiologic temperature were spared.

For use as targeted drug carriers *in vivo*, CPP-ELP$_{BC}$s would be systemically administered and circulate throughout the body in their soluble state. It would only be at the site of the solid tumor that local mild hyperthermia would be applied and induce the self-assembly of CPP-ELP$_{BC}$ micelles that could induce internalization into cancer cells. Translation of CPP-ELP$_{BC}$ function from *in vitro* to *in vivo* environments proved to be quite challenging. Issues such as perturbation of temperature-triggered assembly in serum and interference of CPP-ELP$_{BC}$ internalization by serum proteins likely played a role in preventing the extrinsically targeted accumulation of CPP-ELP$_{BC}$s in hyperthermia treated tumors, as investigated by intravital tumor microscopy and biodistribution studies. Further optimization of the CPP-ELP$_{BC}$ platform is thus required to achieve extrinsically targeted drug carrier delivery *in vivo*.

Dedication

This dissertation is dedicated to Angeline Reagan. All will be well.

Contents

List of Tables

List of Figures

Acknowledgements

I would like to thank my advisor, Ashutosh Chilkoti, for his support and patience. I am grateful for the many opportunities made possible by my advisor to explore creative projects in and beyond that of my dissertation work. For the diverse opportunities to write and collaborate, I am deeply thankful. I am also thankful to my committee members, and in addition Dr. Kam Leong, for their support and valuable feedback.

A special thank you is owed to the lab members that had an incredible impact on my time here at Duke. Especially those that joined the Chilkoti Lab with me in 2007: Jon McDaniel, Vina Tjong, Wafa Hassouneh, Mira Amiram, and by default Felipe Garcia Quiroz. I am also grateful to those members of the lab that provided significant scientific support, particularly Dr. Jayanta Bhattacharyya for his help in the covalent conjugation of small molecule chemotherapeutics, and Xinghai Li and Dr. Wenge Liu for their generous help to perform *in vivo* experiments.

Appreciation is also owed to my collaborators. Although their work is not discussed in this dissertation, their contributions improved the understanding of this drug carrier system. To Dr. Andreas Weinberger at the time at the Institut Charles Sadron in Strasbourg, France, and to Dr. Elisabeth Garanger at the Institut Européen de Chimie et Biologie in Bordeaux, France, I am thankful for their expertise.

Finally, my greatest appreciation goes to my family, especially my mother and father, my brother, my aunt, and my grandmother. I am grateful everyday for their support.

1. Background and motivation

1.1 Cancer

1.1.1 Morbidity, mortality, and cost to society

Cancer is an incredibly diverse disease characterized by the uncontrolled proliferation of abnormal cells. Although cancer can manifest in a variety of pathologies, cancer cells in solid tumors are generally distinguished from normal healthy cells due to genetic aberrations that can change their rate of proliferation and capacity for excessive replication, their ability to recruit vascularization and migrate to invade other tissues, and their evasion of cell death by check points like apoptosis and immunological monitoring [1]. Furthermore, cancer is manifest from abnormal interaction of these cells with their local environment, be it interactions in the tissue with other cell types or interaction with the extracellular matrix [2]. These aspects of the cancer cell, in combination with their abnormal interaction with their environment, result in malignancies of localized primary tumors or the spread of metastasized disease throughout the body.

The cause of many cancers may not be precisely defined, but a variety of factors can contribute to the incidence of cancer including environmental exposure to mutagens and genetic predisposition. For this reason, great efforts are made in the prevention and screening for cancer, as well as the development of effective anti-cancer treatments. Although many cancers are similar due to their characteristics caused by neoplasia, the

variability between each type and instance of cancer has made this a particularly difficult disease to treat. Due to the diversity of cancer the approaches to prevent, diagnose, and treat tumors must often be tailored to each classification of the disease.

Cancer is one of the leading causes of death in the United States with 585,720 individuals expected to die as a result of cancer in 2014. In 2012, approximately 13.7 million living individuals in the United States had been diagnosed with cancer in their lifetimes, with 1,665,540 new cases of cancer expected to be diagnosed in the year 2014. The magnitude of this disease burden leads to a substantial cost, approximated to be $216.6 billion for the United States in 2009 alone [3]. The morbidity, mortality, and extreme cost of healthcare to prevent, diagnose, and treat cancer have made this disease target a major topic in the medical research community.

1.1.2 Standards of cancer treatment

Conventional treatments for solid tumors include surgical resection, radiation therapy, chemotherapy, or some combination thereof. Surgery to remove abnormal tissue has remained a prominent approach in cancer therapy for hundreds of years. Physical removal of the cancer can provide relief of the noxious effects of the tumor and prevent spread of the disease, provided that no cancer cells are left behind whose continued growth can lead to a repopulation of the tumor. Surgery is a feasible option only in tumors deemed resectable, that is, tumors that are well localized in the body, not excessively infiltrating their surrounding tissue, and not adjacent to critical tissues or

organs. These factors, for instance, limit the ability to surgically remove tumors that have spread widely throughout the body, although some measures can be taken to remove migrating cancer cells from areas such as proximal lymph nodes. Additionally, there is a limited feasibility, or increased complexity, of removing tumors in some critical organs, for example the brain, where surgical resection must be balanced with the risk of altering critical biological functions. Furthermore, surgical resection is limited by the realistic risk associated with residual tumor margins, whereby cancer cells left behind after surgery can lead to relapse of disease. Thus, surgery must often be paired with orthogonal treatments to address those cancers cells that may be left behind.

Radiation therapy is an alternative means of eliminating large populations of cancer cells. Exposure of cancer cells to x-rays or gamma rays can induce DNA damage that will lead to cell death. Radiation can be applied from external sources, such as focused x-ray beams, or from internal sources, such as implanted materials impregnated with radioactive isotopes known as brachytherapy seeds. There is some preferential killing of cancer cells with radiation therapy as their vulnerability to DNA damage-induced cell death is enhanced due to their accelerated division, as compared to most healthy cells [4]. However, there are aspects of the tumor environment, such as hypoxia, that can lead to radiation resistance in cancer cells [5]. The cytotoxic effects of radiation are not specific to cancer cells, however, and therefore normal healthy cells surrounding the tumor are susceptible to damage from extraneous radiation. Therefore radiation is

often administered in fractionated doses, to allow repair of radiation-induced damage in normal tissue, and with local precision directed by tumor imaging for planning of either external beam irradiation or surgical placement of brachytherapy seeds.

Chemotherapy is a third common approach in eliminating tumors by inducing cancer cell death. This therapeutic method has the advantage of an ease of administration, as compared to surgical intervention or radiation therapy, as chemotherapeutics can often be delivered systemically by intravenous or oral dosing. There are many types of chemotherapy drugs, which can be classified by the means in which they induce cell death, often by their interaction with DNA and their interference with cellular machinery critical to cell division. These drugs can achieve a degree of apparent therapeutic targeting in the tumor as their action is usually amplified in cancer cells due to their rapid turnover, as compared to many normal healthy cells. However, the cytotoxicity of most of these chemotherapeutics is not completely restricted to cancer cells. Even novel targeted agents, such as those directed at HER2 and EGFR, induce off-target effects including dermatologic and cardiac toxicities, respectively [6]. Therefore systemic administration of these drugs comes at the risk of off-target toxicity that limits the application of chemotherapeutics, as their use must balance anti-tumor efficacy with dose-limiting side effects.

Although not considered a primary treatment for anti-cancer therapy in the United States, the application of heat can be used as a tool to improve outcomes in

combination with orthogonal treatments. In the context of oncology heat may be applied at extreme temperatures to ablate tumors, thereby eliminating large numbers of cancer cells. This technique, for example, has been used to locally treat liver metastases from breast cancers [7]. Alternatively, a much milder application of heat, just slightly above body temperature, can be used to treat the whole body, defined regions of the body, or specific targets in the body, like solid tumors. Mild hyperthermia of solid tumors typically involves heating to approximately 40-44 °C [8]. Localized mild hyperthermia is achieved in the clinic with externally focused microwaves, radiofrequency, or ultrasound [9-11] applied in a variety of tumor sites [12]. Mild hyperthermia can be effectively contained within tumors without significant spillover into adjacent normal tissue because tumors are poor heat exchangers compared to normal tissues. The disorganized vasculature and recirculating blood flow cause heat to be further retained within the tumor mass [13]. A typical session of mild hyperthermia may involve 1 hour of treatment in which the tumor tissue is maintained at approximately 42 °C [14], resulting in minimal side effects that are generally well tolerated by patients [15-17].

Application of mild hyperthermia is most feasible for surface tumors, easily accessible to heating methods. Treatment of breast cancer recurrence on the chest wall [18] and melanoma [19] are examples of superficial targets in which hyperthermia is combined with radiation therapy. However, success has also been achieved with regional heating of internal tumors including retroperitoneal soft-tissue sarcomas (in

combination with chemotherapy) [20], cervical cancers (in combination with radiation therapy) [21], and internal, albeit superficial, bladder carcinomas (in combination with chemotherapy) [22].

In contrast to the high temperatures utilized for destruction of tumors by thermal ablation, mild hyperthermia in itself is not considered to be cytotoxic, however it has been proven useful as an adjuvant therapy to improve the efficacy of other anti-cancer treatments such as radiation and chemotherapy [9, 11, 23]. Effects of mild clinical hyperthermia that may synergize the action of other treatment modalities may include increased blood flow [24], increased cellular uptake [25], and decreased cellular repair of therapy-induced toxicities [26]. Furthermore, for novel therapeutics delivered by drug carriers, hyperthermia may improve delivery by enhanced extravasation of nanoparticles in heated tumors by means of increased tumor vascular pore cutoff size [27]. Tumor heating at 42 °C for 1 hour has been shown to specifically increase the pore size in tumor vasculature to allow extravasation of 400 nm liposomes from tumor vessels that would otherwise exclude extravasation of liposomes greater than 100 nm at physiologic conditions [28]. Heating appears to create a prolonged effect on vascular permeability lasting 6-8 hours after treatment [27, 29], suggesting its applicability toward long circulating drug carriers that can accumulate in the tumor by means of this temporary enhanced permeability and retention effect.

Finally, hyperthermia can be used not only as an adjuvant therapy, but also as a trigger to influence the delivery of stimulus-responsive drug carriers and their cargo. Local heat at the site of cancer can influence aggregation of drug carriers to enhance accumulation in the tumor [30, 31], or alternatively, local heat can influence the stability of drug carriers to trigger drug release only in the tumor [32-34]. Local heat can thereby provide advantages by manipulating the drug carrier for improved drug targeting and confer its advantageous effects on the tumor physiology that may improve efficacy of the delivered drug cargo.

1.2 Systemically delivered tumor-targeted drug carriers

1.2.1 Passive targeting

Advances in the systemic delivery of anti-cancer therapeutics to solid tumors have aimed to increase the accumulation of drug at the disease site while limiting the accumulation in healthy tissues. This is of particular importance when delivering cytotoxic anti-cancer drugs whose therapeutic action culminates in cell death. Exposure of healthy tissues to these drugs can result in toxic side effects that limit drug dosage and thus compromise therapeutic efficacy. Improving the specificity with which the drug can reach the tumor allows the delivery of increased drug dose while minimizing side effects to achieve improved outcomes of treatment. Delivering therapeutics by means of drug carriers can serve to achieve these goals by manipulating the pharmacokinetics and biodistribution of the drug cargo.

Systemic delivery of anti-cancer therapeutics provides an ease of administration, as compared to local delivery at the site of disease, but presents the challenge of directing drug to the tumor while preventing its accumulation in off-target tissues. Inherent characteristics of many cancers are proposed to achieve passive tumor targeting by accumulation via the enhanced permeability and retention (EPR) effect. The abnormal vasculature produced by the rapid angiogenesis accompanying tumor growth often exhibits an enhanced permeability, such that the leakiness of these vessels permits the extravasation of drug carriers into the tumor tissue [35]. Normal vasculature, however, exhibits tight endothelial junctions, which prevent this extravasation in healthy tissues. Furthermore, the lack of well-organized lymphatics in the tumor tissue prevents the clearance of drug carriers once they have accumulated in the extravascular space of the tumor. This lack of clearance thus permits the retention of drug carriers at the disease site.

The permeability of tumor vasculature results from the creation of pores due to the aberrant architecture of the tumor vessels. It is therefore important to consider the size of the tumor vascular pores, in relation to the size of a drug carrier, to exploit the EPR phenomenon. Pore sizes of 400-600 nm, for example, were evaluated in a human colon adenocarcinoma xenograft in mice, which allowed the accumulation of 400 nm liposomes in the tumor, but excluded 600 nm liposomes from escaping the vasculature [36]. This pore size is, of course, heterogeneous across tumor types, but a range of 380-

780 nm pores has been evaluated in many tumors [37]. If relying on bigger pore size to extravasate larger drug carriers it is important to consider that those outliers may be present only infrequently along the tumor vasculature. Thus many drug carriers exploit the EPR effect at size ranges well below the pore size.

Prolonged circulation of the drug carrier is an important factor in exploiting the EPR effect. When high concentrations of the drug carrier are maintained in the circulation, a greater accumulation in the tumor can be achieved over time, whereas healthy tissues are continually spared by their normal vasculature. Drug carriers whose size exceeds that of the renal filtration cutoff, while staying below the pore size of tumor vasculature, can best exploit the EPR effect to passively accumulate in the tumor tissue. As such, an incredible number of macromolecule and nanoparticle drug carriers have been designed to exploit the EPR effect as a primary means of accumulation in the tumor. However, these systems often take for granted that EPR will result in sufficient accumulation in the tumor, without adequate evaluation of this outcome. There are factors in tumor physiology that can work against the EPR effect, such as enhanced tumor interstitial fluid pressure, caused also by the leaky tumor vasculature. Enhanced tumor interstitial fluid pressure leads to equal fluid pressure between the vascular and extravascular space of the tumor, thus providing little driving force for extravasation of drug carrier despite the presence of pores in the tumor vasculature. The propensity of each tumor to exhibit the EPR effect should therefore be included in the list of

heterogeneous features of tumor physiology, whereby the type, size, and location of tumors can be expected to influence the effect of EPR on tumor-targeted accumulation of drug carriers [38].

1.2.2 Active targeting

Alternative to passive targeting via the EPR effect, tumors can be actively targeted when drug carriers are functionalized in such a way as to interact specifically with the cancer cells or tumor tissue. Traditional active targeting relies on unique aspects of the tumor that are upregulated as compared to normal healthy tissues. These intrinsic tumor targets are most often upregulated cell receptors, overexpressed enzymes, or depressed pH in the tumor tissue. Increased tumor accumulation may not be the ultimate measure of success for actively targeted drug carriers, particularly if their accumulation is dominated by the EPR effect. However, their specific interaction with the tumor may cause other advantages such as prolonged retention at the site of disease or internalization of drug into the targeted cancer cells.

Active targeting requires both a valid target specific to the tumor and a means of interacting with high specificity to that target. Antibody-functionalization is one approach to active targeting where the antibody provides highly specific recognition of its binding partner, typically a receptor that is upregulated on the cancer cell. HER2, upregulated on some breast cancer cells [39], and transferrin [40], upregulated on a variety of cancer cells, are two examples of cell surface receptors targeted by antibodies

or antibody-functionalized carriers. Ligand binding is an alternative approach to achieve specific interactions between drug carrier and cancer cells. For example, functionalization of nanoparticles with transferrin can selectively interact with cancer cells overexpressing the transferrin receptor [41]. As an additional example, functionalization of nanoparticles with small molecule substrates can be recognized specifically by cell surface enzymes upregulated on the cancer cell, such as PSMA on prostate cancer cells [42]. Finally, tissue-specific features can be utilized to target accumulation of drug in the tumor, often by exploiting features of overexpressed enzymes and depressed tumor pH. These unique features of the tumor are often used to induce a change in the drug carrier that can improve drug accumulation or distribution in the tumor. Release of small molecule drugs from macromolecular carriers via enzyme-degradable linkers [43, 44], or disassembly and drug release from ionizable nanoparticles in the low tumor pH [45, 46] are both mechanisms of active targeting that serve to increase drug accumulation in the tumor while encouraging distribution of small drug molecules throughout the tumor.

As an alternative to targeting intrinsic features of the tumor, active targeting can also be achieved by stimulus-responsive drug carriers that are controlled by extrinsic triggers. Provided these external stimuli can be applied with local precision at the site of the tumor, these alternative means of targeting can improve delivery of drug carriers to tumors without prior knowledge of the tumor phenotype. Heat is an external trigger

that can be used to induce tumor accumulation of drug carriers that exhibit lower critical solution temperature phase transition behavior. Drug carriers that aggregate in response to an increase in temperature can be accumulated in the vasculature of heated tumors. When the heat is removed the resolubilization of drug carriers in the vasculature creates a concentration gradient that drives the carrier into the extravascular tumor space [30, 31]. Alternatively, interaction of a drug carrier with cancer cells can be controlled by extrinsic triggers such as light. Light-labile molecules on a nanoparticle can be released in response to UV illumination, revealing active targeting moieties on the nanoparticle surface. This approach has shown UV-triggered cellular uptake by controlled presentation of folic acid to cells overexpressing the folate receptor [47]. Finally, external stimuli can also provide means for local drug release, as has been shown with focused ultrasound and its destabilization of drug-loaded micelles. Ultrasound-triggered disruption of drug-loaded micelles has achieved improved anti-tumor efficacy, likely by both the local release of drug and its improved distribution in the tumor [48].

1.3 Cell-penetrating peptides

1.3.1 Non-specific cellular uptake

Cell-penetrating peptides (CPPs) are a family of peptides that can achieve receptor-independent and non-specific cellular internalization [49, 50]. HIV's transactivator of transcription (TAT) was the first to be discovered to achieve efficient cellular uptake by apparent penetration of the cell membrane. Other peptides such as

Antennapedia, a transcription factor from drosophila [49], and bactenecin, an anti-microbial peptide derived from bovine neutrophils [51], were discovered to exhibit similar behavior, and thus CPPs were classified as a family of peptides that achieve uptake in a variety of cell types. The family of CPPs has expanded beyond natural peptides to include biologically inspired CPPs, such as arginine oligomers [52-54], and synthetic CPP derivatives [55-57].

Many CPPs are cationic due to the contribution of either lysine or arginine residues. Arginine is believed to play an important role in the function of CPPs due to their electrostatic interaction and bidendate hydrogen bonding with components on the cell membrane, including anionic lipids and proteoglycans [58, 59]. Although the exact mechanism of cationic CPP uptake is not completely elucidated, it is likely that these interactions initiate the events leading to internalization. For the many types of CPPs, there are a number of proposed additional mechanisms that participate in the internalization of these materials, whether they are charged, amphiphilic, or hydrophobic: pore formation [60, 61], inverted micelle formation [62], and endocytosis [63, 64]. CPPs may therefore directly access the cytoplasm, by their apparent penetration across the cell membrane, or they may be internalized into intracellular compartments. This distinction for some CPPs has been strongly debated, particularly when CPP charge has the potential to induce confounding artifacts depending on the protocol of evaluating internalization.

Arginine oligomers, whose design is inspired by the arginine-rich CPPs like TAT, are an interesting class of CPPs in that their internalization is controlled by the number of sequential arginine residues that make up the peptide. Below 6 consecutive arginine residues is not sufficient to induce significant uptake, whereas above 6 residues is adequate to induce enhanced internalization [55, 65]. Pure arginine oligomers are commonly used, but it has been shown that arginine residues do not have to be arranged sequentially to achieve efficient cellular uptake. Rather, arginine residues can be spaced along a peptide sequence without compromising cellular uptake [66].

1.3.2 CPP-assisted intracellular delivery of drug carriers

The true utility of CPPs in the field of drug delivery is that the non-specific internalization attributed to the CPP can be conferred to large covalently conjugated cargo. Peptides and proteins [67], liposomes [68], micelles [69, 70], and metallic nanoparticles [71, 72] are all carriers whose intracellular uptake has been facilitated by CPP functionalization. The mechanism of cellular uptake for these large CPP-conjugates, however, tends to differ from that of the CPPs alone. Though some CPPs appear to cross the cell membrane and achieve diffuse distribution throughout the cytosol, CPP-conjugates typically exhibit a punctate accumulation within the cell, suggesting their uptake by an endocytic mechanism that leads to their localization within intracellular vesicle compartments. These differences in uptake between CPPs and their CPP-conjugates have been shown with cargo whose size ranges from peptides to proteins [63,

73]. The sensitive nature of this transition in the mechanism of uptake has been demonstrated with fluorescently labeled Arg_7 with increasing addition of amino acid residues as its cargo [73]. Arg_7 alone, or when appended with a single tryptophan, directly traversed the membrane of osteosarcoma cells as evident by their diffuse fluorescence throughout the cell. However, the addition of 9 to 11 amino acid residues resulted in uptake by an endocytic mechanism as suggested by their punctate fluorescence in the cell.

The exact endocytic mechanism that a CPP-conjugate might exploit for internalization is likely dependent on the type and density of CPP as well as the size and composition of the cargo. Arg_8, for example, has been shown to elicit macropinocytosis when decorating liposomal carriers at a high density [74]. With functionalization at lower density, however, Arg_8 decorated liposomes were shown to enter cells via clathrin-mediated endocytosis. The internalization pathway associated with macropinocytosis is believed to be less degradative than that of clathrin-mediated endocytosis, as the former can avoid, to some extent, the trafficking to harsh environments of the lysosome [75], as is typical for the latter. Thus in this case, a high density of CPP-functionalization could provide an advantage to the drug carrier by improving its ability to prevent degradation of its cargo in hopes of delivering intact and active drug to its intracellular target. Due to the variation in their mechanisms of uptake, each CPP-functionalized carrier system should therefore be individually evaluated to

elucidate their mechanism of entry in the cell, which may inform decisions about the design of the carrier to improve function based on the intracellular environments it is likely to encounter on its route of internalization.

Despite the variability in the mechanism of uptake of CPP-conjugates, these CPP-functionalized carriers have been exploited for their non-specific uptake into a variety of cell types. Due to this non-specific uptake, CPPs were initially used for local delivery. Penetratin™ 1 Peptide (Q-Biogene) [76] and Chariot™ Protein Delivery Reagent (Active Motif) [77] are CPP-functionalized laboratory reagents developed for *in vitro* intracellular delivery. *In vivo*, local application of CPP-functionalized carriers has been used for transdermal drug delivery for scarring [78], wrinkles [79], and psoriasis [80]. Beyond local applications, preliminary use of CPP-functionalized conjugates for systemic delivery has been investigated for the treatment of myocardial infarction [81] and stroke [82].

1.3.3 Targeted delivery with activatable CPP-functionalized drug carriers

To use CPPs in systemically administered anti-cancer drug carriers the function of the CPP must be carefully controlled to provide targeted tumor uptake while avoiding uptake in off-target tissues. To achieve this control, stimulus-responsive materials have been used to selectively display CPPs on drug carriers in response to tumor-specific triggers, such as overexpressed enzymes or depressed pH, or extrinsic triggers, such as light. This general approach to control CPP function on drug carriers

has been investigated with four major mechanisms: 1) controlled display of CPPs after removal of stealth polymers, 2) triggered display of CPPs using actuated molecular tethers, 3) controlled display of CPPs by dissociation from ionic inhibitors, and 4) manipulation of CPP charge by ionizable residues.

Decoration of drug carriers with a high density of CPPs would lead to their efficient uptake in many types of cells. If such a carrier were delivered systemically, it could be taken up non-specifically into any tissue it encountered. Hiding CPP-functionalization beneath a coating of stealth polymer, such as polyethylene glycol (PEG), can prevent interaction of the CPP with cell surfaces and thus shield the drug carrier from non-specific cellular uptake. Recovery of the CPP function can then occur when the stealth polymers are removed. This can provide targeted uptake if removal of the stealth coating only occurs in the tumor. Thus, mechanisms of removal have been designed into PEGylated drug carriers to release their PEG in response to tumor-specific intrinsic triggers. For example, PEG attached to TAT-functionalized liposomes via hydrazone linkers can be released by pH-sensitive cleavage of the linker in the acidic conditions of the tumor. After removal of the PEG, TAT-functionalized liposomes could efficiently deliver their cargo, such as chemotherapeutic doxorubicin, into cancer cells [83]. Alternatively, PEG attached to CPP-functionalized nanoparticles by enzyme-cleavable peptide linkers can release their protective coating by digestion of the linker in the enzymatically rich tumor environment. PEG linkers cleaved by matrix

metalloprotease-2 have been used in such designs to achieve controlled cellular uptake of drug carriers such as TAT-functionalized liposomes [84], or imaging agents such as CPP-functionalized quantum dots [85] and iron oxide nanoparticles [86].

When using stealth coatings to selectively shield CPPs, the function of CPPs can alternatively be triggered by actuation of a molecular tether that allows the presentation of CPPs beyond the protective stealth corona. Using an ionizable tether can provide actuation in response to tumor acidity using a self-assembled diblock copolymer micelle as a carrier. When the CPP-functionalized tether is neutral at pH 7 it prefers to sequester itself near the hydrophobic core of the micelle, such that it is buried within the stealth corona and prevents the interaction of the appended CPP with non-specific targets. Only in the acidic conditions of the tumor can the tether be ionized and its increased hydrophilicity can encourage the stretching of the tether across the stealth corona, to ultimately display CPP on the surface of the nanoparticle. This mechanism has been used with TAT-functionalized micelles to achieve targeted delivery of doxorubicin to improve tumor regression of a drug resistant xenograft in mice [87]. This unique approach has the advantage of being reversible, whereby the tether could potentially return the CPP to its hidden position beneath the stealth coating if it were to escape the acidic conditions in the tumor and return to conditions of normal pH.

For those CPPs that are rich in cationic charge, their function can alternatively be controlled by electrostatic interactions. Pairing a cationic CPP with an anionic inhibitor

can electrostatically preoccupy the CPP, such that it will not prematurely interact with off-target tissues. This is commonly achieved with hairpin-like structures in which the CPP and anionic inhibitor are attached by a short linker that strongly encourages their interaction due to their forced proximity. Selective recovery of the CPP function can be achieved when interaction with the inhibitor is disrupted. This is most often achieved by use of a peptide linker that is cleaved by tumor specific enzymes, such as matrix metalloprotease-2. Overexpression of this enzyme in the tumor leads to local cleavage of the linker, dissociation of the CPP and inhibitor, and internalization of the functional CPP in the tumor. This approach has been extensively developed using arginine-rich CPPs for delivery of imaging agents such as dyes for fluorescent imaging [88-90] and gadolinium for magnetic resonance imaging [91, 92]. Their use as tumor-specific imaging agents has been employed as a tool for improved tumor resection, where intraoperative visualization of accumulated CPP-functionalized markers could direct surgical decisions that improved the removal of tumor margins [92].

The function of many CPPs relies, at least in part, on their charge content. A final, although less common, approach to controlling CPP function is to control its inherent charge by the use of ionizable residues. An example of this approach was shown with a mutated transportan CPP. This lysine-rich CPP was mutated such that all lysine residues were substituted with histidine residues, whose pK_a near physiologic pH makes then suitable ionizable residues in the context of biological systems. The neutral charge of this

mutated CPP at pH 7.4 eliminated uptake, while the ionization to positive charge at pH 6.0 increased internalization. This triggered uptake in low pH, typical of acidic tumors, could increase the *in vitro* cytotoxicity caused by chemotherapeutic cargo, such as camptothecin [93]. This is another approach that provides the advantage of reversibility, whereby charge of the CPP can change as it either enters or exits the acidic conditions of the tumor.

The activation of the CPP function in most of these approaches relies on intrinsic triggers characteristic to the tumor tissue, such as overexpression of extracellular enzymes and tumor tissue acidity. While these alternative approaches have their respective merits, they will likely remain limited by three important factors. First, these approaches remain reliant on the intrinsic characteristics of the tumor tissue as their CPP-activating trigger and thus will remain limited by the heterogeneity of tumors. Second, the reliance on enzyme and pH-mediated reactions presents a challenge of slow reaction kinetics, where the slow activation of CPPs by these processes may hinder their function in the time frame of their accumulation in the tumor tissue. And third, the loss of shielding polymers or ionic inhibitors means some of these approaches to CPP activation are irreversible, and thus present concern for the re-entry of activated CPPs into the systemic circulation from which they may accumulate in any tissue within the body.

1.4 Elastin-like polypeptides as drug carriers

1.4.1 Elastin-like polypeptides

Elastin-like polypeptides (ELPs) are a class of materials inspired from human elastin [94], which are composed of a repeating pentapeptide $(VPGXG)_n$, where *X*, the guest residue, is any amino acid other than proline, and *n* indicates the number of pentapeptide repeats that defines the length of the ELP chain. ELPs exhibit a lower critical solution temperature (LCST) phase transition behavior, such that they are soluble below a characteristic transition temperature (T_t) and coacervate into micron-scale aggregates above this T_t [95]. For many ELPs this transition occurs on a short timescale over a few degrees Celsius and is fully reversible when the solution is return to temperatures below the T_t. This reversibility of the ELP transition makes it a useful behavior that can be exploited for the purification of ELPs by a technique termed inverse transition cycling [96].

ELPs are typically expressed recombinantly in *E. coli*, but have also been successfully synthesized in yeast, fungi, and plant expression systems. Due to their repetitive nature, their genetic design requires specialized cloning techniques to create repeating genes of specific length. Such cloning techniques include recursive directional ligation (RDL) [97], recursive directional ligation by plasmid reconstruction (PRe-RDL) [98], and overlap extension rolling circle amplification (OERCA) [99].

As stimuli-responsive materials, ELPs are particularly useful because of the tunability of their behavior. The characteristic T_t of an ELP is dependent both on intrinsic parameters of the ELP design and extrinsic parameters of the ELP environment. Intrinsic parameters, including sequence and length, are most commonly used to manipulate the ELP T_t. The ELP sequence is manipulated by changing the guest residue, where more hydrophilic guest residues raise the T_t and more hydrophobic guest residues lower the T_t [100, 101]. The ELP length is inversely related to ELP T_t, such that the longer the chain length, the more depressed the T_t [102]. Extrinsic parameters that affect the T_t include the ELP concentration and cosolutes, such as salts. ELP concentration is inversely related to T_t, such that higher concentrations result in lower T_ts, in a logarithmic relationship [102]. The presence of kosmotropic anions (Cl^- and higher on the Hofmeister series) lowers the ELP T_t, where increasing concentration of salt amplifies this effect [103]. Tuning these intrinsic and extrinsic parameters allows exceptional control over the ELP T_t, such that the stimulus-response of an ELP can be engineered precisely for its specific application.

As biopolymers, ELPs have distinct material advantages for use in biological applications. First, since the ELP sequence and length are controlled by a genetic template, ELP products are perfectly monodisperse. Maintaining consistent composition and size provides predictability in material performance *in vivo*, in which these material characteristics influence pharmacokinetics and biodistribution. Second, since ELPs are polymers composed of natural amino acids they are biocompatible and, despite their

synthesis in bacterial hosts, illicit minimal inflammatory and immune responses when locally or systemically injected in animal models [104-106]. Finally, this natural composition also provides biodegradability, such that an ELP can be broken down into amino acid building blocks, which are safely cleared from the body.

The rate of degradation of ELPs has been approximated with systemically administered ^{14}C-labeled ELP in mice. These ELPs exhibited a degradation rate of approximately 2.5 weight %/day after systemic administration [30], demonstrating that ELPs remain intact within timescales typical of applications for drug delivery, but also degrade within weeks of administration to be safely cleared from the body. It is important, however, to consider the effect of ELP T_t on the degradation rate, as the degradability of ELPs by some enzymes has been shown to be inhibited when the ELP is coacervated in micron-scale aggregates or coacervated and sequestered within the core of ELP block copolymer micelles [107].

Due to their controlled synthesis, biocompatibility, and tunable stimulus-response, ELPs have been used for a number of biological applications including biosensing [108, 109], tissue engineering [110], and drug delivery [111]. Furthermore, their qualities as biocompatible and stimulus-responsive materials have been extensively exploited in the delivery of therapeutics to cancers, be it as macromolecular and nanoparticle carriers, hyperthermia-targeted vehicles, or temperature-triggered depots [112].

1.4.2 CPP-ELPs as drug carriers

Pseudorandom ELPs have been functionalized with CPPs such as antennapedia and TAT as a means to increase their cellular uptake and thereby increase internalization of drug cargo [113]. When the T_t of the CPP-ELP was tuned between 37 °C and 42 °C, it could be used to further enhance uptake by means of hyperthermia-triggered aggregation, whereby the ELP transition alone had been shown to increase cellular uptake, likely by means of increased endocytosis of the portion of aggregates that are nano-scale [114]. Increased cellular uptake of CPP-ELPs, assisted by mild hyperthermia, has enhanced the delivery of a number of genetically appended therapeutics *in vitro*, including peptide drugs like H1 c-Myc inhibitor [115], p21 kinase inhibitor [116], and L12 cancer cell lytic peptide [117]. Alternatively, CPP-ELPs have also been covalently conjugated with small molecule chemotherapeutics such as doxorubicin [118, 119] and paclitaxel [120]. *In vivo*, these CPP-ELPs have been shown to exhibit anti-tumor efficacy when delivering peptide drugs [121] or small molecule chemotherapeutics [122, 123] by systemic administration in combination with local tumor hyperthermia.

However, the use of pseudorandom or homopolymer ELPs to control the CPP function by ELP coacervation is not an idealized approach, in that the presentation of CPPs in the ELP aggregate is disorderly and not necessarily displayed in a manner that would increase uptake by enhanced interaction with the cell surface. However, the

aggregation of the ELP alone has been shown to increase cellular uptake and the contribution of this effect may compensate for non-optimal presentation of CPP by the aggregate. Furthermore, aggregation of CPP-ELPs may also present complications of toxicity, as not all CPP-ELPs discussed above were found to be suitable materials as drug carriers due to their inherent toxicity in some cell lines [115, 124].

1.4.3 ELP diblock copolymers

ELP diblock copolymers (ELP_{BC}s) are created by the genetic fusion of two ELP sequences. When the two blocks are composed of a hydrophilic ELP (containing more hydrophilic guest residues) and a hydrophobic ELP (containing more hydrophobic guest residues), the ELP_{BC} can undergo temperature-triggered self-assembly into higher order structures, provided the two ELP sequences impart a T_t on each block that is sufficiently different than the other. Raising the solution temperature above the T_t of the hydrophobic block leads to the desolvation of a nanoparticle core, while the hydrophilic block creates a solvated nanoparticle corona. Raising the solution temperature further, above the T_t of the hydrophilic block, leads to complete aggregation of the ELP_{BC}s into micron-scale aggregates.

This behavior has been extensively characterized for ELP_{BC}s that self-assemble into spherical micelles. The first ELP_{BC} to exhibit temperature-triggered micelle assembly was composed of a hydrophilic $[VPGEG(IPGAG)_4]_{14}$ block and a hydrophobic $[VPGFG(IPGVG)_4]_{16}$ block [125]. The extreme difference in the hydrophilicty of guest

residues glutamic acid and alanine as compared to the hydrophobicity of the guests residues phenylalanine and valine drove the temperature-triggered self-assembly of this construct into spherical, and sometimes cylindrical, micelles when above approximately 25 °C, the T_t attributed to the hydrophobic block.

Systematic design of several ELP$_{BC}$s, composed of a hydrophilic $(VPGXG)_n$ [X=$V_1A_8G_7$; n=64, 96, or 128] block and a hydrophobic $(VPGVG)_m$ [m=60, 90, or 120] block, shed light on the design parameters that control temperature-triggered micelle assembly [126]. The combinatorial pairing of these two blocks demonstrated that any ratio of block sizes (n:m) between 1:2 and 2:1 was capable of temperature-triggered self-assembly, whereby straying significantly from this ratio resulted only in unimer-to-aggregate transition. Furthermore, the variation in hydrophobic block size demonstrated that the thermal property of this domain controlled the critical micellization temperature (CMT), the temperature at which the unimer-to-micelle transition occurs. The size of the self-assembled micelles depended not only on the overall size of the ELP$_{BC}$, but also on the hydrophilic-to-hydrophobic block ratio (n:m). Beyond this basic investigation of ELP$_{BC}$ design parameters for micelle self-assembly further elucidation has recently been achieved with modeling of the ELP$_{BC}$ transitions, such that the CMT and micelle-to-aggregate transition of an ELP$_{BC}$ can be predicted by the T_ts of the individual blocks from which the ELP$_{BC}$ is composed [127]. Although this predictive power is limited only to those ELP components used to make such a model, it is a step in the right direction

toward developing procedures for the rational design of ELP$_{BC}$s with precisely predicted thermal properties.

1.4.4 ELP$_{BC}$s as drug carriers

ELP$_{BC}$s have been proposed as suitable drug carriers both as stable self-assembled micelles and as dynamic systems that exploit the temperature-triggered unimer-to-micelle transition. With the goal of tumor targeted delivery, ELP$_{BC}$s have been functionalized at their hydrophilic terminus with peptides [126, 128, 129] and proteins [130, 131] that target upregulated cancer cell receptors to induce cell-specific internalization. In some instances, the thermal properties of the ELP$_{BC}$ were appropriate for temperature-triggered density modulation of the functionalized entity, whereby temperature-triggered micelle assembly could influence internalization in those cell types that overexpressed the target receptor. Very few functionalized ELP$_{BC}$s, however, have been optimized to achieve temperature-triggered micelle assembly in response to conditions of clinically relevant mild hyperthermia.

The use of ELP$_{BC}$s has advantages over the use of homopolymer ELPs to control the activity of functionalized targeting moieties due to the spatial organization of the functionalization on the self-assembled micelle, as opposed to the disordered aggregate created by homopolymer coacervation. The orderly display of RGD, for example, on an ELP$_{BC}$ micelle corona was crucial for amplifying uptake above the CMT in targeted cancer cells, as compared to the ELP$_{BC}$ unimer below the CMT. RGD-functionalized ELP

above its T_t could not achieve increased cellular uptake, by means of its triggered aggregation, of comparable magnitude to the ELP_{BC} by means of its triggered micelle assembly [128].

Despite efforts to design ELP_{BC}s suitable as drug carriers, there is very little evidence in the literature that these materials have been used to successfully deliver drug cargo. In fact, only one instance is reported in which ELP_{BC} functionalized at the hydrophilic terminus with FK506 binding protein 12 (FKBP), a binding partner to the small molecule drug rapamycin, self-assembled into a stable micelle at 37 °C and carried drug cargo, both bound to the micelle corona and sequestered in the micelle core by means of the hydrophobic effect. The immunosuppressant and anti-proliferative properties of this drug provided efficacy in suppressing autoimmune effects in a Sjogren's syndrome mouse model [132] and in regressing tumor growth of a breast cancer xenograft in mice [131]. Delivery of the drug by means of the ELP_{BC} served to reduce toxic side effects as compared to free drug alone.

1.5 Manipulation of CPP density with ELP_{BC} self-assembly for controlled cellular uptake

The success of anti-cancer drugs relies heavily on their delivery to the tumor target. The toxicity of anti-cancer drugs caused by their effects in off-target tissues has significantly limited their safe dosage and thus hindered their therapeutic success. Development of macromolecule and nanoparticle drug vehicles has improved the accumulation of drug cargo in the tumor with passive targeting by the EPR effect.

Furthermore, a number of active targeting strategies have been investigated that exploit distinct features of the tumor such as overexpressed receptors, upregulated enzymes, and depressed pH. These approaches, however, are limited by the heterogeneity of the intrinsic tumor targets. Due to the vast diversity of cancer types, these methods of active targeting are applicable only to specific cancers likely to possess the required target [133]. Their efficacy is also limited by tumor heterogeneity among individual patients, such that all instances of a single cancer type cannot be successfully targeted by these approaches [134-137].

Development of a novel carrier capable of targeted accumulation at the tumor site independent of the tumor characteristics, while simultaneously avoiding uptake in healthy tissue, would provide a delivery method applicable to a wide range of cancer types and would circumvent the need for a prior knowledge of the tumor phenotype. Such a therapeutic carrier has yet to be realized in the clinic and would likely find benefits in the systemic treatment of a variety of solid tumors.

To attain this goal, the method described here exploits CPPs as a means of achieving non-specific and receptor-independent cellular uptake. Because of their non-specific activity, the function of CPPs must be carefully controlled to achieve the desired uptake at the tumor site, regardless of tumor characteristics, while avoiding uptake in healthy tissues throughout the body. To create "on" and "off" states of CPP uptake, a CPP-functionalized ELP_{BC} has been designed whose temperature-triggered micelle

assembly can modulate the density of CPPs in the presence of mild clinical hyperthermia (Figure 1). In the simplest approach, the density of arginine residues—important to CPP function due to their unique guanidinium headgroup—can be modulated between unimer and micelle states of the ELP_{BC}. The threshold of 6 arginine residues required to achieve uptake can prevent the cellular internalization of unimers containing fewer than 6 arginines. Only when assembled into micelles in the presence of heat can this threshold, as sensed by the target cell surface, be overcome by the increased density of arginines presented on the micelle corona.

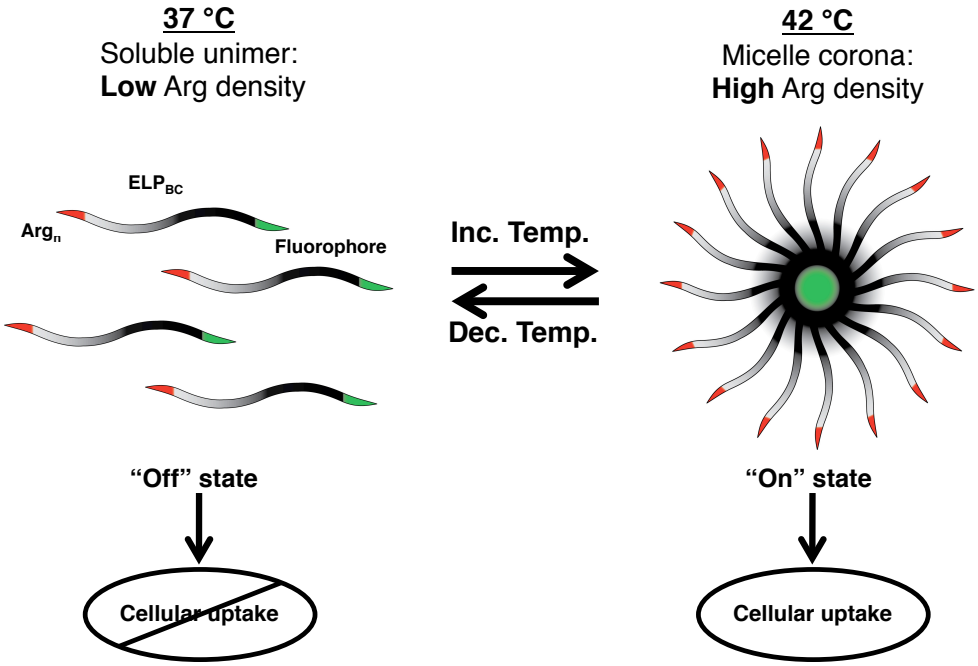

Figure 1: CPP-ELP_{BC}s control cellular uptake by modulation of CPP density. The low density of arginines on each unimer—below the threshold necessary for uptake—limits their internalization into cells in their soluble "off" state at 37 °C. When the temperature is increased above the CMT, the ELP_{BC} self-assembles into micelles with

increased density of CPP on the micelle corona. This increased density of CPP—above the threshold necessary for uptake—permits enhanced internalization in their self-assembled "on" state at 42 °C.

CPP-ELP$_{BC}$s, by means of their temperature-triggered micelle assembly, can thereby control cellular uptake by manipulation of CPP density using an extrinsic trigger. Parameters of controlled uptake, including the magnitude of internalization at both "off" and "on" conditions, can be tuned by the CPP-functionalization beyond arginine oligomers. Creation of a family of CPP-ELP$_{BC}$s thus permits the exploration of variable levels of uptake. This is particularly convenient in the context of delivering variable drug cargo, where the suitable "off" and "on" levels of intracellular delivery necessary to induce controlled therapeutic effect at "on" conditions and spare cells at "off" conditions is likely to be dependent on drug characteristics, such as potency. This modular drug carrier system, capable of extrinsically targeting cellular internalization, thus provides a platform of materials that may be suitable for the delivery of a breadth of drug classes to a variety of cell types with controlled therapeutic effect.

2. Design, synthesis, and thermal characterization of CPP-ELP$_{BC}$s

2.1 Motivation

The temperature-triggered self-assembly of ELP$_{BC}$s was first established for constructs composed purely of two distinct ELP domains [126]. It has since been demonstrated that ELP$_{BC}$s can be functionalized with additional components and retain their temperature-triggered self-assembly. Tumor-targeting peptides, such as NGR and RGD, have been genetically appended to the hydrophilic terminus of ELP$_{BC}$s and resulted in minimal perturbation of the CMT of functionalized ELP$_{BC}$, as compared to non-functionalized ELP$_{BC}$ [126, 128]. Furthermore, tumor-targeting protein fibronectin type III domain, despite its size and hydrophobicity, has been successfully appended to ELP$_{BC}$s that self-assemble into micelles and display the protein on the micelle corona [130]. Thus, it is highly feasible that ELP$_{BC}$s can also be genetically appended to CPPs at their hydrophilic terminus and retain their temperature-triggered self-assembly.

There are three important requirements that must be met when genetically appending a new peptide entity to an ELP$_{BC}$. First, the fusion must be sufficiently expressed in *E. coli*. The sequence and structure of the peptide, as well as its mRNA template, can influence the efficiency of expression. Furthermore, the site of peptide fusion, at the N- or C-terminus of the ELP$_{BC}$, can also affect successful expression and sufficient yield of the ELP fusion.

Second, the fusion must be adequately purified from the *E. coli* lysate. Typically, ELPs are easily purified from the *E. coli* lysate by means of their LCST behavior. However, peptides that are highly charged, such as cationic CPPs, can introduce additional challenges in the purification process by electrostatically binding to contaminants that can then be unintentionally co-purified with the ELP. Modifications in the purification process many therefore be necessary to produce pure peptide ELP_{BC} fusions.

Third, the peptide-functionalized ELP_{BC} must display the desired thermal properties required for its specific application. For applications requiring mild hyperthermia-targeted self-assembly, the CMT must be between 37 °C (corresponding to normal body temperature) and 42 °C (corresponding to mild clinical hyperthermia) over an acceptable range of ELP concentration. The ELP transition is sensitive to its local environment, including those entities that are synthetically or genetically appended to the polypeptide chain, creating what is known as a ΔT_t effect, in which the T_t of the ELP fusion differs from the ELP alone [138]. Thus, it is not unexpected that some peptides will perturb the T_t of the appended ELP and thereby perturb the ELP_{BC}'s CMT and micelle-to-aggregate T_t. Characteristics such as the size, charge, and hydrophobicity of the peptide are likely to influence the magnitude of the peptide's effect on the ELP T_t. Although CPPs are generally short peptides, the high charge content of cationic CPPs may induce changes in the thermal properties of the ELP_{BC}s to which they are appended.

Keeping in mind the potential challenges presented by CPP-functionalization in meeting the requirements discussed above, novel CPP-ELP$_{BC}$s were genetically designed, recombinantly expressed, and purified. Their thermal behavior was then characterized with temperature-regulated turbidimetry, dynamic light scattering, and zeta potential measurements. ELP$_{BC}$ design parameters were manipulated to optimize the thermal behavior of these systems, such that they would exist as soluble unimers at 37 °C and self-assemble into micelles at 42 °C. The behavior of these optimized constructs would best permit the future investigation of controlled cellular uptake by means of modulating CPP density with temperature-triggered ELP$_{BC}$ self-assembly in response to the clinically relevant stimulus of mild hyperthermia.

2.2 Methods

Two cloning methods were utilized in the design of CPP-ELP$_{BC}$s: recursive directional ligation (RDL) and RDL by plasmid reconstruction (PRe-RDL). First and second generation CPP-ELP$_{BC}$s were designed by RDL, whereas third and fourth generation CPP-ELP$_{BC}$s were designed by PRe-RDL. Transition to the PRe-RDL cloning system provided additional ease of genetic design due to the modular nature of this technique, which facilitates the variation of N- and C-terminal functionalization of the ELP$_{BC}$ genes. Each method utilized its own cloning vector with unique enzyme restriction sites for the insertion of ELP, leader, and trailer genes. Once genetically encoded, ELP$_{BC}$s designed with either cloning method were similarly expressed,

purified, and characterized. Design parameters, such as ELP sequence and length, were manipulated to optimize the thermal behavior of CPP-ELP$_{BC}$s for hyperthermia-triggered self-assembly.

2.2.1 RDL cloning method

RDL is one method for oligomerizing repetitive genes with precisely controlled sequence and length [97]. This method exploits a cloning vector that, when cut at a unique restriction site, can receive a gene insert digested out of a separate vector. This method can thereby predictably build the length of an ELP by the addition of the gene in the receiving vector and the gene insert. Digestion at the unique restriction site in the receiving vector results in asymmetric sticky ends that serve two purposes: first, to recognize the insert only in its correct 5′-to-3′ directionality and second, to prevent concatemerization of multiple copies of the insert. These features ensure that the ELP gene sequence and length are precisely controlled with each oligomerization step. Functionalization of the N- and C-terminus of the ELP gene is accomplished by ligating the complete ELP gene into an expression vector at a unique restriction site designed at the junction between the leader and trailer-encoding genes. RDL cloning of ELP$_{BC}$s was performed in a pUC19 vector, while modification of the N- and C-terminal functionalization of ELP$_{BC}$s was performed in a pET-25b(+) vector. Both vectors encoded antibiotic resistance to ampicillin.

2.2.1.1 Synthesis of ELP_{BC} genes by RDL cloning

First and second generation ELP_{BC}s synthesized by RDL cloning were composed of two ELP sequences: E4 and E2. E4 is a hydrophobic ELP with the sequence $(VPGVG)_n$, where the guest residue is valine. E2 is a hydrophilic ELP with the sequence $(VPGXG)_n$ where the guest residue, X, is valine, glycine, or alanine in a ratio of 1:7:8. The sequence and length of an ELP is denoted with the nomenclature *E-n*, where *E* denotes the type of ELP (ex. E4, E2, etc.) and *n* denotes the length, in pentapeptides. Genes encoding both E4 and E2 were readily available in the Chilkoti laboratory, and therefore did not require synthesis beginning at oligomer concatemerization. Only the combination of E4 and E2 genes was required in the creation of new ELP_{BC}s using this RDL cloning method. The oligonucleotide and peptide sequence of ELPs designed with RDL cloning are listed in Table 1.

Table 1: Genetic design of ELPs for RDL cloning.

ELP: (VPG*X*G)*n*	**Peptide and gene sequence**
E4: $(VPGVG)_{30, 60, or 90}$	(V G V P G V G V P G V G V P G V G (gtg ggt gtt ccg ggc gta ggt gtc cca ggt gtg ggc gta ccg ggc gtt ggt V P G V G V P G)$_{6, 12, or 18}$ gtt cct ggt gtc ggc gtg ccg ggc)$_{6, 12, or 18}$

E2: $(VPGXG)_{64 \text{ or } 96}$ *X*=V:G:A=1:7:8	(V G V P G A G V P G G G V P G A G (gtg ggt gtg ccg ggc gca ggt gtt ccg ggt ggc ggt gtg ccg ggc gca ggt V P G G G V P G A G V P G G G V P gtt ccg ggt ggc ggt gtg ccg ggc gca ggt gtt ccg ggt ggc ggt gtg ccg G A G V P G G G V P G A G V P G G ggc gca ggt gtt ccg ggt ggc ggt gtg ccg ggc gca ggt gtt ccg ggt ggc G V P G A G V P G G G V P G A G V ggt gtg ccg ggc gca ggt gtt ccg ggt ggc ggt gtg ccg ggc gca ggt gtt P G G G V P G A G V P G)$_{4 \text{ or } 6}$ ccg ggt ggc ggt gtg ccg ggc gca ggt gtg ccg ggc)$_{4 \text{ or } 6}$

Genes encoding ELP_{BCS} were synthesized by genetic fusion of E4 and E2. The ELP destined for the N-terminus of the block copolymer was identified as the insert, and the ELP destined for the C-terminus of the block copolymer was identified as the receiving vector. The receiving vector was digested with PflMI, dephosphorylated with calf intestinal alkaline phosphatase (CIP), and purified from the reaction using a PCR purification kit. The insert was prepared by digestion with PflMI and BglI, creating 4 distinct fragments: 1377, 1186, and 164 base pairs in length, in addition to a band corresponding to the length of the encoded ELP gene. These fragments were separated by gel electrophoresis and the band corresponding to the ELP fragment was excised from the gel and recovered using a gel extraction purification kit. The receiving vector and insert were then ligated and transformed into competent TOP10 *E. coli*. Successful

ligation was screened with diagnostic digestion using HindIII and EcoRI restriction enzymes and then confirmed with plasmid DNA sequencing using T7 promoter and terminator primers.

2.2.1.2 N- and C-terminal functionalization of ELP_{BC} genes by RDL cloning

To functionalize the N- and C-terminus of the ELP_{BC}, a vector was designed to encode the leader sequence that would precede the ELP and the trailer sequence that would succeed the ELP. A pET-25b(+) cloning vector was digested with NdeI and EcoRI, dephosphorylated by incubation with CIP, and purified from the excised 96 base pair fragment using a PCR purification kit. Oligonucleotides encoding the leader and trailer sequences were designed with 5′ and 3′ sticky ends complementary to the NdeI and EcoRI cut sites and contained a distinct SfiI cut site to allow the insertion of the ELP between the leader and trailer sequences. Annealed oligonucleotides and digested vector were ligated and transformed into competent TOP10 *E. Coli*. Successful functionalization of the vector was screened by colony PCR and diagnostic digestion with SfiI and then confirmed with plasmid DNA sequencing using the T7 promoter primer. Oligonucleotide and peptide sequences of leaders and trailers for those ELPs designed with RDL are listed in Table 2, where pertinent residues of the leader and trailer are noted, functionalizing the N- and C-terminus of the ELP, respectively.

Table 2: Genetic design of leaders and trailers for RDL cloning.

N-	C-	Peptide and oligonucleotide sequence
Arg_3	Cys, Trp	(M) G R R R G P G W P C . . t atg ggc cgc cgt cgc ggg ccg ggc tgg ccg tgc tga t ac ccg gcg gca gcg ccc ggc ccg acc ggc acg act att aa
Cys, Trp	-	(M) G C G W P G G P G G S . . t atg ggc tgc ggg tgg ccg ggc ggg ccg ggc ggt agc tga t ac ccg acg ccc acc ggc ccg ccc ggc ccg cca tcg act att aa
Cys, Trp	Lys	(M) G C G W P G G P G G S K . . t atg ggc tgc ggg tgg ccg ggc ggg ccg ggc ggt agc aaa tga t ac ccg acg ccc acc ggc ccg ccc ggc ccg cca tcg ttt act att aa
Cys, Trp	Arg	(M) G C G W P G G P G G S R . . t atg ggc tgc ggg tgg ccg ggc ggg ccg ggc ggt agc cgc tga t ac ccg acg ccc acc ggc ccg ccc ggc ccg cca tcg gcg act att aa
Cys, Trp	Arg_3	(M) G C G W P G G P G G S R R R . . t atg ggc tgc ggg tgg ccg ggc ggg ccg ggc ggt agc cgc cgt cgc tga t ac ccg acg ccc acc ggc ccg ccc ggc ccg cca tcg gcg gca gcg act att aa
Cys, Trp	Arg_4	(M) G C G W P G G P G G S R R R R . . t atg ggc tgc ggg tgg ccg ggc ggg ccg ggc ggt agc cgc cgt cgc cgt tga t ac ccg acg ccc acc ggc ccg ccc ggc ccg cca tcg gcg gca gcg gca act att aa
Cys, Trp	Arg_5	(M) G C G W P G G P G G S R R R R R . t atg ggc tgc ggg tgg ccg ggc ggg ccg ggc ggt agc cgc cgt cgc cgt cgc tga ac ccg acg ccc acc ggc ccg ccc ggc ccg cca tcg gcg gca gcg gca gcg act . t att aa

The vector encoding the leader and trailer sequence was digested with SfiI, dephosphorylated with CIP, and purified from the reaction using a PCR purification kit.

The vector encoding the ELP_{BC} was digested with PflMI and BglI, resulting in sticky ends that are compatible with the SfiI cut site. The desired fragment that included the ELP sequence was separated by gel electrophoresis and purified with a gel extraction kit. The vector and insert were then ligated and transformed into competent BLR *E. coli*. Successful ligation was screened with diagnostic digestion using AvaI and XbaI restriction enzymes and then confirmed by sequencing with T7 promoter and T7 terminator primers.

2.2.2 PRe-RDL cloning method

PRe-RDL is a modular cloning method that is well suited for the creation and functionalization of ELP_{BC}s [98]. Unlike RDL, which uses a single restriction site as the point of inserting an ELP gene, PRe-RDL uses three restriction enzymes to deconstruct two plasmids encoding the ELP sequences to be combined. After purification of the desired fragments from digestion of the two plasmids, the fragments are ligated to reconstruct a functional vector while combining the desired genes from either original plasmid. A functional plasmid is only recovered by successful ligation of the desired fragments, thus eliminating colony background from undesirable ligation events. This approach therefore greatly improves cloning efficiency, as compared to RDL, by reducing the chances of vector self-ligation prior to ELP gene insertion. Furthermore, PRe-RDL allows independent attachment of leader and trailer sequences at the N- and C-terminus of the ELP gene, which provides greater freedom of gene functionalization.

This is particularly useful for the addition of a family of CPPs at the C-terminus of the ELP_{BC} while the N-terminal functionalization sequence remains the same.

2.2.2.1 Modification of pET-24a(+) vector for PRe-RDL cloning

For third and fourth generation ELP_{BCS}, PRe-RDL cloning was performed using a modified pET-24a(+) vector [98]. This modification was added between XbaI and BamHI restriction sites and contained the ribosomal binding site and restriction enzyme recognition sites for BseRI and AcuI that are necessary for the PRe-RDL cloning method (Figure 2).

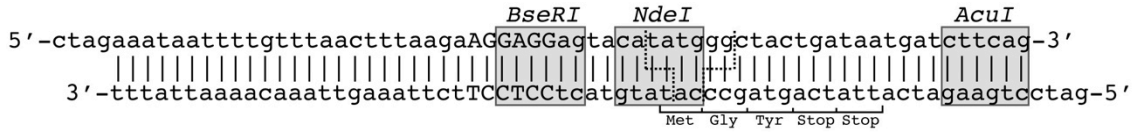

Figure 2: The pET-24a(+) vector was modified for PRe-RDL cloning. Insertion of this oligomer conferred the restriction enzyme recognition sites for BseRI, NdeI, and AcuI enzymes (grey), a ribosomal binding site (capitalized), and a short leader and trailer sequence (MGY). The cut site for NdeI (dotted line) results in ta-5′ overhangs, while the overlapping cut site for BseRI and AcuI (dotted line) results in gg-3′ overhangs. Reproduced from [139].

2.2.2.2 Oligomerization of ELP genes and synthesis of ELP_{BC} genes with PRe-RDL cloning

The ELP sequences used to design ELP_{BCS} with PRe-RDL differed slightly from those utilized in RDL cloning. The hydrophobic domain was still composed of E4 with the sequence $(VPGVG)_n$, where the guest residue was valine. The hydrophilic ELP was composed of a modified E2, identified as E2*, with the sequence $(VPGXG)_n$ where the

guest residue, *X*, is alanine or glycine at a 1:1 ratio. The oligonucleotide and peptide sequences of ELPs used for PRe-RDL cloning are listed in Table 3.

Table 3: Genetic design of ELPs for PRe-RDL cloning.

ELP: VPGXG$_n$	**Peptide and oligonucleotide sequence**
E4: (VPGVG)$_{30, 35, \text{ or } 40}$	(V G V P G V G V P G V G V P G V G V (gtg ggt gtt ccg ggc gta ggt gtc cca ggt gtg ggc gta ccg ggc gtt ggt gtt P G V G V P G)$_{6, 7, \text{ or } 8}$ cct ggt gtc ggc gtg ccg ggc)$_{6, 7, \text{ or } 8}$
E2*: (VPGXG)$_{60}$ X=A:G=1:1	(A G V P G G G V P G A G V P G G G (gca ggt gtt ccg ggt ggc ggt gtg ccg ggc gca ggt gtc ccg ggt ggc ggt V P G A G V P G G G V P G A G V P G gtg ccg ggc gca ggt gtc ccg ggt ggc ggt gtt ccg ggc gca ggt gtc ccg ggt G G V P G A G V P G G G V P G)$_{30}$ ggc ggt gtg ccg ggc gca ggt ggt ccg ggt ggc ggg gtg ccg ggc)$_{30}$

E4 and E2* genes for PRe-RDL cloning were previously synthesized in the Chilkoti lab in a variety of lengths. For the creation of new ELP genes (primarily the synthesis of (VPGSG)$_{80}$ discussed in Section 5.2.6) oligomers encoding five pentapeptide repeats of an ELP were concatemerized in a modified pET-24a(+) vector (Figure 3). ELP oligomers were designed with sticky ends compatible with the restriction site created by BseRI digestion. Sense and anti-sense single stranded oligomers were annealed by mixing, heating to 95 °C for 1 minute on a heat block, and cooling slowly to room temperature over several hours. The pET-24a(+) vector was digested with BseRI and dephosphorylated by incubation with CIP. The vector and an excess of annealed ELP

oligomers were ligated and transformed into competent EB5α *E. coli*. Colonies were screened for variable insertion of the oligomers by colony PCR, in which the inserted genes were amplified using T7 promoter and T7 terminator primers. PCR products were observed by DNA electrophoresis, which directed the selection of colonies to be grown, sequenced, and saved for further cloning. This concatemerization procedure typically produced 1-4 oligomer insertions, corresponding to 5-20 pentapeptide repeats.

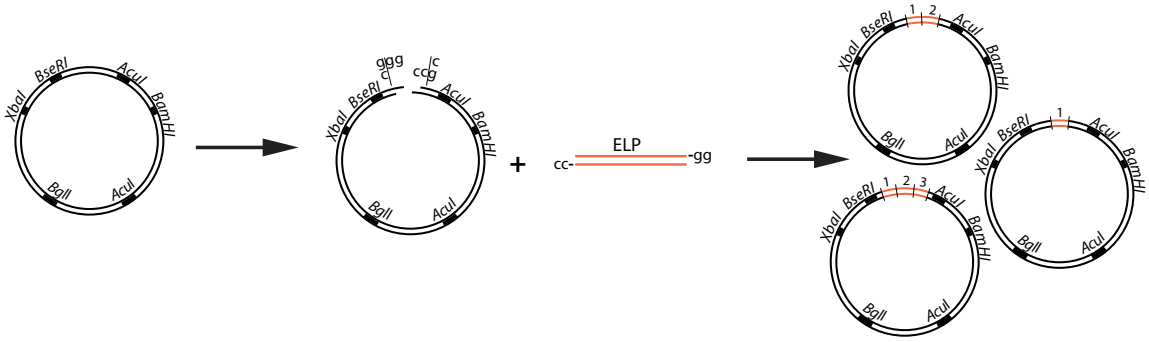

Figure 3: Preliminary synthesis of ELP genes was performed by concatemerization. Modified pET-24a(+) vector was digested with BseRI and ligated with an excess of ELP oligomers designed with sticky ends complimentary to the BseRI cut site. A library of vectors was created in which the ELP gene length varied from 1-4 oligonucleotide inserts, equivalent to 5-20 pentapeptide repeats. Adapted from [139].

The PRe-RDL cloning procedure was used to build an ELP of precisely increasing length or combine two ELP sequences to create an ELP_{BC} (Figure 4). The ELP sequence intended for the N-terminus of the combined construct was used to create an "A cut" by digestion with AcuI and BglI restriction enzymes. The ELP sequence intended for the C-terminus of the combined construct was used to create a "B cut" by

digestion with BseRI and BglI restriction enzymes. The reaction mixtures of the "A cut" and "B cut" were then separated by gel electrophoresis. The "A cut" produced DNA fragments with lengths, in base pairs, of 1586, 1821, and 1891 + the length of the ELP insert. The "B cut" produced DNA fragments with lengths, in base pairs, of 1891 and 3407 + the length of the ELP insert. In each case, the largest band was excised from the gel and the fragments were purified prior to their ligation and transformation into competent EB5α *E. coli*. Colonies were screened by diagnostic digestion with XbaI and BamHI restriction enzymes. Successful oligomerization or ELP_{BC} synthesis was confirmed with plasmid DNA sequencing using T7 promoter and T7 terminator primers.

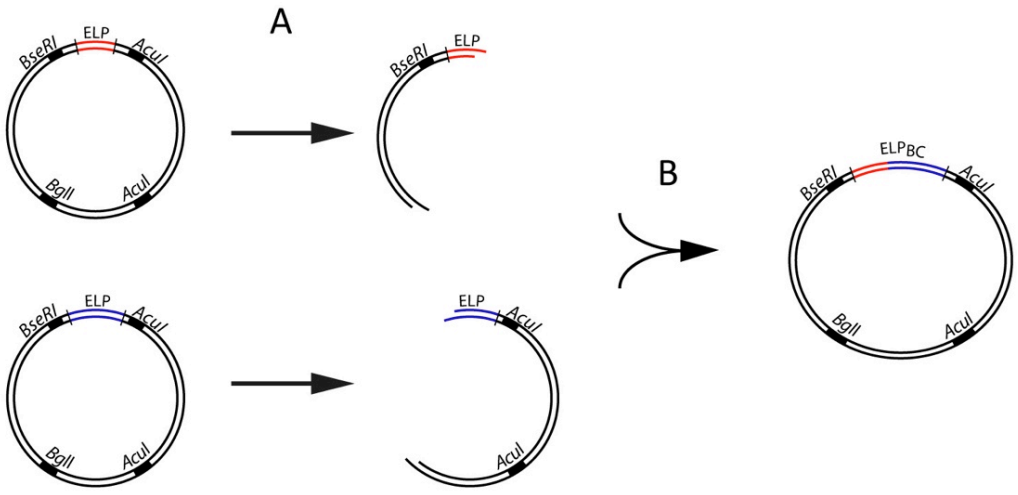

Figure 4: ELP_{BC} genes were synthesized by PRe-RDL cloning. Vectors containing the hydrophobic ELP domain (red) and hydrophilic ELP domain (blue) were combined to form the desired ELP_{BC}. The vector containing the hydrophobic domain was digested

with AcuI and BglI to form an "A cut", while the vector containing the hydrophilic domain was digested with BseRI and BglI to form a "B cut" (A). The desired restriction products were separated by gel electrophoresis and purified prior to ligation to combine the ELP domains and form the ELP$_{BC}$ (B). Adapted from [139].

2.2.2.3 N- and C-terminal functionalization of ELP$_{BC}$ genes with PRe-RDL cloning

The leader sequence applied to all ELP$_{BC}$s for thermal characterization and evaluation of controlled cellular uptake was MGCGWPG, where methionine initiated polypeptide expression, cysteine provided a reactive amino acid for the conjugation of a fluorophore label, and tryptophan provided an optically active amino acid for peptide quantification by absorbance at 280 nm. The oligonucleotide and peptide sequence of the leader used for ELP$_{BC}$s created with PRe-RDL cloning is listed in Table 4, where pertinent residues of the leader are noted, functionalizing the N-terminus of the ELP.

Table 4: Genetic design of the leader sequence for PRe-RDL cloning.

N-	Peptide and oligonucleotide sequence
Cys, Trp	(M) G C G W P t atg ggc tgc ggg tgg ccg gg ac ccg acg ccc acc ggc

The oligonucleotides encoding the leader sequence were designed with sticky ends compatible to those created from vector digestion with BseRI and NdeI and annealed as described previously. The pET-24a(+) vector was digested first with BseRI alone, and then NdeI was added to the reaction mixture. This sequential digestion was necessary to create the desired overhangs in the digested vector, since the NdeI cut site lies between the BseRI recognition site and the BseRI cut site. The plasmid fragments

were dephosphorylated with the addition of CIP and the vector fragment was purified by PCR purification kit. The annealed oligonucleotides and restricted vector were ligated and transformed into competent EB5α *E. coli.* Successful insertion of the oligonucleotides was screened with colony PCR or diagnostic digest using XbaI and BamHI enzymes. The creation of leader-encoding vectors was confirmed with plasmid DNA sequencing using T7 promoter primer.

All trailer sequences encoded a brief flexible spacer of PGGS followed by a CPP sequence and stop codons to terminate peptide synthesis. The oligonucleotide and peptide sequences of the trailers used for ELP_{BCS} created with PRe-RDL cloning are listed in Table 5, where pertinent residues of the trailer are noted, functionalizing the C-terminus of the ELP.

Table 5: Genetic design of trailer sequences for PRe-RDL cloning.

C-	**Peptide and oligonucleotide sequence**
-	P G G S . . g ccg ggc ggt agc tga taa gg ccc ggc ccg cca tcg act att
Arg_5	P G G S R R R R R . . g ccg ggc ggt agc cgc cgt cgc cgt cgc tga taa gg ccc ggc ccg cca tcg gcg gca gcg gca gcg act att
Arg_8	P G G S R R R R R R R R . . g ccg ggc ggt agc cgc cgt cgt cgc cgc cgt cgc cgt tga taa gg ccc ggc ccg cca tcg gcg gca gca gcg gcg gca gcg gca act att
TAT_{47-57}	P G G S Y G R K K R R Q R R R . . g ccg ggc ggt agc tat ggc cgt aaa aaa cgt cgt cag cgt cgc cgt tga taa gg ccc ggc ccg cca tcg ata ccg gca ttt ttt gca gca gtc gca gcg gca act att

$RTAT_{47\text{-}57}$	P G G S Y G R G G R R G R R R . . g ccg ggc ggt agc tat ggc cgt ggc ggt cgt cgt ggc cgt cgc cgt tga taa gg ccc ggc ccg cca tcg ata ccg gca ccg cca gca gca ccg gca gcg gca act att

Oligonucleotides encoding the trailer sequences were designed with sticky ends compatible to those created from vector digestion with BseRI alone. The pET-24a(+) vector was digested with BseRI, dephosphorylated with the addition of CIP, and purified by PCR purification kit prior to ligation with the annealed oligonucleotides encoding the trailer sequences and transformation into competent EB5α *E. coli.* Successful insertion of the oligonucleotides was screened with colony PCR or diagnostic digest using XbaI and BamHI enzymes. The creation of trailer-encoding vectors was confirmed with plasmid DNA sequencing using T7 promoter primer.

PRe-RDL was again performed to functionalize the N- or C-terminus of the ELP_{BC} gene. For functionalization of the N-terminus, a vector encoding the desired leader sequence would be digested to create an "A cut", while the vector encoding the ELP_{BC} would be digested to create a "B cut" (Figure 5A). The desired restriction fragments were separated by gel electrophoresis, purified, and ligated to create a leader-ELP_{BC} gene (Figure 5B). For functionalization of the C-terminus, the vector encoding the leader-ELP_{BC} would be digested to create an "A cut" and the vector encoding the desired trailer sequence would be digested to create a "B cut" (Figure 5C). The desired restriction fragments were separated by gel electrophoresis, purified, and ligated to

create the fully functionalized ELP$_{BC}$ (Figure 5D). The final gene was confirmed by plasmid DNA sequencing using T7 promoter and terminator primers and transformed into competent BL21 *E. coli*, appropriate for overexpression of the ELP product.

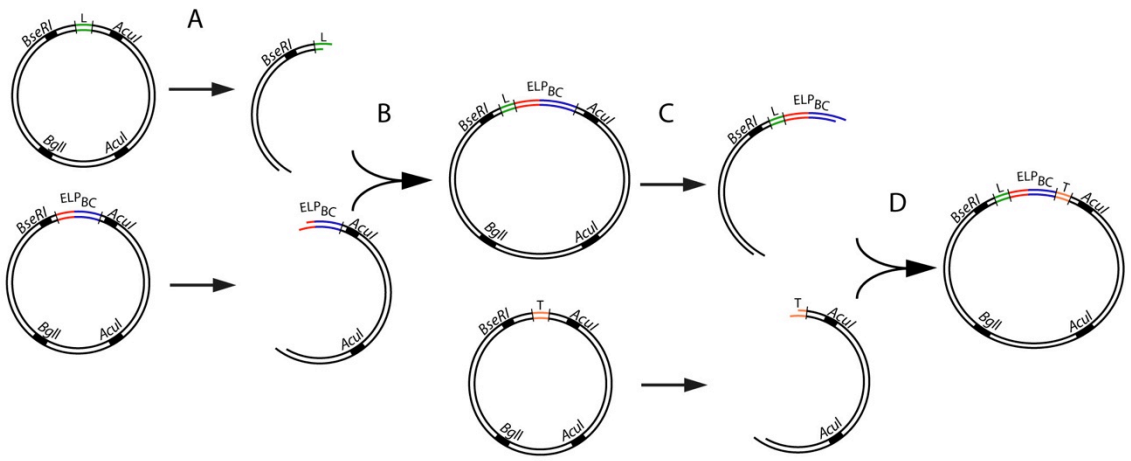

Figure 5: N- and C-terminal functionalization of ELP$_{BC}$s was achieved with PRe-RDL cloning. The vector encoding the leader (L) was digested to create an "A cut" while the vector encoding the ELP$_{BC}$ was digested to create a "B cut" (A). Ligation of desired restriction fragments resulted in the leader-ELP$_{BC}$ gene (B). The vector encoding the leader-ELP$_{BC}$ gene was digested to create an "A cut" while the vector encoding the trailer (T) was digested to create a "B cut" (C). Ligation of the desired restriction fragments created the fully functionalized ELP$_{BC}$ gene (D). Adapted from [139].

2.2.3 Recombinant expression of CPP-ELP$_{BC}$s in *E. coli*

E. coli cells suitable for expression (BLR or BL21) were transformed with the complete plasmid encoding the desired ELP functionalized with a leader and trailer sequence, under control of the T7-*lac* promoter. These cells were grown in 50 mL Terrific Broth (TB) media with appropriate antibiotic overnight at 37 °C while shaking at 200 RPM. *E. coli* cells were collected by centrifugation at 2,000 x *g* for 10 minutes, the

supernatant waste was discarded, cells were resuspended in PBS, and used to inoculate 1 L of TB media with appropriate antibiotic. Cultures were grown for 24 hours at 37 °C while shaking at 200 RPM.

The T7-*lac* system exhibits leaky background expression that results from growth at 37 °C over the course of 24 hours. This background expression level was sufficient for the synthesis of most ELPs discussed in this dissertation, particularly of those ELP_{BC}s in which a more hydrophobic sequence (ex. $(VPGVG)_n$) was expressed proximal to the N-terminus. However, when background expression was not sufficient, overexpression was induced with the addition of 0.2 mM isopropyl-beta-D-thiogalactoside (IPTG) at approximately 10 hours after initiating the culture growth.

2.2.4 Purification of CPP-ELP_{BC}s from *E. coli* lysate

E. coli cells were collected by centrifuging the culture in a 1 L bottle at 2,000 x *g* for 10 minutes at 4 °C. The supernatant was discarded and the cell pellet was resuspended with 20 mL phosphate buffered saline (PBS). Cells were lysed by sonication in 9 minute cycles of 10 seconds "on" and 20 seconds "off" at an output power of 85 W. To condense genomic contaminants, 2 mL of 10% (w/v) polyethylenimine (PEI) was added to the lysate. Insoluble contaminants were collected by centrifugation at 16,000 x *g* for 15 minutes at 4 °C. The supernatant was transferred to a clean tube and ELP purification proceeded by inverse transition cycling (ITC) [96], in which the sample was

centrifuged above and below the ELP T_t to remove soluble and insoluble contaminants, respectively (Figure 6).

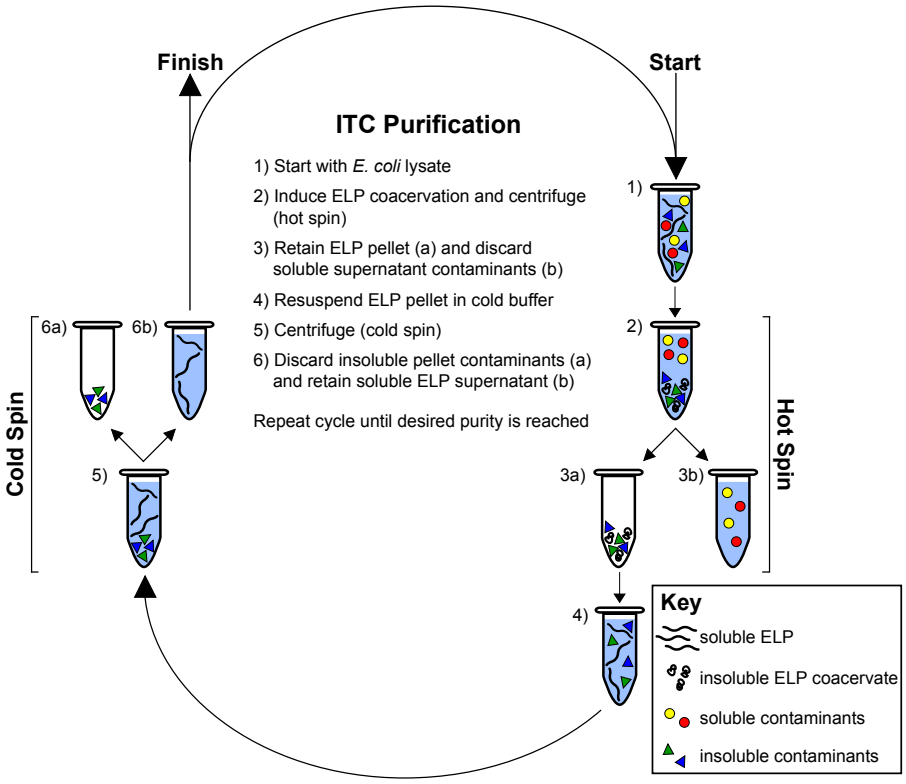

Figure 6: CPP-ELP$_{BCS}$ were purified from *E. coli* lysate by ITC. Repeated centrifugation above and below the ELP T_t removed soluble and insoluble contaminants, respectively. Reproduced from [140].

The ELP transition was induced with the addition of heat (a water bath was used at 37 °C) and/or salt (crystalline NaCl was used at less than 3 M). The ELP coacervate was collected by centrifugation at 16,000 x *g* for 10 minutes at room temperature—this step is termed a "hot spin". Soluble contaminants were discarded and the ELP pellet was resuspended in cold PBS. The solubilized ELP sample was then centrifuged at

16,000 x *g* for 10 minutes at 4 °C—this step is termed a "cold spin". The ELP solution was then transferred to a clean tube, and the insoluble contaminant pellet was discarded. Four rounds of ITC with alternating "hot" and "cold" spins generally produced ELPs of sufficient purity, as determined by SDS-PAGE. Purified ELPs were separated on 4-20% Tris-HCL polyacrylamide gels run at 180 V for approximately 45 minutes. ELPs were visualized by negative staining of the gel using 0.5 M $CuCl_2$. As typical for ELPs, some CPP-ELP_{BC}s ran at an apparent molecular weight (MW) up to 20% higher than the theoretical MW dictated by their genetic design [97].

2.2.5 Thermal characterization of CPP-ELP_{BC}s

2.2.5.1 Temperature-regulated turbidimetry

The thermal behavior of ELPs can be quickly evaluated over a wide range of temperatures using temperature-regulated turbidimetry. A Cary 300 Bio UV-Visible spectrophotometer was used to measure the optical density (OD) at 350 nm of ELP solutions at 5-100 μM over a range of temperatures (ex. 20-90 °C). OD measurements were recorded at every 0.33 °C as the solution temperature was heated at 1 °C/minute. Reversibility of the ELP transition was confirmed by the return of OD to baseline as the solution was cooled at 1 °C/min. Typically, as the solution temperature is raised, a drastic increase in OD (> 2.0 OD units) is indicative of the ELP transition from unimer to micron-scale aggregate (Figure 7A-B). The ELP T_t can be defined as the temperature at which the maximum of the first derivative of OD, with respect to temperature, occurs.

For ELP$_{BC}$s that exhibit temperature-triggered self-assembly a subtle increase in OD (~0.1-0.5 OD units) as the solution temperature is raised is typically indicative of the transition of ELP unimer to ELP nanoparticle (Figure 7C). Further increasing the solution temperature will lead to a drastic increase in OD (> 2.0 OD units) that signifies the complete aggregation of ELP nanoparticles into micron-scale aggregates.

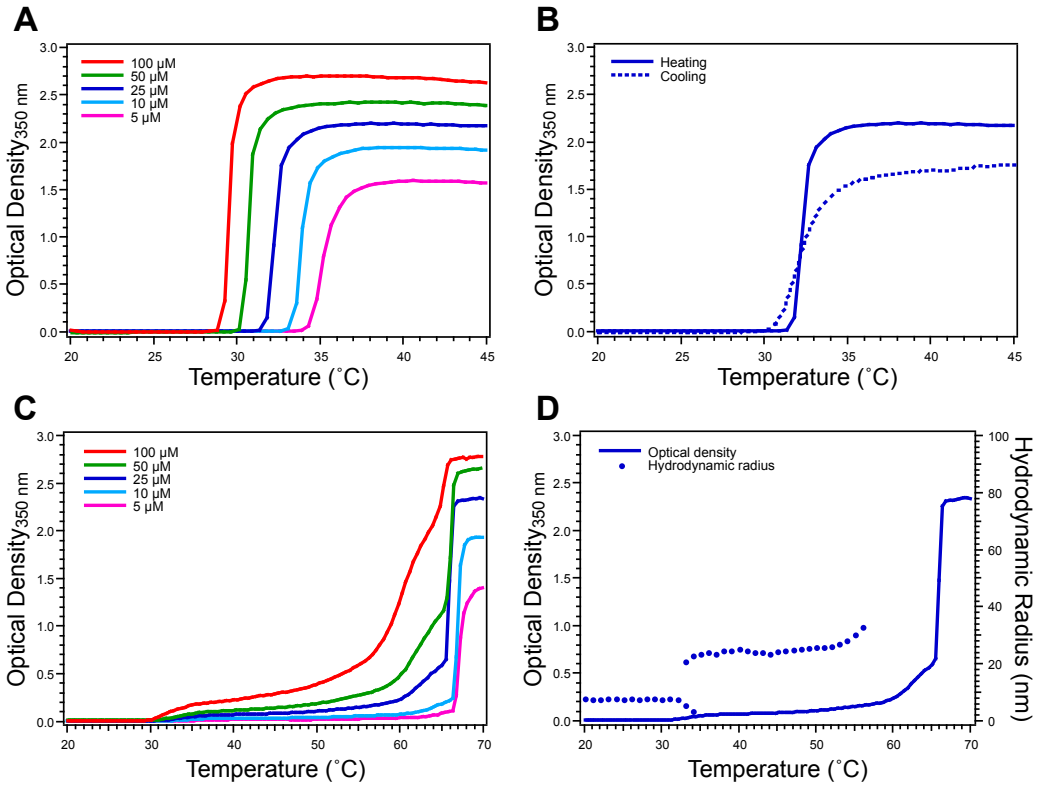

Figure 7: Temperature-regulated turbidimetry and dynamic light scattering demonstrate representative thermal behavior of ELP homopolymers and ELP$_{BC}$s. Rapid increase in OD is indicative of ELP unimer-to-aggregate transition (A), which is typically reversible (B). Representative ELP homopolymer: SKGPG-(VGVPG)$_{80}$-Y (A-B). Subtle increase in OD is indicative of nano-scale ELP$_{BC}$ assembly prior to complete aggregation (C), which can be confirmed by DLS measurements (D). Representative ELP$_{BC}$: GCGWPG-(VGVPG)$_{60}$-(AGVPGGGVPG)$_{30}$-PGGS (C-D). Adapted from [140].

2.2.5.2 Dynamic light scattering

Dynamic light scattering (DLS) was used to corroborate the results from turbidimetry measurements and to determine the size of self-assembled ELP nanoparticles. Samples were filtered prior to analysis by DLS using filters with pore sizes of 20, 100, or 200 nm, depending on the ELP sample. The hydrodynamic radius (R_h) was measured on a Wyatt Technology DynaPro temperature controlled microsampler or Wyatt DynaPro plate reader over a temperature range of interest, as directed by turbidimetry results. ELP unimers typically exhibit an $R_h \leq 10$ nm, ELP nanoparticle assemblies typically exhibit an $R_h \sim 20\text{-}40$ nm, and ELP aggregates typically exhibit an $R_h > 500$ nm (Figure 7D). To confirm R_h measurements at specific thermal conditions, for instance 37 °C and 42 °C, 3 samples were evaluated by DLS and an average $R_h \pm$ standard deviation (SD) or standard error of the mean (SEM) was reported.

2.2.5.3 Zeta potential

The surface charge of self-assembled CPP-ELP_{BC} micelles was investigated by zeta potential measurements. Due to the need to eliminate buffer salts for zeta potential measurements, the thermal behavior of ELP_{BC}s was re-evaluated in H_2O, due to the dependence of ELP T_t on the presence of salts. This characterization defined the increased concentration and temperature at which the measurements must be taken to ensure the self-assembly of ELP_{BC}s in water. Solution temperature was allowed to equilibrate for 10 minutes prior to obtaining zeta potential measurements on a Malvern

Zetasizer Nano ZS90 for CPP-ELP$_{BC}$ or a non-functionalized ELP$_{BC}$ control. Zeta potential measurements were repeated with 3 samples and an average zeta potential, in mV, was reported ± SD.

2.3 Results and discussion

2.3.1 CPP-ELP$_{BC}$ design

Toward the goal of achieving controlled cellular uptake with modulation of CPP density on self-assembled ELP$_{BC}$s, an initial CPP-ELP$_{BC}$ design was proposed to meet the needs of minimizing uptake in the soluble "off" state and maximizing uptake in the self-assembled "on" state. Selection of the first CPP to investigate with this ELP$_{BC}$ system was based on two existing factors in the CPP literature: 1) the threshold of CPP function of arginine oligomer CPPs, dependent on the number of arginine residues, and 2) the charge density typical of existing CPP-functionalized drug carrier nanoparticles.

Due to the high arginine content in many cationic CPPs, and the important role of arginines in CPP function, biologically inspired arginine oligomers have been studied as a model CPP system capable of receptor-independent internalization. The cellular uptake of arginine oligomers demonstrates a functional threshold dependent on the arginine number, where less than 6 consecutive arginine residues are insufficient to achieve uptake, while greater than 6 consecutive arginine residues are sufficient to achieve internalization [55, 65]. Although arginine oligomers are often employed due to their simplicity, it has been shown that arginine residues do not have to be arranged

sequentially to achieve efficient cellular uptake; arginine residues can be spaced to some extent along a peptide backbone without compromising internalization [66]. These characteristics of arginine oligomer CPPs present two distinct advantages for the proposed CPP-ELP$_{BC}$ platform. First, the arginine oligomer length appended to each ELP$_{BC}$ can be selected below the functional threshold to minimize uptake in the "off" state. Second, the resulting presentation of high arginine density on the corona of self-assembled CPP-ELP$_{BC}$ micelles is likely to provide CPP-mediated cell uptake, since arginine proximity on the peptide chain is not a direct requirement for arginine oligomer CPP function.

To further direct the choice of arginine oligomer length for ELP$_{BC}$ functionalization in preliminary experiments, while remaining below the functional threshold of 6 arginine residues, we looked at the standards in the literature of CPP-functionalized nanoparticle drug carriers that successfully deliver drug cargo to intracellular targets. TAT-decorated liposomes, extensively utilized in the laboratory of Vladimir Torchilin at Northeastern University, are one such example of a standard in the field. These TAT-functionalized liposomes, approximately 100 nm in radius, were decorated with the YGRKKRRQRRR peptide with an efficiency of approximately 500 TAT peptides per liposome [141]. Comparing the charge density on this liposomal platform to that of an ELP micelle, approximated to have a radius of 30 nm and coordination number of 100 ELP$_{BC}$ unimers per micelle, gives us the charge balance:

$$\frac{(8)(500)}{4\pi(100)^2} = \frac{(X)(100)}{4\pi(30)^2}$$

where X is 3.6 net positive charge per ELP_{BC} to create a nanoparticle with equivalent surface charge density to that of the TAT-functionalized liposome. This approximation directed the choice to first explore this system with an ELP_{BC} carrying 3 arginines per unimer, in hopes that rounding down to 3 positive charges per unimer would minimize uptake in the unimer "off" state, while still achieving enhanced uptake at the micelle "on" state.

2.3.2 CPP-ELP_{BC} syntax

The first generation ELP_{BC}s synthesized by Dreher *et al.* [126] were designed such that, from N-to-C terminus, the hydrophilic block was expressed first, followed by the hydrophobic block. This ELP_{BC} syntax thus required that any functionalization of the hydrophilic block, which would decorate a micelle corona upon self-assembly, must be expressed at the N-terminus of the ELP_{BC} gene. N-terminal functionalization had previously been successful for genetically appending ELP_{BC}s with both peptides [126] and proteins [130]. This ELP_{BC} syntax was therefore also explored for CPP functionalization. Unfortunately, with the addition of three arginines at the N-terminus of the ELP_{BC}, no recombinant product could be purified from the *E. coli* lysate. SDS-PAGE analysis of the cell lysate confirmed that the Arg_3-ELP_{BC} was not overexpressed, as compared to bacterial proteins.

In retrospect, it was not surprising that this diblock syntax was inappropriate when it required the N-terminal expression of arginine oligomers. Arginines are known to have a destabilizing effect when present at the N-terminus of proteins expressed in *E. coli*, leading to a short half-life in the bacteria as they are quickly degraded [142]. Therefore to successfully functionalize the hydrophilic domain of ELP_{BC}s with arginine oligomers, the syntax of the ELP_{BC} had to be reversed, such that the hydrophobic block was expressed first, followed by the hydrophilic block and finally the C-terminal expression of arginine-rich CPPs.

Prior to the creation of CPP-ELP_{BC}s in this alternative syntax, a non-functionalized ELP_{BC} was designed and synthesized with both possible syntax to determine the effect, if any, that ELP_{BC} expression order had on temperature-triggered self-assembly. Surprisingly, the thermal behavior of the ELP_{BC} changed significantly depending on its syntax, such that the ELP_{BC} with hydrophobic-to-hydrophilic syntax, necessary for CPP-functionalization, had a decreased CMT and increased micelle-to-aggregate T_t, as compared to the ELP_{BC} with hydrophilic-to-hydrophobic syntax (Figure 8).

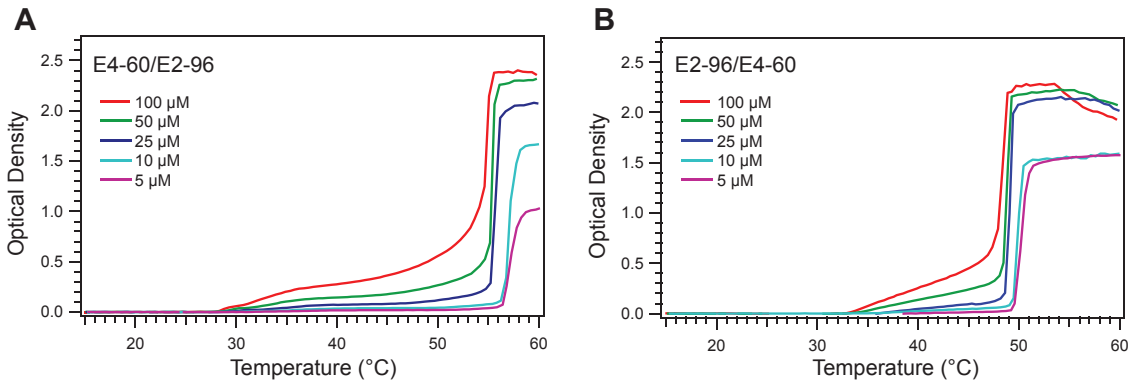

Figure 8: Syntax influences thermal properties of ELP$_{BC}$s as measured by temperature-regulated turbidimetry. Both the CMT and micelle-to-aggregate T_t are affected by the expression order of the ELP$_{BC}$ as evident in comparing an ELP$_{BC}$ with hydrophobic-to-hydrophilic expression order (A: MGCGWPG-E4-60/E2-96-PGGSK) to an ELP$_{BC}$ with hydrophilic-to-hydrophobic expression order (B: MSKGPG-E2-96/E4-60-WPC). Temperature-regulated turbidimetry measurements were taken in PBS at 5-100 µM.

Arg$_3$-functionalized ELP$_{BC}$s were then synthesized in the hydrophobic-to-hydrophilic syntax, where the Arg$_3$ was appended to the C-terminus, and were successfully overexpressed in *E. coli*. Reversing the ELP$_{BC}$ syntax therefore provided efficient expression for constructs genetically appended to an arginine-rich CPP at the terminus of the hydrophilic domain. Arg$_3$-ELP$_{BC}$s, despite their additional charge, were sufficiently purified by means of the ELP LCST behavior, without any modification to the standard ITC protocol. This ease of purification held true for all variations of CPP-ELP$_{BC}$ functionalization, as demonstrated by SDS-PAGE analysis of CPP-ELP$_{BC}$s that exhibited good agreement of recombinant product MW with theoretical MW and good purity by lack of contaminating bands (Figure 9).

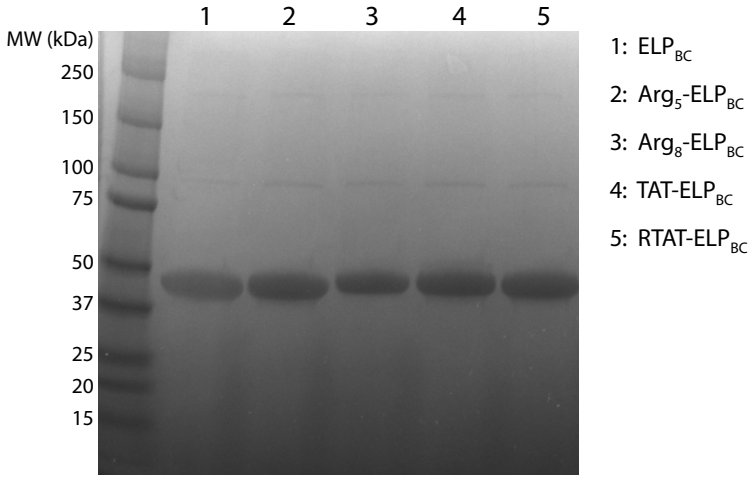

Figure 9: ELP$_{BC}$s with various CPP-functionalization were overexpressed and sufficiently purified from *E. coli* lysate when designed in a hydrophobic-to-hydrophilic ELP$_{BC}$ syntax. SDS-PAGE and $CuCl_2$ staining of CPP-ELP$_{BC}$ products demonstrated agreement of measured and theoretical MW, where the expected MWs varied slightly due to CPP functionalization and were, by lane: 1) 39.72 kDa, 2) 40.05 kDa, 3) 40.97 kDa, 4) 41.26 kDa, and 5) 41.05 kDa.

2.3.3 Characterization of first generation CPP-ELP$_{BC}$s

Three ELP$_{BC}$s were synthesized with a hydrophobic-to-hydrophilic syntax and functionalized with Arg_3 at the hydrophilic terminus. These diblock copolymers had a hydrophobic/hydrophilic block size ratio of E4-90/E2-64, E4-60/E2-96, or E4-60/E2-64, which in their opposite syntax had been designed previously by Dreher *et al.* [126]. The addition of Arg_3 to any of these diblock configurations did not perturb the temperature-triggered micelle assembly (Figure 10). However, the reversed syntax of these diblocks caused a drop in CMT below 37 °C, such that these materials would not be suitable for hyperthermia-targeted self-assembly between normal body temperature and conditions of mild hyperthermia. Although not ideal in achieving our ultimate goal of utilizing a

clinically relevant extrinsic thermal stimulus to trigger micelle assembly, these first generation materials would still permit us to investigate the proof-of-concept of controlled cell uptake with CPP density modulation on self-assembled nanoparticles using thermal conditions of 25 °C and 37 °C as the "off" and "on" conditions, respectively. Indeed, these conditions may inadvertently provide an advantage of evaluating our hypothesis in the absence of the hyperthermia parameter, which could have its own confounding effects on cellular uptake of drug carriers.

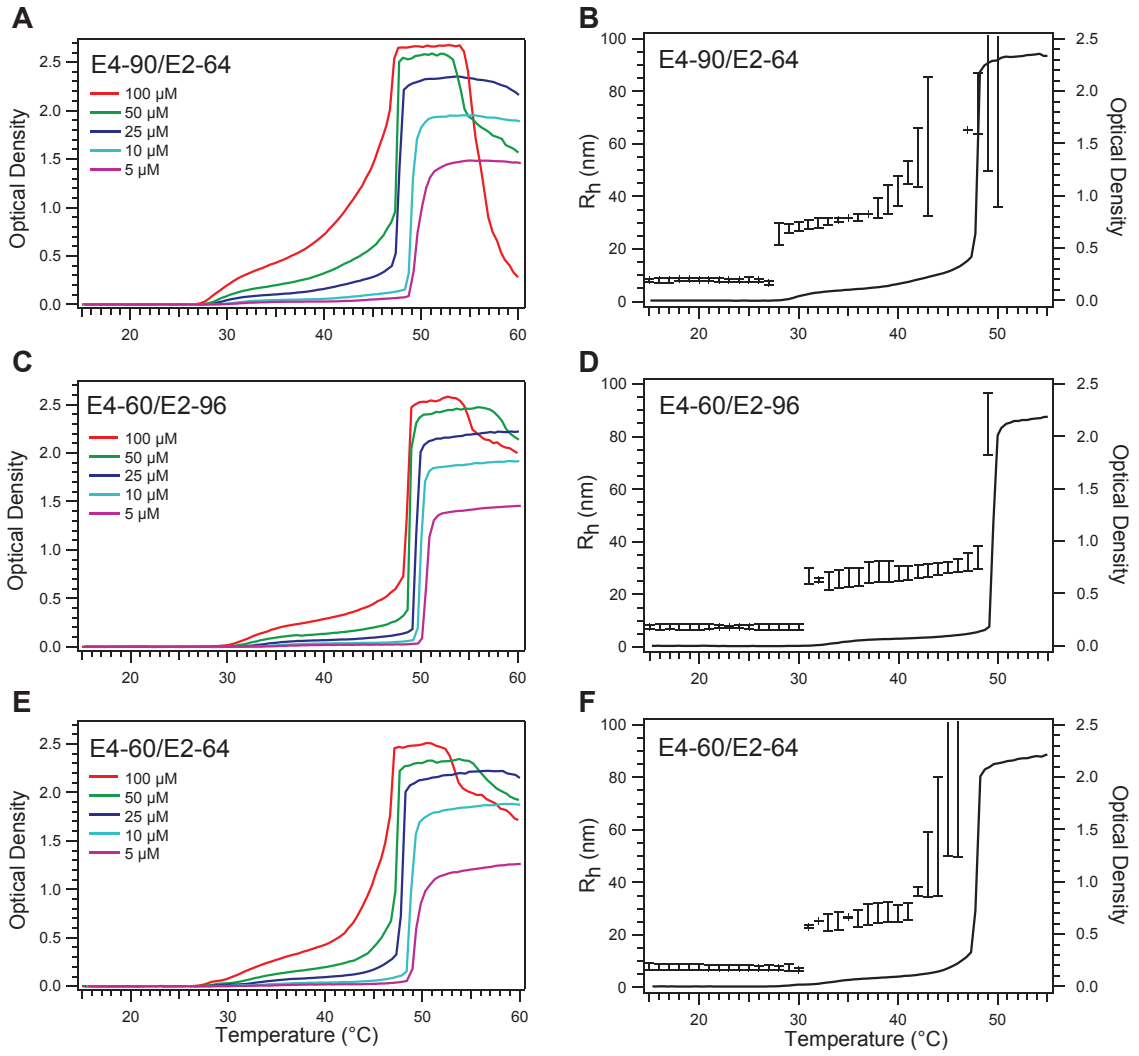

Figure 10: Functionalization of the hydrophilic terminus with Arg_3 CPP did not perturb temperature-triggered self-assembly of ELP_{BC}s E4-90/E2-64 (A-B), E4-60/E2-96 (C-D), or E4-60/E2-64 (E-F), as determined by temperature-regulated turbidimetry (A, C, and E) and DLS (B, D, and F). However, changes in behavior due to ELP_{BC} syntax precluded the use of these materials for triggered self-assembly between body temperature and conditions of mild clinical hyperthermia. Temperature-regulated turbidimetry measurements were taken in PBS at 5-100 μM. DLS data represent mean of three measurements taken in PBS at 25 μM ± SD.

Successful self-assembly was also evident by the change in surface charge, measured by zeta potential, with respect to temperature-triggered micelle formation. As

a CPP-ELP$_{BC}$ solution is heated, an increase in zeta potential is expected when the unimer self-assembles into micelles, transitioning from a low density of cationic CPP on the unimer to high density cationic CPP on the micelle surface. Indeed this was true for Arg$_3$-functionalized E4-60/E2-96 whose zeta potential increased as the solution temperature was raised from 25 °C, to 37 °C, to 42 °C (Figure 11). The change in zeta potential with micelle assembly and the magnitude of the zeta potential in the micelle state is reasonable when compared to other CPP-functionalized carriers. For example, an increase in zeta potential from 0 to 6 mV has been reported for the deshielding of activatable TAT-functionalized micelles [143]. Thus the change in zeta potential from 2 to 6 mV with self-assembly of Arg$_3$-ELP$_{BC}$s is feasible since these materials have some inherent charge in their unassembled state, in contrast to shielded TAT-functionalized micelles, and will likely display less charge on the nanoparticle corona as Arg$_3$ CPP has less net charge than TAT. Interestingly, non-functionalized ELP$_{BC}$ showed the opposite trend, whereby its zeta potential became increasingly more negative as temperature was increased. This is logical, however, in that this construct has a negatively charged carboxyl group on the C-terminus that will decorate the micelle surface upon self-assembly.

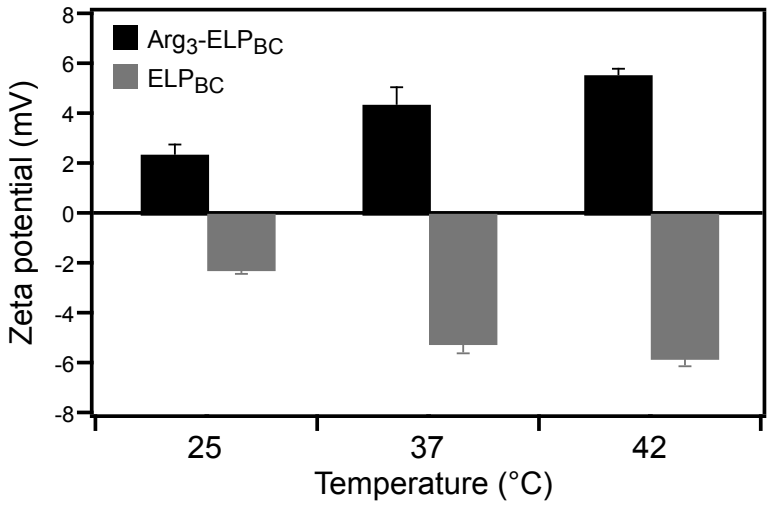

Figure 11: Change in zeta potential is indicative of temperature-triggered micelle assembly of E4-60/E2-96 diblocks. Increasingly positive zeta potential was measured for Arg_3-ELP_{BC} as it was heated from below its CMT at 25 °C to above its CMT at 37 °C and 42 °C. Non-functionalized ELP_{BC} exhibited an increasingly negative zeta potential with micelle assembly, likely due to the negatively charged carboxyl terminus decorating the surface of this control micelle. Data represents mean of 3 measurements taken in low ionic strength buffer at 50 μM ± SD.

Of the three block copolymers investigated, E4-60/E2-96 was chosen for further study, as it achieved stable micelle assembly over the largest temperature range and its CMT was well positioned to be centrally located between the "off" and "on" conditions, 25 °C and 37 °C respectively, to investigate the effects of self-assembly of this non-optimized CPP-ELP_{BC} family. Functionalization of this block copolymer with arginine oligomers of 1, 3, or 5 arginine residues demonstrated that the micelle-to-aggregate T_t was affected by changes in functionalization, but the CMT remained relatively unperturbed such that "off" and "on" conditions of 25 °C and 37 °C could be used consistently for all E4-60/E2-96 diblocks, regardless of CPP-functionalization (Figure 12).

Interestingly, as the functionalization was increased from 1, to 3, to 5 arginines, the micelle-to-aggregate T_t decreased. This is somewhat surprising given the charge of the arginine residues, which one would assume would impart an enhanced hydrophilicity to the ELP_{BC} that would increase the micelle-to-aggregate T_t. However, this effect likely stems from the relative hydrophobicity of the arginine residue, despite its cationic character, due to the delocalized charge of its guanidinium headgroup [144-146].

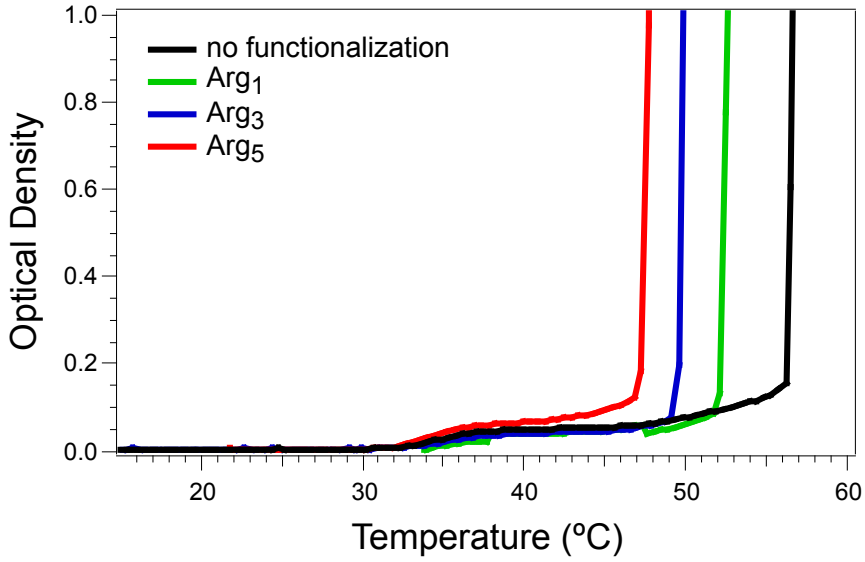

Figure 12: CPP-functionalization affects the micelle-to-aggregate T_t, without perturbing the CMT of ELP_{BC}s, as demonstrated by temperature-regulated turbidimetry. E4-60/E2-96 was functionalized with Arg_1, Arg_3, and Arg_5 CPPs and demonstrated a decreasing micelle-to-aggregate transition as more arginine residues were added to the hydrophilic terminus. The CMT, however, did not change significantly based on CPP functionalization, allowing all constructs to be examined in "off" and "on" states of 25 °C and 37 °C, respectively. Temperature-regulated turbidimetry measurements were taken in PBS at 25 μM.

2.3.4 Characterization of second generation CPP-ELP$_{BC}$s

To achieve materials with the desired response to mild clinical hyperthermia, the block copolymer design was manipulated with the goal of a CMT between 37 °C and 42 °C. Although the rules for predictable ELP$_{BC}$ design are growing [127], there remains a need to intrinsically verify the thermal behavior of ELP$_{BC}$s whose design is guided by educated hypotheses, based largely on the knowledge gleaned from the behavior of the homopolymer ELPs from which the ELP$_{BC}$ is composed. Therefore, knowledge of the ELP T_t's dependence on intrinsic parameters of sequence (ex. guest residue) and length directed the manipulation of the existing CPP-ELP$_{BC}$ design to raise the CMT. Manipulation of these design parameters—sequence and length—among other changes, may be made to the ELP$_{BC}$ to achieve a desirable thermal behavior, as outlined in the flow chart of Figure 13.

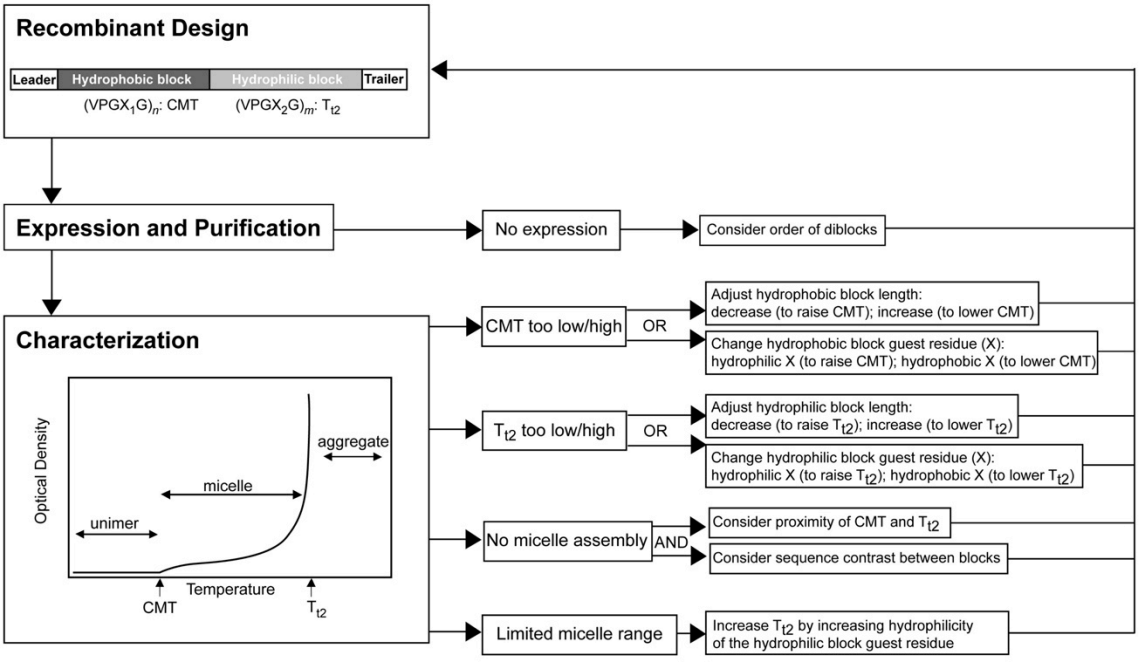

Figure 13: An iterative design process was used to optimize the ELP$_{BC}$ thermal behavior, as measured by the CMT and micelle-to-aggregate T_t. Manipulation of the ELP$_{BC}$ design was performed to achieve temperature-triggered self-assembly in response to conditions of mild clinical hyperthermia.

The CMT is largely dependent on the hydrophobic block whose transition initiates self-assembly and forms the micelle core. To increase the T_t of the hydrophobic block the length of this segment was decreased, while the ELP sequence was kept constant. This new hydrophobic block was E4-30. The shorter hydrophilic block, E2-64, was utilized as it should have a higher T_t than the larger E2-96 block used previously. Combination of these new hydrophobic and hydrophilic blocks yielded an ELP$_{BC}$ of E4-30/E2-64 that achieved the target CMT between 37 °C and 42 °C, as confirmed by temperature-regulated turbidimetry and DLS (Figure 14). Manipulation of the

hydrophobic block also slightly increased the micelle-to-aggregate T_t, as compared to the behavior of first generation E4-60/E2-64 diblock with the same hydrophilic domain.

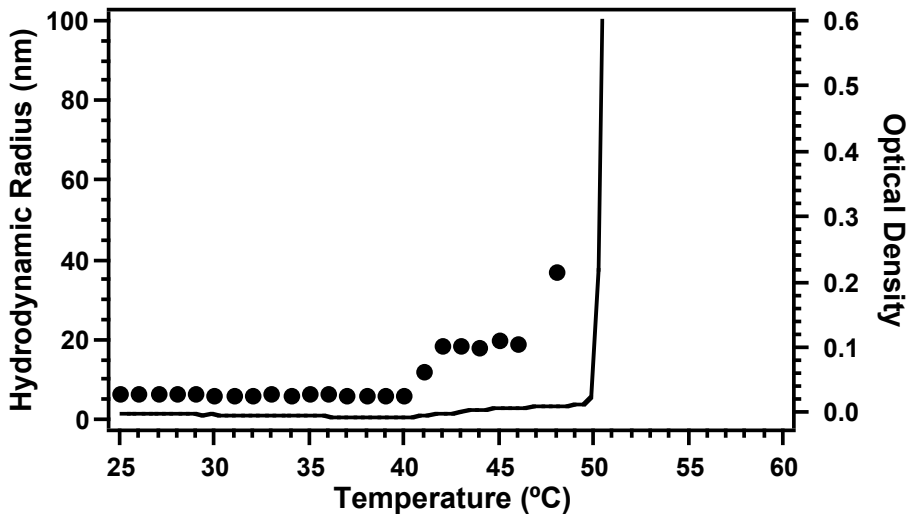

Figure 14: Second generation Arg$_5$-ELP$_{BC}$ achieved self-assembly in response to mild hyperthermia. Decreasing the size of the hydrophobic block achieved a CMT between 37 °C and 42 °C for E4-30/E2-64 as determined by temperature-regulated turbidimetry (line) and DLS (dots). This ELP$_{BC}$, however, exhibited a limited self-assembly range (<10 °C), which would ultimately prevent it from being a broadly applicable construct for the purpose of targeted uptake and drug delivery. Temperature-regulated turbidimetry and DLS measurements were acquired in PBS at 25 μM.

The increase in CMT in combination with the less significant change in the micelle-to-aggregate T_t of the optimized E4-30/E2-64 diblock effectively decreased the range of temperatures over which stable micelle assembly was attained (this range is defined as that between the CMT and micelle-to-aggregate T_t) (Figure 15). Although a minimum micelle assembly range, and thus an implied minimum micelle-to-aggregate T_t, was not an initial requirement of ELP$_{BC}$ optimization, it would become an important

design parameter when the ELP$_{BC}$ was further modified in ways that affected its thermal behavior, such as the attachment of fluorescent labels. For this reason the E4-30/E2-64 diblock would not be the optimal construct for application as a drug delivery vehicle, but it did provide the properties that allowed the initial evaluation of controlled cellular uptake in response to a clinically relevant thermal trigger.

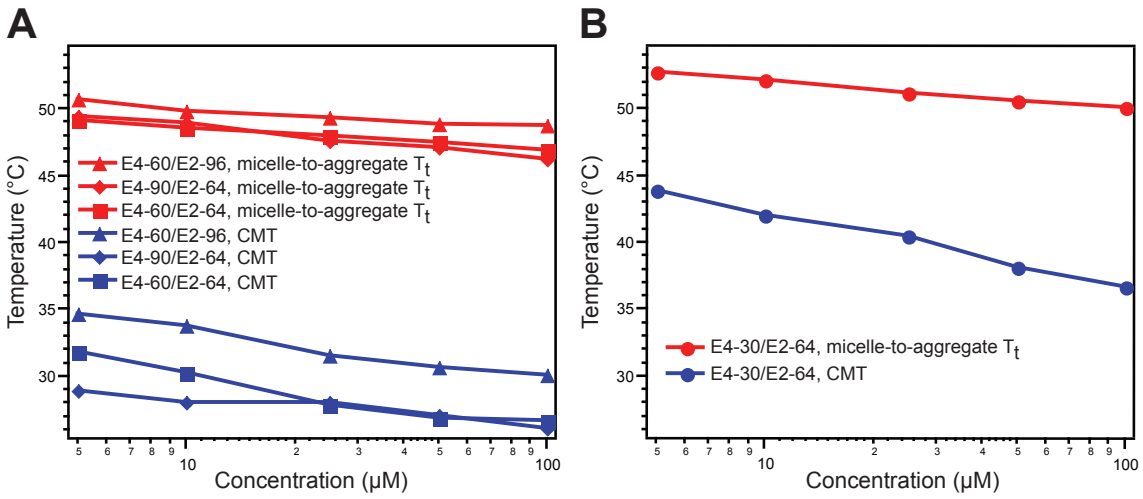

Figure 15: Raising the CMT in second generation ELP$_{BC}$s decreased the temperature range over which stable micelle assembly occurred. Comparison between first generation Arg$_3$-ELP$_{BC}$s (A) and second generation Arg$_5$-ELP$_{BC}$ (B) demonstrated the decreased micelle range that resulted from the increase in the CMT, that was greater than the increase in the micelle-to-aggregate T_t. CMTs and micelle-to-aggregate T_ts were obtained from temperature-regulated turbidimetry measurements in PBS at 5-100 μM.

2.3.5 Characterization of third generation CPP-ELP$_{BC}$s

To further optimize the thermal response of CPP-ELP$_{BC}$s, a new ELP sequence was investigated to raise the T_t of the hydrophilic domain. These third generation ELP$_{BC}$s were synthesized with PRe-RDL cloning. The hydrophilic domain was composed of 60

pentapeptides of E2*, whose sequence $(VPGXG)_{60}$ where $X=A_1G_1$ is more hydrophilic than the previous hydrophilic domain of E2, which alternatively replaced a hydrophilic glycine guest residue with a hydrophobic valine guest residue in every 16th pentapeptide. The hydrophobic domain was still composed of E4, but three lengths of this domain were investigated—30, 35, or 40 pentapeptides—to fine-tune the thermal response by their increasing hydrophobicity. The hydrophobic and hydrophilic genes were fused to create diblocks of E4-30/E2*-60, E4-35/E2*-60, and E4-40/E2*-60 which were functionalized with Arg_5 CPP and characterized by temperature-regulated turbidimetry (Figure 16).

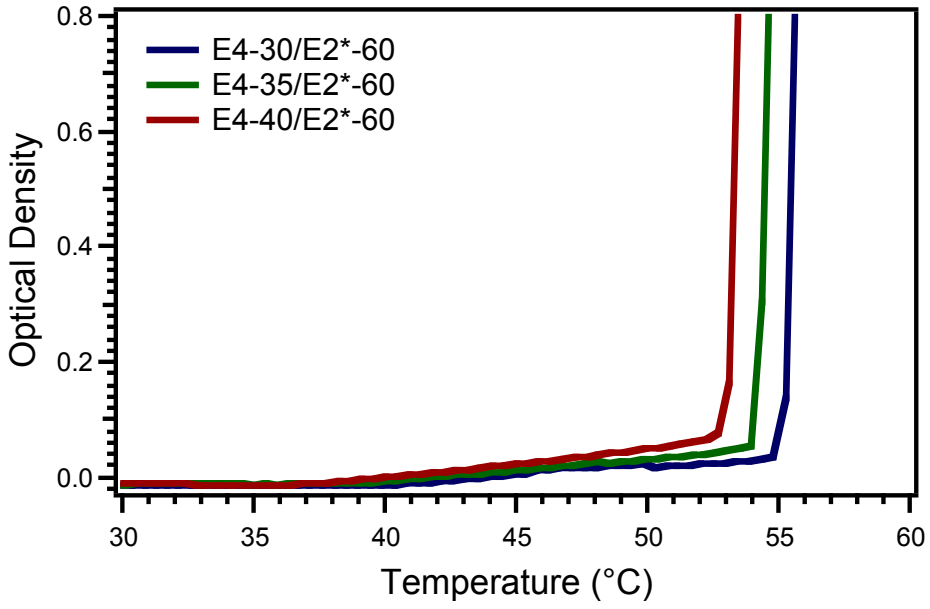

Figure 16: Third generation Arg_5-ELP_{BC}s achieved self-assembly in response to mild hyperthermia and increased the micelle assembly range. A more hydrophilic domain, composed of E2*, increased the micelle-to-aggregate T_t. Three hydrophobic block sizes, composed of E4 with 30, 35, or 40 pentapeptides, provided fine-tuning of the

CMT between 37 °C and 42 °C. Temperature-regulated turbidimetry measurements were taken in PBS at 25 μM.

The more hydrophilic E2* sequence increased the micelle-to-aggregate T_t as much as 5 °C, as compared to previous constructs using E2. This new hydrophilic block, in combination with all three hydrophobic block lengths tested, achieved a desired CMT between 37 °C and 42 °C at 25 μM. As expected, the CMT was fine-tuned by the subtle changes in the hydrophobic block size, such that the CMT increased slightly as the hydrophobic block decreased in length (Table 6). The effect of the hydrophobic block size was also reflected in the micelle-to-aggregate T_t, which decreased slightly with increasing hydrophobic block length.

Table 6: Fine-tuning of the CMT and micelle-to-aggregate T_t of third generation Arg$_5$-ELP$_{BC}$s.

Arg$_5$-ELP$_{BC}$	CMT	Micelle-to-aggregate T_t
E4-30/E2*-60	40.5 °C	55.3 °C
E4-35/E2*-60	38.8 °C	54.1 °C
E4-40/E2*-60	37.5 °C	53.1 °C

DLS of the Arg$_5$-ELP$_{BC}$s with the two extremes in hydrophobic block length further demonstrated the fine-tuned temperature-triggered self-assembly of nanoparticles approximately 20 nm in radius (Figure 17). This library of ELP$_{BC}$s with finely tuned CMT would be particularly important when these constructs were further modified to serve their function as carriers for controlled cellular uptake and drug delivery. Addition of moieties such as fluorescent labels and drug cargo are expected to

slightly perturb the thermal properties of the ELP$_{BC}$s, and thus this library of materials was useful to pull from to conform to those perturbations and maintain an appropriate thermal response for mild hyperthermia-triggered self-assembly.

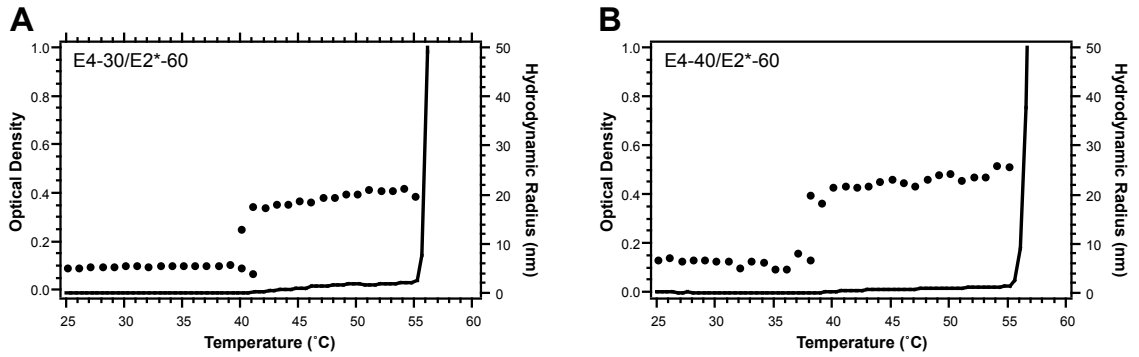

Figure 17: Third generation Arg$_5$-ELP$_{BC}$s finely tune the temperature-triggered behavior, as confirmed by DLS. Arg$_5$-functionalized E4-30/E2*-60 (A) and Arg$_5$-functionalized E4-40/E2*-60 (B) demonstrate CMTs between 37 °C and 42 °C that differ by only 2 °C, as controlled by the length of their hydrophobic domain. Temperature-regulated turbidimetry (lines) and DLS (dots) measurements were taken in PBS at 25 μM.

Zeta potential measurements also confirmed the self-assembly of third generation CPP-ELP$_{BC}$s. To improve the quality of zeta potential measurements, these ELP$_{BC}$s were investigated in water to circumvent the negative effects of salt on this technique. These CPP-ELP$_{BC}$s were thus measured at an elevated concentration (100 μM) and elevated temperature (50 °C) that achieved micelle assembly while considering the change in thermal properties due to the absence of salts. At these conditions, Arg$_5$-functionalized E4-40/E2*-60 and non-functionalized E4-40/E2*-60 micelles exhibited zeta potentials of 14.3 ± 0.5 mV and -4.8 ± 0.8 mV (average of three measurements ± SEM),

respectively. Arg_5-ELP_{BC} exhibited a positive zeta potential, indicative of the high density of cationic CPP on the micelle corona. The negative zeta potential of the non-functionalized ELP_{BC} was likely due to the presentation of the negatively charged ELP C-terminus on the corona of this control micelle.

The role of alternative CPPs was investigated by the functionalization of third generation E4-40/E2*-60 block copolymer. This block copolymer was functionalized with Arg_8, TAT (residues 47-57), and a mutation of TAT, termed RTAT, in which the architecture of arginine could be evaluated without contribution from other charged residues, as achieved by mutation of all non-arginine residues to neutral glycine residues. The thermal behavior of Arg_5-ELP_{BC} as compared to Arg_8-ELP_{BC} confirmed that third generation ELP_{BC}s could be functionalized with new CPPs without significantly perturbing the CMT. Altering the functionalization at the corona does, however, influence the micelle-to-aggregate transition (Figure 18). Yet, the conserved transition from unimer at 37 °C to micelle at 42 °C, despite changes in the charge of functionalized CPP at their most extreme, supported the choice of this third generation ELP_{BC} as a platform for the investigation of a variety of CPPs in the pursuit of controlled cellular uptake by modulation of CPP density with temperature-triggered micelle assembly.

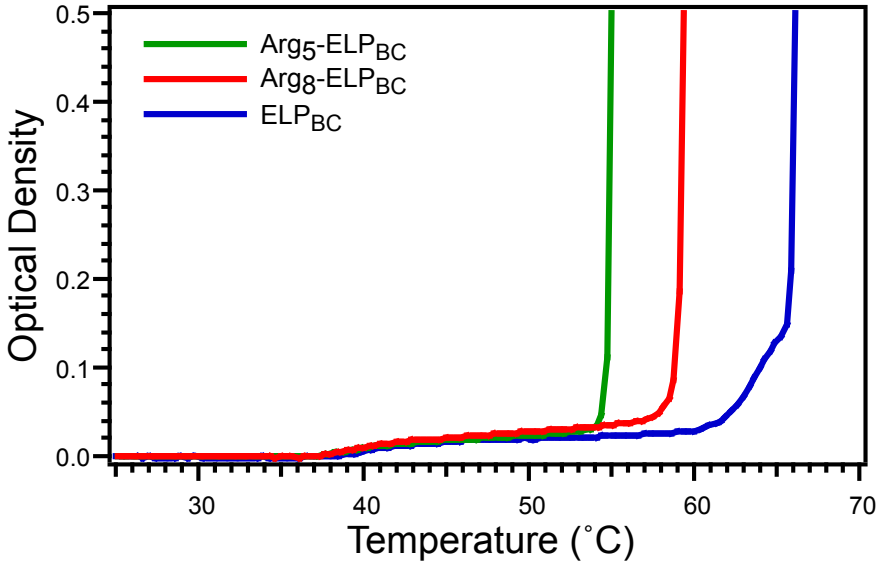

Figure 18: The CMT was conserved between third generation E4-40/E2*-60 block copolymers despite variation in CPP-functionalization. Functionalization of E4-40/E2*-60 with Arg_5 or Arg_8 did not significantly perturb the CMT as compared to a non-functionalized ELP_{BC} control, confirming the utility of this platform to produce various CPP-ELP_{BC}s for controlled cellular uptake and drug delivery. Temperature-regulated turbidimetry measurements were taken in PBS at 15 μM.

2.4 Conclusions

Significant changes in the design of ELP_{BC}s were made to accommodate the addition of CPPs on the hydrophilic terminus and compensate for resulting changes in the ELP_{BC} thermal properties, with the goal of achieving a unimer-to-micelle transition between body temperature and a temperature typical of mild clinical hyperthermia. Prior to CPP-functionalization, the ELP_{BC} syntax was reversed to allow the expression of residues typical to cationic CPPs (ex. arginines) on the hydrophilic terminus of the ELP_{BC}. In this syntax, CPP-functionalization of ELP_{BC}s did not destroy the temperature-triggered self-assembly. However, the syntax did influence the thermal properties of the

ELP_{BC}, such that first generation constructs displayed a CMT below 37 °C, which did not meet the goal of achieving triggered self-assembly in response to mild clinical hyperthermia.

Iterative manipulation of CPP-ELP_{BC} design parameters was performed to improve the thermal behavior, with the goal of achieving a CMT between 37 °C and 42 °C. Decreasing the length of the hydrophobic domain achieved this goal with an E4-30/E2-64 block copolymer, albeit at the negative side-effect of decreasing the temperature range over which stable micelle assembly occurred. This would eventually become a limitation of this block copolymer when additional manipulation of the construct (ex. fluorophore conjugation) would further limit the micelle range and eventually destroy micelle assembly.

Further optimization of the block copolymers was thus necessary to increase the micelle-to-aggregate transition and thereby increase the temperature range over which stable micelle assembly was achieved. This was accomplished with a hydrophilic domain composed of a new ELP sequence, E2*, with an increased T_t. This adjustment of the ELP_{BC} design created a construct that achieved both a CMT between 37 °C and 42 °C and an extended micelle assembly range that could accommodate the perturbations typical of fluorophore conjugation and drug loading. This third generation ELP_{BC} displayed a consistent CMT, regardless of CPP-functionalization, demonstrating its strength as a platform material to test the function of various CPPs for controlled

cellular uptake by modulation of CPP density with temperature-triggered micelle assembly.

Successful design of CPP-ELP$_{BC}$s was primarily measured by the ability to achieve temperature-triggered micelle assembly between conditions of 37 °C and 42 °C. However, additional aspects of the self-assembled micelles may be influenced by the CPP-ELP$_{BC}$ design and have an effect on the performance of CPP-ELP$_{BC}$s as drug carriers. The aggregation number (number of CPP-ELP$_{BC}$ chains per micelle), for instance, may vary with CPP-functionalization or ELP$_{BC}$ design and influence the valency of CPP on each micelle. This could lead to changes in cellular uptake depending on the number of CPPs on each micelle that are capable of interacting with the cell surface. More thorough characterization of the CPP-ELP$_{BC}$ micelle structure and morphology may shed greater light on the relationship between the design and function of CPP-ELP$_{BC}$s.

3. Controlled cellular uptake of CPP-ELP$_{BC}$s *in vitro*

3.1 Motivation

Temperature-triggered CPP-ELP$_{BC}$ micelle assembly provides the mechanism to control the density of CPPs by means of an extrinsic stimulus. CPP-ELP$_{BC}$s below their CMT exist as soluble unimers whose low CPP density (ex. a limited number of arginine residues per ELP$_{BC}$) does not strongly encourage cellular uptake as conferred by the CPP moiety. CPP-ELP$_{BC}$s above their CMT, however, present a high density of CPPs on the self-assembled micelle corona, which encourages enhanced cellular uptake as defined by the CPP component. CPP-ELP$_{BC}$s synthesized in the previous section were characterized to determine "on" and "off" state thermal conditions at which the ELP$_{BC}$ was a unimer (T < CMT) or a micelle (CMT < T < micelle-to-aggregate T_t). This defined the experimental conditions used to evaluate the controlled cellular uptake as triggered by an external thermal stimulus.

To best evaluate controlled cellular uptake, the CPP-ELP$_{BC}$s were labeled with a fluorescent dye to allow them to be visualized by microscopy and quantified by flow cytometry. Comparing internalization below and above the CMT provided a preliminary understanding of cellular uptake, as controlled by the temperature-triggered self-assembly of CPP-ELP$_{BC}$s. As the mechanism of uptake is known to depend on both the CPP and its appended cargo, common routes of endocytosis were

investigated for their role in the uptake of CPP-ELP$_{BC}$s by inhibition and colocalization studies.

3.2 Methods

3.2.1 Fluorophore labeling of CPP-ELP$_{BC}$s

CPP-ELP$_{BC}$s and controls were fluorescently labeled with Alexa Fluor 488. The reactive cysteine residue at the ELP N-terminus permitted conjugation of fluorophore via maleimide chemistry. Purified ELP was reacted with an excess of Alexa Fluor 488 C5-maleimide in 3 mM TCEP-HCl and 10 mM sodium phosphate for 2 hours at room temperature. ELP was collected from the reaction solution by the addition of NaCl to induce ELP coacervation and centrifugation for 10 minutes at 16,000 x *g*. Free fluorophore in the supernatant was discarded and the ELP pellet was resuspended in PBS. Resuspended ELP was passed through a desalting column to remove remaining free fluorophore. Labeling efficiency was determined by absorbance at 495 nm, compensating for fluorophore absorbance occurring at the 280 nm protein peak. Labeled ELP was mixed with respective unlabeled ELP to achieve a labeling efficiency that was equivalent across all CPP-ELP$_{BC}$s and controls compared in an experiment. A labeling efficiency of 50% was typical for most experiments.

3.2.2 Cell culture

HeLa cells were grown in Dulbecco's Modified Eagle's Medium (DMEM) supplemented with 10% fetal bovine serum (FBS), 0.1 M non-essential amino acids, 1.0

mM sodium pyruvate, 100 units/mL penicillin, and 100 μg/mL streptomycin. MCF7 cells were grown in Minimum Essential Medium Eagle with Earle's salts, supplemented with 10% FBS, 0.01 mg/mL bovine insulin, 0.1 M non-essential amino acids, 1.0 mM sodium pyruvate, 100 units/mL penicillin, and 100 μg/mL streptomycin. HUVEC cells were cultured in EBM-2 media supplemented with EGM-2MV SingleQuots and 5% FBS. All cells were maintained at 37 °C and 5% CO_2.

3.2.3 Visualization of CPP-ELP$_{BC}$ uptake with live cell microscopy

Cells were seeded on 8 well coverglass slides and allowed to attach for 24 hours, after which the media was removed and replaced with serum-free media (SF-media) containing Alexa Fluor 488-labeled CPP-ELP$_{BC}$s or controls at concentrations of 10-25 μM. The slides were incubated at 37 °C or 42 °C for 1 hour after which the media was replaced with Hank's balanced salt solution (HBSS) containing 5 μg/mL Alexa Fluor 594 wheat agglutinin and 2 μM Hoechst 33342 to stain the cell membrane and cell nuclei, respectively. After 10 minutes, cells were washed 3 times with PBS before the addition of HBSS. The cells were imaged immediately on a Nikon Eclipse TE2000 widefield fluorescence microscope, using a 60x oil immersion objective, or on a Leica SP5 confocal microscope, using a 63x water immersion objective.

3.2.4 Quantification of CPP-ELP$_{BC}$ uptake with live cell flow cytometry

HeLa, MCF7, or HUVEC cells were seeded in 12-well tissue culture polystyrene plates. After 24 hours the media was removed and replaced with SF-media containing 10

-25 μM of Alexa Fluor 488-labeled CPP-ELP$_{BC}$ or controls. The plates were incubated at 37 °C or 42 °C for 1 hour after which the cells were washed once with PBS and removed from the culture surface with 0.05% trypsin/EDTA. The cells were washed by centrifugation for 3 minutes at 1,200 RPM once with complete media and twice more with PBS before immediate analysis on a BD LSR II flow cytometer. Cells were gated on the live population by forward and side scatter and no less than 10,000 cells were evaluated to determine cellular uptake by measure of mean cellular fluorescence, corrected for autofluorescence of untreated cells.

3.2.5 Investigation of uptake mechanism and intracellular localization of CPP-ELP$_{BC}$s

3.2.5.1 Inhibition of endocytosis pathways

To evaluate the contribution of endocytosis pathways on the cellular uptake of CPP-ELP$_{BC}$s, HeLa cells were co-incubated with CPP-ELP$_{BC}$s or controls at 20 μM in SF-media in combination with inhibitors for clathrin-mediated endocytosis (chlorpromazine (10 μM) or dansylcadaverine (50 μM)), caveolae-mediated endocytosis (filipin (0.5 μg/mL) or genistein (100 μM)), or macropinocytosis (amiloride (50 μM)). Following 1 hour of incubation at 42 °C, cells were analyzed by confocal microscopy or flow cytometry, as described previously. The effect of inhibitors on temperature-triggered micelle assembly was evaluated with DLS.

3.2.5.2 Colocalization with endocytosis markers

To evaluate the intracellular localization of CPP-ELP$_{BC}$s, HeLa cells were coincubated with 20 μM CPP-ELP$_{BC}$ in combination with markers of macropinocytosis (Lucifer yellow, 0.5 mg/mL) [147] or receptor-mediated endocytosis into lysosomes (Lysotracker Red, 75 nM) [148]. The excitation/emission of Lucifer yellow (488/532) corresponded too closely to the Alexa Fluor 488 used previously for ELP labeling. Therefore ELP was alternatively labeled with Alexa Fluor 594 to use in combination with Lucifer yellow. The excitation/emission of Lysotracker Red (577/590) permitted the use of Alexa Fluor 488-labeled ELP, as usual. HeLa cells were co-incubated with CPP-ELP$_{BC}$ and endocytosis markers at 42 °C for 1 hour and then visualized by fluorescence microscopy, as previously described.

3.3 Results and discussion

3.3.1 Controlled cellular uptake of first generation CPP-ELP$_{BC}$s: Proof-of-concept with non-optimized temperature-triggered assembly

First generation CPP-ELP$_{BC}$s exhibited thermal behavior that was not optimized for our ultimate goal of temperature-triggered CPP-ELP$_{BC}$ micelle assembly in response to mild clinical hyperthermia. These constructs displayed unique thermal behavior due to their reversed ELP$_{BC}$ syntax, as compared to the original ELP$_{BC}$s synthesized in the Chilkoti lab [126]. The changes in thermal behavior that accompanied the change in ELP$_{BC}$ syntax included a decrease in the CMT, precluding the use of these constructs for hyperthermia-triggered self-assembly. However, these materials were still useful to

probe our hypothesis regarding controlled CPP density, by defining "off" and "on" conditions appropriate for these constructs. At 25 °C these first generation CPP-ELP$_{BC}$s were soluble unimers in their "off" state and at 37 °C were self-assembled into spherical micelles in their "on" state.

In order to visualize or quantify the cellular uptake of the CPP-ELP$_{BC}$s they had to be labeled with a traceable tag. Alexa Fluor 488 C5 maleimide was chosen to stably label the ELP with a fluorescent tag that would allow visualization by fluorescence microscopy and quantification by flow cytometry. This fluorophore derivative was reacted with the cysteine residue genetically engineered at the N-terminus of the CPP-ELP$_{BC}$, proximal to the hydrophobic domain of the block copolymer, such that the fluorophore would be sequestered into the micelle core upon self-assembly.

Due to the sensitivity of ELPs to their local environment, the effect of this covalent attachment on the thermal properties of the ELP$_{BC}$ was investigated before its use for *in vitro* experiments. The Alexa Fluor 488-labeled non-functionalized ELP$_{BC}$ demonstrated a change in thermal properties with fluorophore attachment that was also evident in all CPP-ELP$_{BC}$s. The effects of Alexa Fluor 488 attachment included a slight increase in the CMT and a more significant decrease in the micelle-to-aggregate T_t (Figure 19). These changes are likely caused by the relatively hydrophilic nature of the fluorophore and its forced sequestration in the hydrophobic micelle core, leading to a decreased stability of micelle assembly apparent in a decreased temperature range over

which stable micelle assembly is achieved. The changes in thermal behavior with fluorophore labeling for first generation CPP-ELP$_{BC}$s did not interfere with their intended behavior at their "off" and "on" thermal conditions and thus these labeled constructs were appropriate for use *in vitro*.

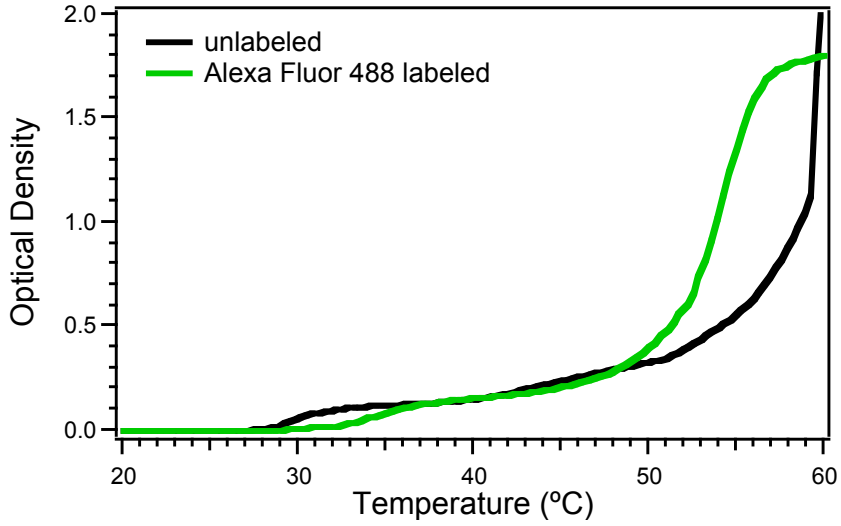

Figure 19: Alexa Fluor 488 labeling affects the thermal properties of first generation ELP$_{BC}$. Attaching Alexa Fluor 488 to the N-terminal cysteine on the hydrophobic domain of the ELP$_{BC}$ raised the CMT and lowered the micelle-to-aggregate T$_t$. Temperature-regulated turbidimetry measurements were acquired in PBS at 25 μM.

Although much of the *in vitro* testing would be performed in SF-media (a standard in the CPP literature), the behavior of first generation Alexa Fluor 488-labeled CPP-ELP$_{BC}$s was evaluated in cell culture media to confirm that serum proteins did not perturb temperature-triggered self-assembly. Arg$_3$-ELP$_{BC}$, Arg$_1$-ELP$_{BC}$, and a non-functionalized ELP$_{BC}$ control all displayed nearly identical thermal behavior in either PBS or cell culture media containing 10% FBS (Figure 20). This suggested that even three

positively charged arginine residues per CPP-ELP$_{BC}$ did not interact significantly with additional serum proteins, permitting temperature-triggered micelle assembly in cell culture media without premature aggregation into larger particles.

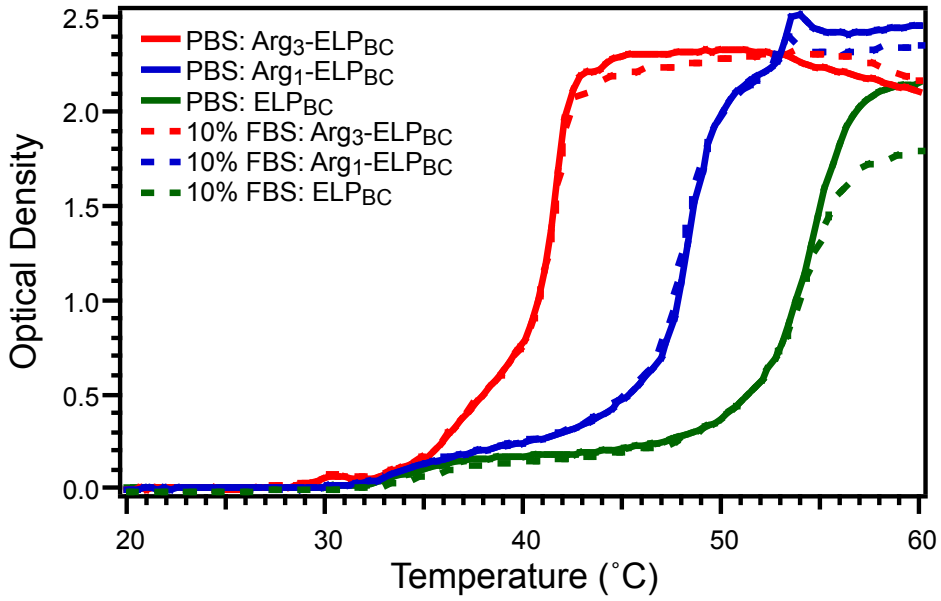

Figure 20: Cell culture media did not affect temperature-triggered micelle assembly of first generation CPP-ELP$_{BC}$s. For Alexa Fluor 488-labeled Arg$_3$-ELP$_{BC}$, Arg$_1$-ELP$_{BC}$, and non-functionalized ELP$_{BC}$ there was no significant difference between thermal behavior in PBS or cell culture media supplemented with 10% FBS. Temperature-regulated turbidimetry measurements were acquired at 25 μM.

Arg$_3$-ELP$_{BC}$s labeled with Alexa Fluor 488 were first evaluated for uptake in HeLa cells at their self-assembled "on" state of 37 °C. Specific intracellular uptake of Arg$_3$-ELP$_{BC}$ micelles was difficult to visualize and distinguish from non-specific adsorption of CPP-ELP$_{BC}$ (Figure 21). Failure to identify significant uptake by fluorescence microscopy with this construct likely culminated from several factors: 1)

the nature of the membrane stain (Cell Tracker Orange), 2) the influence and possible repulsion from the cell culture surface (lysine-functionalized polystyrene), and 3) the insufficiency of Arg_3 to provide the CPP density necessary to significantly enhance cellular uptake in the self assembled state.

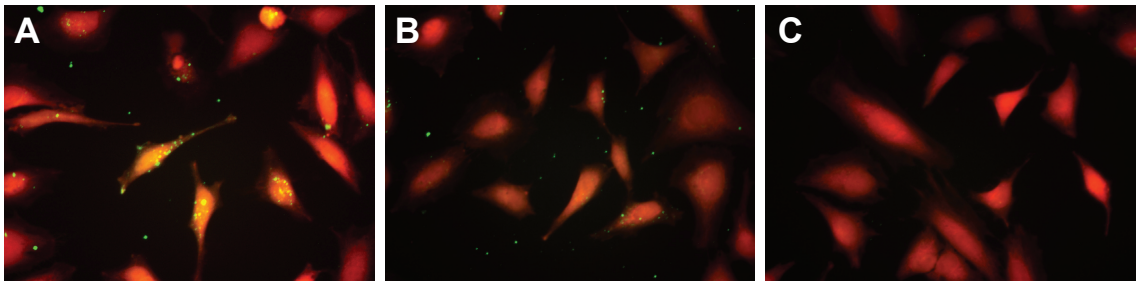

Figure 21: Intracellular uptake of first generation CPP-ELP_{BC}s was not obviously apparent in live cell fluorescence microscopy after 1 hour at 37 °C, at which the ELP_{BC}s were self-assembled into micelles. Specific uptake of Arg_3-ELP_{BC} (A) as compared to Arg_1-ELP_{BC} (B) or non-functionalized ELP_{BC} (C) was not easily distinguished from non-specific adsorption in the cell culture environment. Green—ELP; red—cell tracker; acquired at 60x.

Increasing the valency of arginine on the ELP_{BC} from Arg_3 to Arg_5 significantly enhanced uptake. Visualization of uptake was likely also improved by the modified identification of cell membrane with wheat agglutinin Alexa Fluor 594, in addition to nuclear staining with Hoechst. First generation Arg_5-ELP_{BC} qualitatively demonstrated temperature-controlled cellular uptake by visualization of cells treated with Arg_5-ELP_{BC} at either 25 °C or 37 °C for 1 hour (Figure 22A,D). Very little intracellular signal was apparent in HeLa cells treated with Arg_5-ELP_{BC} at 25 °C, but significant intracellular localization of Arg_5-ELP_{BC} was present at 37 °C. Two controls were also visualized to

ensure that this effect was not due to micelle assembly (independent of CPP-functionalization) or changes in temperature alone. A non-functionalized ELP_{BC} showed minimal intracellular uptake that did not appear to change between 25 °C and 37 °C (Figure 22B,E), suggesting that a change in size from unimer to micelle did not significantly affect uptake. An Arg_5-functionalized unimer control, Arg_5-ELP, incapable of temperature-triggered assembly also showed minimal uptake that was not dependent on thermal conditions (Figure 22C,F). These results confirmed that the enhanced uptake was caused by the change in CPP presentation by Arg_5-ELP_{BC}, from low CPP density on the soluble unimer to high CPP density on the self-assembled micelle.

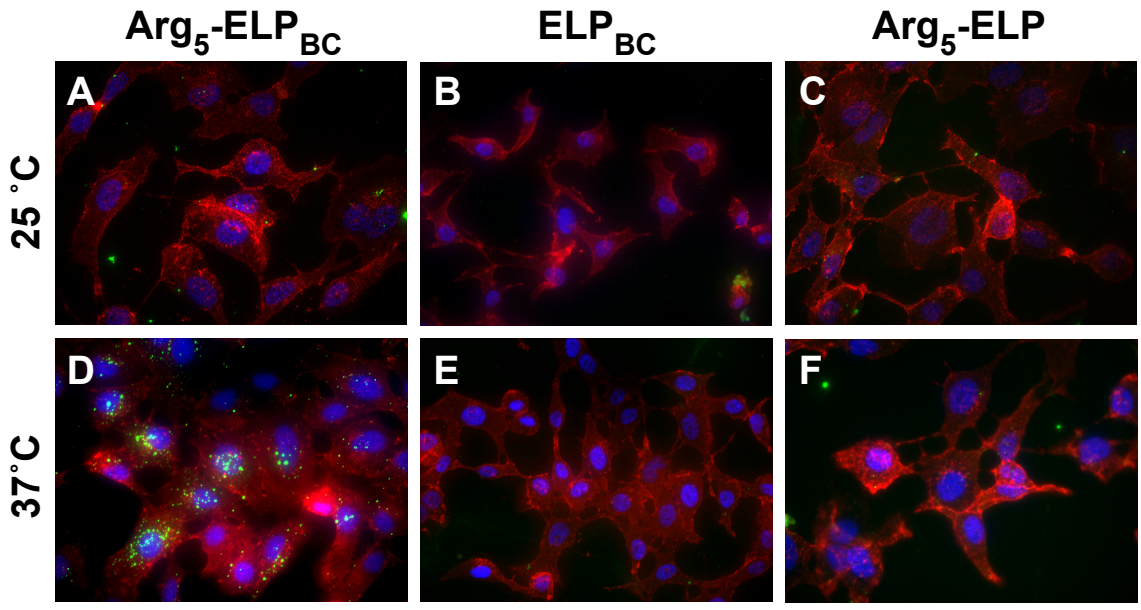

Figure 22: First generation Arg_5-ELP_{BC} achieved controlled cellular uptake as visualized by live cell fluorescence microscopy. Punctate intracellular accumulation was enhanced for Arg_5-ELP_{BC} at 37 °C (D), as compared to 25 °C (A). Minimal internalization was evident for ELP_{BC} (B, E) or Arg_5-ELP (C, F) controls at either

thermal condition. Cells were treated with 20 μM ELP in SF-media. Green—ELP; red—cell membrane; blue—cell nuclei; acquired at 60x.

Controlled cellular uptake was then quantified by live cell flow cytometry. Mean fluorescence of live cells was compared between treatment with Arg_5-ELP_{BC}, non-functionalized ELP_{BC}, or Arg_5-ELP unimer at either 25 °C or 37 °C in SF-media. Histograms of the flow cytometry data demonstrate the shift in cellular fluorescence for Arg_5-ELP_{BC} between 25 °C and 37 °C (Figure 23A). This shift was less exaggerated for non-functionalized ELP_{BC} and insignificant for Arg_5-ELP unimer. Quantification of uptake corroborated the results visualized by microscopy, such that the internalization of Arg_5-ELP_{BC} increased significantly at 37 °C, as compared to 25 °C (Figure 23B). By flow cytometry measurements uptake of the ELP_{BC} control also increased at 37 °C, as compared to 25 °C, albeit less dramatically than for Arg_5-ELP_{BC}, supporting that micelle assembly alone is at least not the major factor driving the function of Arg_5-ELP_{BC}s. However, any change in uptake between thermal conditions for the non-functionalized ELP_{BC} was not expected. This result may be indicative of changes in endocytosis between 25 °C and 37 °C, particularly for these nanoparticle targets of cellular uptake. Although a greatly decreased thermal condition of 4 °C is typically employed to stop energy-dependent mechanisms of endocytosis, it may be that there is some decrease in endocytosis at even 25 °C that causes this change in uptake between the thermal conditions used for these non-optimized first generation ELP_{BC}s. The uptake of the soluble Arg_5-ELP control, however, did not change significantly between either thermal

condition, confirming that heat alone was not responsible for the Arg_5-ELP_{BC} function at 37 °C. Furthermore, although Arg_5-ELP_{BC} significantly increased uptake in its "on" state at 37 °C, it did not greatly exceed the uptake of controls at its "off" state at 25 °C (Figure 23C), demonstrating that the low density of CPP on the soluble Arg_5-ELP_{BC} achieved desirable "off" state behavior, limiting uptake to that which is characteristic of the ELP_{BC} platform alone. Additionally, this result agrees well with the threshold of arginine oligomer CPPs reported in the literature [55, 65], suggesting that those peptides with less than 6 arginine residues do not display significant CPP functionality.

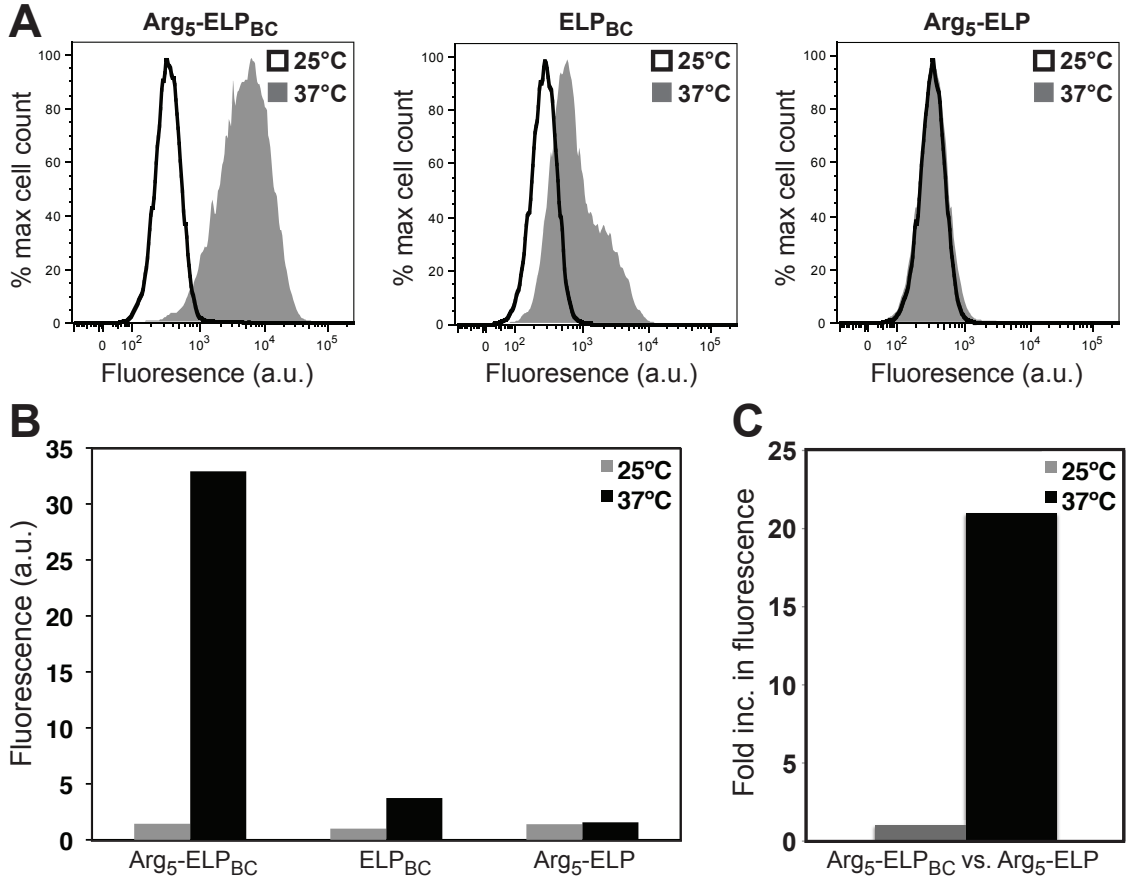

Figure 23: First generation Arg$_5$-ELP$_{BC}$ achieved controlled cellular uptake, as quantified by live cell flow cytometry. Histograms of flow cytometry measurements at 25 °C and 37 °C demonstrated a large shift in cellular fluorescence for Arg$_5$-ELP$_{BC}$ that was less significant for ELP$_{BC}$ and insignificant for Arg$_5$-ELP (A). Quantification of mean fluorescence confirmed that greatly enhanced cell uptake, measured by cellular fluorescence, was evident at 37 °C for Arg$_5$-ELP$_{BC}$, as compared to 25 °C (B). This enhanced uptake was achieved while still maintaining an "off" state uptake that did not greatly exceed that of Arg$_5$-ELP control (C). Cells were treated with 10 μM ELP in SF-media. Flow cytometry measurements were normalized to the uptake of Arg$_5$-ELP$_{BC}$ at 25 °C.

Cellular uptake of first generation Arg$_5$-ELP$_{BC}$ was next evaluated in cell culture media, to determine the effect of serum on the internalization of this CPP-ELP$_{BC}$. Expected temperature-triggered self-assembly of Arg$_5$-ELP$_{BC}$, despite its increased

charge content, was confirmed with temperature-regulated turbidimetry measurement in 10% FBS (Figure 24A), as is typical for the culture media used here. Visualization of cell uptake at the "on" state of 37 °C revealed a decrease in punctate internalization for cells treated in culture media supplemented with 10% FBS (Figure 24B), as compared to those cells treated in SF-media (Figure 24C). Flow cytometry confirmed this decrease in uptake suggested by fluorescence microscopy. Uptake of Arg_5-ELP_{BC} and Arg_5-ELP control were both decreased at 37 °C when in the presence of 10% FBS, as compared to SF-media (Figure 24D). This decreased internalization in the presence of serum could be augmented, however, by increasing the concentration of the ELP. This suggests that, although a decreased cellular uptake should be expected in environments more relevant to *in vivo* conditions, there are controllable parameters of CPP-ELP_{BC} treatment, such as concentration, that may be able to increase uptake in the "on" state *in vivo*, while maintaining minimal uptake in the "off" state.

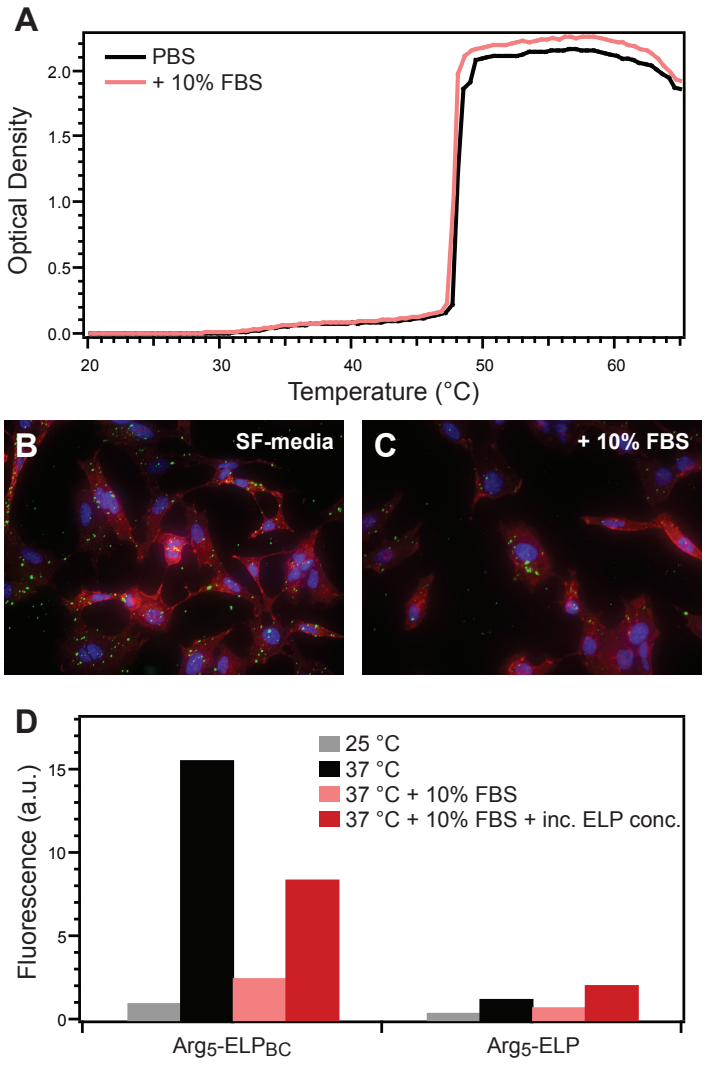

Figure 24: Serum influences the uptake of first generation Arg$_5$-ELP$_{BC}$s. Although temperature-triggered self assembly of Arg$_5$-ELP$_{BC}$ is conserved in 10% FBS (A), its enhanced cellular uptake at 20 μM and 37 °C in serum free media (B) was decreased in the presence of 10% FBS (C). Green—ELP; red—cell membrane; blue—cell nuclei; acquired at 60x. Flow cytometry confirmed the decrease of uptake in the presence of serum for both Arg$_5$-ELP$_{BC}$ and Arg$_5$-ELP control at 10 μM, but demonstrated that enhanced uptake could be partially recovered by increased ELP concentration of 50 μM (D). Flow cytometry measurements were normalized to the uptake of Arg$_5$-ELP$_{BC}$ at 25 °C.

An additional concern about the apparent uptake of Arg_5-ELP_{BC} was that it was indeed internalized into the cell and not just accumulated on the cell surface. This is a significant concern, as the cationic nature of these materials would likely encourage localization on the anionic cell surface. In some instances membrane localization could be useful, for instance to label cell populations for tumor imaging and cell tracking purposes. However, subsequent internalization into the cell is an important function if these materials will be useful as drug carriers to deliver cargo to intracellular therapeutic targets. One approach to probe the location of Arg_5-ELP_{BC}, either inside or outside the cell, is to wash the cells in buffer with high ionic strength to increase charge screening that should elute any materials adherent to the cell surface due to charge interactions. Punctate fluorescence from first generation Arg_5-ELP_{BC} incubated with cells at 37 °C looked similar regardless if the cells were washed in buffer with low ionic strength (PBS) (Figure 25A) or high ionic strength (+ 2M NaCl) (Figure 25B). Thus, although some ELP may be localized on the cell surface, a significant majority of Arg_5-ELP_{BC} was localized within the cell after 1 hour of incubation.

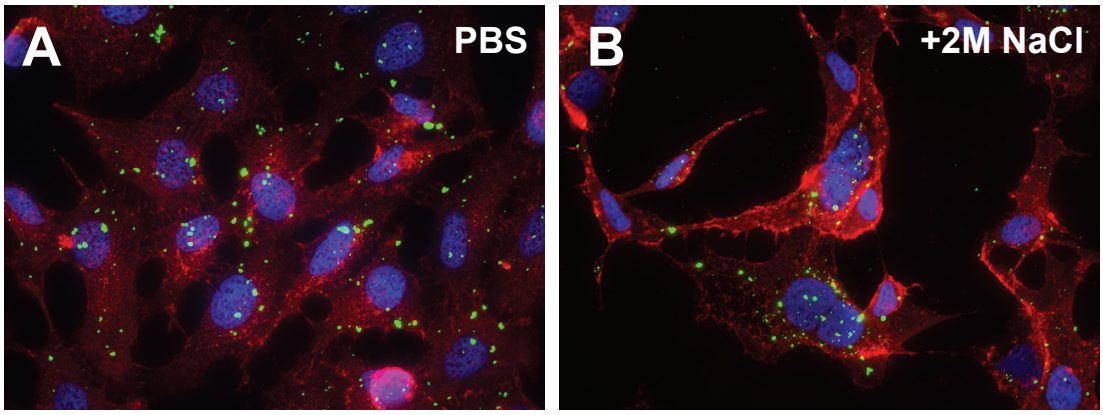

Figure 25: Cellular punctate fluorescence of Arg$_5$-ELP$_{BC}$ was not affected by washing with high ionic strength buffer. Cells treated with 20 μM Arg$_5$-ELP$_{BC}$ at 37 °C exhibited similar punctate fluorescence regardless of washing at low ionic strength (PBS—A) or at high ionic strength (2M NaCl—B), supporting that fluorescence from Arg$_5$-ELP$_{BC}$ was localized within the cells and not on the cell surface. Green—ELP; red—cell membrane; blue—cell nuclei; acquired at 60x.

With Arg$_5$-ELP$_{BC}$s confirming our proof-of-concept of controlled cellular uptake, the valency of the arginine oligomer CPP was revisited to determine the number of arginine residues necessary on each ELP$_{BC}$ to induce this effect. The more sensitive method of quantification, flow cytometry, was used to probe the controlled uptake achieved by ELP$_{BC}$s functionalized with 1, 3, or 5 arginine residues (Figure 26). This uptake was compared to that of the equivalently functionalized soluble unimer controls as well as a non-functionalized ELP$_{BC}$. The "off" state uptake at 25 °C was comparable for all constructs with no apparent trends, suggesting that ELP architecture and functionalization of up to 5 arginines did not significantly affect the uptake when in a soluble unimer form. There was, however, an apparent trend in the uptake achieved at the "on" state of 37 °C, such that an increasing number of arginines induced an

increasing degree of uptake, as measured by cellular fluorescence. The Arg_5-ELP_{BC} thus achieved the biggest fold increase in cellular uptake between thermal conditions.

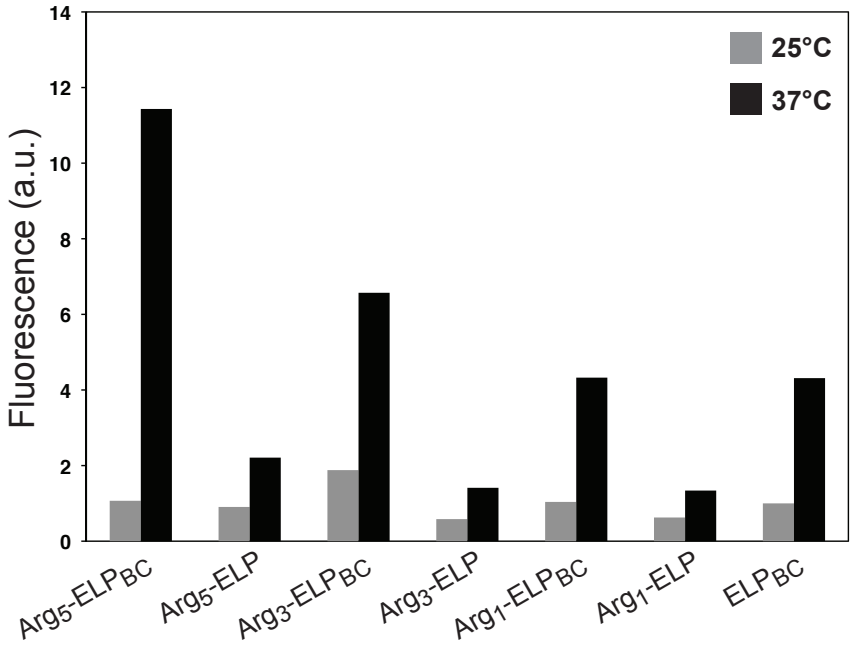

Figure 26: Increasing valency of the arginine oligomer CPP enhanced the fold increase in cellular uptake between 25 °C and 37 °C. Increasing arginine functionalization of 1, 3, or 5 residues increased the uptake achieved at 20 μM and 37 °C without significant effect on the uptake at 25 °C. This trend was less apparent in CPP-ELP controls.

Two additional details are notable from this evaluation of arginine oligomer valency. First, that functionalization of the ELP_{BC} with a single arginine did not achieve any improvement in uptake at the "on" state, as compared to the non-functionalized ELP_{BC} control. So, greater than one arginine is needed to see a desired effect, albeit at a lesser magnitude than is desirable. Second, in this study the non-functionalized ELP_{BC} control, and to a lesser extent the CPP-functionalized soluble controls, continued to

display an increase in uptake at 37 °C, compared to 25 °C. This again suggested that the thermal conditions chosen for this non-optimized construct may have a side-effect of decreasing endocytosis at the hypothermic condition of 25 °C for all constructs. This may, in effect, exaggerate the apparent controlled uptake achieved with these first generation CPP-ELP$_{BC}$s.

3.3.2 Controlled cellular uptake of second generation CPP-ELP$_{BC}$s: Proof-of-concept with mild hyperthermia-triggered assembly

To move on to investigate controlled cellular uptake with a clinically relevant trigger of mild hyperthermia, second generation CPP-ELP$_{BC}$s were prepared with fluorophore-labeling for their initial evaluation *in vitro*. However, as alluded to in Section 2.3.4, the limited micelle range of second generation ELP$_{BC}$s would become problematic when attaching fluorophore, due to the effects of this modification previously gleaned from the labeling of first generation ELP$_{BC}$s. Primarily, the slight increase in CMT and the decrease in micelle-to-aggregate T_t that results from the attachment of fluorophore at the N-terminal cysteine can result in the destruction of micelle assembly if the CMT and micelle-to-aggregate T_t are forced too close to one another and, in effect, cause the ELP$_{BC}$ to transition from unimer-to-aggregate, eliminating the micelle range.

This is exactly the undesirable effect that was seen in the labeling of second generation Arg$_5$-ELP$_{BC}$ with Alexa Fluor 488 C5 maleimide. Temperature-regulated turbidimetry alluded to the loss of micelle assembly (Figure 27), which was further

confirmed by DLS. In an effort to mitigate this undesirable effect, labeling efficiency was decreased by mixing labeled Arg_5-ELP_{BC} with its unlabeled equivalent. DLS measurements of these mixtures suggested a phase separation of unlabeled and labeled Arg_5-ELP_{BC}s, such that both a unimer and micelle population were evident across the temperature range of interest from 37 °C to 42 °C. Manipulation of the labeling efficiency was therefore not a feasible solution to create a clean transition from a purely unimer population to a purely micelle population between "off" and "on" conditions.

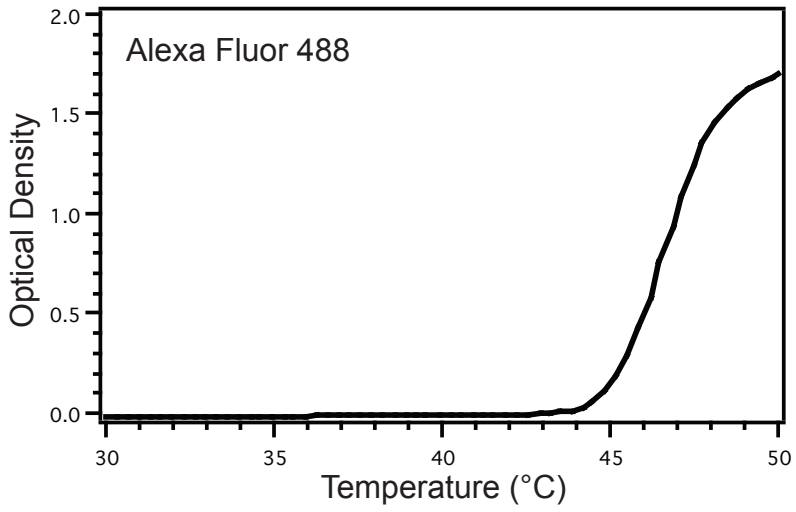

Figure 27: Alexa Fluor 488 labeling at the N-terminal cysteine abolished micelle assembly of second generation Arg_5-ELP_{BC}. Temperature-regulated turbidimetry confirmed the loss of the micelle region and complete aggregation of the labeled construct at approximate 45 °C. Temperature-regulated turbidimetry measurement was acquired at 20 μM in PBS.

It is imaginable that these effects are, in part, dependent on the characteristics of the fluorophore, such as its size, charge, or hydrophobicity. Therefore a number of other

fluorophores with maleimide reactive groups were attached to second generation Arg_5-ELP_{BC} to determine if the desirable thermal properties of this construct could be maintained when fluorescently labeled at the cysteine residue. Alternative fluorophores including Alexa Fluor 594 (Figure 28A), Oregon Green (Figure 28B), and fluorescein (Figure 28C) had the same deleterious effects as Alexa Fluor 488 and destroyed micelle assembly of the Arg_5-ELP_{BC}. However, one fluorophore alternative, BODIPY FL, did not perturb micelle assembly, likely due to its hydrophobic nature (Figure 28D). However, this fluorophore is a poor choice for our intended purpose as the inherent self-quenching of this molecule leads to a decreased fluorescence in the assembled micelle state when fluorophores are packed into close proximity in the micelle core. Preliminary *in vitro* studies of both live cell microscopy and live cell flow cytometry confirmed that BODIPY-labeled Arg_5-ELP_{BC} micelles precluded measurement of controlled cellular uptake at 37 °C due to a lack of punctate fluorescence in cells when observed by microscopy and low fluorescent signal of cells when quantified by flow cytometry.

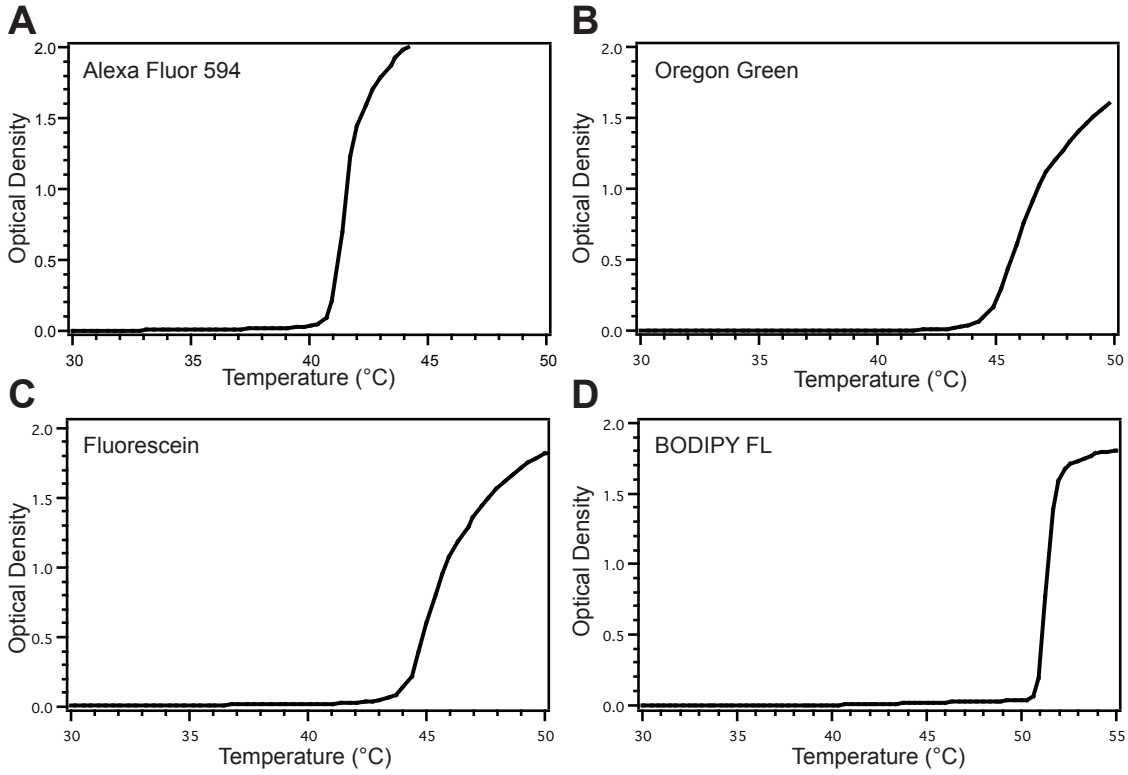

Figure 28: BODIPY was the only alternative fluorophore to maintain micelle assembly of second generation Arg_5-ELP_{BC} with attachment at the N-terminal cysteine. Maleimide derivatives of Alexa Fluor 594 (A), Oregon green (B), and fluorescein (C) abolished micelle assembly as evident by temperature-regulated turbidimetry. Attachment of BODIPY FL did not perturb self-assembly, maintaining a CMT at approximately 40 °C and a micelle-to-aggregate T_t at approximately 50 °C (D). Temperature-regulated turbidimetry measurements were acquired at 20 μM in PBS.

While the characteristics of the fluorophore may be one factor in this undesirable effect on micelle assembly, another factor may the residue to which the fluorophore is being attached. Although the reactive cysteine was included in the block copolymer design for the purpose of fluorophore attachment, it may also serve an unintended purpose of stabilizing micelle formation by means of inter-molecular disulfide bonds that could potentially be formed in the micelle core. If this were to play a role in the

stability of the self-assembled micelles, then occupying these cysteine residues with fluorophore would thereby prevent their function, as such. To investigate this hypothesis, the N-terminal amine on the hydrophobic domain, as opposed to the cysteine residue, was targeted for fluorophore conjugation with Alexa Fluor 488 SDP ester. This approach was feasible, as the ELP contains no other amines, allowing the fluorophore to label the hydrophobic terminus and be buried in the micelle core upon self-assembly. Temperature-regulated turbidimetry and DLS of this labeled variant revealed successful preservation of the thermal properties, whereby pure unimer population was maintained at 37 °C and pure micelle population was achieved at 42 °C (Figure 29). This alternative labeling strategy would allow this construct to serve for initial analysis of controlled cellular uptake in response to mild clinical hyperthermia. However, it was evident from the sensitivity of this construct to functionalization that this second generation ELP_{BC} was not well suited as the ultimate platform for our drug delivery strategy.

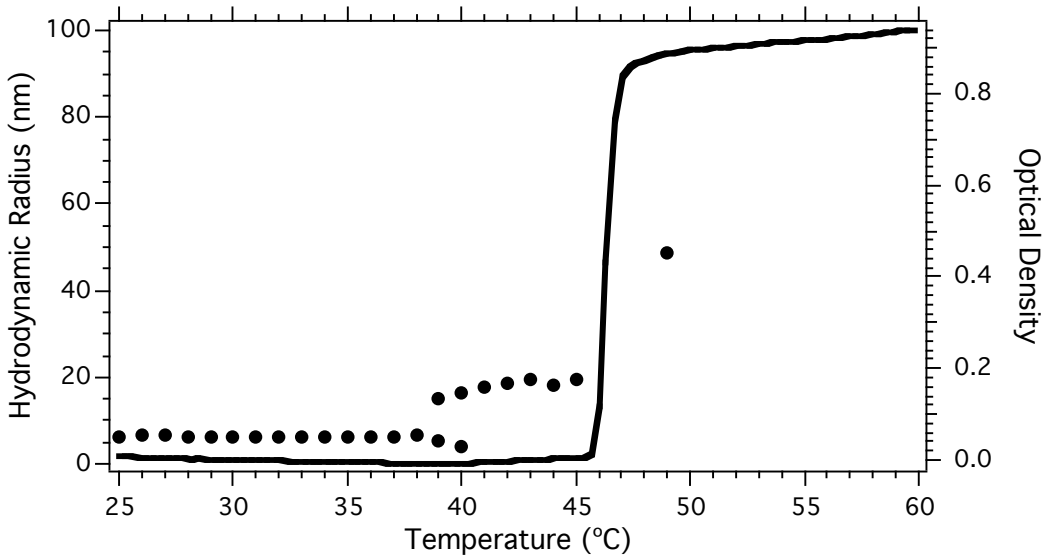

Figure 29: Alexa Fluor 488 labeling at the N-terminal amine of second generation Arg$_5$-ELP$_{BC}$ maintained a desired thermal behavior as confirmed by temperature-regulated turbidimetry (line) and DLS (dots). Temperature-regulated turbidimetry and DLS measurements were acquired at 20 μM in PBS.

With fluorescently labeled second generation CPP-ELP$_{BC}$, the controlled cellular uptake could be investigated under the trigger of mild clinical hyperthermia. Uptake was first visualized by live cell microscopy, in which HeLa cells were incubated with Arg$_5$-ELP$_{BC}$, or appropriate controls, for 1 hour at 37 °C or 42 °C (Figure 30). At the "off" condition of 37 °C all constructs exhibited minimal uptake. However, at the "on" condition of 42 °C Arg$_5$-ELP$_{BC}$ displayed significantly increased uptake as evident by punctate cellular fluorescence. No such uptake was seen with the non-functionalized ELP$_{BC}$ or soluble Arg$_5$-ELP control. These preliminary results confirmed that controlled cellular uptake by means of CPP density manipulation on self-assembled micelles could indeed be translated to clinically relevant conditions, whereby the CPP-ELP$_{BC}$ minimizes

cell uptake at normal physiologic temperature, but induces enhanced cellular uptake at conditions typical of mild clinical hyperthermia.

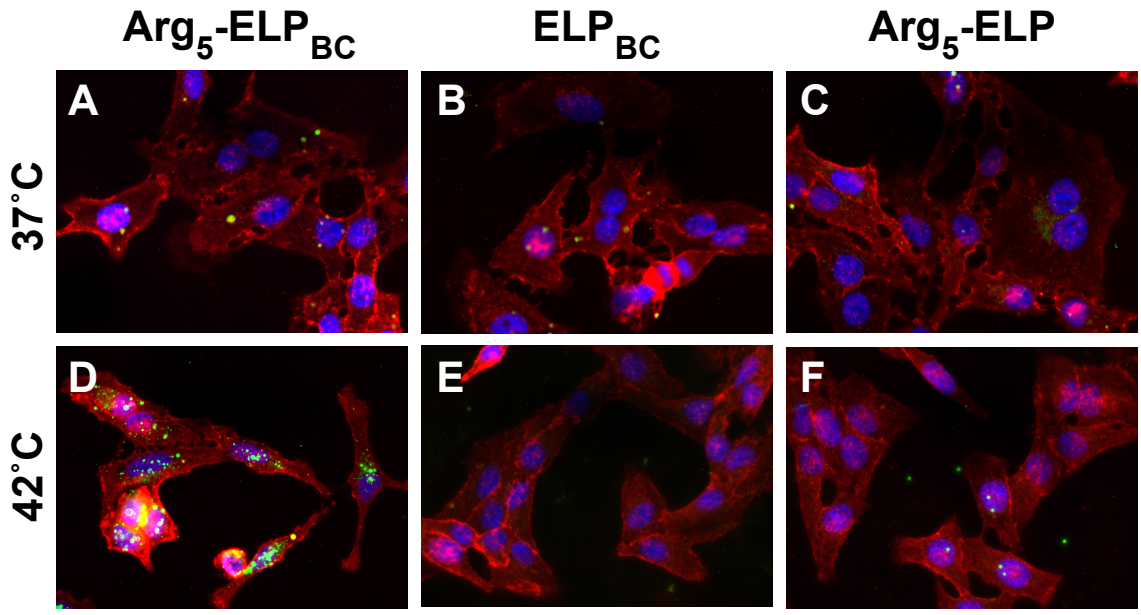

Figure 30: Second generation Arg$_5$-ELP$_{BC}$ achieved mild hyperthermia-controlled cellular uptake, as visualized by live cell fluorescence microscopy. Minimal cellular uptake was seen for all constructs at the "off" state of 37 °C (A-C). Enhanced cellular uptake at 42 °C was seen for Arg$_5$-ELP$_{BC}$ (D), but not for controls ELP$_{BC}$ (E) or Arg$_5$-ELP (F). Green—ELP; red—cell membrane; blue—cell nuclei; acquired at 60x.

Controlled internalization of second generation Arg$_5$-ELP$_{BC}$ was then quantified by flow cytometry. The controlled cellular uptake of Arg$_5$-ELP$_{BC}$ was confirmed, where cellular fluorescence was much greater at the "on" state of 42 °C, as compared to the "off" state of 37 °C (Figure 31A). No change in cellular fluorescence between thermal conditions was observed for the controls of ELP$_{BC}$ or Arg$_5$-ELP. Arg$_5$-ELP$_{BC}$ achieved a 4-fold increase in fluorescence, quantified as the quotient of cellular fluorescence at 42 °C

and 37 °C (Figure 31B). It is of interest to note that, unlike the previous studies with first generation CPP-ELP$_{BC}$s, this family of materials did not exhibit a fold-increase in fluorescence of the non-functionalized ELP$_{BC}$ alone. This suggests that the effects of hypothermia on endocytosis, as were suspected for the thermal condition of 25 °C, were not experienced at the physiologic "off" state of 37 °C for these optimized second generation materials. Furthermore, the controls here also confirmed that the conditions of mild clinical hyperthermia alone—heating to 42 °C for 1 hour—did not appear to have a general effect on endocytosis. Although mild hyperthermia has the potential to induce effects on the cell membrane and cytoskeleton that can influence uptake of nanoparticles, the hyperthermia treatment in the context of these assays did not result in increased uptake of either non-functionalized ELP$_{BC}$ or Arg$_5$-functionalized soluble ELP controls.

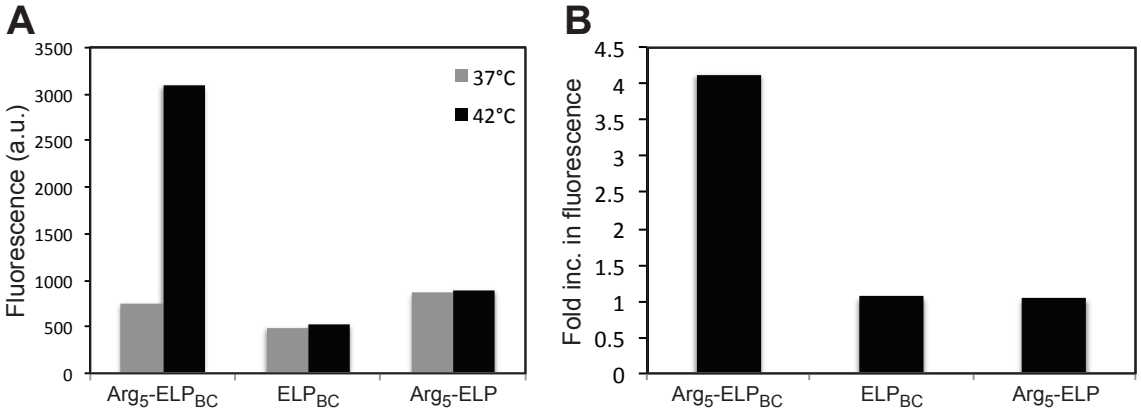

Figure 31: Second generation Arg$_5$-ELP$_{BC}$ achieved mild hyperthermia-controlled cellular uptake, as quantified by live cell flow cytometry. Only Arg$_5$-ELP$_{BC}$ demonstrated an enhanced cellular uptake, as measured by cellular fluorescence, at 42

°C as compared to 37 °C at 10 μM ELP (A), achieving a 4-fold increase in uptake between thermal conditions, above that of the ELP_{BC} or Arg_5-ELP controls (B).

Finally, the effect of serum on the controlled uptake of second generation Arg_5-ELP_{BC} was examined. Flow cytometry confirmed that the uptake of second generation Arg_5-ELP_{BC} micelles with the addition of 10% FBS was similarly influenced by the presence of serum proteins as was first generation Arg_5-ELP_{BC} micelles. However, a decrease in uptake with the addition of 10% FBS was seen only for Arg_5-ELP_{BC} at 42 °C, whereas no significant change in uptake was measured for Arg_5-ELP_{BC} at 37 °C or for non-functionalized ELP_{BC} at either thermal condition (Figure 32). The controlled cellular uptake of second generation Arg_5-ELP_{BC} appeared to be less affected by the presence of serum, as compared to first generation Arg_5-ELP_{BC}. It is not clear whether this is an effect of culture conditions, such as "off" and "on" temperatures, or parameters of the ELP_{BC}, such as size or coordination number. Regardless of the degree of the effect, these results confirmed that controlled cellular uptake could likely still be achieved in *in vivo* environments, but at a decreased magnitude.

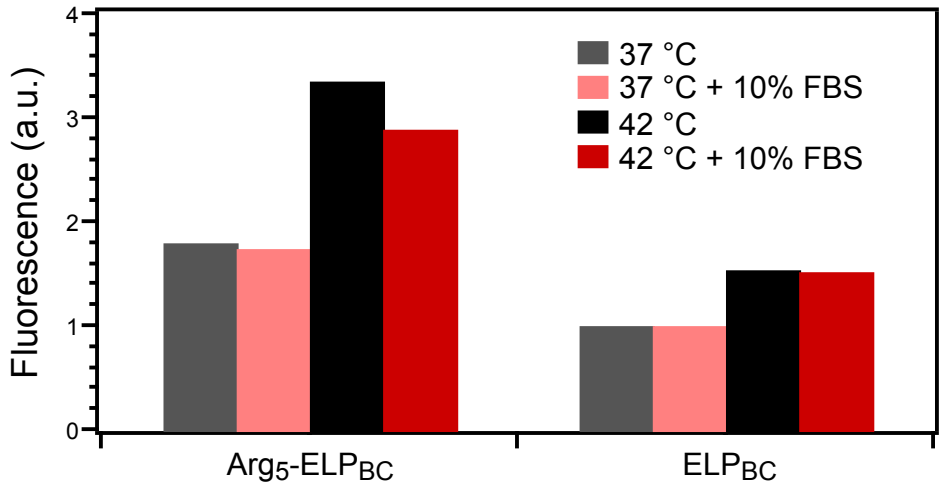

Figure 32: Serum influenced the uptake of second generation Arg$_5$-ELP$_{BC}$s. Flow cytometry confirmed the decrease of uptake in the presence of 10% FBS, as compared to SF-media, for Arg$_5$-ELP$_{BC}$ at 42 °C. Uptake of Arg$_5$-ELP$_{BC}$ at 37 °C or ELP$_{BC}$ at either thermal condition appeared unchanged with the addition of FBS. Cells were treated with 20 μM ELP and flow cytometry measurements were normalized to the uptake of ELP$_{BC}$ at 25 °C.

3.3.3 Controlled cellular uptake of third generation CPP-ELP$_{BC}$s: Optimized mild hyperthermia-triggered assembly

Ultimately, it is the third generation ELP$_{BC}$s that will provide a robust material platform for the evaluation of various CPP-ELP$_{BC}$s as extrinsically targeted carriers. Three variants were designed and characterized in Section 2.3.5: E4-30/E2*-60, E4-35/E2*-60, and E4-40/E2*-60. Unlike the second generation CPP-ELP$_{BC}$, these third generation constructs could be labeled at their N-terminal cysteine with Alexa Fluor 488 without detrimental effect to their self-assembly. This improvement was likely due to the increased micelle range of the third generation ELP$_{BC}$s, created by an increase in the micelle-to-aggregate T_t. This prevented the effects of fluorophore conjugation from

driving the CMT and micelle-to-aggregate T_t so close to one another as to eliminate the micelle assembly range.

Although fluorophore conjugation did not destroy micelle assembly for these constructs, it did increase the CMT slightly, as evident with previous generations of ELP_{BC}s. This change called into play the advantage of having three constructs, with varying hydrophobic block lengths, and thus varying CMTs, to fine-tune the desired CMT following fluorophore conjugation. In the case of E4-30/E2*-60 and E4-35/E2*-60, fluorophore conjugation caused the CMT to rise too close to 42 °C, at 20 μM, to be useful in the intended thermal conditions. Due to the dependence of the ELP T_t on concentration, the CMT will decrease with increasing concentration. Thus, it is feasible to find a concentration range at which each of these three diblocks can function with a desirable CMT. DLS measurements of Alexa Fluor 488-labeled Arg_5-ELP_{BC}s, including E4-30/E2*-60, E4-35/E2*-60, and E4-40/E2*-60, across a range of concentrations confirmed the solution conditions at which the desired CMT was achieved for each construct, such that a population of pure unimers was present at 37 °C and a population of pure micelles was present at 42 °C. For E4-30/E2*-60 with the shortest hydrophobic block of the highest T_t, a concentration of greater than 45 μM was necessary to lower the CMT into a usable range between 37 °C and 42 °C. For E4-35/E2*-60, a concentration of greater than 25 μM was necessary. Finally, for E4-40/E2*-60, a concentration greater than only 5 μM was required. Preferred conditions for *in vitro* evaluation of cellular uptake,

determined from preliminary results with first and second generation CPP-ELP$_{BC}$s, were at ELP concentrations of 10-20 μM. Therefore E4-40/E2*-60 was the construct most suitable to carry forward for thorough characterization of controlled cellular uptake.

Following Alexa Fluor 488 labeling of E4-40/E2*-60, this third generation Arg$_5$-ELP$_{BC}$ was evaluated by DLS to confirm the unimer and micelle population at 37 °C and 42 °C, respectively (Table 7). Arg$_5$-ELP$_{BC}$ was indeed a unimer at 37 °C with an R_h of approximately 5 nm, and a micelle at 42 °C with an R_h of approximately 21 nm. The arginine functionalization did not appear to greatly influence the R_h at either thermal condition, as the non-functionalized ELP$_{BC}$ control had similar R_h measurements of unimer and micelle at 37 °C and 42 °C, respectively. The R_h of the soluble control Arg$_5$-ELP, of approximately 5 nm at both 37 °C and 42 °C, confirmed that it was a unimer at both thermal conditions.

Table 7: Characterization of Alexa Fluor 488-labeled third generation Arg$_5$-ELP$_{BC}$ and controls by DLS at 10 μM in PBS.

Construct	ELP	MW (kDa)	R_h (nm) at 37 °C	R_h (nm) at 42 °C
Arg$_5$-ELP$_{BC}$	E4-40/E2*-60	40.6	5.5 ± 0.1	21.0 ± 1.3
ELP$_{BC}$	E4-40/E2*-60	39.8	5.8 ± 0.2	20.5 ± 0.6
Arg$_5$-ELP	E2*-100	39.2	5.4 ± 0.2	5.2 ± 0.1

The controlled cellular uptake of third generation CPP-ELP$_{BC}$ was then visualized with live cell fluorescence confocal microscopy. Again, limited cellular uptake of Arg$_5$-ELP$_{BC}$ and controls was observed at 37 °C, while only Arg$_5$-ELP$_{BC}$ achieved enhanced cellular uptake at 42 °C (Figure 33). The cellular uptake of non-functionalized

ELP$_{BC}$ and soluble Arg$_5$-ELP did not appear to change between thermal conditions, confirming that micelle assembly and hyperthermia alone were not accountable for the controlled cellular uptake achieved by Arg$_5$-ELP$_{BC}$. In this experiment it was particularly apparent that the internalized Arg$_5$-ELP$_{BC}$ localized to the perinuclear space.

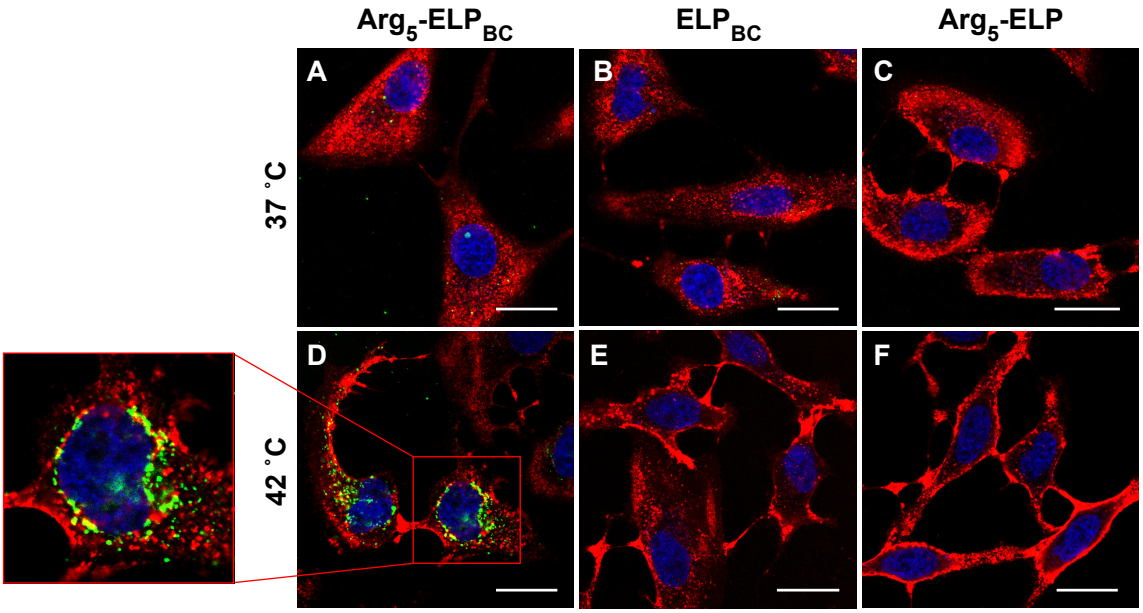

Figure 33: Third generation Arg$_5$-ELP$_{BC}$ achieved controlled cellular uptake, as visualized by live cell fluorescence microscopy. Minimal cellular uptake was observed for all constructs at the "off" condition of 37 °C (A-C). Only Arg$_5$-ELP$_{BC}$ exhibited enhanced cellular uptake at the "on" state of 42 °C (D) while the cellular uptake of non-functionalized ELP$_{BC}$ (E) and soluble Arg$_5$-ELP (F) remained unchanged. The internalized Arg$_5$-ELP$_{BC}$ localized to the perinuclear space (D, box). Green—ELP; red—cell membrane; blue—cell nuclei; scale bars 25 μm. Reproduced from [149].

The sectioning ability of confocal microscopy provided a vote of confidence in the localization of Arg$_5$-ELP$_{BC}$ within the cells, as opposed to on the cell surface. Nonetheless, the effect of cell washing on cellular uptake was investigated to further

confirm the internalization of the Arg_5-ELP_{BC}. Flow cytometry was used to quantify cellular uptake, as measured by cellular fluorescence, after incubation with Arg_5-ELP_{BC} and controls and detachment/washing of cells with trypsin, non-enzymatic cell dissociator, or non-enzymatic cell dissociator followed by a heparin wash. These three conditions were chosen due to their distinct differences in how surface peptides may be removed from the cell during their preparation for analysis by flow cytometry.

Trypsin is an enzyme that dissociates cells by digesting their attachments to the culture surface. Trypsin is also likely to be efficient at removing cell surface-bound arginine-functionalized ELPs. Since the trypsin cleaves at the carboxyl side of an arginine residue it should cut the CPP and release the appended ELP, as well as its attached fluorophore, from the cell surface. Non-enzymatic cell dissociator is a chelator that interrupts cellular interactions responsible for cell surface attachment and thereby does not directly remove surface bound materials. However, non-enzymatic dissociator in combination with a heparin wash should remove surface bound arginine-functionalized ELPs by electrostatic interactions and hydrogen bonding that compete with the cell surface to interact with the cationic CPPs.

Arg_5-ELP_{BC} and controls were incubated with HeLa cells at 37 °C or 42 °C as usual and then removed from the cell culture surface and/or washed with these three conditions, after which the cellular fluorescence was quantified by flow cytometry. Surprisingly, for Arg_5-ELP_{BC} there was hardly any change in cellular fluorescence at

either thermal condition between the three dissociation/washing conditions (Figure 34A). This suggested that the significant majority of Arg_5-ELP_{BC} was internalized and any portion that remained on the surface was likely to be removed by the standard procedure of PBS washing. For both non-functionalized ELP_{BC} (Figure 34B) and Arg_5-ELP (Figure 34C) there was a slight increase in cellular fluorescence detected for non-enzymatic dissociation with and without heparin washing, as compared to the cells processed with trypsin. This suggested that for these controls there was a small portion that existed on the cell surface that was removed efficiently by trypsin, but not by heparin washing. These materials are therefore likely to be adsorbed to the cell by means other than electrostatic effects, such as hydrophobic interactions. This experiment confirmed that the use of trypsin as the dissociator, and PBS as a standard washing buffer, would put all constructs on a level playing field by quantification of only internalized ELP.

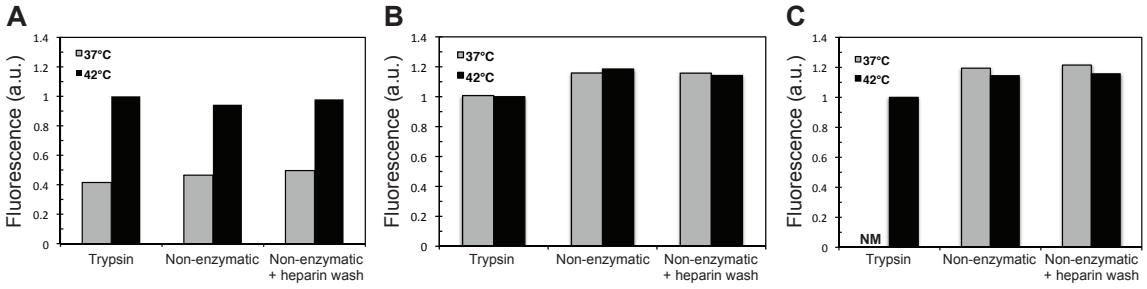

Figure 34: Third generation Arg_5-ELP_{BC} was sufficiently internalized, as evident from dissociator/washing conditions prior to flow cytometry. Arg_5-ELP_{BC} showed no difference in cellular fluorescence between dissociator/washing conditions (A). ELP_{BC} (B) and Arg_5-ELP (C) showed slight increase in cellular fluorescence when treated

with non-enzymatic dissociator. Cells treated with Arg_5-ELP and trypsin at 37 °C were not measured (NM). Flow cytometry measurements from each ELP treatment were normalized to fluorescence at 42 °C with trypsin treatment.

Prior to the thorough quantification of cellular uptake of Arg_5-ELP_{BC} and its controls, the conditions pertaining to flow cytometry measurements were optimized. *In vitro*, the ratio of CPP:cell has been known to be an important parameter affecting the internalization of CPPs, were a greater amount of CPP per cell, independent of CPP concentration, can improve uptake [150]. Thus there are advantages of manipulating the cell density and incubation volume to influence this CPP:cell ratio, while maintaining a constant ELP concentration that fulfills our desired thermal behavior.

The effect of cell density was first investigated by incubating 10 μM Arg_5-ELP_{BC} at 37 °C or 42 °C with cells plated at 25,000, 50,000, or 100,000 cells per well on a 12-well plate. The fold increase in fluorescence (the quotient of uptake at 42 °C compared to 37 °C) revealed decreasing controlled uptake as the cell density was increased (Figure 35A). Although 25,000 cells demonstrated the best performance, the limited number of cells in this case made it difficult to collect the signal from 10,000 cells after cell processing, as was standard for the flow cytometry protocol. Therefore, 50,000 cells per well would be used to improve the fold increase in cellular fluorescence, without burden on the procedures of the flow cytometry measurements.

Next, the effect of incubation volume was investigated by treating 50,000 cells per well at 37 °C or 42 °C with either 400 or 600 μL of Arg_5-ELP_{BC} at 10 μM. Lower

volumes were not feasible, as they would not provide sufficient surface coverage of the wells, while larger volumes were undesirable as they consumed a greater amount of precious Alexa Fluor 488-labeled Arg_5-ELP_{BC}. The fold increase in fluorescence increased with increasing incubation volume (Figure 35B), supporting the choice of 600 μL as the incubation volume for subsequent flow cytometry experiments. These results confirmed those suggestions found in the literature that increasing the CPP:cell ratio, independent of CPP concentration, can enhance cellular uptake.

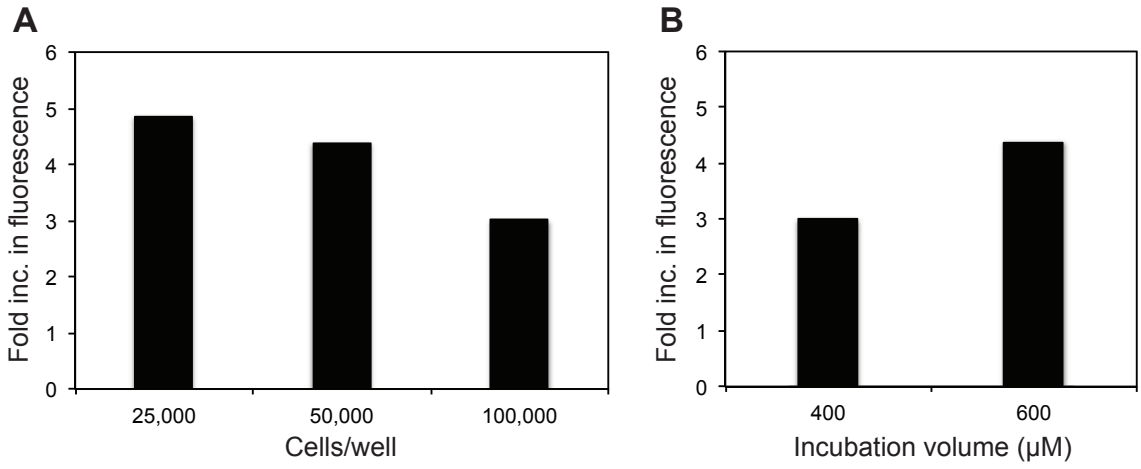

Figure 35: Increasing the CPP:cell ratio optimized controlled cellular uptake of Arg_5-ELP_{BC}, as measured by flow cytometry. Decreasing the cell density enhanced the fold increase in cellular fluorescence (A) and increasing the incubation volume enhanced the fold increase in cellular fluorescence (B).

Using these optimized conditions, the cellular uptake of Arg_5-ELP_{BC} and controls was quantified by flow cytometry over the course of 1 hour. Measurements at 5, 15, 30, and 60 minutes revealed increasing cellular internalization over time for Arg_5-ELP_{BC} at

both 37 °C and 42 °C (Figure 36A). Uptake at 42 °C, however, increased much faster than at 37 °C, after 5 minutes of incubation. The fold increase in uptake at 42 °C, compared to 37 °C, reached its maximum by 30 minutes but was approximately retained until 1 hour. This result is encouraging, to see that the maximum difference in uptake between "off" and "on" state conditions is achieved within the time limitations typical of mild clinical hyperthermia (1 hour at 42 °C [14]). ELP_{BC} and Arg_5-ELP controls also revealed an increase in uptake, albeit modest, over the course of 1 hour, but this increase did not differ between 37 °C and 42 °C for either control (Figure 36B-C).

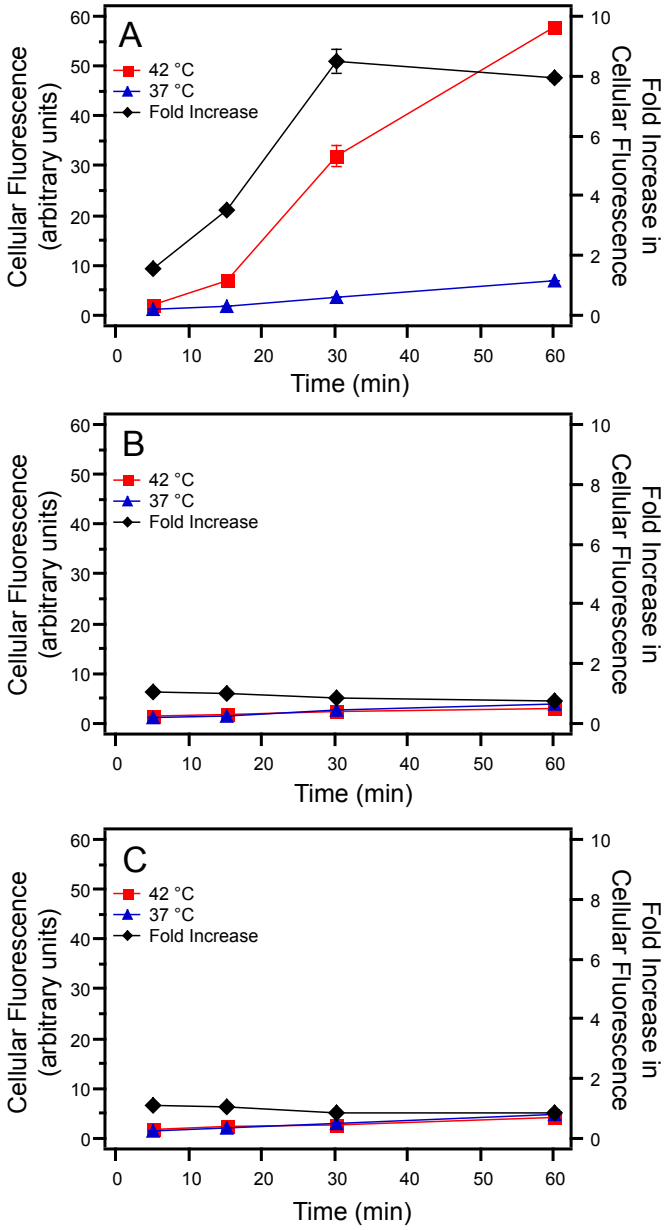

Figure 36: Fold increase in cellular uptake of Arg_5-ELP_{BC} was maximized within the time scale of mild clinical hyperthermia. Cellular uptake, as quantified by flow cytometry, of Arg_5-ELP_{BC} (A), ELP_{BC} (B), and Arg_5-ELP (C) increased over the course of 1 hour, but only Arg_5-ELP_{BC} exhibited an enhanced rate of uptake at 42 °C, maximizing the fold increase in uptake at 42 °C, as compared to 37 °C, within 1 hour. Reproduced from [149].

Due to their non-specific mechanism of uptake, CPPs should achieve efficient internalization in a variety of cell types. To investigate this feature of CPP-ELP$_{BC}$s, the cellular uptake of Arg$_5$-ELP$_{BC}$ and controls was evaluated in three cell lines: HeLa cervical cancer cells, MCF7 breast cancer cells, and primary endothelial HUVEC cells. All cell lines demonstrated the effect of controlled cellular uptake with CPP-density manipulation, such that the fold increase in fluorescence, between 42 °C and 37 °C, was greatest for Arg$_5$-ELP$_{BC}$ in all cases and minimized for ELP$_{BC}$ and Arg$_5$-ELP controls (Figure 37). However, controlled uptake, as measured by fold increase in fluorescence, was best achieved in HeLa cells and to a lesser extent in MCF7 and then HUVEC cells, demonstrating that the level of uptake should not be expected to be consistent between cell lines. The differences detected here suggest that uptake is achieved to a higher level in cancer cells, as opposed to non-cancerous primary endothelial cells, perhaps due to exaggerated endocytosis of malignant cells [151]. These differences in performance could suggest an advantage in targeting cancerous cells over normal cells. However, comparison in uptake between two cancer cell lines and one variant of endothelial cells does not yet provide strong support of this variable uptake. Furthermore, the uptake in HUVECs may vary considerably from other endothelial cell types, such as those found in the microvasculature, causing uptake in the endothelial cell layer to vary in different types of vasculature. Finally, although the uptake is diminished in the endothelial cell line investigated here, it is important to remember that the endothelial cells will

encounter the highest concentration of CPP-ELP$_{BC}$ as it circulates throughout the body, such that even a lower degree of uptake in endothelial cells may result in important biological effects that could be either advantageous or detrimental to the function of CPP-ELP$_{BC}$s as tumor-targeted drug carriers.

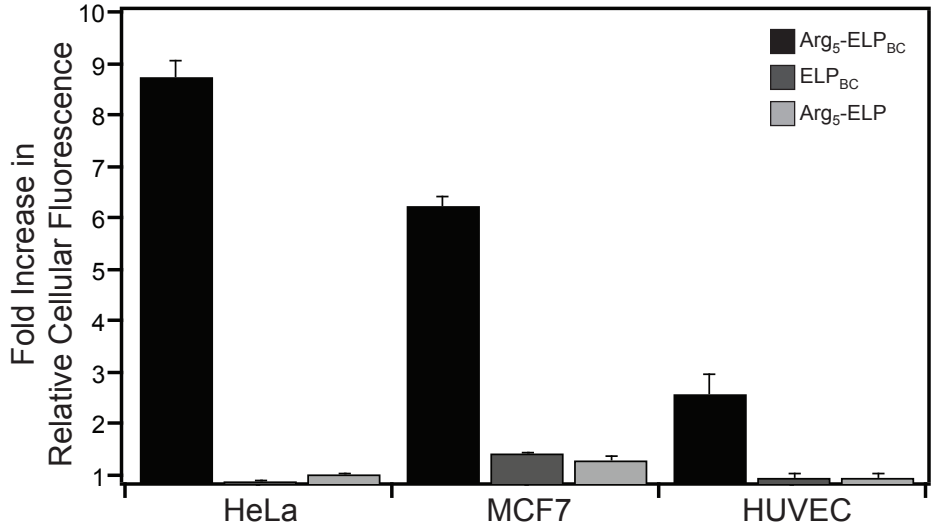

Figure 37: Quantification of the fold increase in cellular fluorescence achieved with Arg$_5$-ELP$_{BC}$, ELP$_{BC}$, and Arg$_5$-ELP between 42 °C and 37 °C in HeLa cervical cancer cells, MCF7 breast cancer cells, and primary endothelial HUVEC cells confirmed that controlled cellular uptake was achieved regardless of cell type. The magnitude of cell uptake, however, was cell-dependent and greatest for cancer cells. Reproduced from [149].

Thus far, CPP-ELP$_{BC}$s for controlled cellular uptake with temperature-triggered micelle assembly have focused on arginine-functionalized constructs where each unimer was functionalized with 5 arginine residues, below the threshold necessary for uptake, to prevent cellular internalization in the soluble "off" state at 37 °C. Thus, only when the Arg$_5$-ELP$_{BC}$ assembled into micelles at their "on" state of 42 °C, could the cell perceive

that the arginine density was above the threshold necessary for uptake. This design therefore took advantage not only of the changing density of arginine residues with micelle assembly, but of the special threshold of arginine content necessary for uptake. The investigation of CPP-functionalized ELP_{BC}s was next expanded beyond the case of arginine oligomers below their functional threshold to include more complex CPP sequences and utilize only the modulation of CPP density with temperature-triggered micelle assembly to achieve enhanced cellular uptake at conditions of mild hyperthermia.

The first expansion of the CPP-ELP_{BC} library involved the extrapolation of arginine oligomers to the biological peptide from which they were inspired, leading to the creation of a TAT-functionalized ELP_{BC} bearing residues 47-57 from the trans-activator of transcription (TAT) of HIV. As each TAT-ELP_{BC} contains a single fully functional CPP, it is no longer expected that cellular uptake will be significantly inhibited at the "off" condition of 37 °C. However, increasing TAT density with temperature-triggered micelle assembly will still likely increase cellular uptake, thus separating the levels of cellular internalization at "off" and "on" conditions.

Preliminary evaluation of TAT-ELP_{BC} was performed with confocal microscopy and flow cytometry and compared to the performance of Arg_5-ELP_{BC}s (Figure 38). As hypothesized, TAT-ELP_{BC} was visualized to have a much greater degree of uptake at the "on" state of 42 °C, as compared to Arg_5-ELP_{BC} (Figure 38B,E), but at the cost of also

increasing uptake, to a lesser extent, at the "off" state of 37 °C (Figure 38A,D). Histograms of cellular fluorescence acquired by flow cytometry confirmed the microscopy results, such that there was a greater increase in cellular fluorescence for TAT-ELP$_{BC}$ between thermal conditions, but this effect was shifted to higher levels of fluorescence for both thermal conditions, as compared to Arg$_5$-ELP$_{BC}$ (Figure 38C,F).

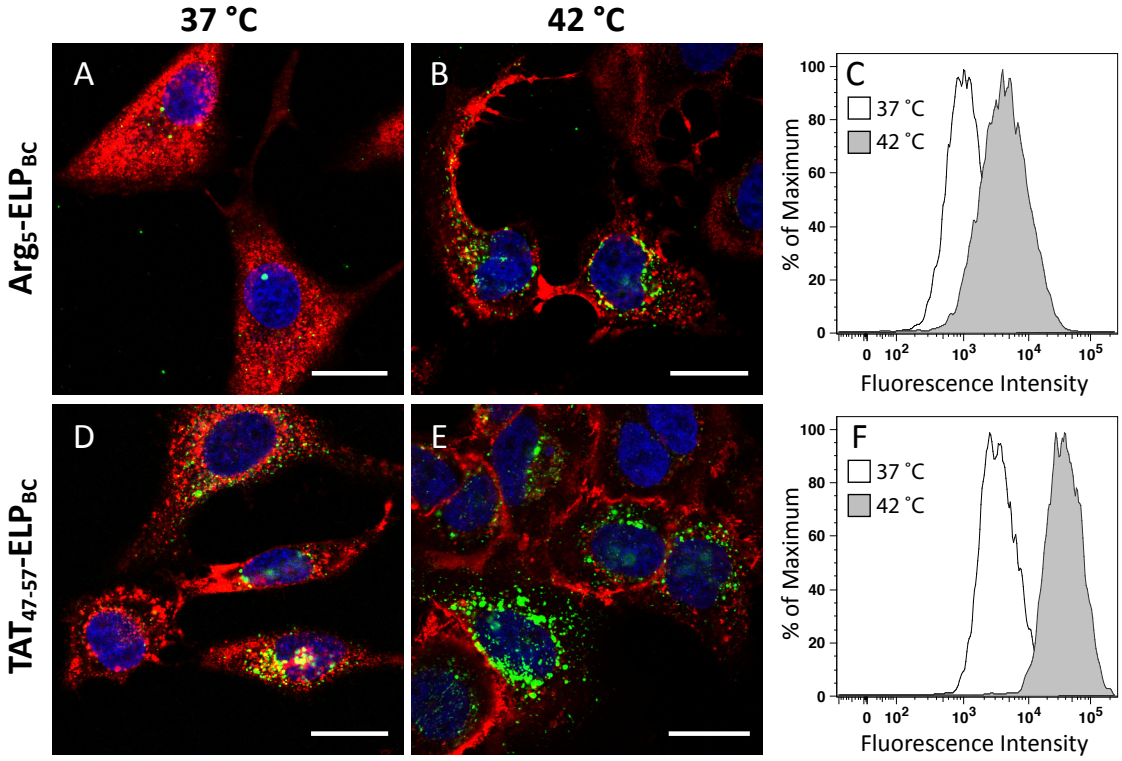

Figure 38: TAT-ELP$_{BC}$ achieved enhanced cellular uptake at both thermal conditions, as compared to Arg$_5$-ELP$_{BC}$. TAT-ELP$_{BC}$ achieved greater uptake at 37 °C (B), as compared to Arg$_5$-ELP$_{BC}$ (A), likely due to its fully functional CPP on each ELP$_{BC}$. Uptake at 42 °C was greatly enhanced for TAT-ELP$_{BC}$ (E), as compared to Arg$_5$-ELP$_{BC}$ (B). Visualized uptake was confirmed by flow cytometry at 37 °C and 42 °C (C and F). Green—ELP; red—cell membrane; blue—cell nuclei; scale bars—25 μm.

These interesting differences in cellular uptake at "off" and "on" states, as well as their implication in the fold-increase in uptake from normothermic to hyperthermic conditions, was further investigated by manipulating the CPP sequence appended to the ELP_{BC}. Additional CPP-ELP_{BC}s were added to the library of third generation ELP_{BC}s to expand the available levels of "off" and "on" state cellular uptake that can maximize internalization at conditions of mild hyperthermia while minimizing uptake at normal body temperature. These additional constructs included functionalization with Arg_8, above the threshold necessary for uptake of arginine oligomer CPPs, and RTAT, a variant of TAT in which the architecture of arginine was explored by mutating all non-arginine residues to neutral glycine residues. This complete family of CPP-ELP_{BC}s was labeled with Alexa Fluor 488 and characterized by DLS to confirm that all constructs existed as unimers (R_h ~ 5-6 nm) at 37 °C and micelles (R_h ~ 20-21 nm) at 42 °C (Table 8).

Table 8: Characterization of the extended library of Alexa Fluor 488-labeled third generation CPP-ELP_{BC}s by DLS at 10 μM in PBS.

Construct	MW (kDa)	R_h (nm) at 37 °C	R_h (nm) at 42 °C
Arg_5-ELP_{BC}	40.50	5.7 ± 0.3	20.8 ± 1.0
Arg_8-ELP_{BC}	40.97	5.4 ± 0.4	21.2 ± 0.3
TAT-ELP_{BC}	41.26	5.7 ± 0.3	21.4 ± 0.3
RTAT-ELP_{BC}	41.05	6.5 ± 0.2	21.8 ± 0.3
ELP_{BC}	39.72	6.2 ± 0.1	20.3 ± 0.3

Controlled cellular uptake of these CPP-ELP_{BC}s was visualized in HeLa cells. Non-functionalized ELP_{BC} showed no visible uptake at either thermal condition (Figure 39A,B), confirming the function of this control as in previous results and demonstrating

that the ELP_{BC} is a useful platform since its function is subsequently conferred entirely by its appended CPP moiety. Arg_5-ELP_{BC} demonstrated minimal uptake at 37 °C in its unimer state, but did achieve greater internalization at 42 °C (Figure 39C,D), again consistent with previous studies. In contrast, ELP_{BC}s appended with Arg_8 (Figure 39E,F), TAT (Figure 39G,H), and RTAT (Figure 39I,J) all exhibited some level of uptake at the "off" condition of 37 °C, consistent with the known ability of these CPPs as single copies to induce cellular uptake. Internalization of these constructs was then dramatically enhanced at the "on" state of 42 °C. All constructs achieved a punctate intracellular fluorescence, suggesting an endocytic route of cellular entry.

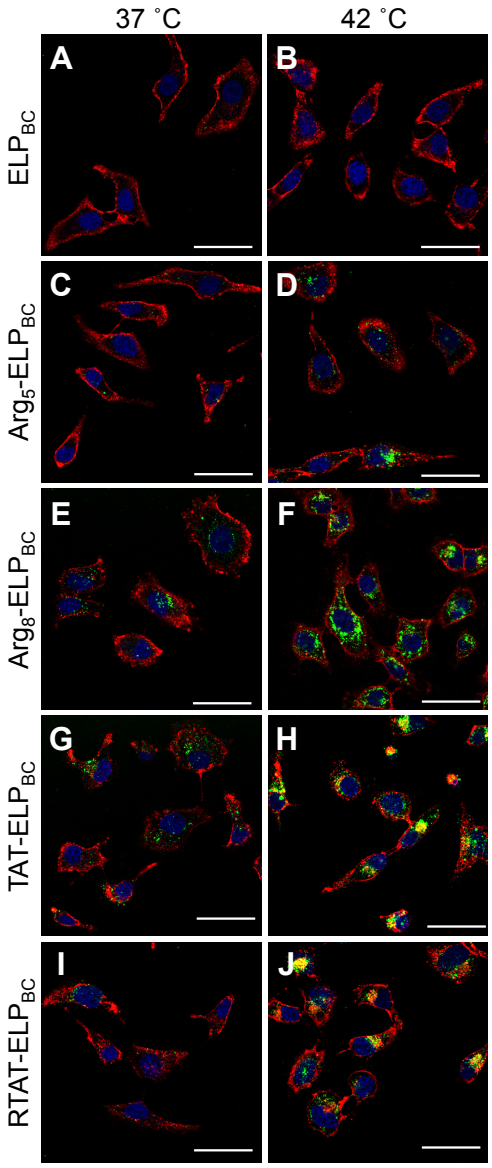

Figure 39: The extended family of CPP-ELP$_{BC}$s achieved a breadth of cellular uptake at "off" and "on" conditions, as visualized by fluorescence microscopy. HeLa cells were incubated for 1 hour at 37 °C or 42 °C with ELP$_{BC}$ (A,B), Arg$_5$-ELP$_{BC}$ (C,D), Arg$_8$-ELP$_{BC}$ (E,F), TAT-ELP$_{BC}$ (G,H), or RTAT-ELP$_{BC}$ (I,J). All CPP-ELP$_{BC}$s demonstrated an increased internalization at 42 °C, as compared to 37 °C. The magnitude of the difference in uptake between thermal conditions was controlled by the appended CPP moiety. Green—ELP; red—cell membrane; blue—cell nuclei; scale bars—50 μm. Reproduced from [152].

Quantification of uptake by flow cytometry confirmed the tunable internalization of these CPP-ELP$_{BC}$s. All CPP-ELP$_{BC}$s achieved amplified uptake at 42 °C, as compared to 37 °C, while the control non-functionalized ELP$_{BC}$ showed no difference in uptake between "off" and "on" conditions (Figure 40A). Although amplification of uptake was apparent for all CPP-ELP$_{BC}$s, the amplitude of uptake at "off" and "on" conditions varied significantly as a function of the CPP potency. The fold increase in cellular fluorescence at 42 °C, as compared to 37 °C, demonstrated the control of cellular uptake afforded by each CPP-ELP$_{BC}$ and also shed light on the variation in CPP-ELP$_{BC}$ performance, dependent on the CPP-functionalization (Figure 40B).

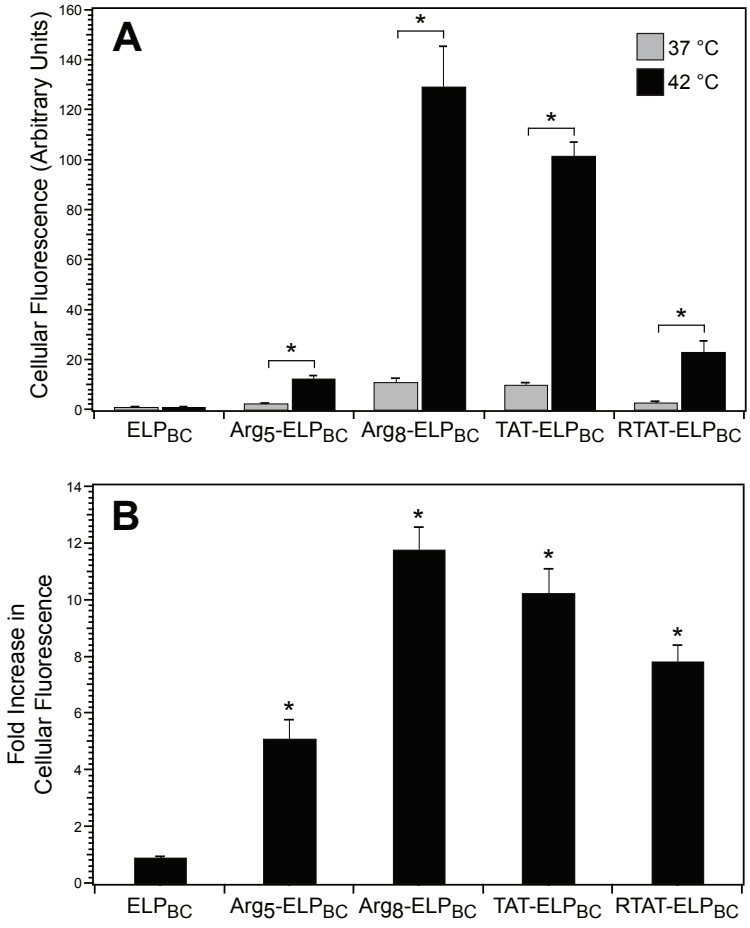

Figure 40: The magnitude of controlled cellular uptake was highly tunable by means of the CPP-functionalization. All CPP-ELP$_{BC}$s achieved greater uptake at 42 °C, as compared to 37 °C, while the non-functionalized ELP$_{BC}$ showed no difference in uptake between thermal conditions (A). *Indicates $p < 0.01$ between thermal conditions (two-way ANOVA, Bonferroni posthoc test for multiple comparisons). Fold increase in cellular uptake between 42 °C and 37 °C demonstrated variability in the controlled cellular uptake that was dependent on CPP functionalization (B). *Indicated $p < 0.0125$ versus ELP$_{BC}$ control (ANOVA, Bonferroni posthoc test for multiple comparisons). Flow cytometry data represents mean of 3 measurements ± SEM. Reproduced from [152].

3.3.4 Mechanism of uptake and intracellular localization of CPP-ELP_{BC}s

Although small CPPs on their own have been suggested to penetrate directly across the cell membrane, the internalization of CPPs appended to the macromolecular ELP carrier should not be expected to do the same. Visualization of internalized CPP-ELP_{BC}s revealed uptake predominantly characterized by punctate fluorescence, suggesting an endocytic route of entry that leads to the entrapment of CPP-ELP_{BC}s in discrete compartments within the cell. There are several generalized means of entering a cell via endocytosis. All of these routes of entry have distinct characteristics, such as the local environment of their intracellular compartments, which may have an effect on how a carrier will function in delivering a therapeutic cargo. For that reason, the mechanism of endocytosis exploited by CPP-ELP_{BC}s was investigated. Mechanisms of uptake including clathrin-mediated endocytosis, macropinocytosis, and caveolae-mediated endocytosis were investigated as potential routes for the internalization of CPP-ELP_{BC}s.

Preliminary investigation of the mechanism of uptake was performed for second generation Arg_5-ELP_{BC} by observing changes in cellular uptake in the presence of endocytosis inhibitors. HeLa cells were co-incubated at 42 °C with Alexa Fluor 488-labeled Arg_5-ELP_{BC} in its micelle state and inhibitors of clathrin-mediated endocytosis (chlorpromazine), macropinocytosis (amiloride), or caveolae-mediated endocytosis (filipin). Uptake was then visualized with fluorescence microscopy. Punctate intracellular fluorescence was observed in chlorpromazine and filipin treated cells, but

very little uptake was evident in amiloride treated cells (Figure 41A). This visual result suggested that macropinocytosis was the primary route of uptake for Arg_5-ELP_{BC} as amiloride, its inhibitor, had the greatest negative effect on uptake. This decrease in uptake was confirmed with flow cytometry, which demonstrated the negative shift in cellular fluorescence in the presence of amiloride, as compared to the other inhibitors that achieved 6-fold higher internalization (Figure 41B). However, DLS of Arg_5-ELP_{BC} in the presence of each of these inhibitors revealed that some were poor choices for this system as they had a tendency to perturb the micelle self-assembly of Arg_5-ELP_{BC} (Figure 41C). Chlorpromazine appeared to perturb the unimer-to-micelle transition such that larger particles were formed prior to the assembly of stable micelles. More drastically, filipin led to a unimer-to-nanoparticle transition in which the self-assembled particles were nearly three times the expected size of the Arg_5-ELP_{BC}s without inhibitor. Only amiloride appeared to have negligible effect on the temperature-triggered Arg_5-ELP_{BC} assembly. Thus, the amiloride data provided useful insight into the potential role of macropinocytosis in Arg_5-ELP_{BC} uptake, but alternative inhibitors were needed to better probe the roles of clathrin-mediated or caveolae-mediated endocytosis.

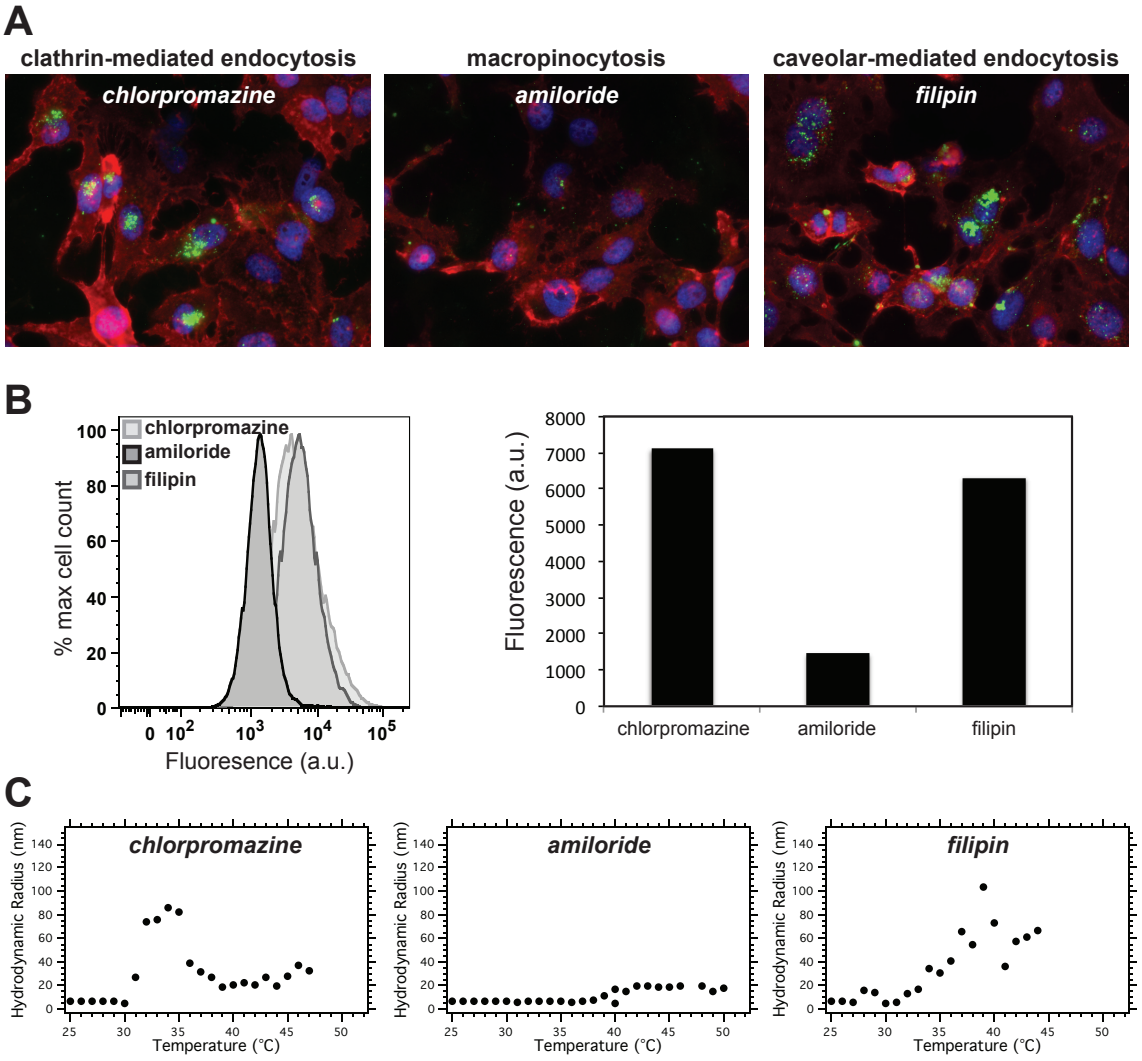

Figure 41: Inhibition of endocytosis pathways suggested the role of macropinocytosis in the uptake of second generation Arg_5-ELP_{BC}. Changes in uptake of Arg_5-ELP_{BC} at 42 °C were visualized with fluorescence microscopy (A) and quantified by flow cytometry (B). Decreased uptake in the presence of amiloride, but not chlorpromazine or filipin, suggested macropinocytosis was the major pathway of Arg_5-ELP_{BC} uptake. However, DLS of Arg_5-ELP_{BC} in the presence of inhibitors revealed that chlorpromazine and filipin perturbed micelle assembly (C).

To better characterize the mechanism of uptake by means of inhibiting endocytic pathways, alternative inhibitors were screened for their effect on temperature-triggered

self-assembly, this time of third generation Arg_5-ELP_{BC} and controls. DLS confirmed that the chosen inhibitors did not perturb assembly as their R_h at 42 °C matched closely to that of their equivalent in the absence of inhibitor (Table 9). The chosen inhibitors were dansylcadaverine, genistein, and amiloride, which are inhibitors of clathrin-mediated endocytosis, caveolae-mediated endocytosis, and macropinocytosis, respectively.

Table 9: R_h (in nm) for CPP-ELP_{BC}s in the absence and presence of endocytosis inhibitors, as measured by DLS.

	Arg_5-ELP_{BC}	**ELP_{BC}**	**Arg_5-ELP**
No Treatment	24.7 ± 0.8 nm	20.7 ± 1.3 nm	5.3 ± 0.4 nm
Dansylcadaverine	23.4 ± 0.5 nm	21.4 ± 0.4 nm	5.7 ± 0.0 nm
Genistein	22.3 ± 0.6 nm	20.3 ± 0.4 nm	5.3 ± 0.0 nm
Amiloride	22.7 ± 0.1 nm	21.1 ± 0.4 nm	5.6 ± 0.1 nm

These inhibitors allowed reliable evaluation of the effect of blocking endocytosis pathways on the uptake of CPP-ELP_{BC}. Cellular fluorescence, as measured with flow cytometry, revealed that dansylcadaverine had little effect on the uptake of Arg_5-ELP_{BC} or controls when co-incubated with HeLa cells at the "on" state of 42 °C (Figure 42A). In contrast, genistein and amiloride both decreased uptake of Arg_5-ELP_{BC} significantly, by 57% and 80%, respectively, as compared to cells treated with Arg_5-ELP_{BC} without inhibitor. These inhibitors did not have a significant effect on the uptake of ELP_{BC} or Arg_5-ELP controls, with the exception of the decrease in uptake by 31% of Arg_5-ELP when co-incubated with amiloride. These results were confirmed visually by confocal microscopy of cells treated with Arg_5-ELP_{BC} at 42 °C in combination with endocytosis

inhibitors. Significantly less intracellular fluorescence was evident in cells treated with amiloride or genistein, as compared to cells treated with dansylcadaverine or treated with Arg_5-ELP_{BC} in the absence of inhibitors (Figure 42B).

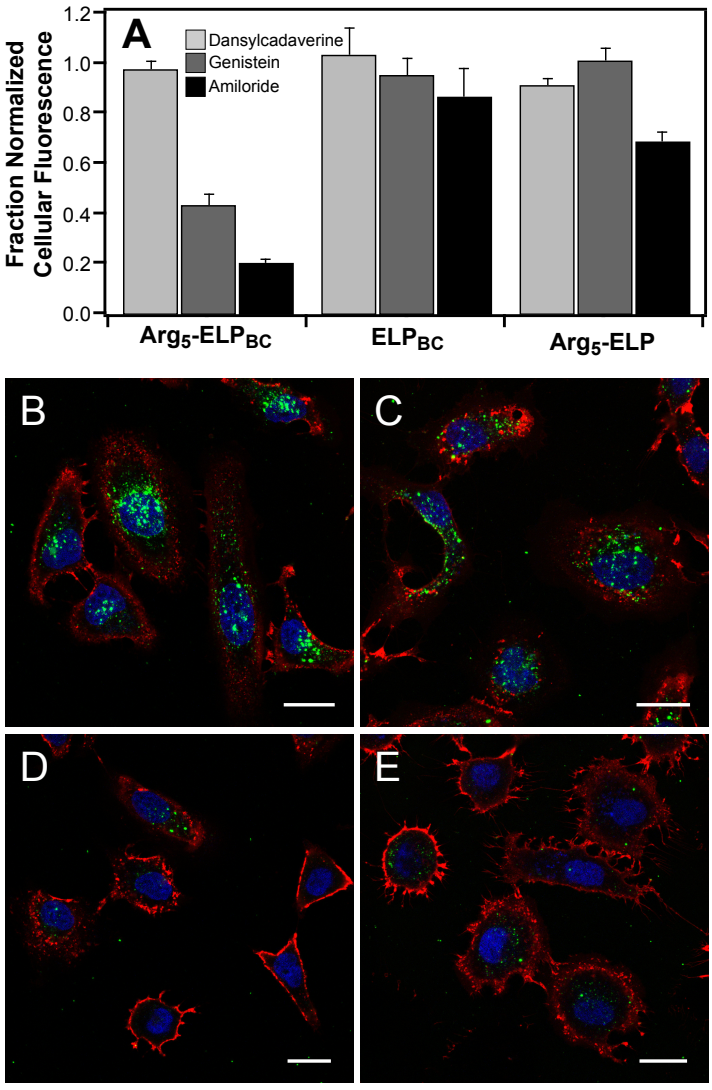

Figure 42: Inhibition of endocytosis pathways suggested the role of macropinocytosis and caveolae-mediated endocytosis in the uptake of third generation Arg_5-ELP_{BC}. Cellular uptake of Arg_5-ELP_{BC} at 42 °C, as measured by cellular fluorescence,

significantly decreased with genistein or amiloride treatment, but not with dansylcadaverine treatment (A). Fluorescence microscopy confirmed that cellular uptake of Arg_5-ELP_{BC} in the absence of inhibitor (B) was largely unperturbed in the presence of dansylcadaverine (C), but greatly decreased in the presence of genistein (D) or amiloride (E). Green—ELP; red—cell membrane; blue—cell nuclei; scale bars 25 μm. Reproduced from [149].

The outcomes of this inhibitor study provided several insights into the route of entry for Arg_5-ELP_{BC} micelles. First, the minimal effect of dansylcadaverine suggested that clathrin-mediated endocytosis, typically associated with receptor-mediated uptake, was not an important route of internalization for Arg_5-ELP_{BC} in its micelle state. Second, the strong effect of amiloride to reduce uptake suggested that macropinocytosis was an important pathway for the uptake of this CPP-ELP_{BC}. This is consistent with reports in the literature that high arginine density directs cellular uptake toward the macropinocytosis pathway [74]. Indeed, we see in our own system that the low arginine density on the Arg_5-ELP control exploits macropinocytosis to some extent, as amiloride also decreased uptake of this soluble unimer construct. The increase in arginine density from Arg_5-ELP unimer to Arg_5-ELP_{BC} micelle appeared to push uptake more toward the macropinocytosis pathway, as evident by the more drastic effect of amiloride on the cellular uptake of Arg_5-ELP_{BC}, as compared to Arg_5-ELP. Finally, it is clear that Arg_5-ELP_{BC} exploits more than one route of cellular entry as demonstrated by the additional effect of genistein on Arg_5-ELP_{BC} uptake, which suggested that caveolae-mediated endocytosis also plays a role in Arg_5-ELP_{BC} micelle internalization.

The results of the inhibitor studies were interesting as they suggested the Arg_5-ELP_{BC} was internalized by mechanisms that may have advantages as routes of intracellular delivery for drug carriers. Primarily, caveolae-mediated endocytosis and macropinocytosis may be less degradative routes of cellular entry, as compared to clathrin-mediated endocytosis. For example, studies have shown that caveolae-mediated endocytosis may avoid, to some extent, lysosomal trafficking [153], while macropinocytosis has been shown to involve leaky macropinosomes that might promote the release of cargo into the cytosol or avoid fusion with lysosome compartments [75]. Together, these pathways present an opportunity for cellular entry that may be less harmful to labile therapeutic cargo, such as biologic drugs, as compared to receptor-mediated uptake via clathrin-mediated endocytosis.

To gain a modest degree of insight on the localization of Arg_5-ELP_{BC} micelles in intracellular compartments, Arg_5-ELP_{BC} was co-incubated with HeLa cells at 42 °C with markers of endocytosis pathways. Lucifer yellow was chosen as a fluorophore that typically accumulates in macropinosomes and Lysotracker Red was chosen as a marker that localizes to lysosomes, classically associated with clathrin-mediated endocytosis. Of note, Lucifer yellow has an excitation/emission spectrum very close to that of Alexa Fluor 488, our ELP label. Therefore, for analysis with Lucifer yellow the Arg_5-ELP_{BC} was attached to an alternative fluorophore, Alexa Fluor 594.

Cellular uptake of Lucifer yellow and Alexa Fluor 594-labeled Arg_5-ELP_{BC} appeared to colocalize strongly within the HeLa cells, indicating the presence of Arg_5-ELP_{BC} in compartments such as macropinosomes (Figure 43). In contrast, the cellular uptake of Lysotracker Red and Alexa Fluor 488-labeled Arg_5-ELP_{BC} appeared to have distinct localization that did not largely overlap in some parts of the cells. These initial results suggested that Arg_5-ELP_{BC}s might, in part, avoid the harsh lysosome environment. However, the most distinctly separate localization of Lysotracker Red and Arg_5-ELP_{BC} appeared to occur in the periphery of the cell, such that this lack of colocalization may just suggest that those intracellular compartments simply had not yet reached their lysosomal endpoint that lies closer to the perinuclear space.

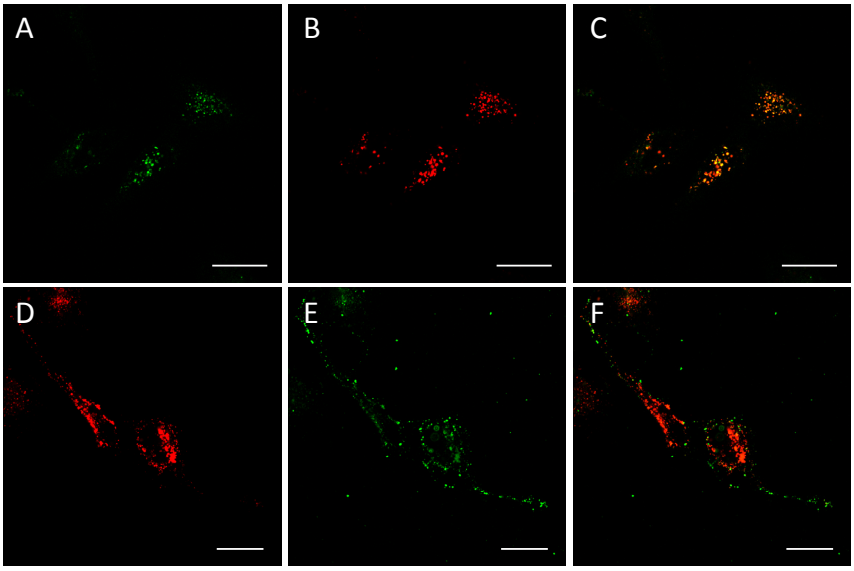

Figure 43: Arg_5-ELP_{BC} micelles co-localized with a macropinocytosis marker, but less significantly co-localized with a marker of lysosomes. Arg_5-ELP_{BC} was incubated with HeLa cells at 42 °C in the presence of markers for macropinocytosis (A-C) or

lysosomes (D-F). Lucifer yellow (A) and Alexa Fluor 594-labeled Arg_5-ELP_{BC} (B) demonstrated intracellular colocalization (C). Lysotracker Red (D) and Alexa Fluor 488-labeled Arg_5-ELP_{BC} (E) demonstrated some separate localization, particularly in the periphery of the cell (F). Scale bars—25 μm.

3.4 Conclusions

We hypothesized that manipulation of CPP density, by means of temperature-triggered micelle assembly, would provide an extrinsic trigger to control cellular uptake by a non-specific mechanism that was thereby applicable to a variety of cell types. To test this hypothesis, CPP-ELP_{BC}s were labeled with a fluorescent tag such that their cellular uptake could be visualized by fluorescence microscopy and quantified by flow cytometry.

First generation CPP-ELP_{BC}s, although not optimized for triggered self-assembly in response to clinically relevant hyperthermia conditions, provided a platform in which to investigate controlled uptake between the "off" condition of 25 °C and the "on" condition of 37 °C. Arg_3-ELP_{BC} was the first CPP-ELP_{BC} whose uptake was investigated in HeLa cells. Difficulty in detecting uptake of this construct by microscopy encouraged the creation of CPP-ELP_{BC}s with increasing arginine content including an Arg_4- and Arg_5-ELP_{BC}. It is with the Arg_5-ELP_{BC} that a striking control in cellular uptake was first observed with microscopy and quantified by flow cytometry. This effect was greatly exaggerated for Arg_5-ELP_{BC}, as compared to ELP_{BC} or Arg_5-ELP controls. However, there were some differences in uptake of these control constructs between "off" and "on" conditions, suggesting that there may have been an unintended side effect of the "off"

state of 25 °C. It is possible that this hypothermic condition generally reduced endocytosis, thus exaggerating the performance of CPP-ELP$_{BC}$s evaluated between 25 °C and 37 °C.

Second generation CPP-ELP$_{BC}$s would provide the first evaluation of this mechanism for controlled uptake using a clinically relevant external trigger, such that the "off" state was at normal physiologic temperature of 37 °C, while the "on" state was in agreement with mild clinical hyperthermia at 42 °C. However, the limited micelle range of these second generation CPP-ELP$_{BC}$s made them highly sensitive to fluorophore conjugation, which would affect the thermal characteristics of these constructs and abolish temperature-triggered self-assembly. Ultimately, it was best to label these constructs with fluorophore at the N-terminal amine, as opposed to the genetically designed cysteine residue, which allowed stable self-assembly with a CMT between 37 °C and 42 °C. Alexa Fluor 488-labeled second generation Arg$_5$-ELP$_{BC}$ demonstrated controlled cellular uptake in HeLa cells, as observed with microscopy and quantified with flow cytometry. At these thermal conditions both ELP$_{BC}$ and Arg$_5$-ELP controls exhibited negligible change in uptake between 37 °C and 42 °C, suggesting that micelle assembly and hyperthermia alone were not responsible for enhanced uptake of Arg$_5$-ELP$_{BC}$, confirming that the change in CPP density triggered the drastic increase in internalization.

Ultimately a more stable construct, less sensitive to modifications such as fluorophore attachment, is desirable as a material platform for drug carriers. Therefore third generation CPP-ELP$_{BC}$s were similarly characterized to demonstrate controlled cellular uptake as visualized by microscopy. Flow cytometry conditions were optimized prior to quantification of uptake in HeLa cells as well as MCF7 and HUVEC cells, demonstrating that controlled cellular uptake was achievable in a variety of cell types, but that the magnitude of uptake was variable and was greater in cancerous cell lines as compared to primary non-cancerous cells. Using third generation ELP$_{BC}$s as a robust material platform, the CPP-ELP$_{BC}$ library was expanded to include alternative CPP-functionalization of Arg$_8$, TAT, and RTAT peptides that all demonstrated controlled cellular uptake with variable magnitudes of internalization both in their "off" and "on" states.

Finally, the mechanism of uptake for Arg$_5$-ELP$_{BC}$s was investigated by inhibition of endocytosis pathways and colocalization with endocytosis markers. Evaluation of both second and third generation Arg$_5$-ELP$_{BC}$s suggested that macropinocytosis was a major endocytic pathway accountable for the internalization of Arg$_5$-functionalized micelles. Caveolae-mediated endocytosis was also indicated as a potential pathway, but clathrin-mediated endocytosis, typical of receptor-mediated uptake, did not appear to be an important pathway for Arg$_5$-ELP$_{BC}$ internalization. Greater colocalization of Arg$_5$-ELP$_{BC}$s with a macropinocytosis marker, as compared to a lysosome marker, suggested

that the intracellular trafficking of Arg_5-ELP_{BC}s might, in part, avoid the degradative environment of the lysosome.

Third generation ELP_{BC}s proved to be a stable material platform that could be functionalized with a number of CPPs to provide controlled cellular uptake that was repeatable and applicable to a number of cell types. The tunable levels of uptake at "off" and "on" conditions, as controlled by CPP-functionalization, provided a variable drug carrier system that could potentially be custom-paired with a therapeutic cargo to meet the needs of that drug in terms of minimizing "off" state uptake to avoid off-target toxicity while providing enhanced "on" state uptake sufficient to induce a therapeutic effect. This functionality of the CPP-ELP_{BC} platform was next tested with two types of therapeutics applicable for anti-cancer therapy: small molecule chemotherapeutics and proapoptotic peptide drugs.

4. Controlled drug delivery by CPP-ELP$_{BC}$s *in vitro*

4.1 Motivation

Successful demonstration of controlled cellular uptake of CPP-ELP$_{BC}$s *in vitro* confirmed that manipulation of CPP density, by micelle self-assembly, could achieve selective internalization in response to an external stimulus. These preliminary experiments demonstrated the ability of CPP-ELP$_{BC}$s as a carrier alone to enter cells in a controlled manner, suggesting any drug cargo associated with these carriers could also be delivered into the cell with the same precision, thereby achieving a therapeutic effect in a controlled fashion. This hypothesis would be tested with drug cargo whose anti-cancer therapeutic effect would be evaluated based on its controlled cytotoxicity in cancer cells.

Two distinct types of anti-cancer drug cargo were investigated with this CPP-ELP$_{BC}$ carrier platform: small molecule chemotherapeutics and proapoptotic peptide drugs. Each drug type had potential advantages and disadvantages in terms of ease of design and drug attachment and their potential for perturbation of the CPP-ELP$_{BC}$ temperature-triggered self-assembly. Furthermore, differences in the potency of each drug type would also contribute to the likelihood of the cargo to achieve controlled therapeutic effect based on the difference in intracellular drug delivery at "off" and "on" conditions.

Small molecule drugs were investigated as a potential cargo due to their prevalence in current cancer treatments and the relative ease in which they could be appended to genetically engineered biopolymers. Inclusion of cysteine residues at precisely controlled locations on the CPP-ELP$_{BC}$ would allow covalent attachment of small molecule drugs via maleimide-functionalized linkers. This approach has been utilized extensively in the Chilkoti laboratory to conjugate hydrophobic chemotherapeutics at one terminus of a soluble pseudorandom ELP, inducing drug-loaded nanoparticle assembly by means of the hydrophobic effect [154]. While this well-established application paves the way in terms of the technical details of small molecule drug attachment, it also provides significant warning of the effect that small molecules can have on ELP self-assembly. For this reason, hydrophobic small molecule drugs were avoided as cargo for CPP-ELP$_{BC}$s, due to the sensitive thermal behavior of this carrier, in hopes to not perturb the optimized CMT of the carrier.

Peptide drugs were chosen as the second potential cargo due to their specificity in targeting therapeutic pathways in cancer cells, their generally poor intracellular uptake as free drug, and their ease with which they can be appended to a recombinant biopolymer carrier. Peptide drugs are a stringent test for CPP-ELP$_{BC}$s, as the delivery of therapeutic peptides remains a major challenge in drug delivery, since peptide drugs typically suffer from limited efficacy due to fast plasma clearance, premature degradation, and difficulty in crossing the cell membrane to reach their intracellular

therapeutic targets [155]. The genetic design of CPP-ELP$_{BC}$s can be modified to encode a peptide drug cargo and a cleavable peptide linker can be embedded between the drug and CPP-ELP$_{BC}$ to provide a mechanism of free drug release within the cell. Peptide drugs also have the potential to perturb ELP$_{BC}$ thermal properties if their sequence encodes residues with extreme characteristics, be it hydrophilicity or hydrophobicity. Indeed a sufficient number of hydrophobic residues localized to one terminus of a hydrophilic ELP homopolymer can also induce self-assembly of nanoparticles [156], reminiscent of those formed with hydrophobic small molecules [154]. Thus, careful attention should be made to the peptide drug's amino acid sequence in predicting its effect on the CPP-ELP$_{BC}$'s optimized CMT.

4.2 Methods

4.2.1 Drug loading of small molecule therapeutics

4.2.1.1 Genetic modification of CPP-ELP$_{BC}$s for small molecule conjugation

CPP-ELP$_{BC}$s were originally designed to include a single cysteine within the N-terminal leader, proximal to the hydrophobic domain. This single cysteine could be used to attach small molecule chemotherapeutics through a maleimide-functionalized linker. However, this single cysteine limited the potential drug loading of these carriers to a maximum of one drug molecule per ELP. To increase the capacity for drug loading, additional cysteine residues were appended to the CPP-ELP$_{BC}$ via a new leader sequence. This leader included eight cysteine residues, each separated by a di-glycine

spacer intended to provide space around each reactive cysteine residue to prevent suboptimal drug conjugation due to steric hindrance between attachment sites. The genetic design of this leader sequence is shown in Table 10, where pertinent residues at this N-terminal functionalization are noted.

Table 10: Genetic design of leader sequence for attachment of small molecule chemotherapeutics to CPP-ELP$_{BC}$s.

N-	Peptide and oligonucleotide sequence
Cys$_8$, Trp	(M) G C G G C G G C G G C G G C G G C G G t atg ggc tgc ggt ggt tgc ggc ggt tgc ggt ggc tgc ggc ggc tgc ggt ggc tgc ggc ggt ac ccg acg cca cca acg ccg cca acg cca ccg acg ccg ccg acg cca ccg acg ccg cca C G G C G G W P tgc ggt ggc tgc ggc ggt tgg ccg gg acg cca ccg acg ccg cca acc ggc

Oligonucleotides encoding this leader sequence were inserted into the PRe-RDL cloning vector, and the N-terminus of the CPP-ELP$_{BC}$ was functionalized by PRe-RDL cloning, as described previously. Successful modification of the CPP-ELP$_{BC}$ was screened by diagnostic digestion and confirmed with plasmid DNA sequencing. Although the thermal properties of this functionalized CPP-ELP$_{BC}$ allowed typical ITC purification by centrifugation above and below the ELP T_t, these CPP-ELP$_{BC}$s had the potential to co-purify contaminants, likely due to their many cysteine residues that could form disulfide bonds with extraneous *E. coli* proteins. To prevent these undesirable interactions, CPP-ELP$_{BC}$s appended to this Cys$_8$ leader were purified in 10 mM TCEP-HCl/H_20 at pH 7, to

break disulfide bonds and release contaminating proteins to be cleared as normally by ITC.

4.2.1.2 Covalent conjugation of gemcitabine small molecule chemotherapeutic

Covalent conjugation of gemcitabine to CPP-ELP$_{BC}$s was performed by Dr. Jayanta Bhattacharyya [157]. Gemcitabine was conjugated to the cysteine(s) genetically engineered at the N-terminus of the hydrophobic domain of the ELP$_{BC}$ by a maleimide-functionalized linker. The reactive acid groups, 3′-OH and 5′-OH, of the gemcitabine molecule were selectively protected with BOC (t-butyloxycarbonyl) to permit specific coupling of a BMPA (N-β-Maleimidopropionic acid) linker only at the reactive gemcitabine amine. EDC (1-Ethyl-3-[3-dimethylaminopropyl]carbodiimide) was added with BMPA to the protected gemcitabine molecule, to attach the –COOH group of the BMPA to the gemcitabine amine via EDC crosslinker. The acid groups of the gemcitabine molecule were deprotected with trifluoroacetic acid prior to reaction of the gemcitabine-BMPA conjugate with the cysteine residue(s) on the CPP-ELP$_{BC}$.

The cysteine(s) on the CPP-ELP$_{BC}$ was reduced by the addition of TCEP-HCl, with excess TCEP in solution then removed by phase transition of the ELP and resuspension in sodium phosphate reaction buffer, to which the reactive gemcitabine-BMPA linker, in methanol, was added. Reaction proceeded overnight to attach the maleimide reactive group of the gemcitabine-BMPA to the sulfydryl group(s) on the CPP-ELP$_{BC}$ cysteine(s), after which methanol in the reaction buffer was evaporated such

that unconjugated gemcitabine-BMPA could be removed by centrifugation of precipitates. The CPP-ELP$_{BC}$-gemcitabine conjugate was then collected by triggering the phase transition, centrifuging to concentrate the ELP pellet, and resuspending the ELP pellet in PBS prior to purification by size-exclusion PD-10 chromatography.

This conjugation strategy using the gemcitabine amide group was chosen as it has been proposed to improve pharmacokinetics compared to the short half-life achieved with conjugation to the acid groups of gemcitabine through ester linkages [158]. Attachment at the amide group may enhance the half-life of the drug by protecting against inactivation by deaminase activity. Although the BMPA linker used here does not impart a practical mechanism of cleavage, ELP-BMPA-gemcitabine conjugates have achieved therapeutic efficacy *in vitro*. It is possible that the inherent degradability of ELPs provides sufficient breakdown of the peptide backbone in the endosome of the cell such that small gemcitabine-conjugated peptides are capable of inducing therapeutic effects, without the encumbrance of the intact macromolecular ELP carrier.

4.2.2 Drug loading of peptide therapeutics

4.2.2.1 Genetic modification of CPP-ELP$_{BC}$s for appending peptide drugs

Peptide drugs, due to their amino acid composition, can be genetically encoded along with the CPP-ELP$_{BC}$ to create a drug-loaded macromolecular carrier in a single recombinant synthesis step. Peptide drugs were encoded at the N-terminus of the CPP-

ELP_{BC}, proximal to the hydrophobic domain, such that they would be sequestered into the micelle core upon self-assembly. Two anti-cancer peptide drugs were investigated as cargo of the CPP-ELP_{BC} drug carrier platform (Table 11).

Table 11: Genetic design of leader sequences encoding anti-cancer peptide drugs.

N-	Peptide and oligonucleotide sequence
H1	(M) G N E L K R A F A A L R D Q I G C G W t atg ggc aac gaa ctg aaa cgt gcg ttt gcg gcg ctg cgt gat cag att ggc tgc ggg tgg ac ccg ttg ctt gac ttt gca cgc aaa cgc cgc gac gca cta gtc taa ccg acg ccc acc P ccg gg ggc
BH3	(M) G Q V G R Q L A I I G D D I N R R Y G t atg ggt cag gtg ggc cgt cag ctg gcg att atc ggc gat gat att aac cgt cgc tat ggc ac cca gtc cac ccg gca gtc gac cgc taa tag ccg cta cta taa ttg gca gcg ata ccg C G W P tgc ggg tgg ccg gg acg ccc acc ggc

The first drug, the H1 peptide, is a c-Myc inhibitor derived from helix-1 of the basic-helix-loop-helix-zipper domain found in c-Myc [159]. The H1 peptide used here is a derivative of wild-type H1, containing F8A and S6A mutations, which purportedly increase c-Myc binding due to increased peptide helicity. H1 can induce an anti-cancer therapeutic effect when it binds to c-Myc and prevents the interaction of this transcription factor with its DNA binding targets. H1 can thus change transcription and protein expression controlled by c-Myc, which is often upregulated in cancers cells, and

lead to cellular instability that culminates in apoptosis. This drug was chosen simply to validate our drug delivery carrier as this peptide drug has functioned successfully with other CPP-ELP systems that utilize pseudorandom ELPs as a macromolecular drug carrier [115].

The second drug, BH3 peptide, corresponds to residues 71-89 of the proapoptotic Bak protein [160, 161]. The BH3 peptide sensitizes cells to apoptosis by inhibiting prosurvival proteins. For example, this BH3 peptide can bind to prosurvival Bcl-x_L [160] and displace the proapoptotic molecules that were neutralized by this Bcl-x_L interaction. These released factors can then contribute to triggering the apoptotic cascade [162]. This BH3 peptide is thereby not the most potent of its class, as it does not directly activate apoptosis, but rather primes a cell toward this death pathway. However, this BH3 peptide has demonstrated efficacy in cancer cells, such as HeLa cells, demonstrating that this perturbation of prosurvival protein function can indeed induce apoptosis [161]. This BH3 peptide was chosen as a therapeutic cargo since it is known to have poor activity as a free drug, which is recovered when it is delivered in assistance with CPP-functionalized carriers [161, 163, 164].

Both of these peptides were feasible candidates as their sequences were not dominated by hydrophobic or hydrophilic character, but were rather a mixture of both types of residues. This was encouraging, in hopes that the mixed qualities of each

peptide would neutralize their effect on the ELP_{BC} and thereby have minimal effect on the CMT.

4.2.2.2 Exploring cleavable linkers with BH3 peptide drug

As would become apparent with preliminary *in vitro* testing, BH3 peptide drug cargo would require release from the ELP carrier within the cell to achieve a therapeutic effect. For this reason, a number of cleavable linkers were investigated to join the BH3 peptide and the ELP carrier. For ease of design and synthesis, only peptide linkers were considered, as they could easily be genetically encoded along with the peptide cargo. As peptides, these linkers are all enzymatically cleavable, providing a mechanism of release when encountering enzymes localized in the endosomes. A number of linkers were chosen for testing to determine which was capable of enzyme-mediated free peptide drug release, while not perturbing the CPP-ELP_{BC} CMT. For those linkers with predominant hydrophobic character, including GFLG and FK linkers, the GCGWPG portion of the leader, otherwise included for consistency with previous constructs, was removed to decrease overall hydrophobicity. The design of peptide drug in combination with cleavable linkers is summarized in Table 12.

Table 12: Genetic design of leaders encoding BH3 peptide drug and enzyme-cleavable linkers.

N-	Linker	Peptide and oligonucleotide sequence
BH3	GFLG	(M) G Q V G R Q L A I I G D D I N R R t atg ggt cag tgt ggc cgt cag ctg gcg att atc ggc gat gat att aac cgt cgc ac cca gtc cac ccg gca gtc gac cgc taa tag ccg cta cta taa ttg gca gcg Y G F L G tat ggc ttt ctg gg ata ccg aaa gac
BH3	FK	(M) G Q V G R Q L A I I G D D I N R R t atg ggt cag gtg ggc cgt cag ctg gcg att atc ggc gat gat att aac cgt cgc ac cca gtc cac ccg gca gtc gac cgc taa tag ccg cta cta taa ttg gca gcg Y F K G tat ttt aaa gg ata aaa ttt
BH3	GGGGG	(M) G Q V G R Q L A I I G D D I N R R t atg ggt cag gtg ggc cgt cag ctg gcg att atc ggc gat gat att aac cgt cgc ac cca gtc cac ccg gca gtc gac cgc taa tag ccg cta cta taa ttg gca gcg Y G G G G G C G W P G tat ggc ggt ggc ggt ggc tgc ggg tgg ccg gg ata ccg cca ccg cca ccg acg ccc acc ggc
BH3	GGG	(M) G Q V G R Q L A I I G D D I N R R t atg ggt cag gtg ggc cgt cag ctg gcg att atc ggc gat gat att aac cgt cgc ac cca gtc cac ccg gca gtc gac cgc taa tag ccg cta cta taa ttg gca gcg Y G G G C G W P G tat ggc ggt ggc tgc ggg tgg ccg gg ata ccg cca ccg acg ccc acc ggc

BH3	RVRR	(M) G Q V G R Q L A I I G D D I N R R t atg ggt cag gtg ggc cgt cag ctg gcg att atc ggc gat gat att aac cgt cgc ac cca gtc cac ccg gca gtc gac cgc taa tag ccg cta cta taa ttg gca gcg Y R V R R G C G W P G tat cgt gtg cgc cgt ggc tgc ggg tgg ccg gg ata gca cac gcg gca ccg acg ccc acc ggc
none	RVRR	(M) G R V R R G C G W P G t atg ggt cgt gtg cgc cgt ggc tgc ggg tgg ccg gg ac cca gca cac gcg gca ccg acg ccc acc ggc

Cleavage of the peptide linker was evaluated *in vitro* by incubation with enzymes that specifically recognized the linker sequence as a cut site and were localized to intracellular compartments that the CPP-ELP$_{BC}$ carrier was likely to encounter. Two such enzymes were evaluated in the cleavage of the RVRR peptide linker: furin and cathepsin B.

Furin reaction buffer was prepared with 100 mM HEPES containing 0.5% TritonX-100, 1 mM $CaCl_2$, and 1 mM 2-mercapto-ethanol at pH 7.5. CPP-ELP$_{BC}$s were incubated with 2 units of Furin in reaction buffer for 6 hours at 37 °C. The reaction was mixed 1:1 with tricine sample buffer containing 2-mercaptoethanol and heated to 95 °C for 2 minutes. Reaction products were separated on a SDS-PAGE 10-20% Tris-tricine gel and stained with $CuCl_2$ to visualize the ELP by negative staining (minimally charged ELPs do not stain well with conventional coomassie staining), washed with water, and subsequently stained with coomassie blue to visualize the released BH3 peptide.

Cathepsin B reaction buffer was prepared with 100 mM potassium phosphate, 15 mM sodium phosphate, 1 mM ethylenediaminetetraacetic acid, 2 mM L-cysteine hydrochloride, and 0.1% (v/v) Brig 35 at pH 6.5. CPP-ELP$_{BC}$s were incubated with 50 units of cathepsin B for 1 hour at 37 °C. Digestion products were visualized by SDS-PAGE as described above.

4.2.3 Evaluation of controlled cytotoxicity

4.2.3.1 Modified *in vitro* cell survival assay

Cells were seeded on 96-well tissue culture treated polystyrene plates. Cells were allowed to adhere for 24 hours before the cells were washed with PBS and incubated with drug-loaded CPP-ELP$_{BC}$ in SF-media. Cells were incubated for 1 hour at 37 °C or 42 °C after which the cells were washed with PBS, provided complete media, and returned to 37 °C for 24-72 hours. Untreated cells and cell media alone were included as controls on each plate.

4.2.3.2 Quantification of cytotoxicity by MTS assay

Cell survival was approximated by the measurement of cell metabolism using the MTS assay. 24-72 hours after treatment, cell titer 96 aqueous non-radioactive cell proliferation solution (MTS) was diluted in cell media and equal amounts were added to each well containing treated cells, untreated cells, or media alone. The cell plate was returned to 37 °C for 15 minutes to 1 hour, until a sufficient color change had occurred. This color change, indicative of reduction of MTS into formazan, was quantified by

absorbance at 490 nm. Treated cell wells were corrected for the signal from media alone and normalized to untreated cells incubated at 37 °C.

4.2.4 Evaluation of the mechanism of therapeutic effect

4.2.4.1 *In vitro* apoptosis assay

HeLa cells were seeded on 12-well tissue culture treated polystyrene plates and were allowed to adhere for 24 hours. Cell media was removed and cells were washed with PBS prior to the addition of CPP-ELP$_{BC}$ drug carrier in SF-media. Cell plates were incubated for 1 hour at 37 °C or 42 °C. The cells were then washed with PBS, provided complete media, and returned to 37 °C for an additional 5 hours.

4.2.4.2 Quantification of apoptosis by caspase activation

Cells were gently removed from the culture surface with 0.05% trypsin/EDTA and analyzed for caspase-3 activity with an EnzChek Caspase-3 Assay Kit #2. Cells were incubated with lysis buffer on ice for 30 minutes and insoluble cell debris was removed by centrifugation at 5,000 RPM for 5 minutes. The cell lysate was incubated with Z-DEVD-R110 substrate for 1 hour and the fluorescent reaction products were quantified by absorbance at 520 nm on a plate reader. Protein content was evaluated in each sample by BCA assay. Caspase-3 activity, as measured by the fluorescent products from the EnzChek assay, was corrected to protein content to compensate for slight variations in cell number between samples. Caspase-3 activity was further normalized to the level of caspase-3 activity seen in untreated cells incubated at 37 °C.

4.3 Results and discussion

4.3.1 Cytotoxicity of CPP-ELP$_{BC}$ carriers alone

Prior to drug loading, the cytotoxicity of CPP-ELP$_{BC}$s without drug cargo was determined by modified survival assay in HeLa cells to confirm that the carrier alone did not contribute significantly to cell death. Third generation Arg$_5$-ELP$_{BC}$ and Arg$_8$-ELP$_{BC}$, along with the non-functionalized ELP$_{BC}$ control, were chosen to evaluate the cytotoxicity of CPP-ELP$_{BC}$s as these constructs spanned the breadth of both CPP charge and CPP-ELP$_{BC}$ uptake and would thereby provide insight into the cytotoxicity of the complete CPP-ELP$_{BC}$ library.

None of the CPP-ELP$_{BC}$s or the ELP$_{BC}$ control induced significant cell death, as approximated by absorbance at 490 nm, as compared to untreated controls, at either 37 °C or 42 °C in this modified survival assay (Figure 44). Additionally, untreated cells incubated at 37 °C or 42 °C showed no significant difference in cell survival between these thermal conditions, confirming that mild hyperthermia alone had no effect on cytotoxicity in the context of this *in vitro* survival assay. These results confirm that any cytotoxicity detected from drug-loaded CPP-ELP$_{BC}$s in the format of this assay is inherent to the drug cargo and not the drug carrier.

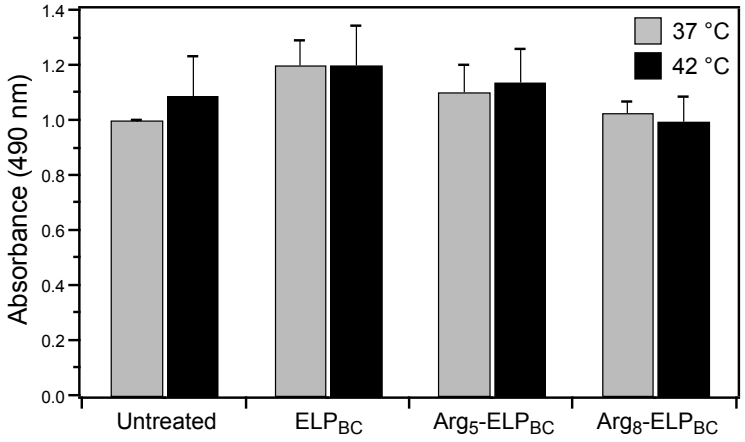

Figure 44: CPP-ELP$_{BC}$s alone did not induce cell death in a modified assay of cell survival. Cell survival, approximated from absorbance at 490 nm, did not change between 37 °C and 42 °C for CPP-ELP$_{BC}$ carriers without drug cargo or for treatment with mild hyperthermia alone. Absorbance was normalized to untreated cells incubated at 37 °C. Data represents mean of 3 experiments ± SEM. Reproduced from [152].

4.3.2 CPP-ELP$_{BC}$s as drug carriers for small molecule therapeutics

Small molecule therapeutics were investigated as drug cargo due to their applicability to anti-cancer therapy and their ease of attachment to ELPs due to prerequisite expertise in the Chilkoti laboratory. Small molecules, however, had shown their power in influencing the self-assembly of ELPs [154, 157] and therefore their effect on the thermal behavior of the optimized CPP-ELP$_{BC}$s was a primary concern. The small molecule chemotherapeutic cargo for CPP-ELP$_{BC}$s was thus carefully chosen.

Gemcitabine was chosen to investigate the feasibility of small molecule chemotherapeutic cargo for CPP-ELP$_{BC}$s due to the following reasons. First, the relative hydrophilicity of gemcitabine (LogD ~ -2.2 [157]) may not alter the thermal properties of the ELP$_{BC}$, unlike hydrophobic drugs whose conjugation induces the self-assembly of

ELP micelles by the hydrophobic effect [154]. This was supported by previous experiments by Dr. Jayanta Bhattacharyya in which the conjugation of 8 gemcitabine molecules to C-terminal cysteine residues on a pseudorandom hydrophilic ELP did not induce premature self-assembly into ELP micelles nor significantly perturb the T_t of the parent ELP [157]. These results suggested that gemcitabine, when conjugated to the hydrophobic terminus of an ELP_{BC}, may indeed leave the thermal properties of that ELP_{BC} unchanged, maintaining a CMT controlled by the T_t of the hydrophobic ELP_{BC} domain.

The second reason for selecting gemcitabine as a small molecule chemotherapeutic cargo is due to its therapeutic action within the cell. Gemcitabine is a nucleoside analog whose cytotoxicity derives from its replacement of cytidine in DNA replication and its inhibition of the enzyme ribonucleoside reductase, which interferes with DNA and deoxyribonucleotide synthesis, respectively [165]. The cytotoxicity of gemcitabine relies on its cellular internalization and intracellular activation by phosphorylation [165], which makes it an ideal candidate to be delivered by efficiently internalized CPP-ELP_{BC} carriers. Furthermore, although small molecules are typically well internalized into cells on their own, traversing the cellular membrane with ease, this may be less true for gemcitabine due to its hydrophilic nature, as compared to the many hydrophobic small molecule drugs. Gemcitabine may thereby gain an additional advantage by efficient delivery into the cell by a CPP-ELP_{BC} carrier.

Third, gemcitabine was also chosen due to its applicability to relevant cancer targets. Gemcitabine has been indicated in the treatment of pancreatic, bladder, and breast cancers [166-168]. These prospective cancer targets are particularly suited to our proposed system as they are all suitable for concurrent treatment with localized clinical hyperthermia [8].

Finally, gemcitabine is an interesting drug cargo for temperature-targeted CPP-ELP$_{BC}$ delivery because treatment with gemcitabine in combination with hyperthermia has been shown to synergistically improve the efficacy of gemcitabine both *in vitro* [169] and in the clinic [170]. Therefore the inherent aspect of heating used to target our CPP-ELP$_{BC}$s may increase the local efficacy of a gemcitabine drug cargo.

Preliminary investigation of a CPP-ELP$_{BC}$ gemcitabine conjugate (CPP-ELP$_{BC}$-GEM) was investigated in a simplified drug carrier system. This carrier, E4-60/E2*-60, was chosen due to its CMT below body temperature and its incorporation of only a single cysteine residue at its N-terminus. This CPP-ELP$_{BC}$ thereby permitted the investigation of drug delivery by self-assembled micelles at 37 °C and limited the drug loading to a maximum of one drug molecule per ELP. The behavior of this carrier thus allowed characterization of drug delivery without involving new effects of hyperthermia and high drug loading. Gemcitabine was attached to Arg$_8$-ELP$_{BC}$ with a conjugation efficiency of approximately 87%, as determined by MALDI-TOF of carrier with and without gemcitabine cargo. Thermal characterization of Arg$_g$-ELP$_{BC}$-GEM by

temperature-regulated turbidimetry revealed an increase in CMT upon drug conjugation (Figure 45). This is not surprising, in that the attachment of hydrophilic drug may increase the T_t of the proximal hydrophobic ELP domain and may also provide resistance to self-assembly as it does not prefer to be sequestered into the hydrophobic micelle core, thereby increasing the CMT. However, this increase in CMT was not so extreme as to interfere with self-assembly at the thermal condition of 37 °C, therefore this drug conjugate could be used to test the cytotoxicity of Arg_8-ELP_{BC}-GEM micelles at physiologic conditions.

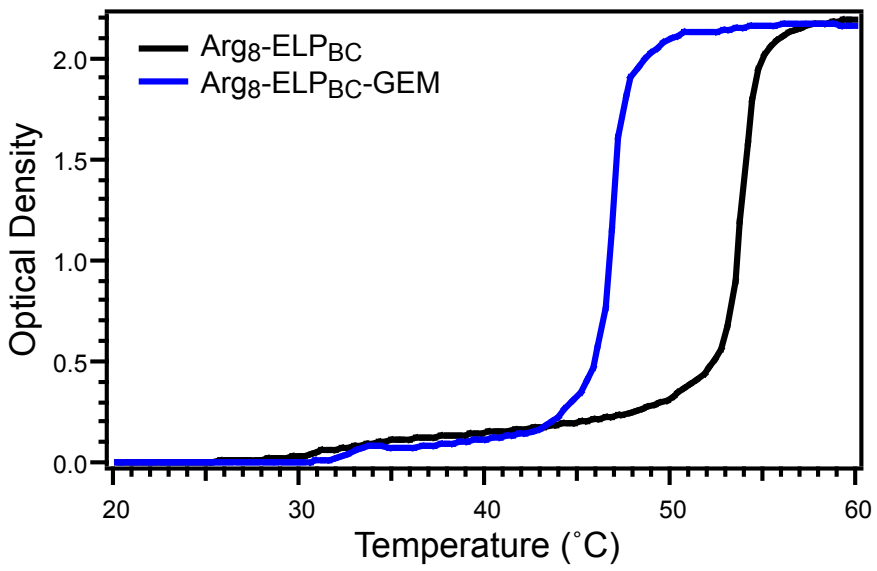

Figure 45: Gemcitabine conjugation increased the CMT of Arg_8-ELP_{BC}. Temperature-regulated turbidimetry confirmed a change in thermal behavior between Arg_8-ELP_{BC} and Arg_8-ELP_{BC}-GEM, whereby drug conjugation increased the CMT and decreased the micelle-to-aggregate T_t. Turbidimetry measurements were acquired at 25 μM in PBS.

This Arg_8-ELP_{BC}-GEM carrier was evaluated for anti-cancer efficacy by measurement of cytotoxicity in gemcitabine sensitive HCT116 colon carcinoma cells [171]. A modified cell survival assay was performed, in which adherent cells were incubated with Arg_8-ELP_{BC}-GEM or free gemcitabine at 37 °C for 1 hour. After this incubation the drug treatment was removed and cells were provided fresh media and returned to 37 °C. After 72 hours cell survival was approximated by measurement of cell metabolism using an MTS assay. This modified survival assay includes an abbreviated exposure to drug as compared to typical survival assays in which the cells are exposed to drug over a total of 72 hours. Therefore this modified assay was a stringent test for CPP-ELP_{BC}s to deliver drug in only 1 hour to provide a prolonged therapeutic effect, reminiscent of the *in vivo* setting in which 1 hour of clinical hyperthermia will be used to achieve intracellular drug delivery of CPP-ELP_{BC}s in the tumor, after which extracellular CPP-ELP_{BC}s will be cleared.

In vitro, Arg_8-ELP_{BC}-GEM achieved increasing cytotoxicity, approximated by absorbance at 490 nm, with increasing concentration from 20-100 μM gemcitabine (equivalent CPP-ELP_{BC} concentration of 23-115 μM based on drug conjugation efficiency) (Figure 46). In comparison, free gemcitabine had little effect on cell survival over this range of concentrations. This may in part be due to the inefficiency of intracellular delivery of this free drug, suggesting this hydrophilic small molecule does not traverse the cell membrane significantly over the course of only 1 hour. Due to this

modified cell survival assay, it is difficult to compare the efficacy of Arg_8-ELP_{BC}-GEM to that of free gemcitabine reported in the literature (IC_{50} ~14 nM [171]) and determine what effect the carrier has on the drug function, whereby covalent attachment of drug via non-cleavable linkers will typically significantly decrease the drug activity. However, the cancer cell death achieved in even the limited exposure used in this modified assay provided motivation to investigate this drug cargo with hyperthermia-responsive CPP-ELP_{BC}s.

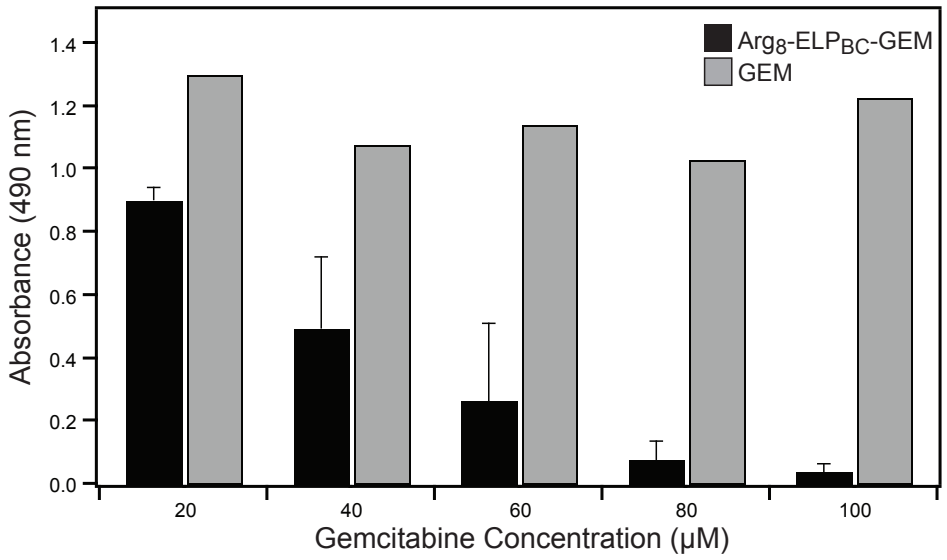

Figure 46: Arg_8-ELP_{BC}-GEM enhanced cytotoxicity, approximated by absorbance at 490 nm, of free gemcitabine in a modified cell survival assay in HCT116 colon carcinoma cells. Drug delivery over the course of just 1 hour produced significant cancer cell death with Arg_8-ELP_{BC}-GEM, but not free drug. Absorbance was normalized to untreated cells. Arg_8-ELP_{BC}-GEM data represents mean of 3 samples ± SEM.

Next, the third generation CPP-ELP_{BC}s were investigated as drug carriers for gemcitabine to determine if this drug cargo could achieve controlled cytotoxicity by

means of controlled intracellular delivery with hyperthermia-triggered micelle assembly. Gemcitabine was conjugated to third generation Arg_5-ELP_{BC}, Arg_8-ELP_{BC}, and non-functionalized ELP_{BC}, all with a single genetically engineered cysteine. Since an increase in the CMT was previously seen with gemcitabine conjugation of CPP-ELP_{BC}, the thermal behavior of these third generation CPP-ELP_{BC}-GEM conjugates were checked by DLS, to determine the unimer and micelle populations at 37 °C and 42 °C, over a range of concentrations. Analysis of the thermal behavior of ELP_{BC}-GEM confirmed an increase in CMT, whereby distinct unimer and micelle populations were not achieved at 37 °C and 42 °C, respectively, at the concentration range utilized in previous *in vitro* experiments (10-20 μM). At an increased concentration range of 30-50 μM, the ELP_{BC}-GEM carrier began to display temperature-triggered micelle assembly, but of a mixed population of unimer and micelle at 42 °C (Figure 47). It was not until an elevated concentration of 60 μM that a pure population of unimer and micelle were achieved at 37 °C and 42 °C, respectively. Therefore treatment concentrations of 60 μM and higher would be necessary to truly elucidate the effect of triggered micelle assembly on controlled drug delivery and controlled cytotoxicity.

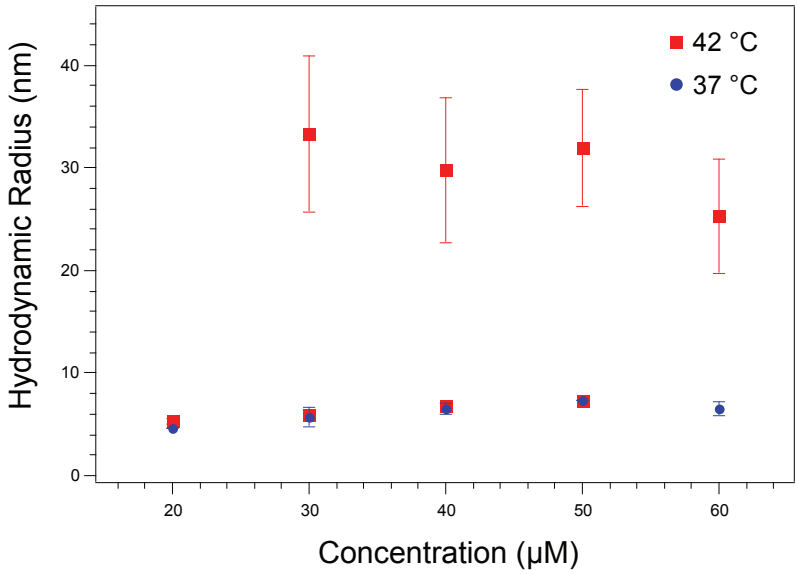

Figure 47: Gemcitabine conjugation increased the CMT of third generation ELP$_{BC}$-GEM. A minimum concentrations of 60 μM was necessary to achieve a pure population of unimer or micelle at 37 °C or 42 °C, respectively. DLS data was acquired in PBS and represents the mean of 3 measurements ± SEM.

Controlled cytotoxicity was investigated with third generation CPP-ELP$_{BC}$-GEM in CFPAC-1 cells. This change in cell type was made to help with the high concentrations of drug carrier necessary to evaluate the unimer and micelle conditions, since CFPAC-1 cells have a reported decreased sensitivity to gemcitabine (IC_{50} ~ 1 μM [172]). Cells were treated with 60 μM at 37 °C or 42 °C for 1 hour, per the modified survival assay described previously. No significant differences in cell survival, as approximated from absorbance at 490 nm, were seen between 37 °C and 42 °C for Arg$_5$-ELP$_{BC}$-GEM, Arg$_8$-ELP$_{BC}$-GEM, or ELP$_{BC}$-GEM control (Figure 48). Approximately 20% of cells were surviving at the end of this assay, regardless of treatment type. This residual cell population may represent those cells with decreased sensitivity to gemcitabine or

may represent those cells that did not take up a significant amount of the drug carrier. The 72 hour duration of this assay could allow either of such cell populations to proliferate and constitute the signal suggesting a 20% cell survival.

There are two possible explanations for the lack of controlled cytotoxicity. The first possibility is that temperature-triggered micelle assembly did not affect the amount of drug delivered into the cell to the extent of producing a difference in cell survival. The second possibility is that, regardless of differences in intracellular delivery, the amount of drug taken up into the cells at either thermal condition was enough to dominate a cytotoxic effect. There was no difference in cell survival between thermal conditions with the treatment of free gemcitabine and in this cell line free gemcitabine was significantly cytotoxic at 60 μM, equivalent to the CPP-ELP$_{BC}$ delivered drug. This suggests that in the context of this modified survival assay CFPAC-1 cells are more sensitive to gemcitabine than the HCT116 cells used previously, contrary to their reported sensitivity in standard survival assays in the literature. The equivalence in cytotoxicity between all CPP-ELP$_{BC}$ drug conjugates and free drug suggest that the latter of the two explanations above may be the reason for the lack of controlled cytotoxicity seen here, where enough drug was delivered into the cells in all cases that the cytotoxic effect was overwhelming. This phenomenon sheds light on the true disadvantage of the increased CMT caused by drug conjugation, forcing the use of CPP-ELP$_{BC}$-GEM at high concentrations.

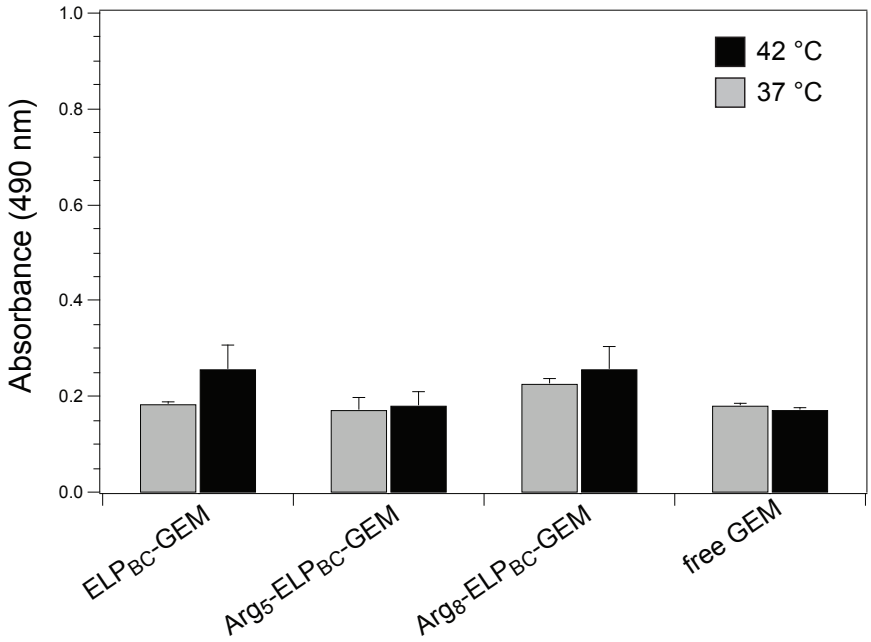

Figure 48: Equivalent cytotoxicity, as approximated by absorbance at 490 nm, was achieved with CPP-ELP$_{BC}$-GEM and free GEM, regardless of thermal conditions at 60 μM in CFPAC-1 cells. Neither Arg$_5$-ELP$_{BC}$-GEM, Arg$_8$-ELP$_{BC}$-GEM, or ELP$_{BC}$-GEM achieved controlled cytotoxicity with temperature-triggered micelle assembly. Absorbance was normalized to untreated cells at 37 °C. Data represents mean of 3 samples ± SEM.

To see if controlled cytotoxicity emerged at other concentrations, the cytotoxicity of these CPP-ELP$_{BC}$-GEM carriers was investigated over a range of concentrations, now in HeLa cells, even less vulnerable to gemcitabine (IC_{50} ~ 26.8 μg/mL [173]), in hopes of mitigating the necessary use of high drug concentration. Interestingly, ELP$_{BC}$-GEM showed little difference in cytotoxicity, approximated from absorbance at 490 nm, as compared to free gemcitabine and did not change significantly between thermal conditions, suggesting uptake did not change significantly with this control carrier (Figure 49). However, neither Arg$_5$- or Arg$_8$-ELP$_{BC}$-GEM demonstrated a consistent trend

in cytotoxicity of unimer versus micelle at 37 °C and 42 °C, respectively. Although neither CPP-ELP$_{BC}$-GEM conjugate demonstrated consistent controlled cytotoxicity, it was interesting that Arg$_5$-ELP$_{BC}$-GEM did consistently produce increased cytotoxicity as compared to Arg$_8$-ELP$_{BC}$-GEM. This suggested that the predictable uptake, controlled by CPP-functionalization, was also perturbed in this set of gemcitabine-loaded drug carriers.

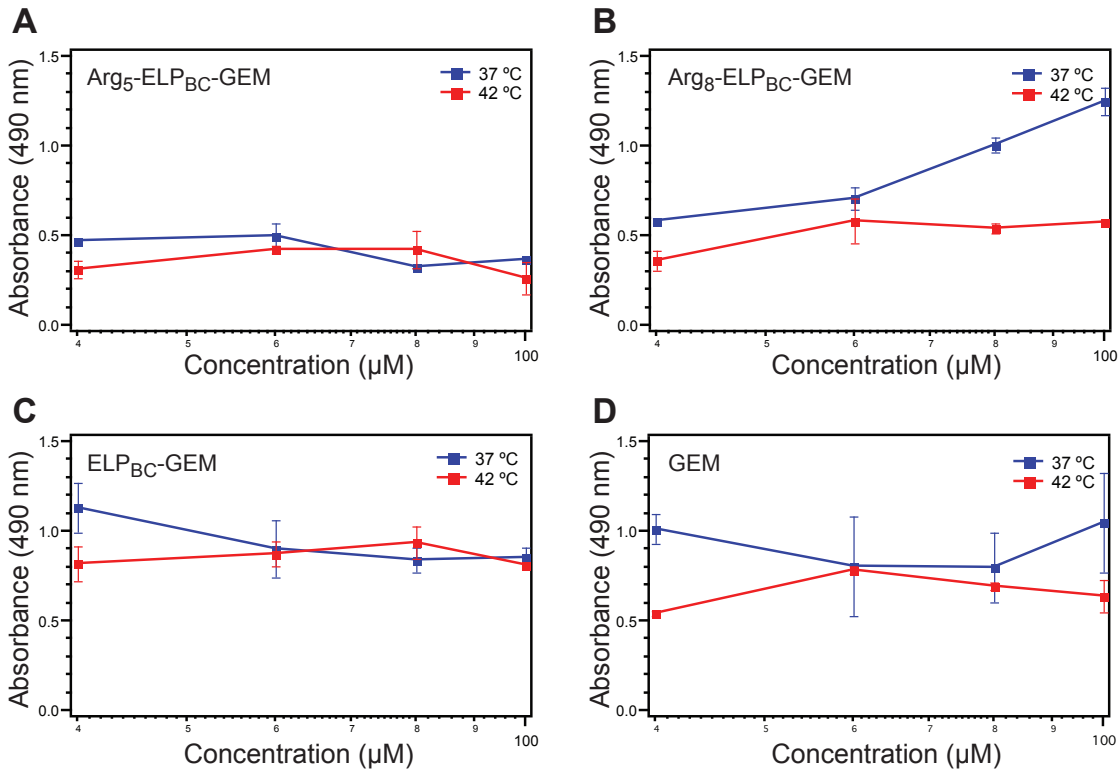

Figure 49: No consistent trends in controlled cytotoxicity, approximated from absorbance at 490 nm, were seen with CPP-ELP$_{BC}$-GEM carriers in HeLa cells. Free gemcitabine and ELP$_{BC}$-GEM control displayed little difference in cytotoxicity between 37 °C and 42 °C, but controlled cytotoxicity did not emerge for Arg$_5$-ELP$_{BC}$-

GEM or Arg_8-ELP_{BC}-GEM between thermal conditions. Absorbance was normalized to untreated cells at 37 °C. Data represents mean of 3 measurements ± SEM.

Despite a lack of cytotoxic control with drug loading of a single gemcitabine molecule for each CPP-ELP_{BC}, more heavily drug loaded constructs were characterized to better understand the effects of drug conjugation on ELP_{BC} thermal properties. To increase the amount of drug loading per ELP_{BC} a new leader sequence—$MG(CGG)_8WPG$—was genetically appended to the hydrophobic terminus of the ELP_{BC}, providing eight reactive cysteine residues for conjugation of small molecule chemotherapeutics. The effects of encoding additional cysteine residues at the CPP-ELP_{BC} hydrophobic terminus on self-assembly were examined by temperature-regulated turbidimetry measurements, which revealed a decrease in the CMT with the addition of eight cysteine residues (Figure 50). This was not surprising as the interaction between cysteines likely encouraged the interaction between ELP_{BC}s, which lowered the transition temperature of the hydrophobic ELP_{BC} domain. Conjugation of gemcitabine to this Arg_5-ELP_{BC} yielded an average conjugation of 5.4 gemcitabine molecules per CPP-ELP_{BC}, occupying approximately 68% of the cysteine residues on each CPP-ELP_{BC}. Conjugation of gemcitabine to this CPP-ELP_{BC} did not greatly perturb the CMT of the $MG(CGG)_8WPG$-functionalized ELP_{BC}, suggesting that the cysteines that remain free after drug conjugation (approximately 2.6 per ELP_{BC}) may continue to exert their effects on self-assembly after the conjugation reaction. This effect currently limits the possibility to test this conjugate effectively in our standard conditions, as in this state the drug

conjugate exists as a micelle at 37 °C, eliminating its useful triggered self-assembly between 37 °C and 42 °C at realistic ELP concentrations.

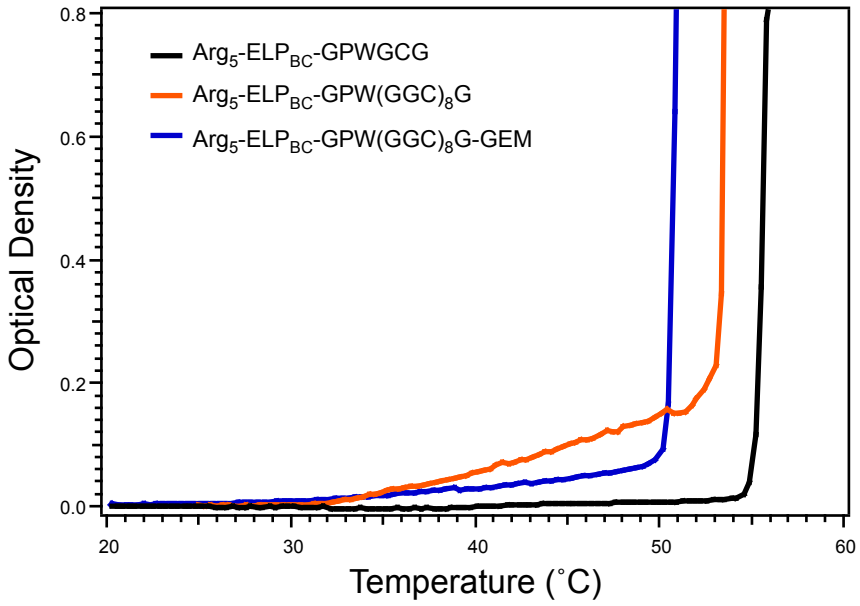

Figure 50: Genetically appending a drug conjugation domain with 8 cysteine residues lowered the CMT of third generation Arg$_5$-ELP$_{BC}$. The CMT was not significantly changed with the conjugation of approximately 5 gemcitabine molecules to each Arg$_5$-ELP$_{BC}$. This decrease in CMT, below 37 °C, precluded the use of this carrier with increased drug loading for mild hyperthermia-controlled delivery. Turbidimetry measurements were acquired at 25 μM in PBS.

These preliminary results with CPP-ELP$_{BC}$s and small molecule cargo suggested a great deal of material optimization was needed to ensure that the desired thermal properties of the CPP-ELP$_{BC}$ were achieved after drug loading. This would be necessary to ensure that a reasonable concentration of CPP-ELP$_{BC}$ and drug cargo could be delivered with the desired thermal behavior. Since extensive optimization was already invested in the third generation CPP-ELP$_{BC}$ constructs, it was most practical to turn

attention to a different drug cargo that could perhaps exploit the CPP-ELP$_{BC}$ platform that was readily available. Thus, due to the complexities of small molecule conjugation and the desired preservation of the precisely tuned thermal properties of the ELP$_{BC}$, the alternative drug cargo of peptide therapeutics was investigated with the third generation CPP-ELP$_{BC}$s.

4.3.3 CPP-ELP$_{BC}$s as drug carriers of peptide therapeutics

Peptide drugs are an alternative cargo for conjugation to CPP-ELP$_{BC}$s with several advantages over small molecule chemotherapeutics. First, peptide drugs are extremely easy to conjugate to the CPP-ELP$_{BC}$. The peptide drug is simply genetically encoded at the N-terminus of the ELP$_{BC}$ gene and the drug conjugate can thereby be created with perfect drug loading and monodispersity in a single recombinant synthesis step. Second, the composition of the peptide drug from natural amino acid constituents makes it easier to predict the effect of peptide drug on ELP properties based on the well-known effects of each amino acid on the ELP thermal behaviors, at least as guest residue components of the polypeptide chain. These predictive behaviors may be more reliable than the largely unknown effects of covalently attached molecules based on their size and hydrophobicity, as well as that of their intervening linker between the drug and ELP. For these reasons it is likely that peptide drug cargo will be more amenable to conserving the optimized thermal properties of CPP-ELP$_{BC}$s, as compared to small molecule drug cargo.

Preliminary investigation of peptide cargo was performed with a drug that had been previously validated by a CPP-ELP drug delivery system [115]. This H1 peptide, a c-Myc inhibitor, was appended to third generation Arg_5-ELP_{BC}. DLS measurements of Arg_5-ELP_{BC}-H1 confirmed that a concentration of greater than 20 μM was required to achieve desirable temperature-triggered self-assembly, such that the drug carrier was a unimer at 37 °C and a micelle at 42 °C. The controlled cytotoxicity of this peptide-loaded construct was evaluated in MCF7 breast cancer cells, in the same modified survival assay employed for evaluation of small molecule drugs described above. Arg_5-ELP_{BC}-H1 demonstrated controlled cytotoxicity, approximated from absorbance at 490 nm, over the concentration range of 20-100 μM (Figure 51). Cytotoxicity was much greater at 42 °C with the delivery of micelle drug carrier, as compared to unimer carrier at 37 °C. Cytotoxicity increased with concentration at 42 °C and to a lesser extent at 37 °C. The controlled cytotoxic effects of this construct confirmed those results in the literature for CPP-ELP-H1 carrier [115], although higher concentrations of the CPP-ELP_{BC} was needed, likely due to differences in CPP-functionalization that led to both differences in drug uptake and differences in the inherent toxicity of the carrier itself. This preliminary evaluation of peptide drug cargo confirmed that CPP-ELP_{BC}s could indeed control cytotoxicity by controlling cell uptake of anti-cancer peptide therapeutics.

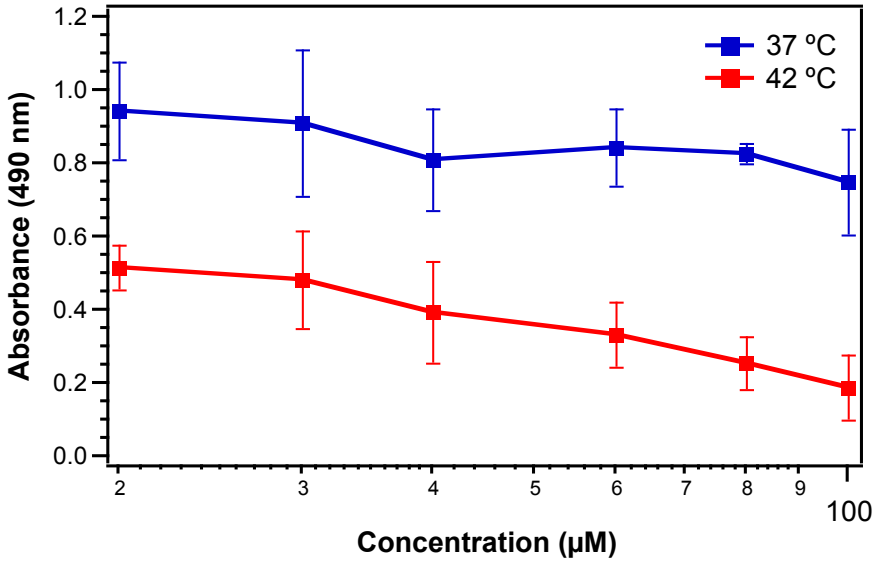

Figure 51: Arg$_5$-ELP$_{BC}$-H1 achieved controlled cytotoxicity, approximated from absorbance at 490 nm, in MCF7 breast cancer cells. Cell killing was enhanced at 42 °C with the delivery of CPP-ELP$_{BC}$ micelles as compared to the delivery of CPP-ELP$_{BC}$ unimers at 37 °C. Absorbance was normalized to Arg$_5$-ELP$_{BC}$ without drug cargo. Data represents mean of 3 measurements ± SEM.

An anti-cancer peptide drug new to ELP delivery was next investigated as a cargo of CPP-ELP$_{BC}$s to demonstrate the flexibility of this platform to accommodate other peptide therapeutics. The BH3 peptide, derived from the Bak protein, was chosen as a proapoptotic therapeutic for anti-cancer applications. The BH3 peptide was suitable for delivery with CPP-ELP$_{BC}$s for several reasons. First, its sequence, like that of H1, was a mixture of residues with variable qualities, not swayed to a distinct hydrophobic or hydrophilic content suggesting it could be incorporated into the ELP$_{BC}$ design without detrimental effects on thermal behavior. Second, this peptide had shown cytotoxicity in HeLa cells, in which uptake of CPP-ELP$_{BC}$s had been extensively validated. This efficacy in HeLa cells, however, was only apparent when BH3 delivery was facilitated with a

CPP-functionalized carrier. Finally, the internal therapeutic target of BH3 suggested that this peptide could be greatly improved by the efficient cellular uptake afforded by CPP-ELP$_{BC}$s, only when targeted by hyperthermia-triggered micelle assembly.

Delivery of BH3 peptide drug was first evaluated with Arg$_5$-ELP$_{BC}$-BH3, similar to that for delivery of H1 peptide described above. Unlike H1, however, the delivery of BH3, even up to 80 μM, showed little controlled cytotoxicity, approximated from absorbance at 490 nm, between thermal conditions and indeed showed little cytotoxicity in general despite increasing drug concentrations (Figure 52). Since activity of this drug against this cell line was well supported in the literature, this result suggested two potential problems with the Arg$_5$-ELP$_{BC}$ delivery system. The first potential problem could be that the steric hindrance of the macromolecular CPP-ELP$_{BC}$ carrier disrupted the interaction of BH3 with its therapeutic target. This problem could be alleviated with the incorporation of a cleavable linker between the peptide drug and the ELP. The second potential problem could be the delivered amount of drug if the extent of internalized Arg$_5$-ELP$_{BC}$ did not fulfill the necessary dose to induce a therapeutic effect. This problem could be alleviated by testing alternative CPP-ELP$_{BC}$ carriers, whose degree of cellular uptake could be tuned by their CPP-functionalization.

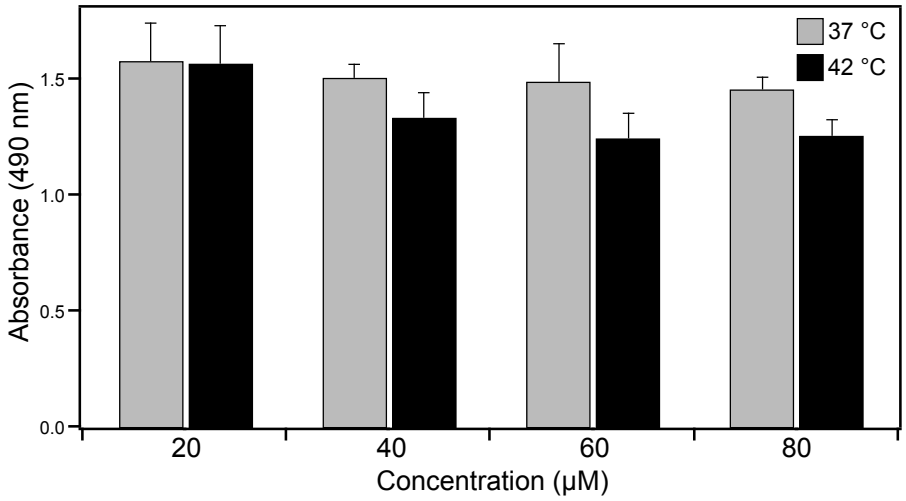

Figure 52: Arg$_5$-ELP$_{BC}$-BH3 failed to achieve significant cytotoxicity, approximated from absorbance at 490 nm, in HeLa cells. Neither micelle assembly at 42 °C nor increasing concentration induced significant changes in cytotoxicity. Absorbance was normalized to untreated cells at 37 °C. Data represents mean of 3 measurements ± SEM.

To address the first issue, cleavable linkers were investigated for use with this BH3 peptide drug cargo. Peptide linkers were easiest to employ since they could be genetically engineered between the peptide drug and ELP. Furthermore, peptide linkers were appropriate as many are cleavable by enzymes that CPP-ELP$_{BC}$s are likely to encounter in the endosomal compartment when internalized. Of common peptide cleavable linkers, many are high in hydrophobic character and it was unclear whether the strong hydrophobicity of the linker would perturb self-assembly of the CPP-ELP$_{BC}$. Preliminary incorporation of the commonly used GFLG [174] and FK [175] linkers, cleavable by cathepsin B, confirmed that their hydrophobicity, attributed to phenylalanine in combination with leucine or alone, did perturb the self-assembly of Arg$_5$-ELP$_{BC}$ (Figure 53). It is likely that the incorporation of these hydrophobic linkers

induced premature assembly, pushing the CMT below 25 °C. This is not completely unexpected, as a higher number of hydrophobic residues like phenylalanine have been used to induce spontaneous self-assembly of ELPs by asymmetric conjugation similar to that of hydrophobic small molecule drugs [156].

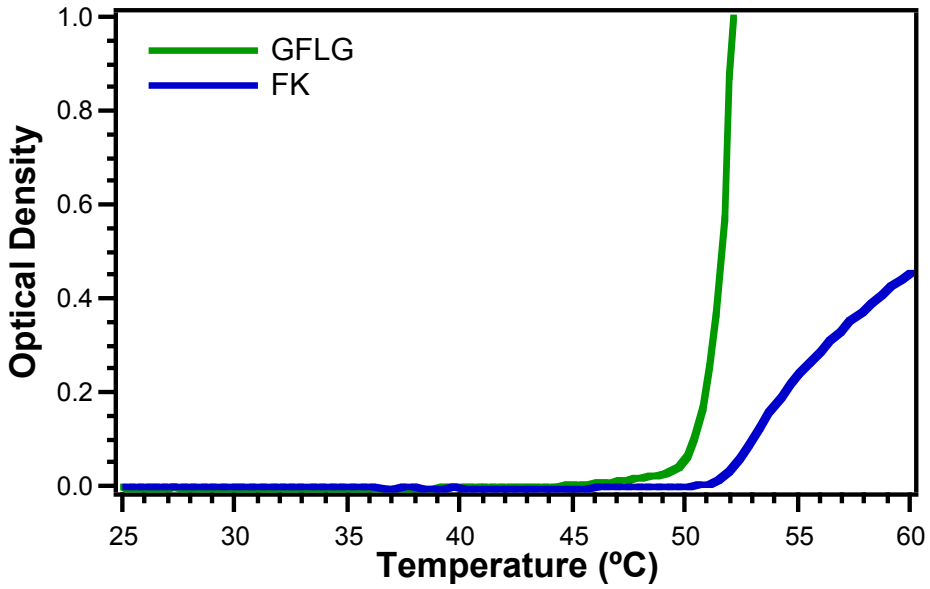

Figure 53: Hydrophobic cleavable linkers GFLG and FK significantly changed the thermal behavior of Arg$_5$-ELP$_{BC}$-BH3. The hydrophobicity of these linkers perturbed the CMT, such that they no longer achieved unimer and micelle conditions at 37 °C and 42 °C, respectively. Turbidimetry measurements were acquired at 15 μM in PBS.

Due to the significant effect of hydrophobic linkers on the self-assembly of Arg$_5$-ELP$_{BC}$-BH3, alternative linkers with more neutral or hydrophilic character were investigated. RVRR, cleavable by furin and cathepsin B [176-178], was investigated as a relatively hydrophilic linker and glycine oligomers GGG and GGGGG, cleavable by cathepsin B [179], were investigated as relatively neutral linkers. These alternative

linkers were genetically encoded between the Arg_8-ELP_{BC} and the BH3 peptide drug and their thermal properties were evaluated by temperature-regulated turbidimetry. Contrary to the hydrophobic linkers GFLG and FK, these alternative linkers did not significantly affect the thermal behavior of the Arg_8-ELP_{BC} (Figure 54). Without perturbation of the CMT, the RVRR, GGG, and GGGGG linkers could be incorporated into the drug carrier design such that unimers alone were present at 37 °C and micelle assembly was achieved at 42 °C.

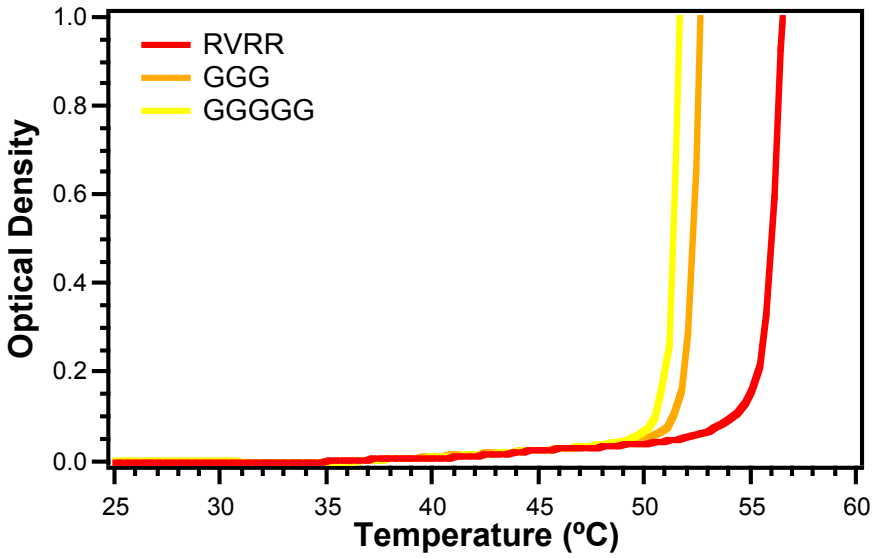

Figure 54: Hydrophilic and neutral cleavable peptide linkers RVRR, GGG, and GGGGG did not significantly change the thermal behavior of Arg_8-ELP_{BC}-BH3. Preservation of the CMT would permit constructs containing these linkers to achieve mild hyperthermia-triggered self-assembly. Turbidimetry measurements were acquired at 15 μM in PBS.

Since the RVRR, GGG, and GGGGG linkers all maintained the desirable thermal properties of the Arg_8-ELP_{BC} each was a feasible option to create a drug carrier capable

of hyperthermia-triggered micelle assembly that was also potentially capable of releasing free peptide drug within the cell. These three linkers were screened in a preliminary *in vitro* test of controlled cytotoxicity. The Arg_8-ELP_{BC} carrier was used here to circumvent the additional question of drug dose, such that the maximum intracellular dose could be delivered in this experiment to tease out only the effect of linker on drug efficacy. In the modified survival assay in HeLa cells all three linkers were capable of achieving controlled cytotoxicity, measured by absorbance at 490 nm, between 37 °C and 42 °C (Figure 55). The greatest fold change in cell survival was achieved with the RVRR linker, which was therefore chosen for future use as the linker to characterize the delivery of peptide drug using variable CPP-ELP_{BC} carriers.

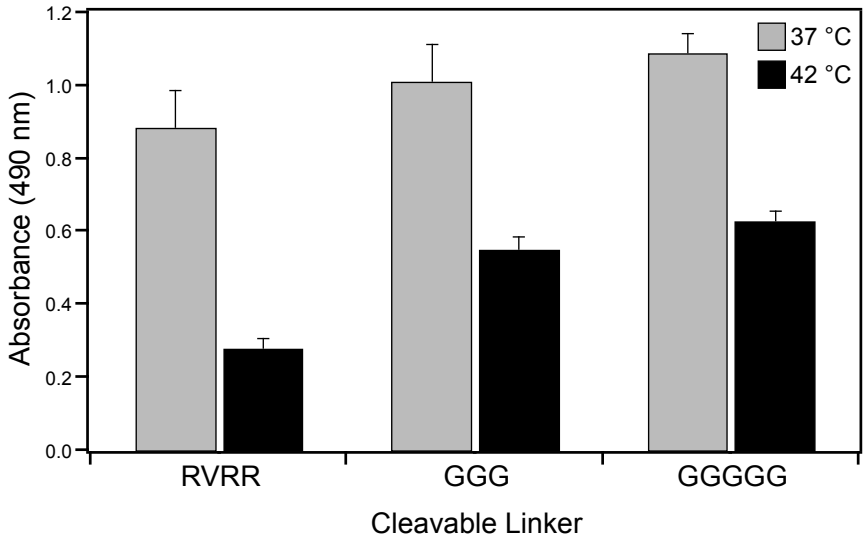

Figure 55: Arg_8-ELP_{BC}-BH3 achieved controlled cytotoxicity, approximated from absorbance at 490 nm, with RVRR, GGG, and GGGGG cleavable linkers, inducing cell death at 42 °C, with minimal cell death at 37 °C. RVRR cleavable linker achieved

the greatest fold increase in cell death between thermal conditions. Absorbance was normalized to untreated cells at 37 °C. Data represents mean of 3 measurements ± SEM.

Now with a chosen drug linker, a family of CPP-ELP$_{BC}$ drug carriers was created to investigate the role of CPP-functionalization on the delivery of cleavable drug cargo to achieve controlled cytotoxicity. Arg$_5$- and Arg$_8$-ELP$_{BC}$s were chosen as the carriers as they encompass the breadth of "off" and "on" levels of uptake within the extended CPP-ELP$_{BC}$ family. Drug carriers that included the cleavable RVRR linker were designated CPP-ELP$_{BC}$-cBH3. Beyond the Arg$_5$-ELP$_{BC}$-cBH3 and Arg$_8$-ELP$_{BC}$-cBH3 drug carriers, three controls were included to probe the effects of CPP-functionalization, cleavable drug cargo, and linker toxicity. These controls were non-functionalized ELP$_{BC}$-cBH3, Arg$_8$-ELP$_{BC}$-BH3 without the RVRR linker, and Arg$_8$-ELP$_{BC}$-RVRR, which included the RVRR linker without the BH3 peptide drug cargo. All constructs were efficiently expressed in *E. coli* and sufficiently purified by ITC (Figure 56).

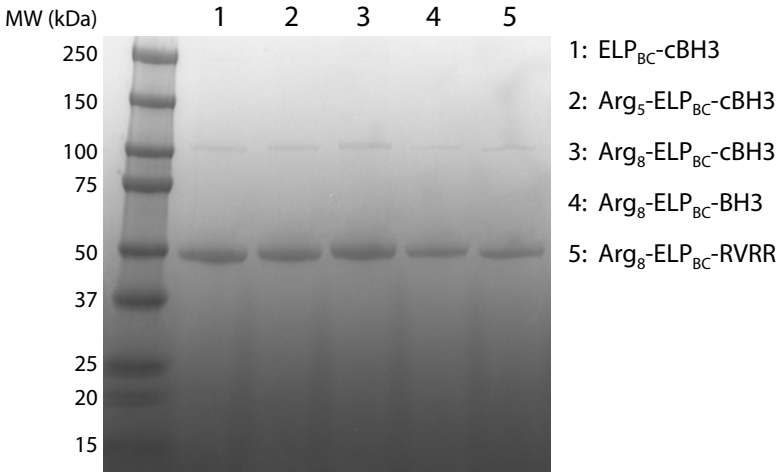

Figure 56: CPP-ELP$_{BC}$ drug carriers and controls were efficiently expressed and sufficiently purified from *E. coli*, as confirmed by SDS-PAGE. The expected molecular weight of the CPP-ELP$_{BC}$ drug carriers varied slightly due to CPP, drug, and linker functionalization and were, by lane, 1) 42.32 kDa, 2) 43.10 kDa, 3) 43.57 kDa, 4) 43.00 kDa, and 5) 41.60 kDa. Reproduced from [152].

The thermal behavior of these drug carriers and controls was investigated by temperature-regulated turbidimetry to confirm that manipulation of CPP, linker, and drug cargo did not perturb the CMT at the concentration intended for *in vitro* cytotoxicity assays. Characterization at 15 μM confirmed that the desired thermal behavior was conserved across all five constructs in this drug carrier family, whereby the CMT did not change significantly between constructs although the micelle-to-aggregate transition did change depending on CPP, drug, and linker functionalization (Figure 57).

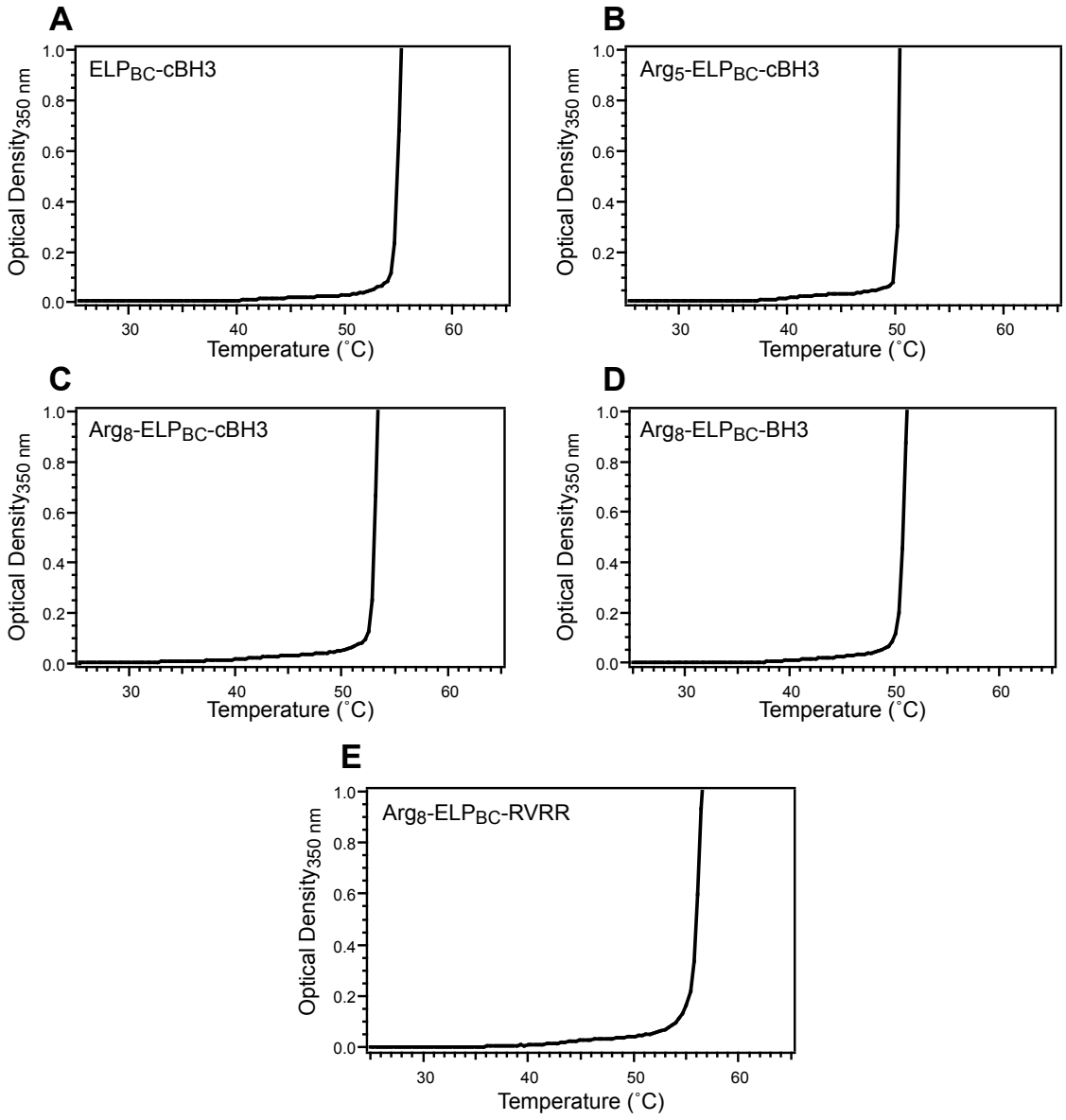

Figure 57: Desirable thermal behavior was conserved in this family of CPP-ELP$_{BC}$-BH3 drug carriers, regardless of CPP, drug, or linker functionalization. Temperature regulated turbidimetry confirmed that ELP$_{BC}$-cBH3 (A), Arg$_5$-ELP$_{BC}$-cBH3 (B), Arg$_8$-ELP$_{BC}$-cBH3 (C), Arg$_8$-ELP$_{BC}$-BH3 (D), and Arg$_8$-ELP$_{BC}$-RVRR maintained a CMT between 37 °C and 42 °C. Turbidimetry measurements were acquired at 15 μM in PBS. Reproduced from [152].

DLS further confirmed that the desired thermal behavior was conserved across this family of drug carriers and controls. All drug carriers and controls demonstrated a pure unimer population at 37 °C and a pure micelle population at 42 °C at 15 μM (Table 13). These results demonstrated the ability of optimized third generation CPP-ELP$_{BC}$s to support a variety of functionalization while retaining desirable thermal properties, at least for peptide therapeutics and peptide linkers. This conservation of thermal properties affords the opportunity to compare the role of CPP-functionalization in modulating intracellular drug dose and assess the role of each component in the drug carrier using controls to probe the contribution of the CPP, drug, and linker toward the anti-cancer efficacy of this drug carrier.

Table 13: Characterization of CPP-ELP$_{BC}$-BH3 peptide drug carriers and controls by DLS at 15 μM in PBS. Data represents mean of 3 measurements ± SEM.

Construct	BH3 drug	RVRR linker	R_h at 37 °C (nm)	R_h at 42 °C (nm)
ELP$_{BC}$-cBH3	+	+	9.7 ± 0.1	23.6 ± 0.8
Arg$_5$-ELP$_{BC}$-cBH3	+	+	7.8 ± 0.2	24.1 ± 1.7
Arg$_8$-ELP$_{BC}$-cBH3	+	+	8.2 ± 0.1	27.5 ± 0.3
Arg$_8$-ELP$_{BC}$-BH3	+	-	7.4 ± 0.3	22.1 ± 0.4
Arg$_8$-ELP$_{BC}$-RVRR	-	+	7.7 ± 0.3	24.4 ± 1.2

Prior to the *in vitro* evaluation of drug delivery, the function of the cleavable peptide linker was verified. Each CPP-ELP$_{BC}$ or control containing the cleavable BH3 drug via the RVRR linker, as well as the uncleavable control, were incubated with furin to mimic the digestion of these constructs by this enzyme that it would encounter in the intracellular endosome [176, 180, 181]. The digestion products of this reaction were then

separated by SDS-PAGE and visualized by coomassie staining with comparison to undigested constructs. Since coomassie staining is specific to a handful of residues (such as cationic or aromatic residues), which are not prevalent in all constructs investigated here, the gel was also stained by $CuCl_2$, which provides negative staining to visualize all ELP constructs. Free BH3 peptide was detected only for those constructs exposed to furin and for only those constructs containing the RVRR linker (Figure 58). This confirmed the function of this cleavable linker, at least with respect to its susceptibility of cleavage by the furin enzyme.

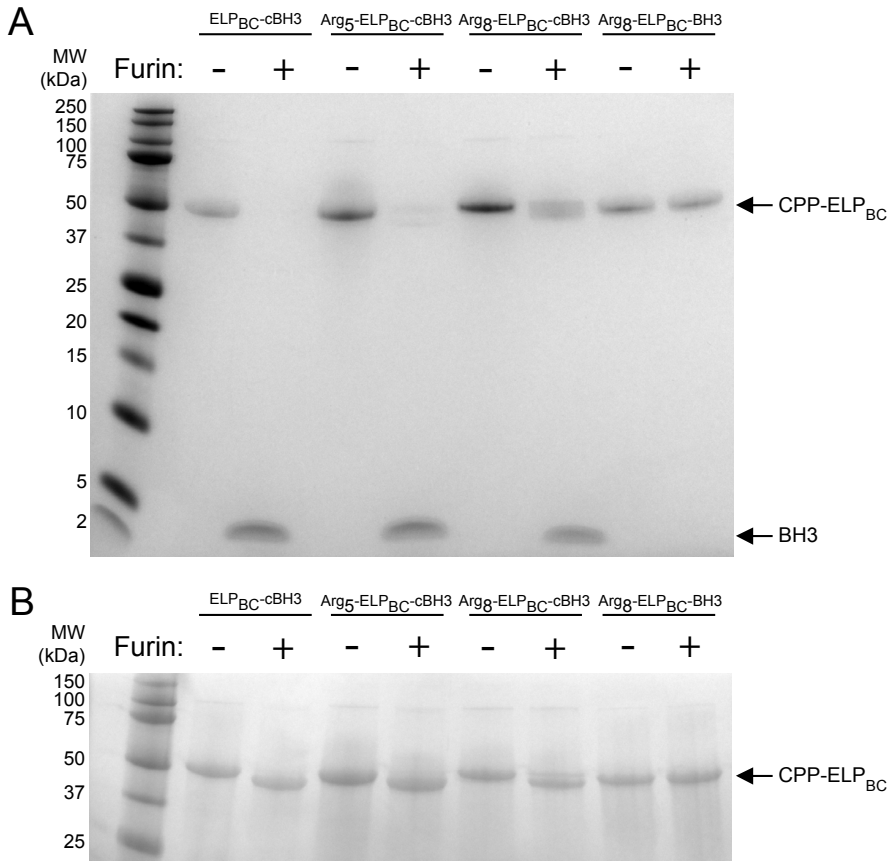

Figure 58: BH3 peptide was released from CPP-ELP$_{BC}$s containing the RVRR linker when incubated with furin. Coomassie staining visualized cleaved BH3 peptide (MW: 2.74 kDa, where furin cleaves at the C-terminus of the RVRR linker producing the fragment MGQVGRQLAIIGDDINRRYRVRR) from the CPP-ELP$_{BC}$ (approximate MW: 40 kDa, depending on CPP functionalization) (A). $CuCl_2$ staining visualized all CPP-ELP$_{BC}$s with and without furin digestion (B). Reproduced from [152].

The RVRR linker is also a recognition sequence for cathepsin B cleavage, another enzyme localized in the endosome [182]. Incubation of CPP-ELP$_{BC}$ drug carriers and controls with cathepsin B led to a much different digestion product than was seen with furin. The first difference was that the free peptide was not visualized by coomassie staining (Figure 59). The second difference was that there appeared to be digestion of the

Arg_8-ELP_{BC}-BH3 control lacking the RVRR linker. The third difference was seen in the $CuCl_2$-stained gel, which revealed a digestion of each CPP-ELP_{BC} drug carrier and control into a large fragment whose size was consistent across all constructs at approximately 20 kDa.

Reflecting on the size of this fragment with respect to the overall design of the ELP_{BC} made it clear that this fragment was composed of the hydrophobic domain of the ELP_{BC}. In retrospect this is not surprising as linkers that were evaluated for this system, such as GGG, exhibit sensitivity to cathepsin B cleavage and these consensus sequences are indeed repeated along the hydrophilic domain of the ELP_{BC}. This domain has an alternating guest residue of alanine or glycine, and for each pentapeptide in which glycine is the guest residue a GGG peptide is created due to the VPGXG repeat of the ELP motif. The inherent sequence of E2* thus makes it degradable by cathepsin B. Without seeing the free peptide band, it is unclear if the peptide is being degraded into smaller fragments, or if it is being retained on the hydrophobic ELP domain. With plentiful cut sites along the hydrophilic ELP domain (30 fold more than the single RVRR site on each construct), there may be significant competition for cleavage of the RVRR sequence if it is indeed recognized by cathepsin B. Although conclusive cleavage by cathepsin B was not characterized, the release of free drug by at least one intracellular enzyme confirmed the potential for this linker to serve its ultimate purpose of free drug release within the cell.

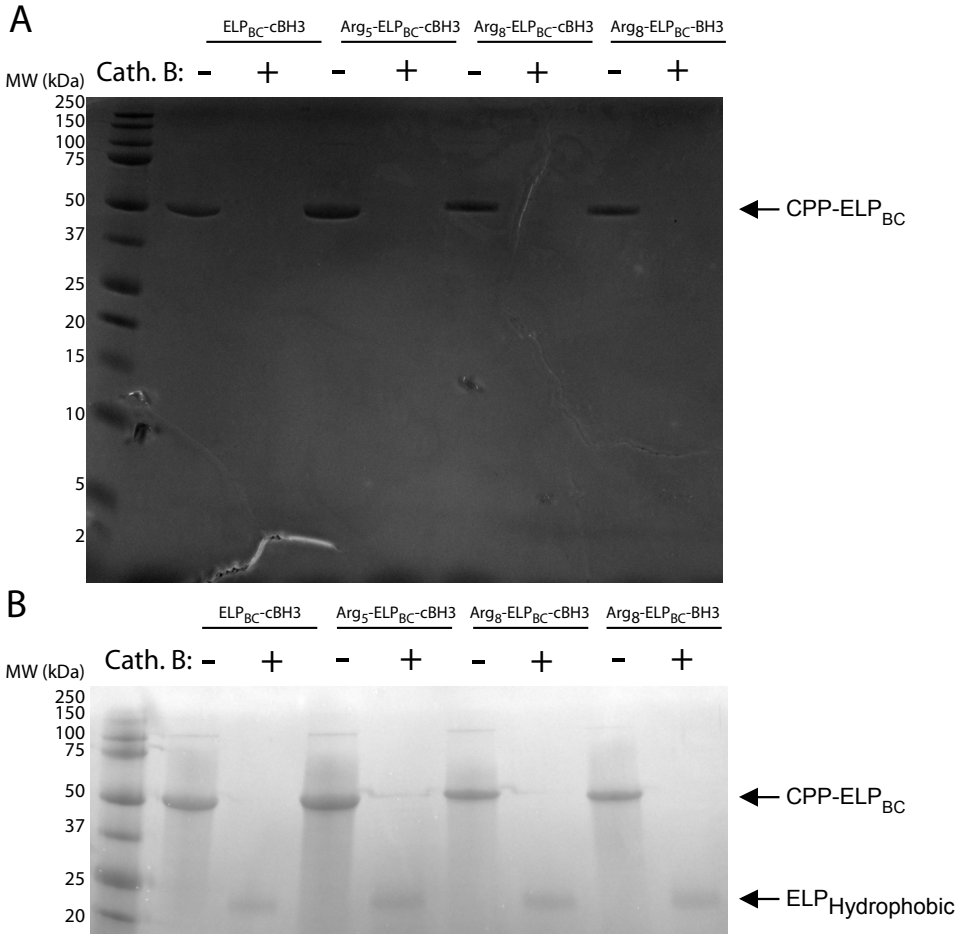

Figure 59: BH3 peptide drug release was not apparent by cathepsin B cleavage. However, this enzyme did appear to digest the hydrophilic domain of the CPP-ELP$_{BC}$. Coomassie staining of cleavage products did not visualize free BH3 peptide (MW: 2.74 kDa, where furin cleaves at the C-terminus of the RVRR linker producing the fragment MGQVGRQLAIIGDDINRRYRVRR) independent of the CPP-ELP$_{BC}$ (approximate MW: 40 kDa, depending on CPP functionalization) (A). $CuCl_2$ staining of CPP-ELP$_{BC}$s with and without cathepsin B digestion revealed a product of approximately 20 kDa that was likely the hydrophobic domain of the ELP$_{BC}$ (approximate MW: 16.4 kDa +/- 2.74 kDa for drug cargo and linker).

Extensive characterization of these drug carriers and control confirmed their expected therapeutic function. The *in vitro* cytotoxicity was evaluated in HeLa cells,

again using the modified survival assay which includes exposure of the cells to drug carrier for only 1 hour at either 37 °C or 42 °C, after which the treatment is removed and the cells are returned to fresh media at 37 °C. For this peptide drug cell survival, approximated from absorbance at 490 nm, was evaluated only 24 hours after treatment. Arg_8-ELP_{BC}-cBH3 induced significantly greater cell death at 42 °C, as compared to 37 °C, while no significant change in cell survival was measured for Arg_5-ELP_{BC}-cBH3 or non-functionalized ELP_{BC}-cBH3 control between thermal conditions (Figure 60). The greater uptake of Arg_8-ELP_{BC} at 42 °C was thus necessary to deliver a drug dose sufficient to induce a therapeutic effect, while the uptake of Arg_8-ELP_{BC} at 37 °C was low enough to spare cells at 37 °C from a cytotoxic effect. The difference in cell survival between 37 °C and 42 °C was less pronounced for Arg_8-ELP_{BC}-BH3, which lacked the cleavable RVRR linker. This supports the importance of releasing free peptide drug within the cell for this drug carrier and drug cargo combination. Free BH3 was also included in this assay to demonstrate the therapeutic effect of this drug without the assistance of a delivery vehicle. Free BH3 peptide alone showed no significant cytotoxicity at either thermal condition, likely due to its poor intracellular delivery caused by the impermeable barrier of the cell membrane to this drug.

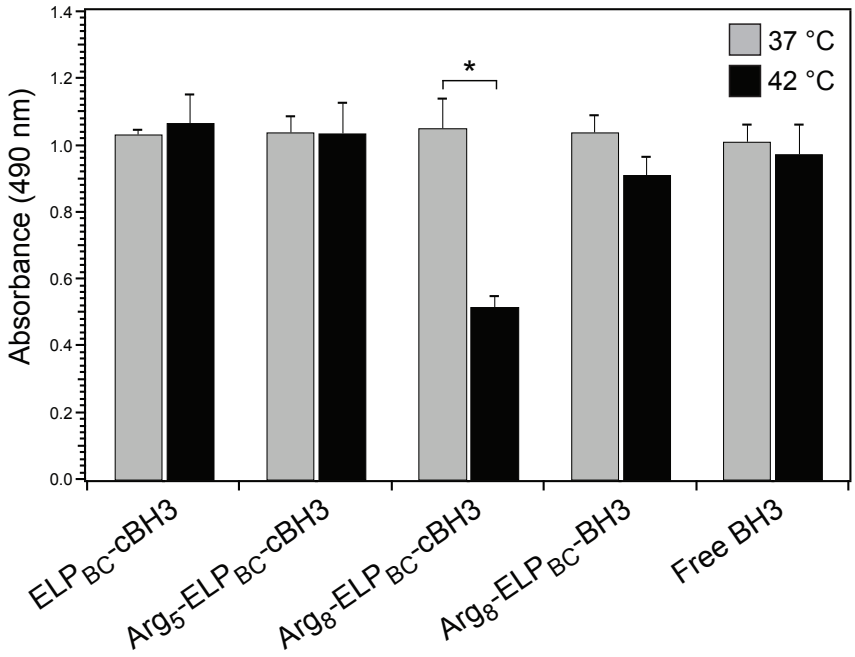

Figure 60: Only Arg$_8$-ELP$_{BC}$-cBH3 achieved controlled cytotoxicity in HeLa cells, as measured by absorbance at 490 nm, with significant cell death at 42 °C, while cells at 37 °C were spared. Absorbance was normalized to untreated cells at 37 °C. Data represents mean of 3 experiments ± SEM. *Indicates $p < 0.005$ between thermal conditions (two-way ANOVA, Bonferroni posthoc test for multiple comparisons). Reproduced from [152].

While the controls included in the experiment above confirmed the importance of including a cleavable linker in the drug carrier design to induce a therapeutic effect, they did not examine the role of the linker itself in contributing to this cytotoxic effect. The toxicity of the cleavable RVRR linker was therefore evaluated with the Arg$_8$-ELP$_{BC}$-RVRR construct using the same cell survival assay. Cell survival with treatment of Arg$_8$-ELP$_{BC}$-RVRR at 42 °C was lower than those cells treated at 37 °C, as approximated by absorbance at 490 nm, but this effect was not significant (Figure 61). However, this

small, albeit statistically insignificant, effect may suggest a minor role of the RVRR linker in the cytotoxicity of Arg_8-ELP_{BC}-cBH3 cleavable drug carrier.

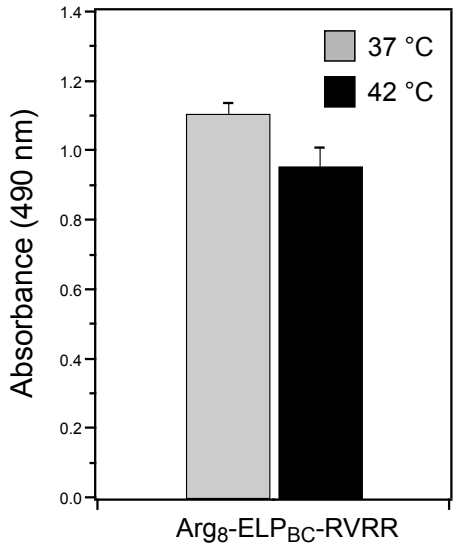

Figure 61: Cell survival, approximated from absorbance at 490 nm, did decrease with Arg_8-ELP_{BC}-RVRR at 42 °C, as compared to 37 °C, but this effect was not significant. Absorbance was normalized to untreated cells at 37 °C. Data represents mean of 3 experiments ± SEM. Reproduced from [152].

Finally, the mechanism of cytotoxicity induced by Arg_8-ELP_{BC}-cBH3 was investigated by the contribution of apoptosis, measured by the activation of effector enzyme caspase-3. Enzyme activity of caspase-3 was evaluated in cells treated with CPP-ELP_{BC} drug carriers and controls and quantified by the fluorescent cleavage fragments from caspase-specific targets. Arg_8-ELP_{BC}-cBH3 showed a significant increase in caspase-3 activation in cells treated at 42 °C, as compared to those treated at 37 °C (Figure 62). This result supports that the controlled cytotoxicity achieved with this drug carrier was

attributed to the induction of apoptosis by the BH3 peptide drug cargo. The caspase-3 activation was, however, elevated slightly at 37 °C as well, when compared to the other drug carrier controls. However, the increased caspase-3 activation triggered at 37 °C by Arg_8-ELP_{BC}-cBH3 did not correlate to an increase in cytotoxicity, suggesting that a threshold of caspase-3 activation was not met at this treatment condition to induce a significant cytotoxic effect. No significant changes in caspase-3 activation were seen between cells treated with ELP_{BC}-cBH3, Arg_5-ELP_{BC}-cBH3, or free BH3 at either 37 °C or 42 °C, supporting the conclusion that only the delivery afforded by Arg_8-ELP_{BC} was capable of achieving controlled cell death by apoptosis.

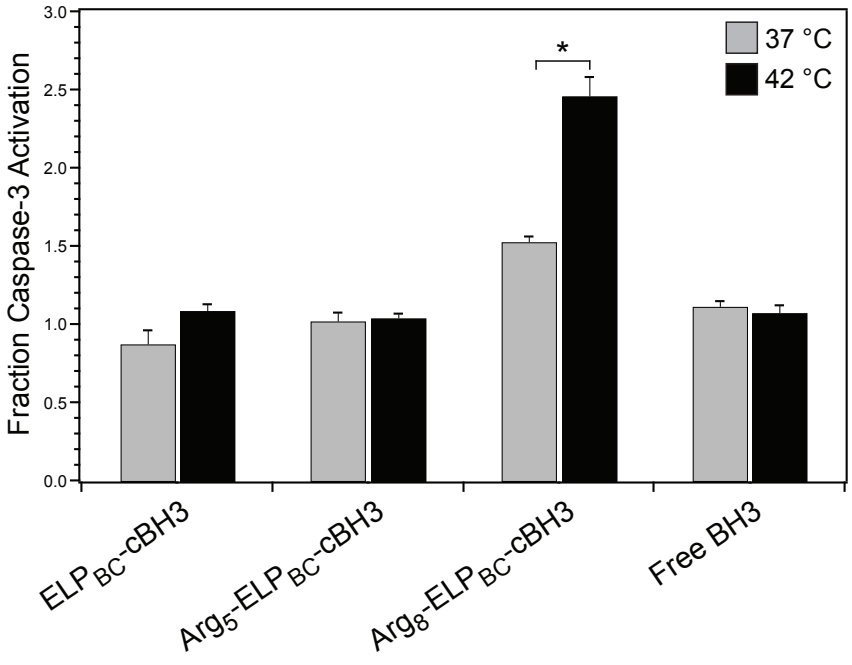

Figure 62: Only Arg_8-ELP_{BC}-cBH3 achieved elevated caspase-3 activation at 42 °C, as compared to 37 °C. Caspase-3 activation was normalized to untreated cells at 37 °C.

Data represents mean of 3 experiments ± SEM. *Indications $p < 0.01$ between thermal conditions (two-way ANOVA, Bonferroni posthoc test for multiple comparisons). Reproduced from [152].

To evaluate all factors of this drug delivery platform, the role of hyperthermia alone was also investigated as a potential contributor toward apoptosis. Therefore the effect of hyperthermia on the induction of apoptosis was evaluated by quantification of caspase-3 activity in untreated cells exposed to 37 °C or 42 °C. No significant difference in caspase-3 activity was detected between cells incubated at 37 °C or 42 °C (Figure 63), confirming that mild hyperthermia alone did not induce apoptosis in the context of this *in vitro* assay.

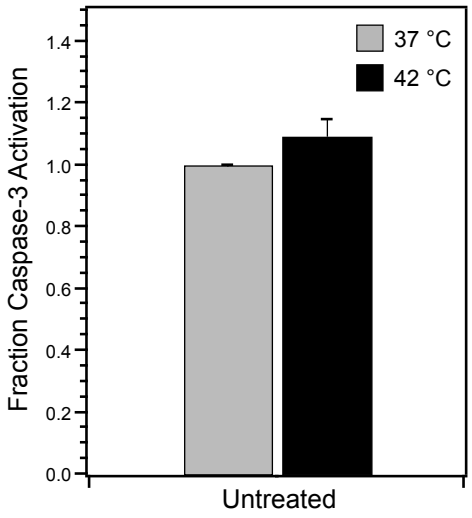

Figure 63: No significant difference in caspase-3 activity was detected between untreated cells incubated at 37 °C or 42 °C confirming that hyperthermia alone did not contribute to the induction of apoptosis. Caspase-3 activation was normalized to untreated cells at 37 °C. Data represents mean of 3 experiments ± SEM. Reproduced from [152].

The results with this family of CPP-ELP$_{BC}$ drug carriers confirm several factors in the successful control of therapeutic effect with hyperthermia-triggered micelle assembly that drives intracellular drug delivery. For BH3 peptide cargo the critical parameters included a drug carrier functionalized with Arg$_8$ CPP, capable of maximizing uptake at 42 °C to cause significant cell death at this "on" state, while keeping uptake at 37 °C low enough to avoid cytotoxicity at this "off" state. Furthermore a cleavable peptide linker, such as RVRR, was critical in allowing free drug release in the cell that could perform its therapeutic function.

While the experiments performed here confirmed the importance of these parameters, there are likely several additional factors that contributed to the controlled cytotoxicity achieved with the Arg$_8$-ELP$_{BC}$-cBH3 drug carrier. First, the positive charge contributed to the BH3 peptide by the residual RVRR linker, following cleavage at the C-terminus of this peptide, could potentially increase the cytotoxicity of the peptide drug by electrostatically localizing the peptide to the mitochondrial membrane [183]. This localization could either increase activity of BH3 by increasing its interaction with prosurvival proteins anchored in the mitochondrial membrane or could increase cytotoxicity by directly destabilizing the mitochondrial membrane [184]. Second, mild hyperthermia used to trigger micelle assembly may contribute to cytotoxicity by influencing components of the apoptosis cascade, such as down-regulation of apoptosis-related proteins [185] or direct destabilization of the mitochondrial membrane [186].

Since hyperthermia alone did not induce cytotoxicity in untreated cells, these effects may only become apparent when synergized with delivery of a proapoptotic signal, such as is provided by the BH3 peptide. The factors of BH3 peptide delivery, charge, and heat may all synergistically contribute to a controlled cytotoxicity achieved at conditions of mild hyperthermia, while sparing cells at physiologic temperatures.

4.4 Conclusions

Due to their genetic design, CPP-ELP$_{BC}$s are well suited for drug loading, be it by genetically appending biologic drugs, or incorporating unique reactive residues for covalent attachment of non-biologic therapeutics. The major concern in the attachment of drug cargo of all kinds is the preservation of the desired thermal properties of the ELP$_{BC}$ if they have been optimized for the intended application. As was the case for third generation CPP-ELP$_{BC}$s, the desired unimer and micelle conditions were previously attained by careful optimization of the ELP$_{BC}$ to achieve a CMT between 37 °C and 42 °C, independent of CPP-functionalization. With significant effort applied in optimizing the behavior of the CPP-ELP$_{BC}$, a drug cargo without detrimental effect on the thermal behavior was sought for this family of drug carriers.

Attachment of small molecule drugs was investigated by covalent conjugation to N-terminal cysteine residues. The hydrophilic small molecule gemcitabine was chosen as the drug cargo to guarantee that it would not induce premature self-assembly of the ELP, as is known for hydrophobic small molecules. Although the conjugation of

gemcitabine did not cause premature self-assembly of the ELP_{BC}, this drug attachment did induce changes in the CPP-ELP_{BC} thermal behavior that either prevented its use for hyperthermia-triggered self-assembly or forced its use at high concentrations to achieve the desired "off" and "on" states of the drug carrier platform. Controlled cytotoxicity with small molecule drug cargo was not achievable with the current drug carrier design and it became clear that significant optimization of the carrier would need to be assessed at each step in small molecule drug loading to truly evaluate the potential to deliver small molecule drugs in a controllable manner at relevant doses. These complications lead to the search for alternative drug cargo that could potentially exploit the optimized CPP-ELP_{BC}s that were available.

Peptide drug cargo proved to be significantly less destructive to the ELP_{BC} thermal properties. Even peptides that include residues with hydrophobic or charged character could be incorporated into the CPP-ELP_{BC} design and not perturb the optimized thermal response of these carriers. Controlled cytotoxicity was achieved with proapoptotic BH3 peptide drug cargo when delivered with Arg_8-ELP_{BC} in combination with a cleavable linker that provided release of free peptide within the cell. While this carrier system proved suitable for BH3 peptide drug it is imaginable that for other peptide drugs the ideal intracellular drug dose at "off" and "on" conditions will likely vary to achieve controlled cytotoxicity depending on the drug's potency. The CPP-ELP_{BC} drug carrier platform provides the ability to tune these delivery parameters, as

controlled by the CPP-functionalization. This drug delivery platform may therefore be quite tunable depending on the needs of the drug cargo.

5. Targeted delivery of CPP-ELP$_{BC}$s *in vivo*

5.1 Motivation

CPP-ELP$_{BC}$s successfully controlled cellular uptake and drug delivery *in vitro* in response to a trigger of mild clinical hyperthermia that induced self-assembly of the drug carriers. For targeted delivery *in vivo* the CPP-ELP$_{BC}$s would be injected systemically. At physiologic temperature of 37 °C, the CPP-ELP$_{BC}$s should circulate in the blood as unimers in their "off" state. This should minimize the internalization of CPP-ELP$_{BC}$s in off-target tissues that they encounter as they circulate throughout the body. It is only in the solid tumor, to which local hyperthermia is applied, that the CPP-ELP$_{BC}$s should self-assemble into micelles at 42 °C, thereby transitioning to their "on" state only at the site of disease. This should achieve enhanced cellular uptake and intracellular drug delivery targeted only to the tumor.

There are many aspects of targeted drug carrier delivery that must be evaluated to determine the function of such materials in a living system. These factors include the behavior of the drug carrier in blood, the rate of clearance of the drug carrier from circulation, the interaction of drug carrier with its target tissue, and the biodistribution of the drug carrier in both the target tissue as well as off-target organs. Combined, all of these factors contribute to the success or failure of the drug carrier *in vivo*.

The hypothesis that drove the creation of cationic CPP-ELP$_{BC}$s originally assumed a relatively low charge content of 3 arginine residues per ELP$_{BC}$ to achieve

controlled cellular uptake at 42 °C that was comparable to other CPP-functionalized systems like TAT-decorated liposomes. However, analysis of arginine oligomer valency suggested that greater than 3 arginine residues was necessary to achieve significant uptake in the "on" state of self-assembled CPP-ELP$_{BC}$ micelles at 42 °C that was enhanced in comparison to 37 °C. Indeed, 5 or 8 arginine residues worked best to demonstrate controlled cellular uptake with variable magnitudes of uptake at "off" and "on" conditions. Furthermore, only Arg$_8$-ELP$_{BC}$ was capable of inducing controlled cytotoxicity of some drug cargo, suggesting that the high level of uptake afforded by this CPP-ELP$_{BC}$ was necessary to deliver a sufficient intracellular dose of some drugs in order to induce a therapeutic effect. Therefore, the CPP-ELP$_{BC}$s we found to have useful behaviors *in vitro* had a much greater cationic content than we had originally anticipated. Not surprisingly, this charge content would be a major challenge in achieving the desired behavior of these cationic drug carriers *in vivo*.

These challenges would have the opportunity to present themselves at all stages of the evaluation of CPP-ELP$_{BC}$s *in vivo*, where charge can have negative effects on the thermal behavior of CPP-ELP$_{BC}$s in blood, on the clearance of CPP-ELP$_{BC}$s from circulation, and on the non-specific interaction of CPP-ELP$_{BC}$s with off-target organs. It was therefore unlikely that these highly cationic CPP-ELP$_{BC}$s would achieve successful tumor targeting *in vivo*. However, it was useful to evaluate the behavior of those CPP-ELP$_{BC}$s that were thus far developed to perhaps elucidate factors in the CPP-ELP$_{BC}$

design that could be tuned to achieve successful performance of temperature-triggered micelle assembly *in vivo,* which could be applicable to future generations of functionalized ELP$_{BC}$s.

5.2 Methods

5.2.1 Preparation of CPP-ELP$_{BC}$s for *in vivo* administration

For visualization and quantification *in vivo*, CPP-ELP$_{BC}$s were fluorescently labeled with Alexa Fluor 488, as previously described. One additional purification step was included for materials destined for *in vivo* administration to remove residual endotoxin resulting from the recombinant synthesis of CPP-ELP$_{BC}$s in *E. coli*. Labeled CPP-ELP$_{BC}$s were added to Pierce high capacity endotoxin removal resin in a spin column and mixed for 1 hour at room temperature while protected from light. Endotoxin free sample was then collected by centrifugation of the spin column at 500 x *g* for 1 minute.

5.2.2 Thermal characterization of CPP-ELP$_{BC}$s in serum

To characterize the thermal behavior that would be expected of CPP-ELP$_{BC}$s in the circulation, temperature-regulated turbidimetry was repeated in fluids that could mimic the complex composition of blood. Mouse serum, 90% FBS, and 1 mM bovine serum albumin (BSA) were all employed to shed light on the behavior of CPP-ELP$_{BC}$s in buffers beyond that of PBS, SF-media, and cell culture media supplemented with 10%

FBS. Turbidimetry in these alternative fluids provided efficient analysis of changes in the CMT and micelle-to-aggregate T_t in the presence of serum proteins.

5.2.3 Pharmacokinetics of systemically administered CPP-ELP$_{BC}$s

To evaluate the duration of blood circulation, fluorescently labeled CPP-ELP$_{BC}$s were administered intravenously via the tail vein of balb/c mice. At select time points over the course of 24-48 hours, 10 μL of blood was sampled from a tail vein prick. The blood sample was diluted in 100 μL of heparinized PBS and red blood cells were removed by centrifugation at 5,000 x *g* for 5 minutes. The supernatant was loaded onto black 96-well microplates and the fluorescence of Alexa Fluor 488 was measured on a microplate reader and corrected for background signal from the plasma of untreated mice. The fluorescent signal was either normalized to the first time point and reported as a fraction of fluorescence over time or it was converted to absolute concentration using fluorescent standard curves created for each of the administered CPP-ELP$_{BC}$s. SAAM II software was used to approximate the distribution half-life (α $t_{1/2}$), elimination half-life (β $t_{1/2}$), and area under the curve (AUC) for pharmacokinetic data, assuming a two compartment pharmacokinetic model.

5.2.4 Intravital microscopy of systemically administered CPP-ELP$_{BC}$s

5.2.4.1 Surgical implantation of dorsal fold window chambers

Six-week-old female nude mice were used for the implantation of dorsal fold window chambers for intravital microscopy of CPP-ELP$_{BC}$ interactions with vascular

and extravascular tumor tissue. The mice were anesthetized for surgery with intraperitoneal delivery of ketamine (100 mg/kg) and xylazine (10 mg/kg). The back of the mouse was washed with soap and then sterilized with 70% alcohol. The dorsal line of the mouse was marked with a sterile pen and the mouse was wrapped in a sterile drape that left the surgical site exposed. Four points along the dorsal line were used to fix the mouse skin to a metal C-shaped rack using nylon sutures to stretch the skin. The window chamber was used as a template to mark the area of skin to be removed on one side of the dorsal fold and to mark the holes for the three bolts of the window chamber. Holes for the bolts were made using a skin hole punch and a circular incision was made where marked on the dorsal fold, removing the skin and ensuring that the fascia from the proximal side was also removed. The wound was kept moist by the application of warm saline. One half of the window chamber, containing the bolts, was fit onto the dorsal fold, threading through the three holes made in the skin. The other half of the window chamber was aligned to the first, and secured with three nuts.

FaDu human squamous carcinoma cells were used to inoculate the window chamber. This cell type was found to be best suited for the window chamber model due to its slow growth that allowed tumors to reach several millimeters in the course of 10 days after inoculation, allowing sufficient time for healing of the injury caused by window chamber implantation. FaDu cells were harvested when they reached 80% confluence, washed, prepared at a concentration of 2 million cells/mL in phenol-red-free

media, and stored on ice for the duration of the surgical procedure. 10 μL of the tumor cell suspension (approximately 20,000 cells) were injected under the fascia of the opposing skin, forming a bubble. The injection site was washed with saline prior to fixing a glass cover slip over the tissue and securing it with an expandable plastic ring. The mouse was then removed from the C-shaped rack and the window chamber was secured with sutures at four total points, two at the top and bottom of the window chamber. Antibiotic was applied to the suture lines and incision site and the animals were allowed to recover on a warmed plate. The animals were returned to their cages and tumors were allowed to grow 7-10 days reaching a diameter of 2-3 mm in the window chamber.

5.2.4.2 Intravital confocal imaging of dorsal fold window chambers

For intravital imaging of the dorsal fold window chamber, mice were anesthetized with nembutol and placed on the microscope stage, securing the window chamber on the heating element coupled to a water bath. The temperature of the window was maintained at either 37 °C or 42 °C by means of the heated water bath circulating through the heating element mounted on the microscope stage. A catheter was installed in the mouse tail vein, enabling ease of dosing while imaging. To label the vascular space, 2 MDa rhodamine-labeled dextran was injected. Visualization of the vasculature helped in locating an area of interest for imaging, preferably in the tumor as characterized by the disorganized and tortuous nature of the neovasculature. Achieving

this goal was often difficult as the tumors tended to grow proximal to the outer diameter of the window, where the window chamber limited the working distance of the objective. With an area of interest identified, Alexa Fluor 488-labeled CPP-ELP$_{BC}$ was then administered via tail vein. A z-stack of images was taken over the depth of the vasculature, as defined by the vascular mask signal, every 3 minutes over the course of 1 hour.

This standard imaging protocol was later modified due to concerns about the interaction of high molecular weight dextran with the CPP-ELP$_{BC}$s. In later experiments Alexa Fluor 488-labeled CPP-ELP$_{BC}$ alone was injected intravenously and imaged over time in the absence of a vascular mask. At the end of imaging, 1 hour after administration, rhodamine-labeled high molecular weight dextran was added to help define the vascular space at this end point. In these modified experiments Hoechst was also administered at the end of imaging to localize the cellular components of the tumor tissue.

5.2.5 Biodistribution of systemically administered CPP-ELP$_{BC}$s

To determine biodistribution of CPP-ELP$_{BC}$s in the tumor and other critical organs, a FaDu xenograft was used on the right hind leg of nude mice. When the tumors reached approximately 100 mm^3 the mice were assigned to groups split by CPP-ELP$_{BC}$ treatment and thermal condition to normalize the average tumor volume in each group. For hyperthermia-treated tumors, mice were anesthetized with nembutol, catheters were

installed in the tail vein, and rectal temperature probes were placed in each mouse. The mice were then mounted in custom holders that permitted just their leg bearing the tumor to be immersed in a water bath that maintained a tumor temperature of 42 °C. Tumors were preheated for 10 minutes to allow internal temperatures to reach 42 °C prior to intravenous administration of Alexa Fluor 488-labeled CPP-ELP$_{BC}$s. Tumor heating continued for a total of 1 hour while monitoring the core body temperature of the mice. After 1 hour of tumor heating, mice were removed from the water bath and allowed to recover from anesthesia. For tumors without heat treatment the mice were simply administered CPP-ELP$_{BC}$ via tail vein injection.

2 or 24 hours after CPP-ELP$_{BC}$ administration, the mice were sacrificed and tissues were collected including the tumor, muscle, heart, lungs, kidney, spleen, and liver. A portion of each organ sample was homogenized by beating with zirconia beads. The homogenized tissue and beads were centrifuged and the supernatant was loaded on a black 96-well microplate. Alexa Fluor 488 fluorescence was measured on a microplate reader. The fluorescent signal from each sample was corrected for the background fluorescence typical for each organ (by mass), measured from an animal not receiving CPP-ELP$_{BC}$ treatment. The fluorescence concentration was then determined from standard curves, created for each CPP-ELP$_{BC}$ treatment, and accumulation in each organ was expressed as percent dose per tissue weight.

5.2.6 Optimizing material design with fourth generation CPP-ELP$_{BC}$s

It would become apparent in preliminary *in vivo* studies of third generation CPP-ELP$_{BC}$s that a larger ELP$_{BC}$ might provide advantages in avoiding uptake or clearance via the kidney. Increase in the size of the ELP blocks composing the ELP$_{BC}$ would cause a drop in their T_t, due to the inverse relationship between ELP length and T_t [102]. Alternative ELP sequences were thus investigated to compensate for this change in T_t due to increased length. A guest residue of serine was used to create a hydrophilic domain with increased T_t at 80 pentapeptides in length. The genetic design of this hydrophilic ELP is listed in Table 14.

Table 14: Genetic design of an alternative hydrophilic block for fourth generation CPP-ELP$_{BC}$s.

ELP: VPGXG$_n$	Peptide and oligonucleotide sequence
(SGVPG)$_{80}$	(S G V P G S G V P G S G V P G S G V (agc ggt gtt ccg ggc tct ggt gtc cca ggt tcc ggc gta ccg ggc agc ggt gtt P G S G V P G)$_{16}$ cct ggt tct ggc gtg ccg ggc)$_{16}$

Since the CMT is largely controlled by the hydrophobic domain of the ELP$_{BC}$, a family of alternative hydrophobic domain sequences were investigated to aid in the fine-tuning of the CMT between 37 °C and 42 °C. These hydrophobic domain sequences were composed of alanine and valine guest residues, where the increasing fraction of alanine residues raised the T_t of these ELP sequences. The synthesis, design, and

characterization of most of these sequences were performed by Dr. Jon McDaniel [187, 188]. The genetic designs of these hydrophobic ELPs are listed in Table 15.

Table 15: Genetic design of alternative hydrophobic blocks for fourth generation CPP-ELP$_{BC}$s.

ELP: VPGXG$_n$	Peptide and oligonucleotide sequence
(XGVPG)$_{80}$ [X=A:V=7:3]	(A G V P G A G V P G V G V P G A G (gcc gga gtg cct ggt gca ggt gtg cca ggc gtg ggt gtt cca gga gca ggc V P G V G V P G A G V P G A G V P G gtt cca ggt gtg ggt gtt cct ggc gcc gga gtg cct ggt gca ggt gtg cca ggc V G V P G A G V P G A G V P G)$_8$ gtg ggt gtt cca gga gca ggc gtt cca ggt gcg ggt gtt cct ggc)$_8$
(XGVPG)$_{80}$ [X=A:V=3:2]	(A G V P G A G V P G V G V P G A G (gcc gga gtg cct ggt gca ggt gtg cca ggc gtg ggt gtt cca gga gca ggc V P G V G V P G A G V P G A G V P G gtt cca ggt gtg ggt gtt cct ggc gcc gga gtg cct ggt gca ggt gtg cca ggc V G V P G A G V P G V G V P G)$_8$ gtg ggt gtt cca gga gca ggc gtt cca ggt gtg ggt gtt cct ggc)$_8$
(XGVPG)$_{80}$ [X=A:V=1:1]	(A G V P G V G V P G A G V P G V G (gcc gga gtg cca ggc gtg ggt gtt cca gga gca ggc gtt cca ggt gtg ggt V P G A G V P G V G V P G A G V P G gtt cct ggc gcc gga gtg cca ggc gtg ggt gtt cca gga gca ggc gtt cca ggt V G V P G A G V P G V G V P G)$_8$ gtg ggt gtt cct ggc gcc gga gtg cca ggc gtg ggt gtt cca gga)$_8$

$(X\text{GVPG})_{80}$ [*X*=A:V=4:6]	(A G V P G A G V P G V G V P G A G (gcc gga gtg cct ggt gca ggt gtg cca ggc gtg ggt gtt cca gga gca ggc V P G V G V P G V G V P G V G V P G gtt cca ggt gtg ggt gtt cct ggc gtg ggt gtt ccg ggc gta ggt gtc cca ggt A G V P G V G V P G V G V P G)$_8$ gcg ggc gta ccg ggc gtt ggt gtt cct ggt gtc ggc gtg ccg ggc)$_8$
$(X\text{GVPG})_{80}$ [*X*=A:V=1:4]	(V G V P G V G V P G A G V P G V G (gtg ggt gtt ccg ggc gta ggt gtc cca ggt gcg ggc gta ccg ggc ggt ggt V P G V G V P G V G V P G V G V P G gtt cct ggt gtc ggc gtg ccg ggc gtg ggt gtt ccg ggc gta ggt gtc cca ggt A G V P G V G V P G V G V P G)$_8$ gcg ggc gta ccg ggc gtt ggt gtt cct ggt gtc ggc gtg ccg ggc)$_8$
$(\text{VGVPG})_{80}$	(V G V P G V G V P G V G V P G V G V (gtg ggt gtt ccg ggc gta ggt gtc cca ggt gtg ggc gta ccg ggc ggt ggt gtt P G V G V P G V G V P G V G V P G V cct ggt gtc ggc gtg ccg ggc gtg ggt gtt ccg ggc gta ggt gtc cca ggt gtg G V P G V G V P G V G V P G)$_8$ ggc gta ccg ggc gtt ggt gtt cct ggt gtc ggc gtg ccg ggc)$_8$

The new hydrophilic and hydrophobic blocks were combined to form fourth generation CPP-ELP$_{BCS}$. Their thermal behavior was evaluated in PBS and mock serum solutions to direct the choice of an optimized construct to best test the mechanism of temperature-triggered micelle assembly *in vivo*.

5.3 Results and discussion

5.3.1 Evaluation of first generation CPP-ELP$_{BC}$s *in vivo*

First generation CPP-ELP$_{BC}$s were not suitable for mild hyperthermia-triggered self-assembly and were thus not appropriate to probe temperature-targeted delivery *in vivo*. These CPP-ELP$_{BC}$s would be in their self-assembled "on" state at 37 °C, and therefore would have the potential to interact non-specifically with any and all tissues if they were systemically administered in the blood stream. These materials should thereby behave as non-activatable CPP-functionalized carriers and therefore are likely to interact with off-target tissues and be cleared quickly from circulation. It was unclear whether these effects would eliminate any possibility that these CPP-ELP$_{BC}$s could also interact with the tumor, albeit in a non-activatable mechanism. Intravital microscopy of dorsal fold window chamber tissue at 37 °C was performed with first generation Arg$_5$-ELP$_{BC}$s and controls to shed light on these questions.

Vasculature was labeled with a high molecular weight rhodamine-dextran and Arg$_5$-ELP$_{BC}$ and controls were delivered at a final blood concentration of 10 μM. Images were acquired for 30-60 minutes after administration, depending on the compliance of the mouse. Both Arg$_5$-ELP$_{BC}$ and non-functionalized ELP$_{BC}$ appeared to extravasate from the vasculature over the course of imaging, whereas the signal from Arg$_5$-ELP soluble unimer only seemed to fade over time (Figure 64). This preliminary experiment suggested that the extravasation with time at 37 °C was governed by micelle

nanoparticle carriers, not their CPP-functionalization. Although the exact parameters of this experiment and the characteristics of these first generation materials do not match with those investigated in second generation carriers and beyond, this information served as the first harbinger that Arg_5-functionalization of ELP_{BC} micelles was not sufficient to achieve targeted delivery *in vivo*.

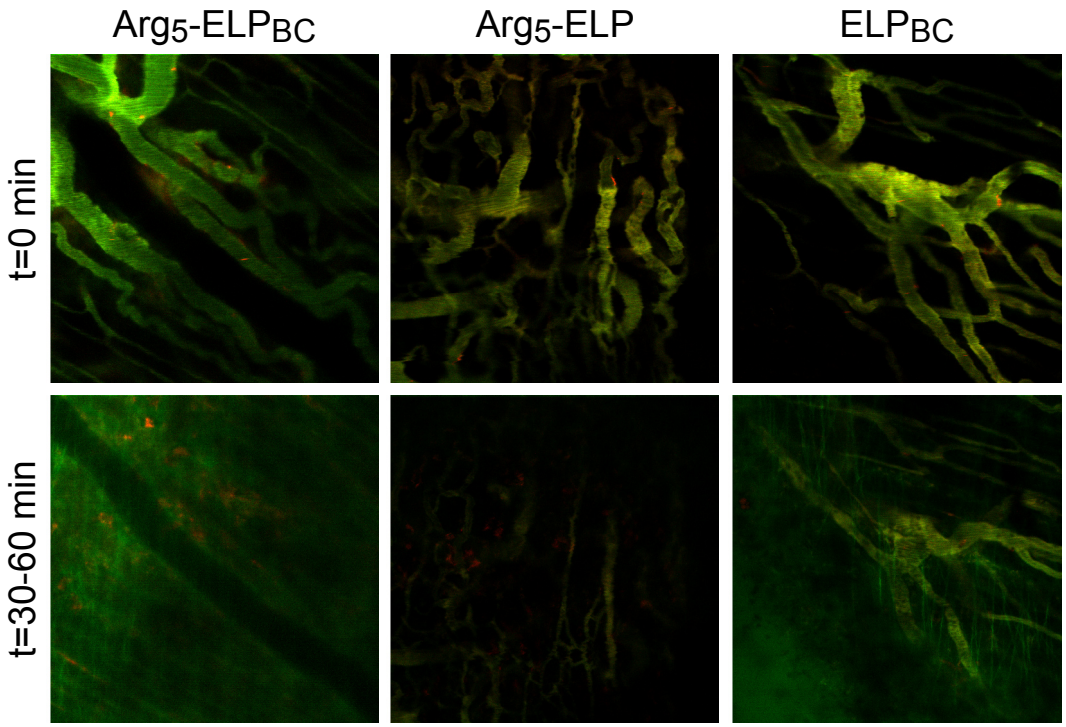

Figure 64: First generation Arg_5-ELP_{BC} and ELP_{BC} micelles extravasated in dorsal fold window chamber tissue at 37 °C. Extravasation was less evident for Arg_5-ELP unimer. Green—ELP; red—vascular mask; acquired at 20x.

5.3.2 Evaluation of second generation CPP-ELP_{BC}s *in vivo*

Second generation CPP-ELP_{BC}s provided the first opportunity to test hyperthermia-triggered micelle assembly. Once validated *in vitro*, their behavior was

visualized *in vivo*, after intravenous administration at a final concentration of 25 μM in the blood and in dorsal fold window chambers heated to 37 °C or 42 °C. It was difficult to identify any trends in behavior by this imaging technique and the constructs delivered here. For instance, when looking at potential tissue interaction that could lead to differences in extravasation, there did not seem to be a particular pattern dependent on material type or tissue temperature. Arg_5-ELP_{BC} (Figure 65) and Arg_5-ELP (Figure 66) both appeared to extravasate over the course of 1 hour regardless of tissue temperature. ELP_{BC}, however, appeared to extravasate to a greater extent at 37 °C, as compared to 42 °C (Figure 67). Furthermore, there did not appear to be any obvious differences in the localization of fluorescent extravasation that would suggest these materials were interacting with the tissue in different ways. It was unclear by these results what role tissue and vascular heterogeneity played in this variability.

What was most important in looking at these imaging results was that punctate fluorescence from the Arg_5-ELP_{BC} was seen at 42 °C in the vasculature just after administration (Figure 65). This fluorescence quickly disappeared in the matter of minutes. It was unclear if the Arg_5-ELP_{BC} was interacting with cell or extracellular components as it was injected. In retrospect, however, it was likely that this construct was aggregating in the presence of serum and mild hyperthermia. Due to the sensitivity of this construct to fluorophore conjugation, it would not be surprising that the presence of serum could disturb its thermal properties in such a way as to destroy micelle

assembly. The quickness with which the punctate fluorescence disappeared from the vasculature suggested that the decrease in concentration of this Arg_5-ELP_{BC} as it was cleared from circulation likely brought it below its critical micelle concentration at this hyperthermic condition. This behavior further confirmed the need for third generation CPP-ELP_{BC}s, and other optimized materials, to address the effects of the *in vivo* environment.

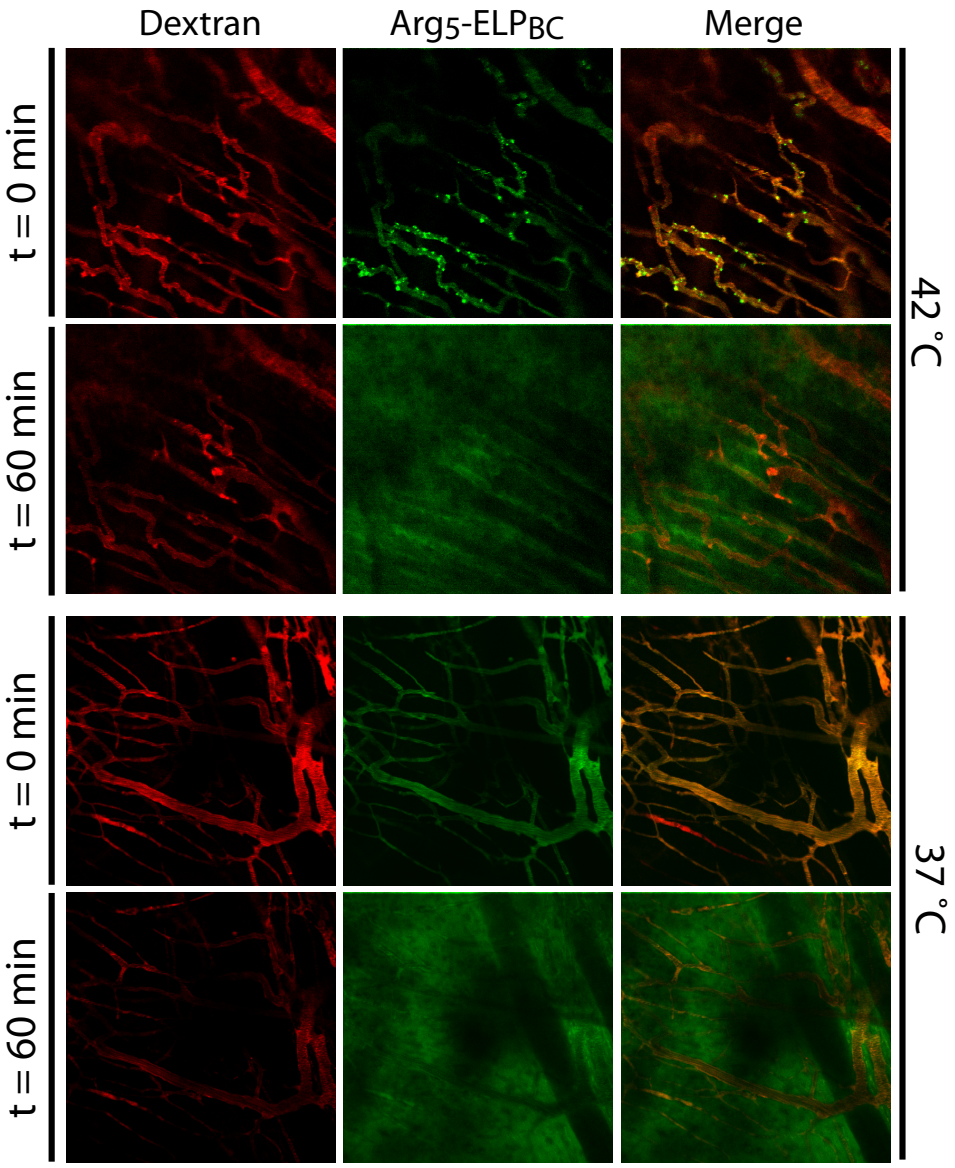

Figure 65: Second generation Arg_5-ELP_{BC} appeared to aggregate upon administration to hyperthermia treated tissue. Arg_5-ELP_{BC} accumulated in the extravascular space over the course of 1 hour, regardless of tissue temperature. Green—ELP; red—vascular mask; acquired at 20x.

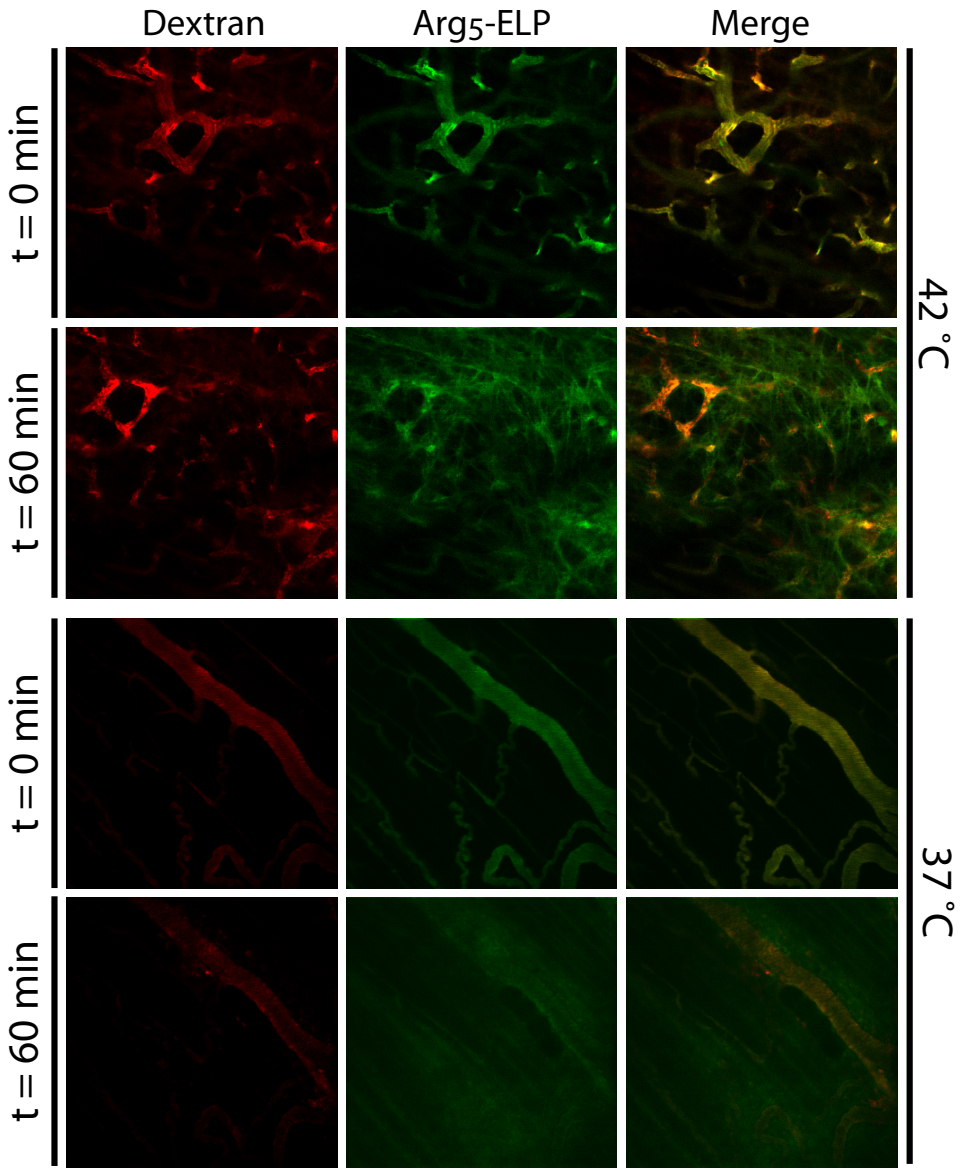

Figure 66: Second generation Arg$_5$-ELP unimer appeared to accumulate in the extravascular space over the course of 1 hour, regardless of tissue temperature and despite distinct vascular architecture. Green—ELP; red—vascular mask; acquired at 20x.

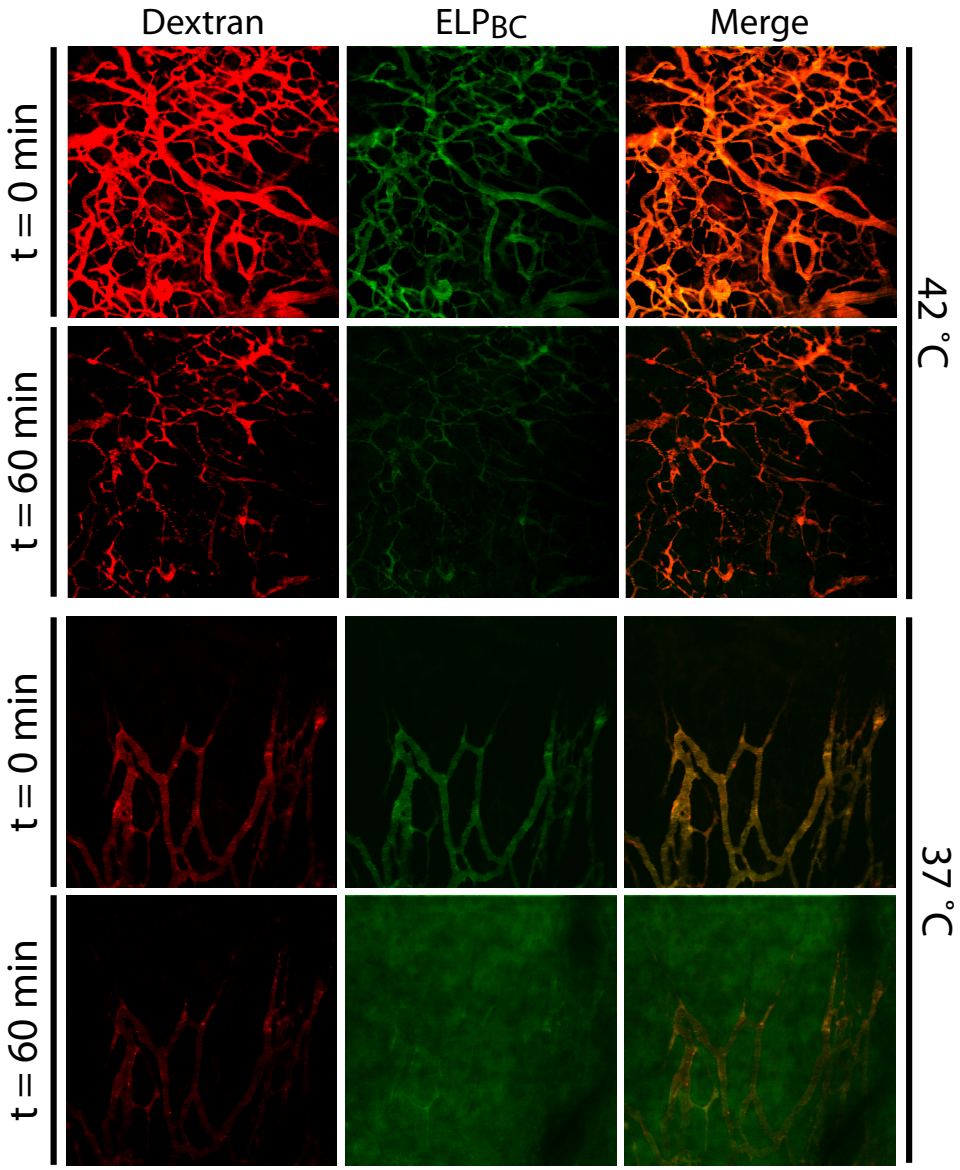

Figure 67: Second generation non-functionalized ELP$_{BC}$ achieved variable accumulation in the extravascular space of tissues at 37 °C or 42 °C, which had distinct vascular architecture. Green—ELP; red—vascular mask; acquired at 20x.

5.3.3 Evaluation of third generation CPP-ELP$_{BC}$s *in vivo*

Third generation CPP-ELP$_{BC}$s were the family of carriers to provide reliable and robust behavior *in vitro*. These optimized constructs were therefore thoroughly

evaluated *in vivo* to determine their circulation time, their interaction with the tumor tissue, and their distribution to the tumor and other organs. Pharmacokinetics of systemically administered third generation CPP-ELP$_{BC}$ and controls was first investigated to provide insight into the clearance of carrier from the blood over time. This is an important parameter in evaluating the function of the CPP-ELP$_{BC}$ relying on the temperature-triggered micelle assembly, which is dependent on concentration. It is therefore important that the concentration of CPP-ELP$_{BC}$ in the blood remains above that which is necessary to maintain a CMT between 37 °C and 42 °C. To our advantage, however, this requirement on the blood concentration must only be achieved over the time course of hyperthermia, typically 1 hour, in which triggered micelle assembly is exploited. Third generation Arg$_5$-ELP$_{BC}$ as well as non-functionalized ELP$_{BC}$ and soluble Arg$_5$-ELP controls were fluorescently labeled and systemically administered via tail vein injection in balb/c mice. The blood was sampled over the course of 48 hours and the concentration of CPP-ELP$_{BC}$ or controls was quantified by fluorescence and normalized to the measurement immediately following administration (40 second time point), making a naive assumption that this concentration would be near to that of the intended dose of 100 μM.

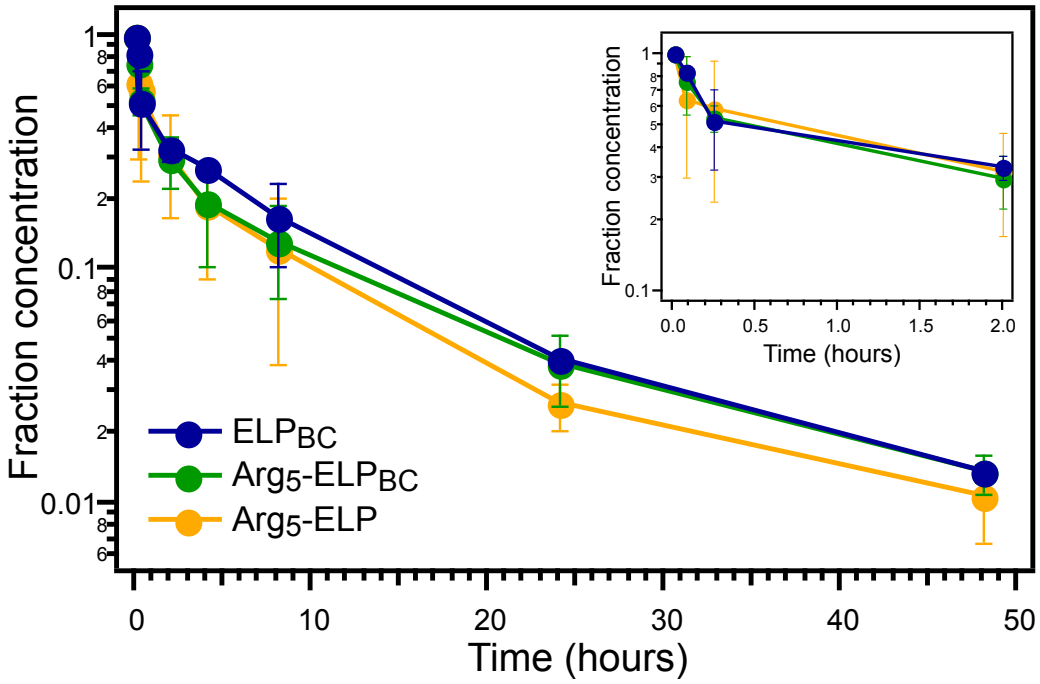

Figure 68: Arg$_5$-functionalization in third generation constructs caused more rapid clearance from the blood, as compared to non-functionalized ELP$_{BC}$ control. Yet, greater than 30% of the dose of all constructs was maintained in the blood over 2 hours (inset).

Both Arg$_5$-ELP$_{BC}$ and Arg$_5$-ELP control were cleared more quickly from the blood when compared to non-functionalized ELP$_{BC}$. The effect of Arg$_5$-functionalization to decrease the presence in circulation was evident from clearance profiles (Figure 68) and pharmacokinetic parameters approximated from this data (Table 16). ELP$_{BC}$ achieved the highest elimination half-life of approximately 14 hours, while both Arg$_5$-ELP$_{BC}$ and Arg$_5$-ELP had shortened elimination half-lives of approximately 11 hours. Furthermore, non-functionalized ELP$_{BC}$ achieved the largest area under the curve (AUC), such that it achieved the greatest carrier exposure in the blood through its prolonged circulation, as compared to Arg$_5$-functionalized constructs. This effect was not surprising since it

would be expected that the cationic charge, albeit small, would result in some non-specific interactions that would lead to a decreased presence in the blood. Despite the increased clearance of these Arg_5-functionalized constructs, they both greatly outperformed free arginine oligomer CPPs, such as Arg_9, whose circulation half-life has been reported as only 1.9 hours [189].

Table 16: Pharmacokinetic parameters of second generation Arg_5-ELP_{BC}, Arg_5-ELP, and ELP_{BC} after systemic administration at 100 μM.

Construct	α $t_{1/2}$ (min)	β $t_{1/2}$ (hour)	AUC (μM•h)
Arg_5-ELP_{BC}	12.4 ± 5.5	10.7 ± 0.9	378.4 ± 27.2
Arg_5-ELP	9.3 ± 5.8	11.0 ± 1.5	199.5 ± 23.0
ELP_{BC}	100.4 ± 19.1	14.2 ± 1.9	438.8 ± 22.7

Most important to the CPP-ELP_{BC}s was the clearance of constructs with respect to the time frame of mild hyperthermia. Despite the increased clearance of Arg_5-functionalized materials, all constructs maintained 30% of their delivered dose in circulation over the course of 2 hours (Figure 68—inset). Assuming that the earliest time point corresponded to concentration near the intended does of 100 μM, this blood concentration would be sufficiently above the critical micelle concentration to achieve a CMT between 37 °C and 42 °C.

Pharmacokinetics suggested sufficient concentration in the blood was maintained by third generation CPP-ELP_{BC} and controls such that temperature-triggered micelle assembly should be achievable with hyperthermia over the course of 1 hour following administration. It was therefore feasible to investigate the temperature-

triggered behavior with intravital microscopy, providing insight into the interaction of Arg_5-ELP_{BC} with the tumor as a function of the "off" or "on" condition of the carrier in either non-heated or hyperthermia-treated tumors in a dorsal fold window chamber. High molecular weight rhodamine-dextran was systemically administered to provide visualization of the vascular space over the course of imaging. Alexa Fluor 488-labeled Arg_5-ELP_{BC} was then administered via tail vein at a final blood concentration of 50 μM. The dorsal fold window chamber in which the tumor was inoculated was heated to either 37 °C or 42 °C using a heating chamber controlled by a circulating water bath. This preliminary evaluation of third generation Arg_5-ELP_{BC} demonstrated differences in extravascular accumulation of Arg_5-ELP_{BC} in the presence or absence of tumor hyperthermia (Figure 69A) and revealed an interesting accumulation pattern for Arg_5-ELP_{BC} in tumors heated to 42 °C. Enhanced magnification of hyperthermia treated tumors revealed perivascular localization of Arg_5-ELP_{BC} after 1 hour (Figure 69B). The significance of this extravasation was unclear in whether the CPP-ELP_{BC} was escaping the vascular space by means of hyperthermia-induced increased permeability, was binding to the extravascular space, or was being taken up by cells adjacent to the vasculature. Furthermore, it was unclear if these visualized differences would lead to a meaningful change in tumor accumulation, as compared to other off-target organs.

An encouraging result, as compared to second generation Arg_5-ELP_{BC}, was that no vascular punctate fluorescence was seen with this third generation construct

immediately after administration to hyperthermia treated tumors. This gave the impression that this optimized CPP-ELP$_{BC}$ platform was more stable in blood and may have avoided the issues of aggregation that were detected with second generation materials. In retrospect, however, this may not have been the case.

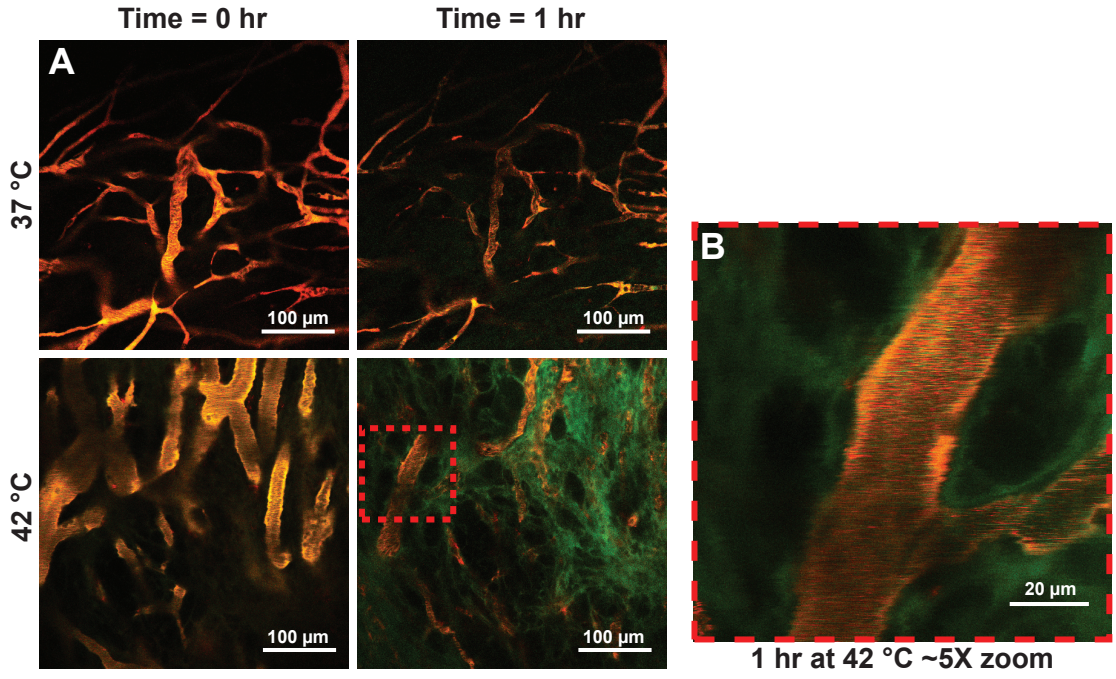

Figure 69: Mild hyperthermia appeared to influence the extravascular accumulation of third generation Arg$_5$-ELP$_{BC}$ over the course of 1 hour, as compared to non-heated tissue (A). Perivascular accumulation in hyperthermia treated tumors after 1 hour was revealed by enhanced magnification (B). Green—ELP; red—vascular mask.

To probe the question of tumor targeting in the context of whole body distribution, the accumulation of Arg$_5$-ELP$_{BC}$ was evaluated in tumors with or without hyperthermia as well as other critical off-target organs. Subcutaneous tumors were induced on the mouse hind limb. For those mice receiving tumor hyperthermia, their

hind limb bearing the tumor was locally heated with a water bath at 42 °C for 1 hour, while maintaining the body temperature of the mouse at, or below, 37 °C. The tumor and critical organs were excised 2 hours after treatment and the percent dose of the CPP-ELP_{BC} found in each organ was determined by fluorescence. There was no significant difference in the amount of Arg_5-ELP_{BC} or non-functionalized ELP_{BC} that was found in the tumor with or without hyperthermia treatment (between thermal conditions, two-way ANOVA, Bonferroni posthoc test for multiple comparisons) (Figure 70).

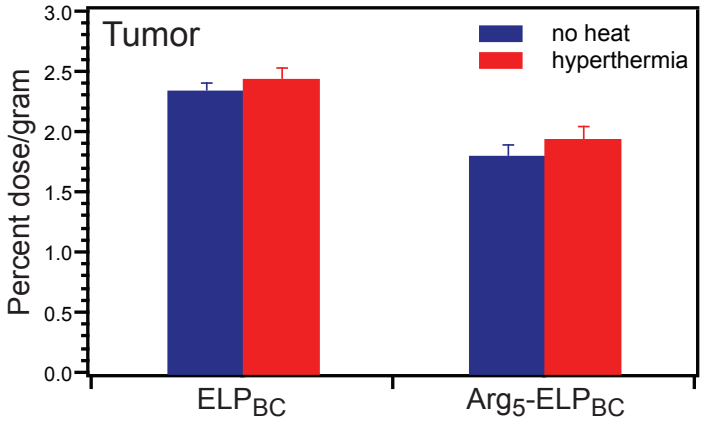

Figure 70: No significant difference in tumor accumulation was seen with Alexa Fluor 488-labeled Arg_5-ELP_{BC} or non-functionalized ELP_{BC} in hyperthermia-treated tumors or tumors receiving no heat. Mice were administered CPP-ELP_{BC} or control at a total blood concentration of 100 μM. Data represents mean of 3 measurements ± SD.

There were several interesting aspects of accumulation elsewhere in the body when looking at the other collected organs (Figure 71). First, little accumulation was apparent in the heart, liver, lung, and spleen, suggesting minimal off-target uptake in these tissues. Second, the uptake in the muscle, which serves as a non-heated

contralateral control, was less than that seen in the tumor with and without heat for both Arg$_5$-ELP$_{BC}$ and ELP$_{BC}$, suggesting a contribution of passive targeting of these carriers to the tumor. Third, and most striking, was the high percent of the dose that was found in the kidney for both Arg$_5$-ELP$_{BC}$ and the ELP$_{BC}$ control. This preliminary result suggested the molecular weight of this CPP-ELP$_{BC}$ (approximately 40 kDa) might be below the renal filtration cutoff and allow significant clearance via the kidney.

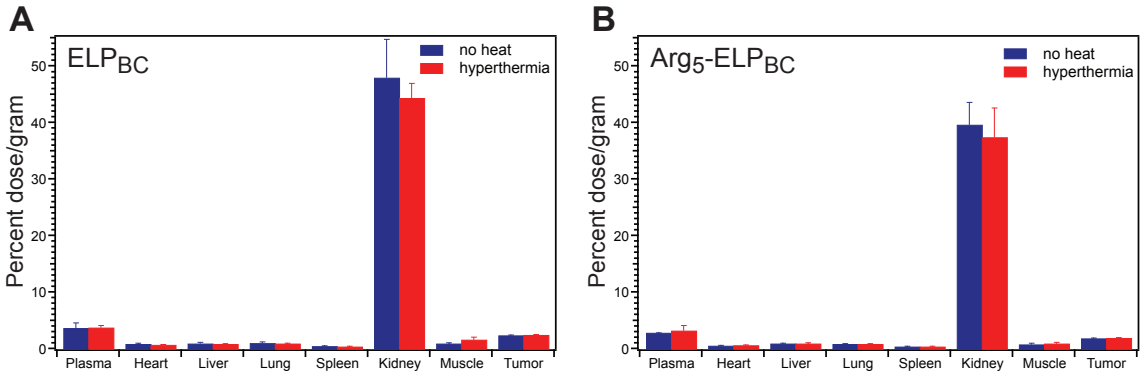

Figure 71: Accumulation of Alexa Fluor 488-labeled Arg$_5$-ELP$_{BC}$ and non-functionalized ELP$_{BC}$ in critical organs did not differ significantly between carriers or thermal conditions of the tumor. A significant fraction of the dose of both Arg$_5$-ELP$_{BC}$ and ELP$_{BC}$ was detected in the kidney. Data represents mean of 3 animals ± SD.

The results of the preliminary pharmacokinetic, intravital imaging, and biodistribution studies for third generation Arg$_5$-ELP$_{BC}$ together suggested several issues preventing successful tumor targeting *in vivo*. First, although the concentration of CPP-ELP$_{BC}$ in the circulation appeared to be sufficient for hyperthermia-triggered micelle assembly over at least 1 hour, it seemed that a significant amount of the carrier was localized in the kidney, perhaps suggesting clearance through this renal pathway. The

consumption of the dose present in the kidney suggested a large amount of carrier was unavailable for tumor targeting, perhaps limiting the ability of the carrier to sufficiently accumulate in the tumor tissue. Second, although no adverse behavior of the CPP-ELP$_{BC}$ was visualized with intravital microscopy, the lack of hyperthermia-controlled tumor uptake as seen in the biodistribution study suggested that the CPP-ELP$_{BC}$ may not be behaving as expected in the *in vivo* environment.

It was only in retrospect of these preliminary studies that the temperature-triggered self-assembly of third generation Arg$_5$-ELP$_{BC}$ was tested in mock serum conditions. Evaluation by temperature-regulated turbidimetry in 90% FBS revealed that Arg$_5$-ELP$_{BC}$ self-assembly was abolished in this mock serum solution (Figure 72), thereby Arg$_5$-ELP$_{BC}$ was unlikely to function with its expected unimer-to-micelle transition *in vivo*. It was interesting that aggregation of the CPP-ELP$_{BC}$ was not seen with *in vivo* imaging, suggesting several factors that may have masked this effect. First, the significant clearance of Arg$_5$-ELP$_{BC}$ may have decreased the concentration of carrier reaching the tumor, preventing aggregation at this temperature and local concentration. Second, although unintended, there may be an interaction effect between the dextran and Arg$_5$-ELP$_{BC}$ as they circulate together throughout the body. Although neutral dextran was utilized, this large molecule does contain charge of a zwitterionic nature. Local concentration of anionic charge on these large molecules may interact with the cationic CPP-ELP$_{BC}$, preventing aggregation or preventing its favorable interaction with

target cells in the tumor. Third, this contradiction between *in vivo* imaging and *ex vivo* characterization by turbidimetry may simply suggest that the mock serum condition of 90% FBS is a poor substitute for the actual conditions the carrier encounters in circulation.

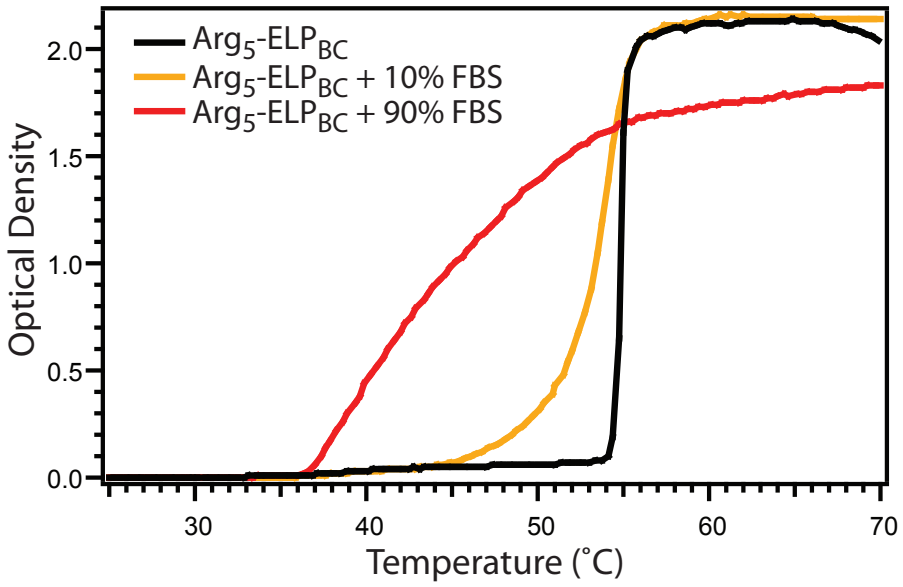

Figure 72: Temperature-regulated turbidimetry revealed the effect of mock serum on the self-assembly of third generation Arg$_5$-ELP$_{BC}$. In the presence of 10% FBS, typical of cell culture conditions, Arg$_5$-ELP$_{BC}$s self-assembled into micelles with a CMT between 37 °C and 42 °C. In 90% FBS, however, micelle assembly was abolished, and Arg$_5$-ELP$_{BC}$ appeared to transition from unimer to aggregate in response to mild hyperthermia. Turbidimetry measurements were acquired at 25 μM.

5.3.4 Synthesis and characterization of fourth generation CPP-ELP$_{BC}$s for optimized use *in vivo*

Two of the potential problems identified by preliminary examination of third generation CPP-ELP$_{BC}$s could be addressed by further optimization of the ELP$_{BC}$ design:

the overall size of the carrier and the stability of micelle assembly in the presence of serum. The CPP-ELP$_{BC}$ design again went under iterative optimization to increase the molecular weight of the carrier while still achieving the desired thermal properties to ensure the transition from unimer to micelle in response to mild hyperthermia. A family of potential CPP-ELP$_{BC}$s was then screened in mock serum conditions to determine the carrier that would display predictable and stable triggered micelle assembly *in vivo*.

To increase the overall molecular weight of the ELP$_{BC}$, an increase in the size of both domains in the block copolymer, each to 80 pentapeptides, was proposed. Due to the inverse relationship of ELP length and T_t, any increase in the ELP size would result in a decrease in the T_t of that block. Therefore, simply increasing the size of the blocks in the existing CPP-ELP$_{BC}$ design would surely lead to a carrier that would display temperature-triggered micelle assembly well below 37 °C, making it inappropriate for hyperthermia-targeted micelle assembly. The sequence of each of the domains therefore had to be changed, such that a more hydrophilic ELP with a higher T_t could compensate for the decrease in T_t caused by the increase in length. An ELP with serine as the guest residue (Table 14) was proposed as a new hydrophilic domain, as the hydrophilicity of the serine residue should increase the T_t as compared to the guest residues alanine and glycine in E2*. The hydrophilicity of this alternative block was exemplified in the measurement of its T_t in excess of 100 °C at 25 μM (Figure 73). Increasing the T_t of the hydrophilic domain was also proposed to aid in the stable micelle assembly of CPP-

ELP$_{BC}$s in serum, by preventing premature aggregation that would lead to a unimer-to-aggregate transition, as opposed to the desired unimer-to-micelle transition.

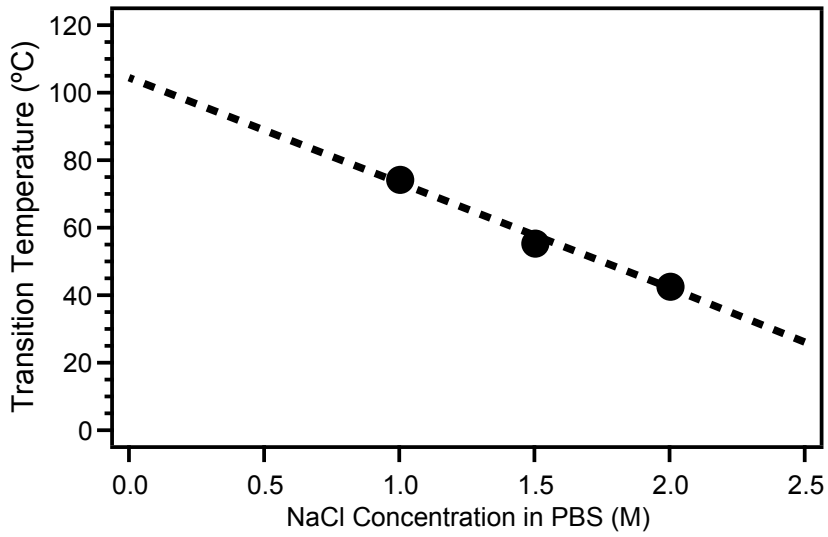

Figure 73: An ELP with serine guest residues was synthesized to increase the T_t of the hydrophilic domain of the block copolymer. This ELP, at 80 pentapeptides in length, displayed a T_t that exceeded 100 °C at 25 μM in PBS, as determined from the extrapolation of T_ts measured by temperature-regulated turbidimetry at increasing concentrations of NaCl in PBS.

The hydrophobic block would control the CMT of the CPP-ELP$_{BC}$, so multiple sequences were investigated for this domain. A family of ELPs with a tunable fraction of alanine and valine residues, as developed by Dr. Jonathan McDaniel [187], were utilized to investigate a range of T_ts to ensure an optimized CMT could be achieved for *in vivo* applications (Table 15). The design scheme to create these optimized fourth generation CPP-ELP$_{BC}$s is shown in Figure 74.

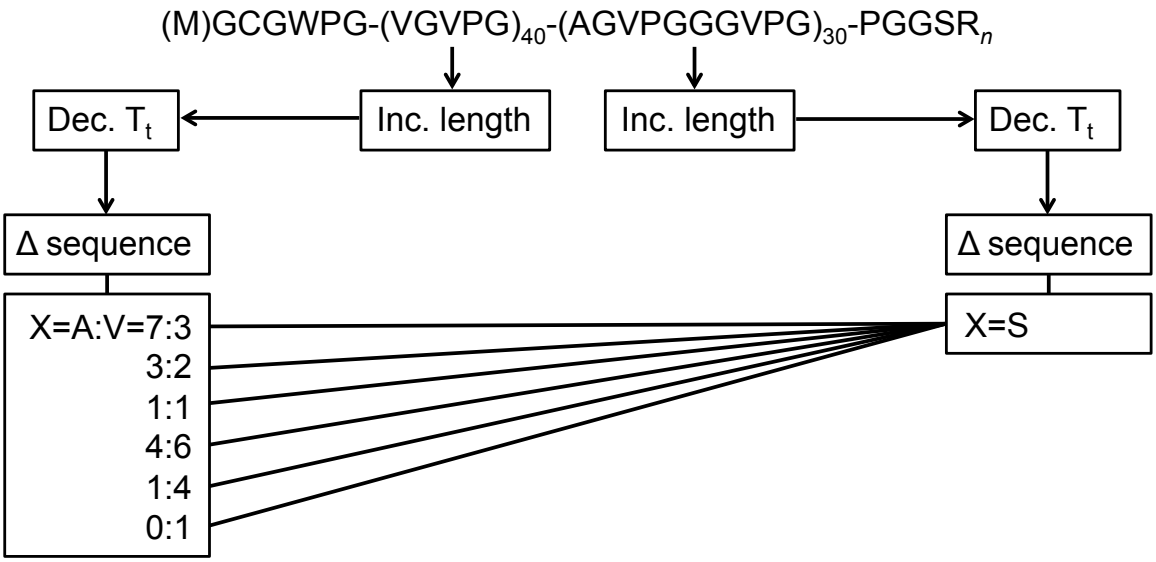

Figure 74: The CPP-ELP$_{BC}$ design was changed to accommodate larger block sizes while maintaining an optimized thermal response. Increased block size required a change in block sequence to avoid a decrease in CMT. A library of ELPs with varying fraction of alanine and valine guest residues was paired with an ELP with serine guest residues to create a family of fourth generation CPP-ELP$_{BC}$s for *in vivo* testing.

The resulting six ELP$_{BC}$s, all 160 pentapeptides in length and with Arg$_5$-functionalization, were characterized by temperature-regulated turbidimetry. A range of CMTs was achieved, among which some were potentially useful for temperature-triggered micelle assembly at 42 °C (Figure 75). As expected, increase in the hydrophobicity of the hydrophobic block, correlating with the fraction of valine guest residues, decreased the CMT of the ELP$_{BC}$. Interestingly, the micelle-to-aggregate transition also changed in response to manipulating the hydrophobic domain, shedding light on the interaction effect between the sequences of the hydrophilic and hydrophobic blocks. When the hydrophobic and hydrophilic block T$_t$s were most different (ex. containing 100% valine and 100% serine guest residues, respectively), there appeared to

be the least interaction between blocks, such that the CMT of this construct was the lowest and the micelle-to-aggregate T_t was at its highest of the ELP$_{BC}$ family evaluated here. As alanine was titrated into the hydrophobic block, the CMT increased and the micelle-to-aggregate T_t decreased, leading to a more limited temperature range over which stable micelle assembly was achieved. This trend continued across the family of ELP$_{BC}$s, such that the ELP$_{BC}$ with the hydrophobic domain containing alanine:glycine guest residues at a ratio of 7:3 only displayed a unimer-to-aggregate transition that was predictable given the trend in decreasing micelle range.

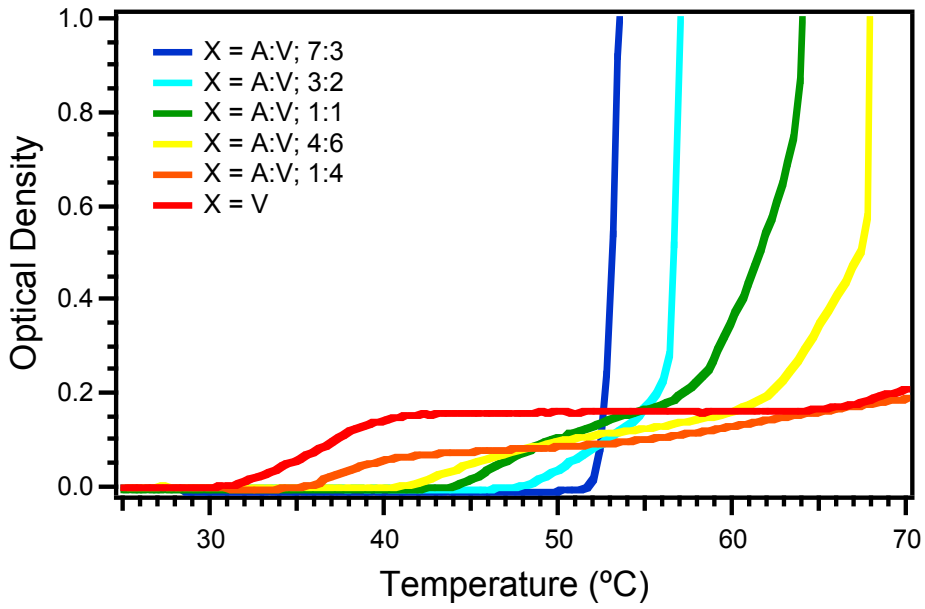

Figure 75: The CMT of fourth generation CPP-ELP$_{BC}$s was tuned by manipulation of the hydrophobic block sequence composed of alanine and valine residues (X) in varying ratios. Temperature-regulated turbidimetry confirmed a range of CMTs, some of which could be feasible for hyperthermia-triggered micelle assembly *in vivo*. All ELP$_{BC}$s were functionalized with Arg$_5$ and characterized at 25 μM in PBS.

Of the six new CPP-ELP$_{BC}$s, the four constructs with the lower CMTs were chosen for preliminary characterization in mock serum. All constructs demonstrated a slight decrease in CMT and a more significant decrease of the micelle-to-aggregate T_t in the presence of 90% FBS (Figure 76). Although this result confirmed a limited micelle range in the presence of serum, it was encouraging to see that these fourth generation ELP$_{BC}$s could support the self-assembly of Arg$_5$-functionalized micelles in the presence of serum, unlike the third generation ELP$_{BC}$ before it.

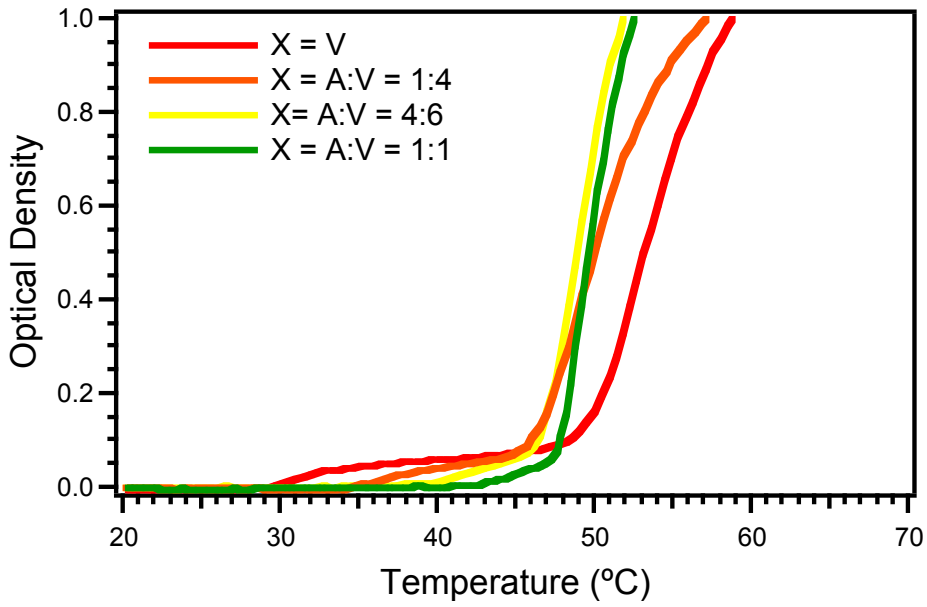

Figure 76: Temperature-regulated turbidimetry of fourth generation Arg$_5$-ELP$_{BC}$s at 25 μM in 90% FBS demonstrated their potential behaviors in blood. All constructs demonstrated a decreased CMT and micelle-to-aggregate T_t in the presence of serum.

The two ELP$_{BC}$s who displayed a CMT closest to 37-42 °C were then selected from this family of four ELP$_{BC}$s and their concentration-dependent temperature-

triggered micelle assembly was measured over a range of 5-100 μM. Evaluation of the CMT with respect to concentration would provide insight into what dose was best to inject *in vivo*, and how wide a concentration range was permitted in which the CMT would remain between 37 °C and 42 °C. The ELP_{BC} with hydrophobic block $(XGVPG)_{80}$[X=A:V=4:6] was selected as the ideal candidate, as its CMT remained between 37 °C and 42 °C over a concentration range of 10 to 100 μM (Figure 77). This construct was selected for future evaluation *in vivo*.

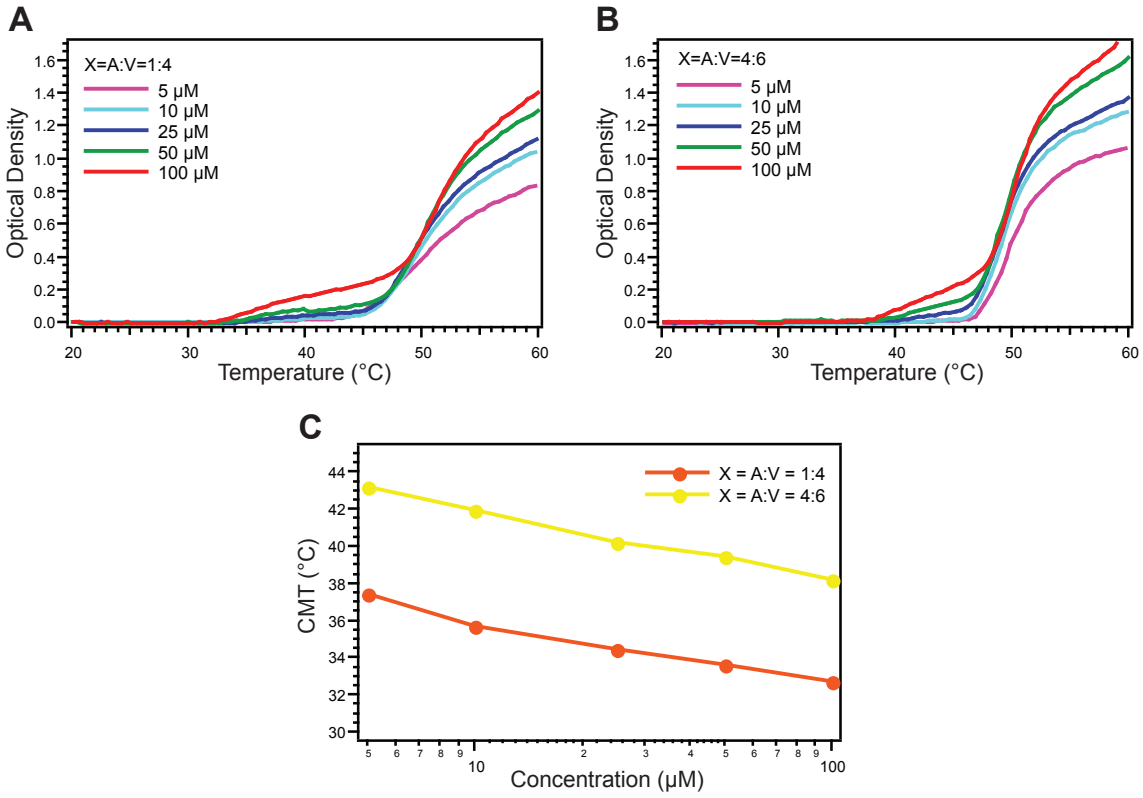

Figure 77: Temperature-regulated turbidimetry was used to measure the thermal behavior of Arg_5-ELP_{BC}s whose hydrophobic blocks contained guest residues X=A:V=1:4 or X=A:V=4:6 in 90% FBS over a concentration range from 5-100 μM. The

ELP_{BC} with hydrophobic guest residues X=A:V=4:6 was selected for further analysis *in vivo*, as its CMT remained between 37 °C and 42 °C over a concentration range of 10-100 μM, ensuring temperature-triggered micelle assembly *in vivo* over the course of hyperthermia treatment as the ELP is gradually cleared from the blood.

With a chosen ELP_{BC}, a family of constructs was then thoroughly characterized prior to its evaluation *in vivo*. This ELP_{BC}, MGCGWPG-$(XGVPG)_{80}$[X=A:V=4:6]-$(SGVPG)_{80}$-$PGGSR_n$ was functionalized with Arg_5 or Arg_8 to evaluate those CPPs that encompassed the breadth of charge and the breadth of cellular uptake as determine by *in vitro* studies. These CPP-ELP_{BC}s and a non-functionalized control were first characterized in PBS across a concentration range of 5-100 μM (Figure 78A-C). The turbidimetry curves for Arg_8-ELP_{BC} looked different than those for Arg_5-ELP_{BC} or ELP_{BC}, suggesting differences in the stability of micelle formation between these constructs. The CMT was approximated from turbidimetry curves and plotted versus concentration (Figure 78D). Arg_5-ELP_{BC} and non-functionalized ELP_{BC} demonstrated nearly identical CMTs over the concentration range, all between 40 °C and 45 °C over 5-100 μM. Arg_8-ELP_{BC} however, displayed a depressed CMT that dropped below 37 °C at concentrations above 25 μM.

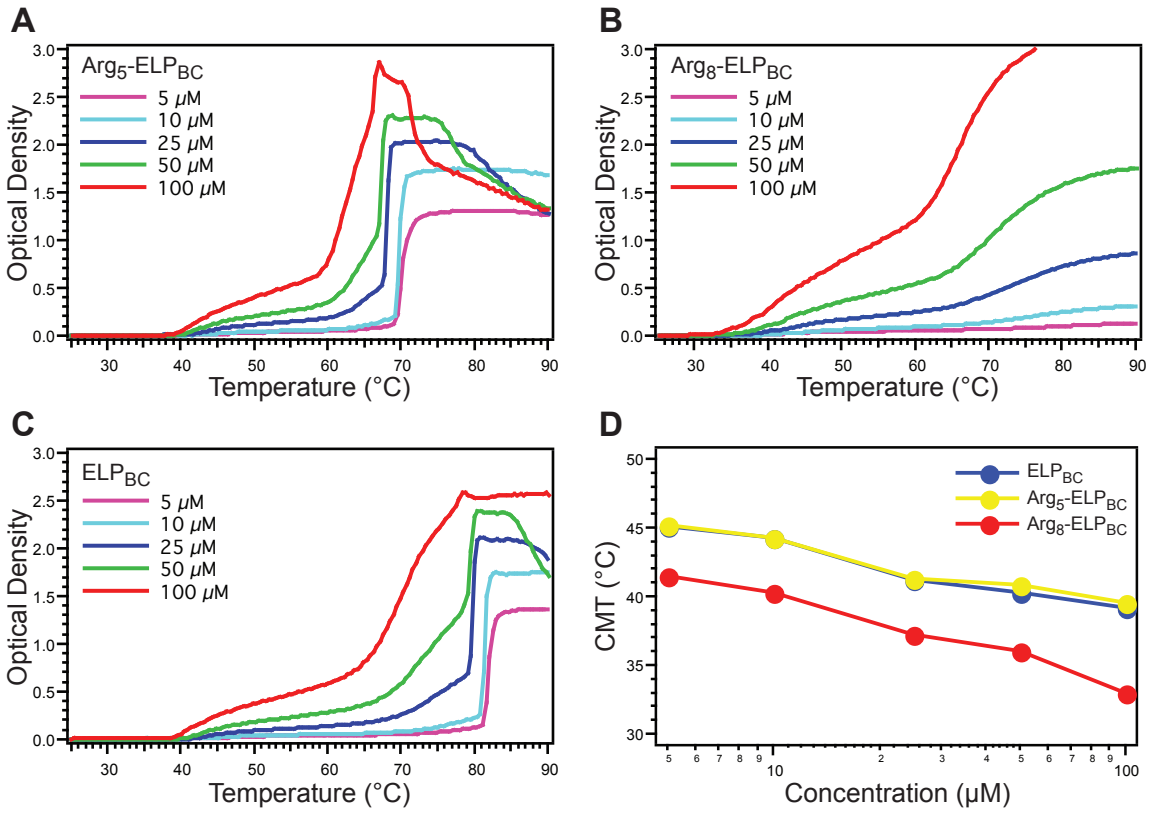

Figure 78: Optimized fourth generation ELP$_{BC}$ was characterized with Arg$_5$ (A), Arg$_8$ (B), or no functionalization (C) across a range of concentrations in PBS. While a CMT between 40-45 °C was conserved for Arg$_5$-ELP$_{BC}$ and ELP$_{BC}$, the CMT was depressed for Arg$_8$-ELP$_{BC}$, dropping below 37 °C at concentrations above 25 μM (D).

This characterization was then repeated, this time in 90% FBS to mimic the environment in circulation. Again the turbidimetry curves for Arg$_8$-ELP$_{BC}$ looked significantly different than those for Arg$_5$-ELP$_{BC}$ or non-functionalized ELP$_{BC}$ (Figure 79A-C). However, this time the Arg$_8$-ELP$_{BC}$ did not appear to exhibit temperature-triggered micelle assembly, but rather appeared to transition from unimer to aggregate in the presence of mock serum. This suggested that Arg$_8$-ELP$_{BC}$ would not display the desired hyperthermia-triggered micelle assembly *in vivo*. So, although the optimized

fourth generation ELP$_{BC}$ could improve stable micelle formation to support the assembly of Arg$_5$-functionalized micelles, it could not do the same for Arg$_8$-functionalized constructs. Arg$_5$-ELP$_{BC}$ and non-functionalized ELP$_{BC}$, however, continued to display a well-conserved CMT between constructs and across concentrations (Figure 79D). Each maintained a CMT between approximately 37 °C and 44 °C from 5 μM to 100 μM.

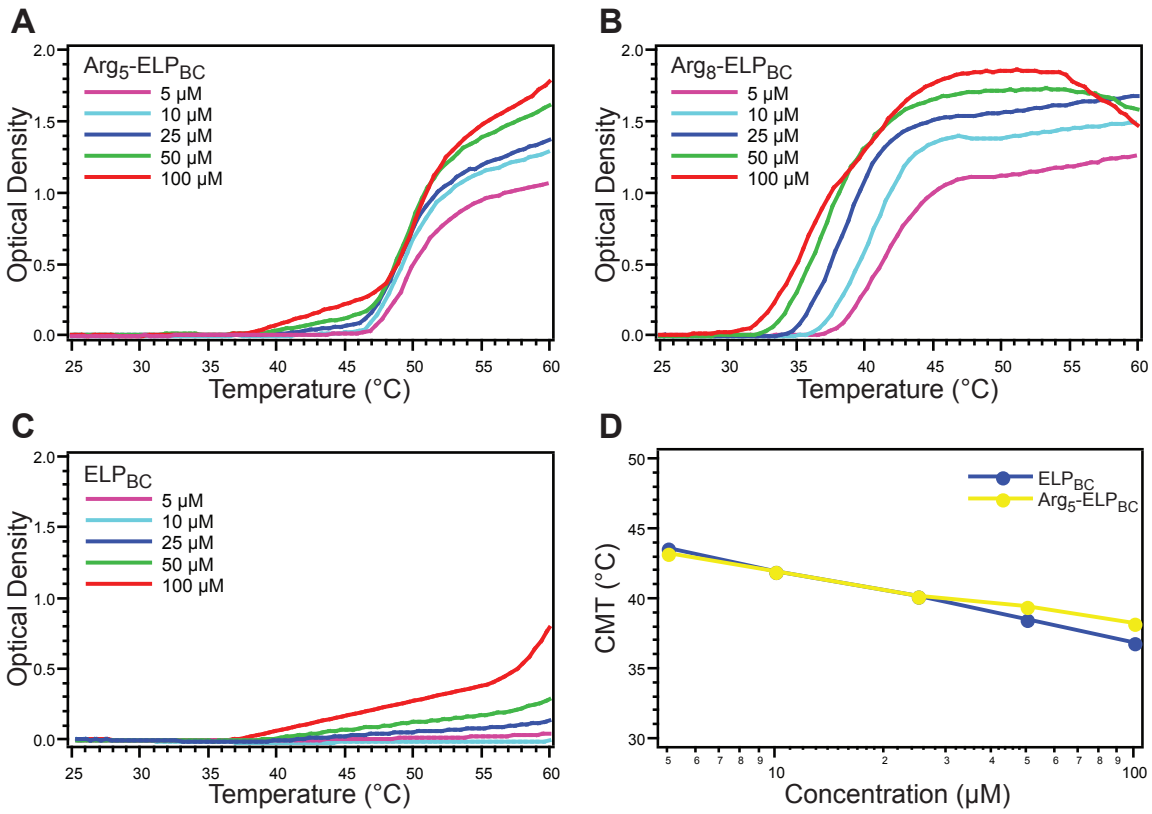

Figure 79: Optimized fourth generation ELP$_{BC}$ was characterized with Arg$_5$ (A), Arg$_8$ (B), or no functionalization (C) across a range of concentrations in 90% FBS to mimic the environment in circulation. While a CMT between 37-44 °C was conserved for Arg$_5$-ELP$_{BC}$ and ELP$_{BC}$ (D), the Arg$_8$-ELP$_{BC}$ did not self-assemble into micelles in mock serum, but rather exhibited a unimer-to-aggregate transition.

Due to confounding results with the third generation Arg_5-ELP_{BC} thermal behavior and its visualization *in vivo*, it was a concern that perhaps 90% FBS was not an appropriate solution in which to approximate the serum conditions *in vivo*. 90% FBS has been used extensively in the Chilkoti lab as a mock serum solution [188] and has provided similar results to 3 mM BSA, another mock serum solution whose effect on ELP T_t has been verified with comparison to mouse serum. However, to cross check the results seen in the mock serum of 90% FBS, thermal characterization was further performed in mouse serum. In this experiment fluorophore-labeled ELP_{BC}s were injected intravenously by tail vein and then blood was collected immediately from the mouse by heart puncture. Cells were removed from the collected blood by centrifugation and the resulting liquid was characterized by temperature-regulated turbidimetry.

The first attempt to analyze the ELP_{BC} micelle assembly in mouse serum was performed in balb/c mice with fourth generation Arg_8-ELP_{BC}, Arg_5-ELP_{BC}, and an ELP_{BC} control. The collected blood was heparinized to yield serum, which was diluted with PBS to reach the volume requirements for solution analysis by temperature-regulated turbidimetry. All three constructs demonstrated turbidimetry curves that suggested a unimer-to-micelle transition between 40-45 °C, where Arg_8-ELP_{BC} surprisingly did not portray a drastic increase in absorbance that suggested its complete aggregation in serum, contradicting the results obtained in the mock serum of 90% FBS (Figure 80A).

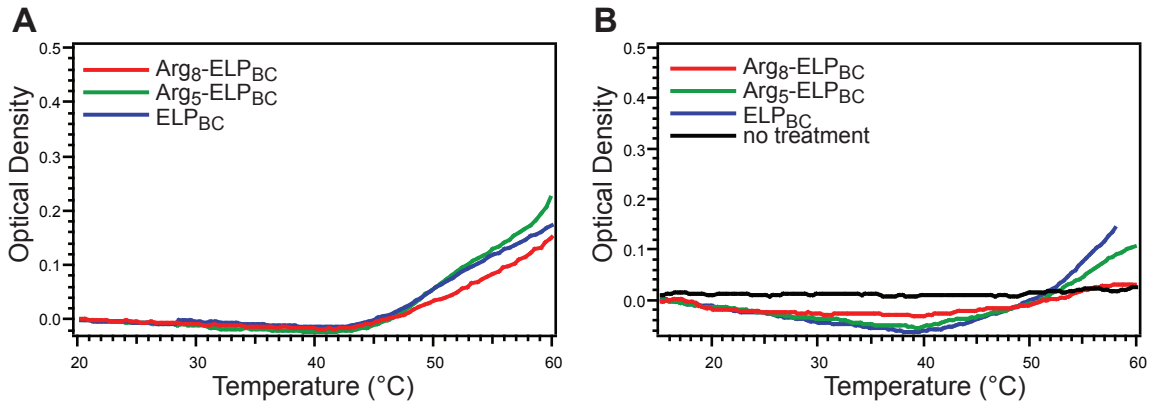

Figure 80: Temperature-regulated turbidimetry was attempted in mouse serum to approximate CPP-ELP$_{BC}$ behavior *in vivo*. The first attempt (A) and modified second attempt (B) both supported the expected micelle assembly of Arg$_5$-ELP$_{BC}$ and ELP$_{BC}$, but neither attempt provided sufficient support that Arg$_8$-ELP$_{BC}$ would exhibit temperature-triggered aggregation in blood.

Upon further reflection, it was questionable whether several aspects of this protocol could have contributed to this unexpected result for Arg$_8$-ELP$_{BC}$. First, the addition of heparin to these samples may have interacted with the positively charged CPP-ELP$_{BC}$s, removing some fraction of material along with the cells and coagulation factors in the centrifugation step. Second, the dilution of samples to meet the volume requirements of turbidimetry measurements may have reduced the concentration of serum proteins to the extent that Arg$_8$-ELP$_{BC}$ could self-assemble in this diluted serum. Third, both of the factors above may have resulted in the decrease of Arg$_8$-ELP$_{BC}$ to a concentration that would not aggregate at the temperatures measured. This may have contributed to the CMT of all constructs at temperatures higher than what is preferable for hyperthermia-triggered micelle assembly at 42 °C.

To address these potentially confounding factors, this experiment was reattempted in a new format. Arg_8-ELP_{BC}, Arg_5-ELP_{BC}, and ELP_{BC} were intravenously injected, this time into nude mice due to their apparent increased blood volume, as compared to balb/c mice. The increased blood volume of this mouse strain should help prevent the need for dilution for turbidimetry measurements. The blood was collected immediately via heart puncture, but this time no heparin was added so the blood was stored on ice and allowed to clot. Again the blood was centrifuged to remove cells and clotted factors. The fluorescence of the supernatant was then measured to back-calculate the concentration of the ELP_{BC} based on standard curves of each treatment, to ensure that a significant amount of the constructs was not lost in the process of recovery from the blood sample. If necessary, the samples were pooled between mice receiving the same treatment to meet the volume requirements for turbidimetry measurements and prevent the need for sample dilution.

In this modified second attempt at evaluating the thermal behavior of CPP-ELP_{BC}s in mouse serum the turbidimetry curves exhibited a gradual decrease in absorbance as the temperature increased, then exhibited an inflection point near the expected CMT of 40 °C, based on their back-calculated concentration, and increased in absorbance thereafter as temperature continued to rise (Figure 80B). This behavior, however, was less evident for the Arg_8-ELP_{BC}, as compared to the Arg_5-ELP_{BC} or non-functionalized ELP_{BC}, perhaps suggesting a different behavior for this most highly

charged construct. However, Arg_8-ELP_{BC} more closely resembled the control curve from a mouse receiving no ELP treatment, which did not change absorbance over the temperatures examined. Still, there was no strong evidence from the mouse serum experiments that supported that Arg_8-ELP_{BC} would undergo only a unimer-to-aggregate transition in blood. It thus remained unclear what approach was best to approximate the behavior *in vivo* using *ex vivo* turbidimetry measurements.

5.3.5 Evaluation of fourth generation CPP-ELP_{BC}s *in vivo*

Fourth generation CPP-ELP_{BC}s were characterized as best as possible *ex vivo* in attempts of creating a material that would behave predictably in the *in vivo* setting. Further characterization of these constructs was then attempted by means of evaluating their functional performance as carriers *in vivo*. Pharmacokinetics was again the first parameter to be tested *in vivo* to provide insight into the best dosage and the range of concentration that could be maintained in the blood over time.

Mice were injected intravenously with Alexa Fluor 488-labeled fourth generation CPP-ELP_{BC} or non-functionalized ELP_{BC} and blood was sampled from the tail vein over the course of 24 hours. The fluorescence of the sampled blood at each time point was used to determine the blood concentration of the CPP-ELP_{BC} based on standard curves from the injected construct. Charge played an important factor in the clearance of fourth generation CPP-ELP_{BC}s from circulation. The ELP_{BC} control exhibited the most prolonged circulation, while in comparison, Arg_5-ELP_{BC} was cleared slightly more

quickly and Arg$_8$-ELP$_{BC}$ was cleared the fastest from circulation (Figure 81). However, all constructs maintained a concentration of 20 μM or greater over the course of 2 hours, such that a CMT between 37 °C and 42 °C should be achieved at this concentration over a time frame suitable for mild hyperthermia.

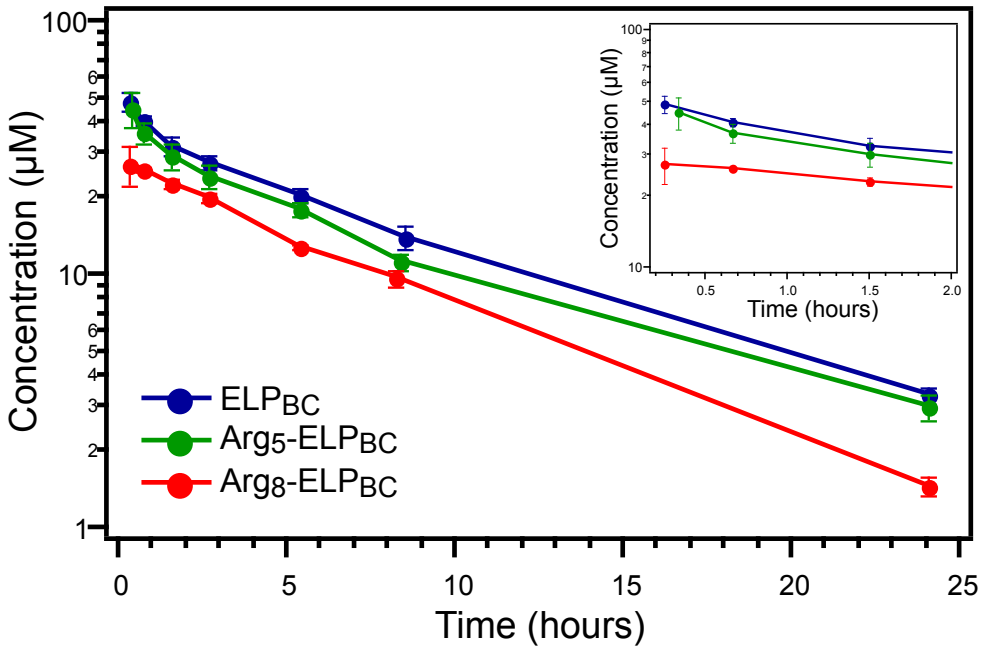

Figure 81: CPP-functionalization led to more rapid clearance of fourth generation CPP-ELP$_{BC}$s, where Arg$_8$-ELP$_{BC}$ was cleared the fastest from circulation. Yet all constructs maintained a blood concentration of greater than 20 μM over the course of 2 hours (inset). CPP-ELP$_{BC}$s and non-functionalized ELP$_{BC}$ were delivered intravenously at a final blood concentration of 100 μM.

Approximation of the pharmacokinetic parameters supported the trend visualized in clearance profiles, whereby non-functionalized ELP$_{BC}$ achieved the greatest AUC as compared to Arg$_5$-ELP$_{BC}$ or Arg$_8$-ELP$_{BC}$ (Table 17). However, Arg$_5$-ELP$_{BC}$ was actually approximated to have a longer elimination half-life, as compared to ELP$_{BC}$,

although the subtle difference in this parameter suggested that the Arg_5-functionalization was not detrimental to the clearance of this construct. The effect of Arg_8-functionalization, however, was much greater and indeed the data obtained from this pharmacokinetic experiment were difficult to fit to pharmacokinetic parameters, perhaps due to their rapid decline in concentration at early time points. Interestingly, fourth generation constructs all exhibited faster clearance, as determined by approximated pharmacokinetic parameters, as compared to third generation constructs, despite their increased molecular weight. This was likely due to the change in the quantification of data between these experiments, whereby third generation constructs were normalized to early time points that were assumed to be near the delivered dose, whereas fourth generation constructs were evaluated by actual concentration values back-calculated from their fluorescence. The later approach improved the quantitative validation of circulating CPP-ELP_{BC}s and controls, thus suggesting that previous data for third generation carriers more than likely overestimated the pharmacokinetic performance.

Table 17: Pharmacokinetic parameters of fourth generation CPP-ELP_{BC}s and control. *Arg_8-ELP_{BC} clearance could not be confidently fit to determine some parameters, the unreasonably high SD suggested they should be used only for qualitative comparison.

Construct	α $t_{1/2}$ (minute)	β $t_{1/2}$ (hour)	AUC (μM•h)
ELP_{BC}	7.5 ± 0.8	6.8 ± 0.1	377.4 ± 5.9
Arg_5-ELP_{BC}	9.4 ± 1.0	7.2 ± 0.2	325.9 ± 7.3
Arg_8-ELP_{BC}	0.6 *	5.8 ± 0.3	220.9*

Pharmacokinetics suggested that all constructs would maintain the necessary concentration in circulation over the course of 1 hour to exhibit a CMT between 37 °C and 42 °C and thus provide hyperthermia-triggered self-assembly *in vivo*. The effect of hyperthermia-triggered micelle assembly was first evaluated *in vivo* by visualizing the interaction of constructs with the tumor vascular and extravascular space using intravital microscopy. CPP-ELP$_{BC}$ was injected systemically and the tumor space was imaged over the course of 1 hour while heated to 37 °C or 42 °C. At the end of imaging, dextran was injected to mark the vascular space and Hoechst was injected to locate cellular nuclei.

Non-functionalized ELP$_{BC}$ administered to non-heated tumors was confined to the vascular space immediately after injection (Figure 82). Over the course of 1 hour the ELP$_{BC}$ traversed from the vascular to the extravascular space, leading to fluorescence across the entire imaging window. Dextran labeling confirmed that although the ELP$_{BC}$ did extravasate, a portion of the construct did still remain in the vasculature at 1 hour. Hoechst staining demonstrated that the fluorescence in the extravascular space was not localized specifically to cells, marked by their nuclei, in the tissue. The extravasation pattern was similar for ELP$_{BC}$ in a tumor heated to 42 °C, suggesting that the accumulation of ELP$_{BC}$ in the extravascular space was not affected significantly by tumor hyperthermia.

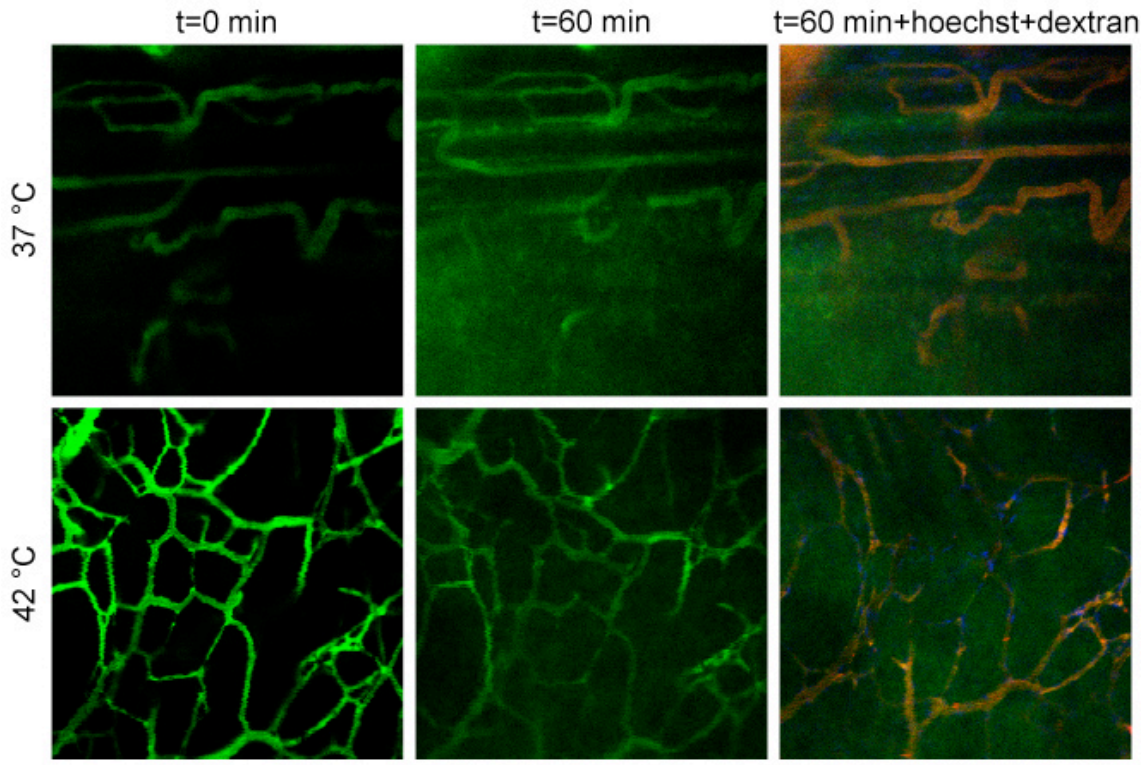

Figure 82: Intravital imaging of ELP$_{BC}$ demonstrated accumulation in the extravascular space over the course of 1 hour that did not change significantly with tumor hyperthermia. Green—ELP; red—vascular mask; blue—cell nuclei; acquired at 20x.

The behavior of Arg$_5$-ELP$_{BC}$ did not appear to be distinctively different than the control non-functionalized ELP$_{BC}$. Similarly to that seen with ELP$_{BC}$, Arg$_5$-ELP$_{BC}$ was at first confined to the vascular space and extravasated into the tumor tissue over 1 hour (Figure 83). The degree or specificity of extravasation didn't seem to change significantly with tumor hyperthermia, suggesting that differences between unimer and micelle Arg$_5$-ELP$_{BC}$, if any, were not easily visualized. Subtle differences may, however, be revealed by more thorough image processing to quantify parameters such as extravasation, permeability, and penetration using a larger sample number of mice for each treatment

condition. Of note however, were distinct areas in the hyperthermia treated tumor that strongly excluded the Arg_5-ELP_{BC} in the extravascular space. The shape and association of these areas with an adjacent nuclei suggested that these might be adipocytes that do not take up Arg_5-ELP_{BC} into their fat reservoirs.

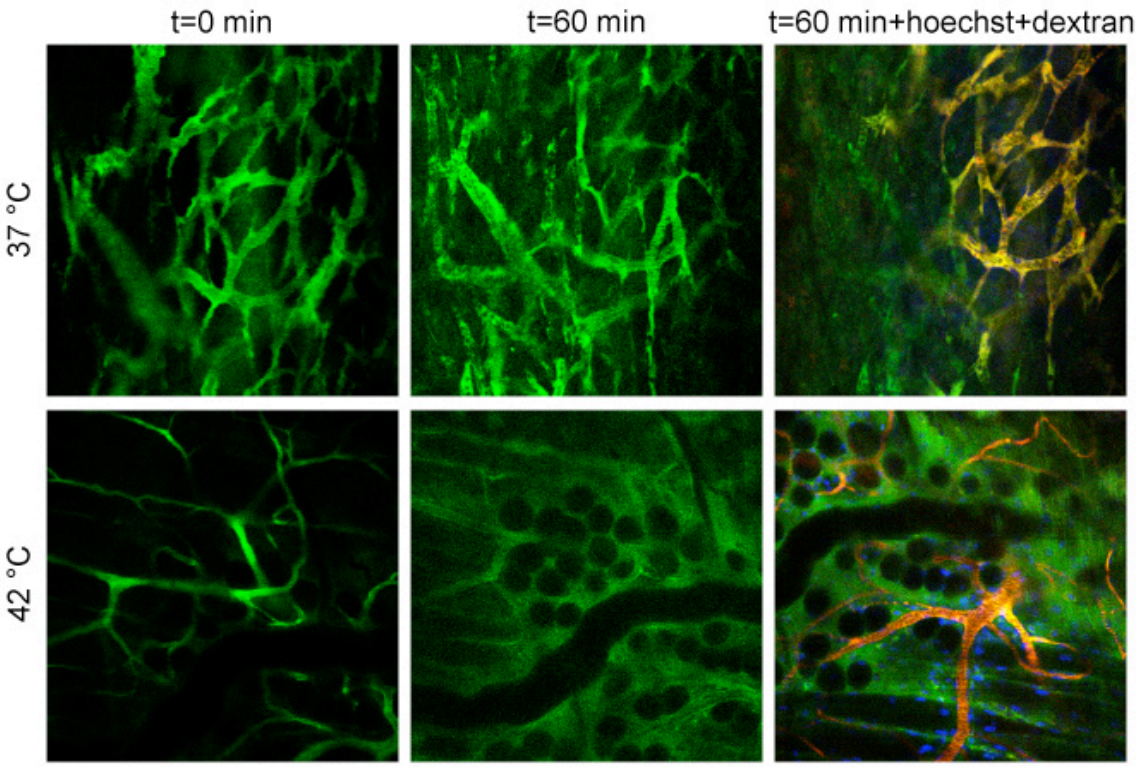

Figure 83: Intravital imaging of Arg_5-ELP_{BC} demonstrated accumulation in the extravascular space over the course of 1 hour that did not change significantly with tumor hyperthermia. The extravasation, with time, did not appear to differ greatly from the non-functionalized ELP_{BC} control. Green—ELP; red—vascular mask; blue—cell nuclei; acquired at 20x.

Intravital imaging of Arg_8-ELP_{BC} in a hyperthermia treated tumor demonstrated a different behavior than that seen with Arg_5-ELP_{BC} or ELP_{BC}. Arg_8-ELP_{BC} looked similar

to the other constructs upon injection, with relatively homogenous fluorescence confined to the vascular space. However, Arg_8-ELP_{BC} quickly aggregated in the heated tumor as indicated by the formation of punctate fluorescence in the vasculature at 20 minutes (Figure 84). To confirm that this punctate fluorescence was a result of the ELP aggregation, and not an interaction of the construct with the vasculature, the tumor was cooled to below 37 °C. The punctate fluorescence disappeared as the aggregated ELP resolubilized and continued to circulate in the vasculature. Visualization of the Arg_8-ELP_{BC} therefore finally clarified the confounding findings made in trying to predict the behavior of this construct *in vivo* and confirmed that Arg_8-ELP_{BC} did aggregate in circulation. Furthermore this validated the use of 90% FBS as a mock serum, as it best predicted the behavior of Arg_8-ELP_{BC}, which was confirmed by intravital imaging in a hyperthermia treated tumor.

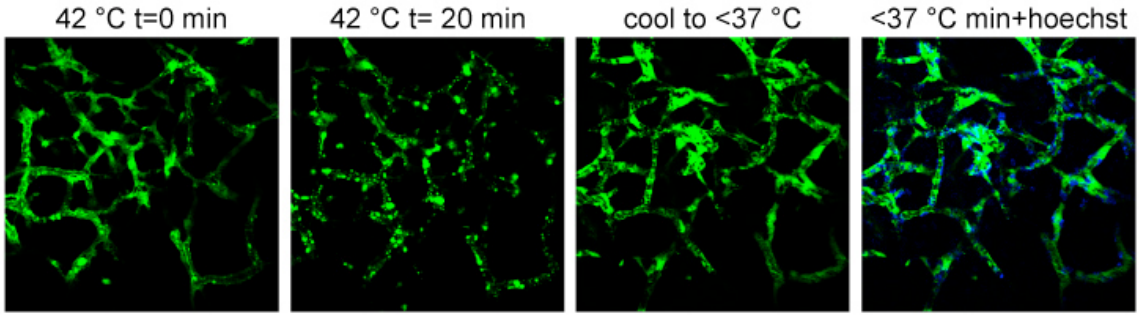

Figure 84: Intravital imaging of Arg_8-ELP_{BC} demonstrated aggregation in a hyperthermia treated tumor. Punctate fluorescence confirmed that Arg_8-ELP_{BC} aggregated in hyperthermia-treated tumors and could be resolubilized when the tumor was cooled below 37 °C. Green—ELP; blue—cell nuclei; acquired at 20x.

Although there were no obvious differences between the behavior of Arg_5-ELP_{BC} and ELP_{BC} as visualized by intravital microscopy, and although Arg_8-ELP_{BC} aggregated as opposed to forming micelles in response to hyperthermia *in vivo*, the biodistribution of these constructs in tumor and critical organs was evaluated as an alternative approach to identify differences, if any, between the *in vivo* behavior of these constructs that could shed light on their potential to achieve tumor-targeted accumulation in response to a hyperthermia trigger.

Biodistribution was evaluated in critical organs and tumors, treated with hyperthermia or receiving no heat, for fourth generation Arg_8-ELP_{BC}, Arg_5-ELP_{BC}, and non-functionalized ELP_{BC} control. In one group of animals the organs were collected and the dose in each organ was quantified at approximately 2 hours after administration. In a second group of animals the organs were collected and dose in each organ was quantified at approximately 24 hours after administration. This extended time point was included to investigate if CPP-ELP_{BC}s may provide an advantage of prolonged presence in the tumor, as compared to non-functionalized ELP_{BC}, by means of their intended local internalization with hyperthermia-triggered micelle assembly in the tumor.

Biodistribution data retrieved 2 hours after administration revealed several interesting points about the uptake in various organs of these fourth generation CPP-ELP_{BC}s (Figure 85A-C). First, none of the constructs appeared to accumulate significantly in the muscle, heart, lung, or spleen, with slightly increased accumulation in the liver in

all cases. Second, despite the increased size of these fourth generation ELP$_{BC}$s there was still the most significant amount of the dose present in the kidney, albeit at lower levels than was observed in the smaller third generation constructs. This persistent accumulation in the kidney, despite the increased molecular weight of the ELP$_{BC}$, may suggest specific interaction of the CPP-ELP$_{BC}$ with the kidney tissue. Higher salt concentration in the kidney tissue, for example, could induce aggregation of CPP-ELP$_{BC}$s and result in their prolonged presence in the kidney. Third, all constructs showed accumulation in the tumor higher than the muscle at either thermal condition, demonstrating a passive mechanism of tumor uptake in all cases. Finally, accumulation in the tumor followed a subtle trend dependent on carrier and tumor heating (Figure 85D). No difference in tumor accumulation of ELP$_{BC}$ was seen between hyperthermia treated tumor and tumor receiving no heat. Arg$_5$-ELP$_{BC}$ achieved a slight increase in accumulation with tumor hyperthermia and temperature-triggered micelle assembly. Arg$_8$-ELP$_{BC}$ achieved the greatest increase in accumulation with tumor hyperthermia and temperature-triggered aggregation, although this effect appears exaggerated due to the lowest tumor accumulation in non-heated tumor with this construct. This increase in tumor accumulation of Arg$_8$-ELP$_{BC}$ with tumor hyperthermia was statistically significant (p<0.0167 between thermal conditions, two-way ANOVA, Bonferroni posthoc test for multiple comparisons). These trends exhibit modest efficacy, at best, of a targeted carrier system and suggest that of the constructs tested, a material that aggregates as opposed

to assembles into predictable nanoparticle morphologies, can achieve greater tumor accumulation in response to hyperthermia.

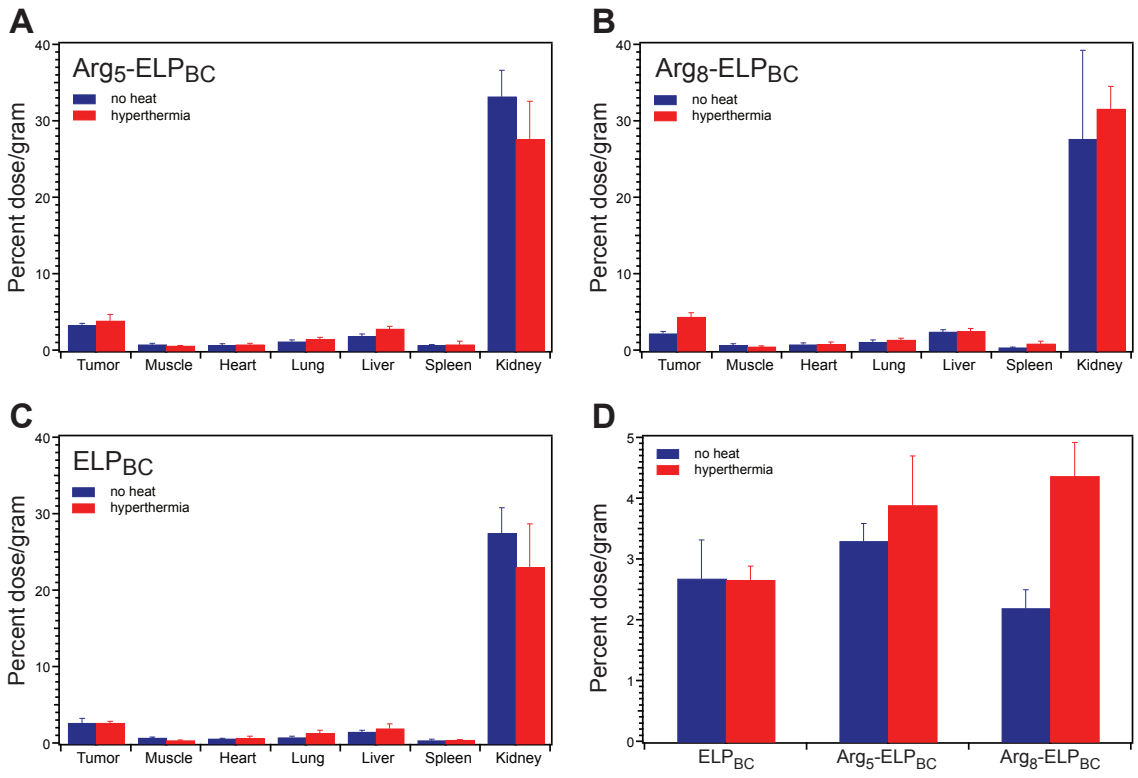

Figure 85: Biodistribution of fourth generation CPP-ELP$_{BC}$s in tumor and critical organs collected 2 hours after administration. Significant percentage of the dose still accumulated in the kidney, despite the high molecular weight of these constructs. Arg$_5$-ELP$_{BC}$ and Arg$_8$-ELP$_{BC}$ achieved modest increase of accumulation in hyperthermia-treated tumors, as compared to tumors receiving no heat. Data represents mean of 3-4 mice ± SEM.

Biodistribution data collected 24 hours after administration confirmed that all constructs were significantly cleared from the muscle, heart, lung, and spleen at this longer time point (Figure 86A-C). Surprisingly the high dose accumulated in the kidney persisted, as did a lower percentage of dose in the liver. Tumor accumulation at 24 hours

remained higher than muscle as well, confirming the retention of passively accumulated constructs in the tumor. However, no trend remained in tumor accumulation at this later time point for CPP-ELP$_{BC}$ treatment or tumor heating, such that no significant difference was detected for any of the constructs between tumors treated with hyperthermia and those treated with no heat (between thermal conditions, two-way ANOVA, Bonferroni posthoc test for multiple comparisons) (Figure 86D). This suggested that constructs were either cleared from the tumor or their fluorescent labels were destroyed over the course of 24 hours following administration.

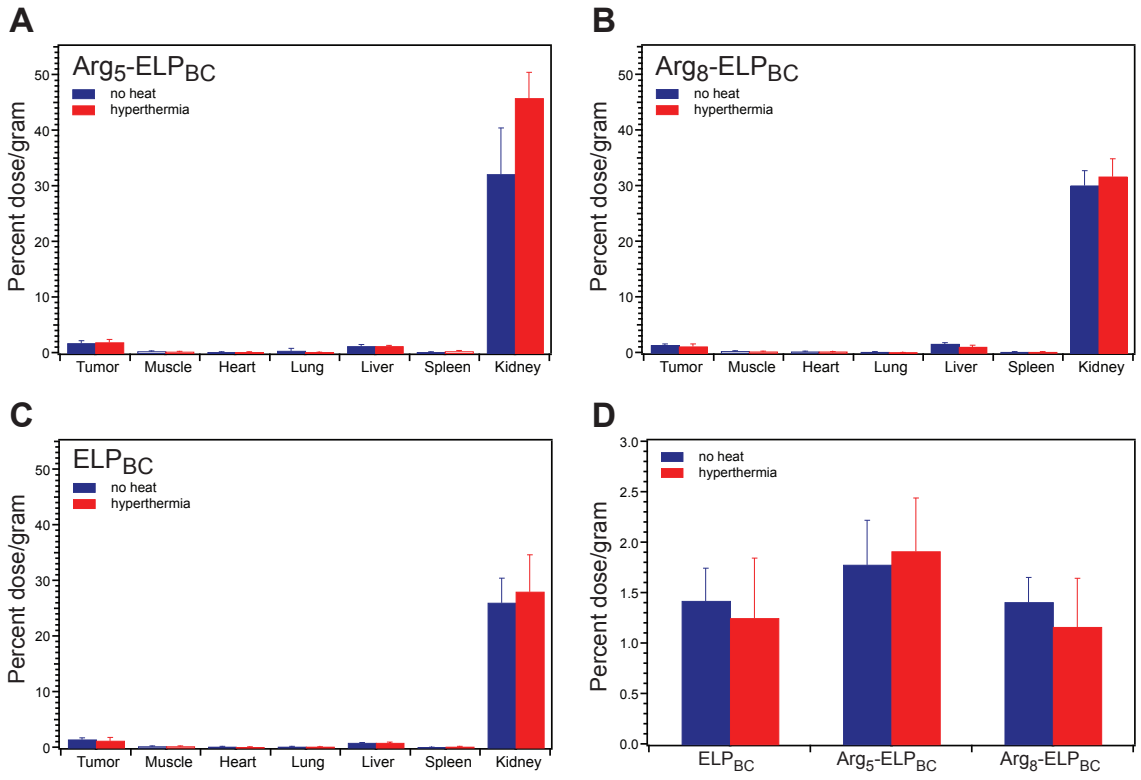

Figure 86: Biodistribution of fourth generation CPP-ELP$_{BC}$s in tumor and critical organs collected 24 hours after administration. No trends were evident between CPP-ELP$_{BC}$ treatments or between tumors receiving hyperthermia and those receiving no heat at this later time point. Data represents mean of 4 mice ± SEM.

5.4 Conclusions

A major challenge in the translation of CPP-ELP$_{BC}$s for use as stimulus-responsive carriers in the body is the optimization of their design to achieve their intended behavior *in vivo*. Starting from the characterization of third generation CPP-ELP$_{BC}$s *in vivo*, it became apparent that the size and thermal behavior of the ELP$_{BC}$s optimized for *in vitro* studies were not appropriate for *in vivo* studies. A new family of CPP-ELP$_{BC}$s—the fourth generation constructs—were redesigned in such a way to have an increased molecular weight, in hopes of avoiding renal clearance, increased

hydrophilicity in the corona, to encourage stable assembly of micelles decorated with positive charge in the presence of serum proteins, and a conserved thermal response to hyperthermia, such that unimers at 37 °C could assemble into micelles at 42 °C.

With an optimized family of CPP-ELP$_{BC}$s, it was apparent that characterization should be performed in conditions that would attempt to mimic the complex environment that the carriers would be exposed to upon systemic injection in a living system. FBS and mouse serum were employed to best choose the ELP$_{BC}$ that would perform properly and predictively *in vivo*. However, confounding results between these mock serum conditions made it unclear whether or not the most heavily charged construct, Arg$_8$-ELP$_{BC}$, could self-assemble into micelles in blood or if the high charge density of this carrier caused it to transition directly from unimer to aggregate in circulation.

The ultimate characterization of CPP-ELP$_{BC}$s was a measurement of its function based on circulation time, interaction with the tumor tissue, and biodistribution. Not surprisingly, increased charge led to decreased circulation time as measured by pharmacokinetics, but all constructs appeared to maintain a blood concentration that was sufficient for hyperthermia-targeted self-assembly over the required 1 hour for hyperthermia treatment following CPP-ELP$_{BC}$ administration. Intravital imaging was used to visualize the interaction of CPP-ELP$_{BC}$s with the tumor vasculature and extravascular space. No significant differences in extravascular accumulation or

localization of Arg_5-ELP_{BC} was seen as compared between heated and non-heated tumors or compared to the ELP_{BC} control. However, intravital imaging did elucidate the thermal behavior of Arg_8-ELP_{BC}, confirming that it did aggregate in hyperthermia treated tumors and could be resolubilized with tumor cooling.

Biodistribution studies had the potential to reveal information about the bigger picture of tumor-targeted delivery in terms of quantifying the accumulation in the tumor and other off-target organs. Modest trends in tumor accumulation suggested that Arg_5-ELP_{BC} and Arg_8-ELP_{BC} achieved increased accumulation in hyperthermia treated tumors, as compared to non-heated tumors, whereas non-functionalized ELP_{BC} showed no difference in accumulation between thermal conditions. From the biodistribution studies of fourth generation CPP-ELP_{BC}s the concern remained regarding the high percentage of dose accumulating in the kidney, which persisted for at least 24 hours after administration, despite the increased molecular weight of these constructs. It was unclear if these results suggested that free fluorophore was easily removed from the labeled construct *in vivo* and if this signal was attributed to the clearance of these small molecules. If this was the case, it is unclear why this signal persisted for so long, as opposed to these molecules being cleared from the body.

In summary, successful tumor-targeted delivery of CPP-ELP_{BC}s by means of their hyperthermia-triggered micelle assembly was not achieved with the generations of constructs that progressively improved upon the qualities and functions of the CPP-

ELP$_{BC}$ platform. Although evidence of significantly enhanced tumor accumulation was not found, that is not to say that there could be other advantages of CPP-ELP$_{BC}$ delivery, for example, if these carriers could still improve upon the internalization, beyond accumulation, of the carrier and its drug cargo. Optimized CPP-ELP$_{BC}$ drug carriers with drug cargo and conserved thermal properties could next address this therapeutic measure of CPP-ELP$_{BC}$ function *in vivo*.

6. Conclusions and future directions

6.1 Conclusions

Although this dissertation does not conclude by achieving the ultimate goal of targeted drug delivery, a great deal was learned along the way about the design and application of ELP$_{BC}$s as stimulus-responsive carriers. The efforts described here contributed to the synthesis, characterization, and optimization of ELP$_{BC}$ materials, shedding light on the parameters that can assist in predictable design of tunable stimulus-responsive ELP$_{BC}$ self-assembly. Within the Chilkoti Lab, this work embodies the first application of ELP$_{BC}$s for the controlled delivery of drug cargo manipulated by the clinically relevant stimulus of mild hyperthermia.

6.1.1 ELP$_{BC}$s as tunable stimulus-responsive biopolymers

The LCST phase transition behavior of ELPs is highly tunable by both intrinsic design parameters and extrinsic environmental factors. Large libraries of homopolymer and pseudorandom ELPs have been synthesized and characterized to build models that can predict the ELP transition temperature as a function of intrinsic parameters including ELP length, concentration, and sequence [102, 187]. Predictive design of ELP$_{BC}$s with desirable thermal properties, such as CMT and micelle-to-aggregate transition temperature, is a more complicated problem. Although progress is being made in modeling the design and behavior of ELP$_{BC}$s [127], to create a ELP$_{BC}$ with novel functionalization at its N- and C-terminus while achieving precisely defined thermal

behavior still requires a great deal of iterative material synthesis, characterization, and optimization. Using those design principles known for homopolymer and pseudorandom ELPs, characteristics of each of the blocks in the ELP$_{BC}$ can be changed to manipulate the thermal properties of the construct. This design process was repeated several times to achieve ELP$_{BC}$s that displayed the desired thermal properties, existing as soluble unimers at 37 °C, while self-assembling into spherical micelles at 42 °C, while accommodating CPP functionalization at the C-terminus and drug loading at the N-terminus of the ELP$_{BC}$.

6.1.2 CPP-ELP$_{BC}$s for controlled cellular uptake *in vitro*

The hypothesis driving the design of the CPP-ELP$_{BC}$ platform was that manipulation of CPP density with micelle assembly could control cellular uptake. In this case of ELP$_{BC}$s, this self-assembly was achieved by means of a thermal stimulus, creating the possibility to control cellular uptake by a clinically relevant external trigger. Successful design of CPP-ELP$_{BC}$s with a CMT between 37 °C and 42 °C allowed this hypothesis to be tested *in vitro* and evaluated by the internalization of fluorescently labeled constructs. As hypothesized, CPP-ELP$_{BC}$s demonstrated enhanced cellular uptake at 42 °C, as compared to 37 °C, demonstrating the effect of manipulating CPP density to modulate cellular internalization. Neither non-functionalized ELP$_{BC}$ or soluble CPP-ELP unimer controls displayed a change in uptake between thermal conditions, confirming that micelle assembly and hyperthermia alone were not responsible for this

effect of amplified cell uptake at hyperthermic conditions. The magnitude of uptake at the "off" state of 37 °C and the magnitude of amplified uptake at the "on" state of 42 °C were tunable by means of the CPP-functionalization of the ELP_{BC}.

Although the mechanism of uptake of CPP-ELP_{BC}s was not thoroughly characterized, preliminary analysis suggested that these materials exploited pathways of macropinocytosis or caveolae-mediated endocytosis more so than that of clathrin-mediated endocytosis, typical of receptor-mediated internalization. More complete analysis of the mechanism of uptake and intracellular localization of CPP-ELP_{BC}s could better direct their design as drug carriers to deliver intact drug cargo to their intracellular therapeutic target.

6.1.3 CPP-ELP_{BC}s for controlled drug delivery *in vitro*

The controlled cellular uptake of CPP-ELP_{BC}s suggested that any drug cargo associated with these carriers could also be selectively delivered into the cell and thereby achieve a controlled therapeutic effect. This translation of controlled cell uptake to controlled drug delivery and controlled therapeutic effect was, however, complicated by the variable effect of drug conjugation on the thermal behavior of the CPP-ELP_{BC} carrier. Many types of drugs have been appended to homopolymer and pseudorandom ELPs, including small molecules, peptides, and proteins, but this was the first attempt in the Chilkoti lab to attach a drug at the hydrophobic terminus of an ELP_{BC} while having minimal tolerance for the perturbation of temperature-triggered self-assembly. This

restriction of the effect of drug attachment on the ELP$_{BC}$ CMT limited the choice of drug cargo.

Preliminary investigation into the covalent attachment of small molecule chemotherapeutics to genetically engineered cysteine residues at the hydrophobic block terminus revealed the complexity of using this class of drug with CPP-ELP$_{BC}$ carriers. A hydrophilic small molecule drug must be used to avoid inducing premature self-assembly of the CPP-ELP$_{BC}$ by means of the hydrophobic effect. However, attachment of hydrophilic drugs drives up the CMT, requiring elevated concentration of drug carrier to compensate for changes in thermal behavior such that unimer and micelle conditions can be achieved at 37 °C and 42 °C, respectively. These high drug concentrations seemed to be overwhelmingly cytotoxic *in vitro*, obliterating any controlled therapeutic effect. Furthermore the pursuit of increased drug loading with this approach created an opposite problem, whereby an increased number of cysteine residues for drug loading induced a decrease in CMT likely due to inter-ELP disulfide bonding that encouraged premature self-assembly. Unfortunately the effects of attaching the hydrophilic drug did not reverse this effect significantly, such that CPP-ELP$_{BC}$s with higher drug loading could not be tested for hyperthermia-targeted drug delivery. An extensive amount of CPP-ELP$_{BC}$ optimization would be required to achieve the desired thermal properties of CPP-ELP$_{BC}$s covalently loaded with small molecule drugs. Therefore an alternative drug cargo was selected for use with the existing CPP-ELP$_{BC}$ platform.

Peptide therapeutics proved to be much more amenable for attachment to CPP-ELP$_{BC}$s without significantly perturbing the thermal behavior of the drug carrier. With peptide drug cargo the controlled cellular uptake conferred controlled therapeutic effect between 37 °C and 42 °C. Peptide drug cargo also provided motivation to characterize the parameters of successful drug carriers, such as the magnitude of intracellular drug delivery afforded by the CPP-ELP$_{BC}$s and the release of free drug within the cell by cleavable linkers. Arg$_8$-ELP$_{BC}$ provided an advantageous balance for the delivery of BH3 peptide, whereby the magnitude of intracellular delivery of drug at 42 °C was high enough to induce significant cytotoxicity at this "on" condition. However, the magnitude of intracellular drug delivery at 37 °C was low enough to spare cells and cause minimal cytotoxicity at this "off" condition. This was the idealized behavior in terms of controlled therapeutic effect. However, the needs of ideal "on" and "off" state intracellular delivery is likely to be dependent on the drug cargo and its potency, stability, and therapeutic mechanism. The CPP-ELP$_{BC}$ platform is well suited to meet the needs of a variety of peptide drugs, as the CPP-functionalization controls the "on" and "off" state uptake and thus far has been shown to be a malleable parameter of the drug carrier design that can be changed without perturbing the optimized thermal properties. The CPPs investigated in this dissertation provided a breadth in magnitude of "off" and "on" uptake, but the family of CPP-functionalized ELP$_{BC}$s can be further expanded to explore the boundaries of amplified uptake at 42 °C and minimized uptake at 37 °C.

6.1.4 CPP-ELP$_{BC}$s for targeted delivery *in vivo*

With successful control of cellular uptake, control of drug delivery, and control of therapeutic effect *in vitro*, the next test was the translation of CPP-ELP$_{BC}$s *in vivo* as tumor-targeted carriers. A great number of challenges were present in this transition from *in vitro* to *in vivo* conditions. The preliminary design of CPP-ELP$_{BC}$s, based on approximations of charge density of TAT-decorated liposomes, had relatively low charge content of only 3 arginine residues per ELP$_{BC}$. A greater number of arginine residues were found to be necessary to achieve meaningful control of intracellular delivery with temperature-triggered micelle assembly. An even greater number of arginine residues were found to be necessary to achieve meaningful control of therapeutic effect with temperature-triggered micelle assembly, at least with one example of peptide drug cargo. The family of optimized CPP-ELP$_{BC}$s therefore had much greater charge content than was originally envisioned for this drug carrier platform.

This high cationic charge leads to a multitude of complications in the translation of drug carriers from the cell culture environment *in vitro* to the complex environment of blood encountered by systemically administered carriers *in vivo*. The primary concern is non-specific interaction of the cationic CPP-ELP$_{BC}$ with materials in the body that are anywhere but the desired tumor target. These non-specific interactions can have negative effects that manifest as changes in clearance of the CPP-ELP$_{BC}$ from systemic

circulation, changes in the thermal properties of the CPP-ELP$_{BC}$, and changes in the level of cellular uptake of CPP-ELP$_{BC}$ micelles. Although charge did appear to affect the clearance of CPP-ELP$_{BC}$s, whereby greater charge lead to faster clearance, none of the CPP-ELP$_{BC}$s investigated *in vivo* demonstrated pharmacokinetics that suggested clearance was happening fast enough to preclude their useful concentration over the course of mild clinical hyperthermia of just 1 hour. Changes in thermal properties were evident for all ELP$_{BC}$s in serum, as compared to PBS or SF-media, even in the absence of CPP functionalization. This was expected as most ELPs demonstrate a decreased T_t in serum. For ELP$_{BC}$s the decrease in T_t was typically more apparent for the micelle-to-aggregate transition as opposed to the CMT. For highly charged Arg$_8$-ELP$_{BC}$ the presence of serum was detrimental to temperature-triggered micelle assembly, and this construct would transition from unimer-to-aggregate in serum. The effect of serum on the cellular uptake of CPP-ELP$_{BC}$s and their self-assembled micelles was less clear and measured only indirectly by visualization of the interaction of drug carrier with tumor tissue using intravital microscopy and quantification of localization within the body by biodistribution studies of the tumor and select organs. CPP-ELP$_{BC}$s did not achieve significantly controlled tumor targeting with micelle assembly in hyperthermia treated tumors, as compared to tumors that were not heated, suggesting that cellular uptake was not robust enough in this *in vivo* setting to create a detectable difference in the extrinsically controlled accumulation of drug carrier.

6.2 Future directions

Many questions remain about the potential of CPP-ELP$_{BC}$s to function successfully in an *in vivo* setting. The material properties of new ELP$_{BC}$s have yet to be optimized to accommodate a variety of CPP-functionalization while maintaining temperature-triggered micelle assembly in blood. Furthermore, the limitations of cationic CPPs, which were not overcome in this dissertation, could be circumvented by investigation of alternative CPP moieties with decreased cationic content but equivalent potential for facilitating the internalization of self-assembled micelles.

6.2.1 Investigation of alternative hydrophilic block copolymer domains

The effect of serum on the thermal behavior of ELP$_{BC}$s seems to be exaggerated with respect to the micelle-to-aggregate transition, as compared to the unimer-to-micelle transition. Furthermore, the CPPs that are responsible for destruction of micelle assembly in serum are of course localized to the terminus of the hydrophilic domain of the ELP$_{BC}$. It is thus imaginable that it is ultimately the change in the apparent thermal behavior of this hydrophilic domain that causes its T_t to decrease in serum to a point at which it collapses collectively with the hydrophobic domain, in effect eliminating the ability of the ELP$_{BC}$ to self-assemble into micelles. Thus, attention was put on manipulation of the hydrophilic domain of the ELP$_{BC}$ in an attempt to alleviate the negative effects of serum on CPP-ELP$_{BC}$ self-assembly. A new hydrophilic block, composed with the guest residue serine, was therefore created in an attempt to increase

the transition temperature of the hydrophilic domain. This particular change in the ELP_{BC} design fixed the problem for Arg_5-functionalization, but not Arg_8-functionalization. However, this approach was only one of many ways in which the hydrophilic domain could be manipulated.

Alternative ELP sequences may impart qualities on the ELP_{BC} that could produce temperature-triggered micelle self-assembly in serum, even when presenting high cationic charge density on the micelle corona. A modest change in the hydrophilic ELP sequence could be the replacement of the serine guest residue with a glycine guest reside. Although these guest residues should have similar hydrophilicity based on Urry's many scales [100, 101], the simple chemistry of the glycine residue may reduce interactions with extraneous materials in the body as compared to serine and its hydroxyl side chain, capable of interactions such as hydrogen bonding. More extreme changes in the hydrophilic block could be the use of anionic guest residues to help offset undesirable electrostatic CPP interactions by charge repulsion. Of course this approach would create a significant risk of CPP interaction with the carrier itself, preoccupying the CPP from its intended target of the cancer cell surface. A zwitterionic ELP sequence may provide the best advantage, avoiding direct interaction with the CPP while serving to decrease extraneous interactions with cells and proteins prior to reaching the heated tumor target.

6.2.2 Investigation of alternative hydrophobic block copolymer domains

All of the effort thus far for improving the ELP_{BC} design for triggered micelle assembly *in vivo* has focused on manipulation of the hydrophilic domain of the block copolymer. However, the hydrophobic domain likely also plays a role in successful micelle assembly in the presence of serum, as the genetic fusion of hydrophobic and hydrophilic domains in the ELP_{BC} causes them to influence each other, as seen in their effects on the CMT and micelle-to-aggregate transition as compared to the T_t of either block alone. Alternative hydrophobic blocks may therefore improve micelle assembly in serum. For instance, others have incorporated cysteine residues at the interface of the hydrophobic and hydrophilic domains to encourage stable micelle assembly in serum by means of intra-micelle disulfide bonding upon self-assembly [190].

The difficulty in exploring alternative hydrophobic domains is that the CMT is controlled by the transition of this block, and therefore the thermal properties of the ELP_{BC} are likely to be perturbed significantly by changes in this design parameter. However, since success has been elusive for self-assembly of highly charged CPP-ELP_{BC}s in serum, it may be best to step back and first achieve an ELP_{BC} that can attain the goal of self-assembly with this functionalization, regardless of CMT. From there the possibility of optimizing the thermal properties can next be evaluated.

An advantage may emerge from pursuing change in both the hydrophilic and hydrophobic domains, in that new ELP materials with extremes in T_t or stability may

combine in an ELP$_{BC}$ in such a way that the advantages of each component are maintained, but the extreme thermal properties are neutralized by their interaction in the genetic fusion. This is of course a lofty proposal, but nonetheless, interesting parameters in ELP$_{BC}$ design and behavior would surely be gleaned from exploring the combination of new hydrophobic and hydrophilic ELP domains in next generation ELP$_{BC}$s.

6.2.3 Investigation of alternative CPP families

Cationic CPPs were the primary focus of this dissertation, based on our hypothesis related to the threshold of arginine oligomers. However, alternative CPPs may also provide controlled cellular uptake in a similar manner depending on their material characteristics and their mechanism of CPP function. Although many CPPs are positively charged, not all rely on a cationic content to induce cellular uptake by initiating electrostatic interactions with the cell surface. Those outlier CPPs, in terms of neutral or even anionic charge, may be suitable for triggered cellular uptake and also circumvent the problems *in vivo* that largely stem from the cationic nature of CPP-ELP$_{BC}$s investigated in this dissertation. Of particular interest is the sweet arrow protein (SAP), a neutral CPP shown to achieve efficient uptake of functionalized oligonucleotides [191], lipid nanoparticles [192], and gold nanoparticles [193], as it has been genetically mutated to incorporate anionic residues, without detrimental effect on its CPP functionality [194]. As such, it is believed to be the first anionic CPP of its kind.

These CPPs may be an interesting place to start for investigating alternative CPPs that may function well *in vitro* and carry their function over into an *in vivo* environment.

If alternative CPPs are pursued as a solution to the undesirable thermal behavior, seen for example with Arg_8-ELP_{BC}, to would be wise to screen for both *in vitro* and *in vivo* function to eliminate immediately those CPPs that may not be amenable to self-assembly on ELP_{BC} micelles in serum but also to not overlook those CPPs that may not have stellar function *in vitro*, yet can perform appropriately in an animal host. Certainly this would be a cumbersome task to screen a large number of CPP candidates, but experience with arginine oligomer CPPs has shown that *in vitro* and *in vivo* environments are greatly disparate conditions in which to achieve intracellular delivery of drug carriers. It is therefore not unreasonable to think that what does not function in one condition may well function in another.

Appendix A

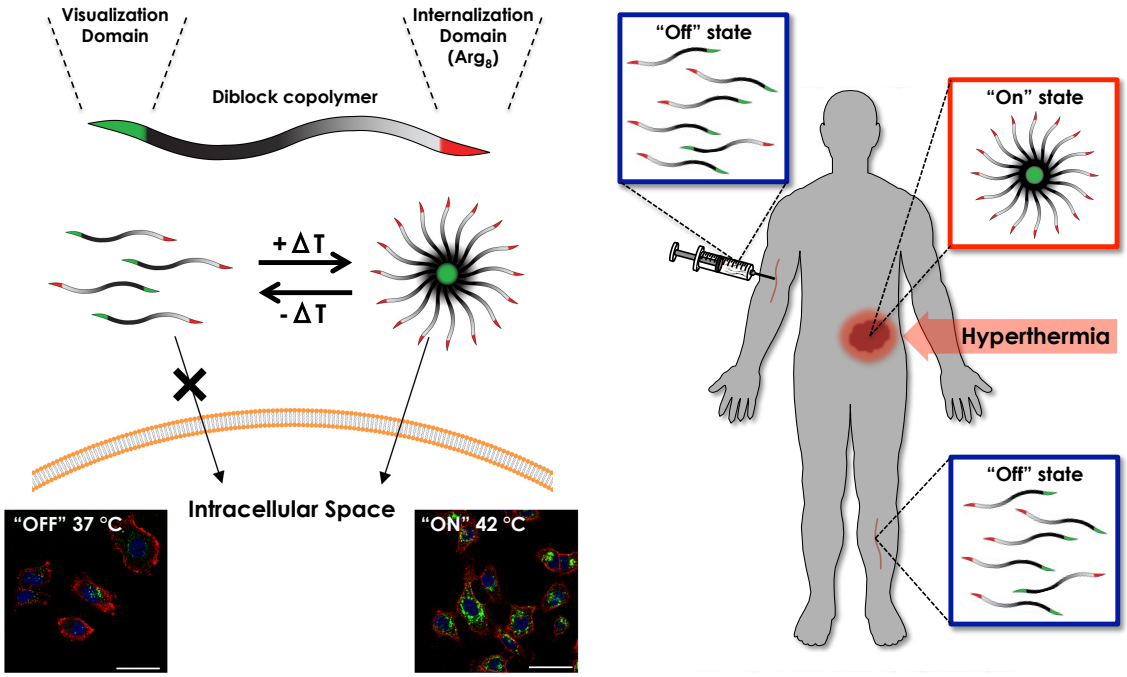

Figure 87: Extrinsically controlled intracellular drug delivery

Intrinsic targets in tumors may be

Receptors or enzymes or acidity

But intrinsic targets in tumors are tough

Some cancers and patients just don't have enough

To deliver drug to sites of disease

Without side effects just wherever you please

Instead we can use an extrinsic cue

To gain some control from an external view

For this approach we can use ELPs

Reacting to heat with the slightest of ease

With careful design these can assemble

And spherical micelles they will resemble

This just occurs in conditions of heat

Without which as unimers they stay discrete

Add an internalization domain

Non-specific cell uptake this will obtain

How can we control this uptake you cry

Change the density from low levels to high

High density (micelles) - means uptake galore

Low density (unimers) - uptake is poor

And there you have with a flip of a switch

A toggle from low to the density rich

Labeled with fluorophore ELPs glow

To see in the microscope or count with flow

Just in the presence of heat are they seen

Inside HeLa cell where they show up in green

Thus it is *in vitro* we can portray

That cell uptake can be controlled in this way

What we can propose to one day obtain

Is delivery control on *in vivo* terrain

Here we inject in a unimer state

Where uptake remains at a diminished rate

If tumor alone is treated with heat

The micelle assembly will here be replete

Uptake is much greater here where it's hot

Whereas normal cells uptake diddly-squat

Assembly targets the tumor you see

With the unheated healthy tissues left be

Thus tumor target we successfully meet

With an external trigger that is simply heat

Appendix B

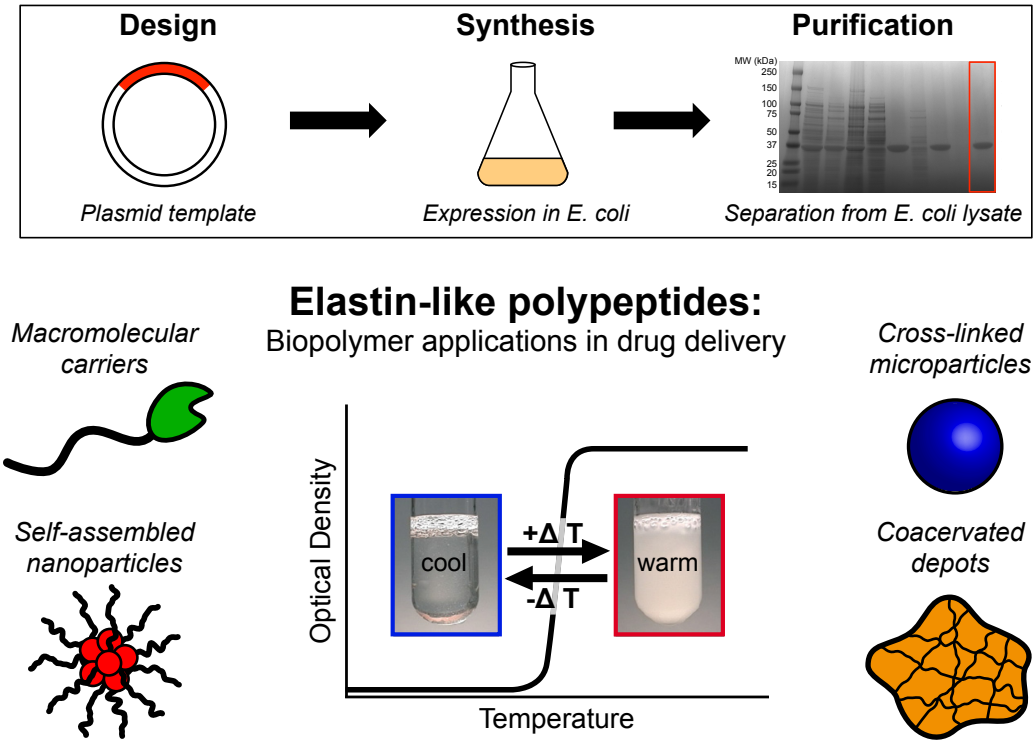

Figure 88: An Ode to Biopolymers

Polymers are swell for delivering drugs

Small molecule, biologics they are happy to lug

Throughout your body with the greatest of ease

Delivering drug to the site of disease

Now polymers made from a synthetic route

Won't have the same qualities day-in and day-out

The reactive site where the drug can attach

May vary in number and place with each batch

RAFT, ROMP, ATRP

Each is controlled, but to what degree?

So sometimes you'll get what you need with some luck

And others might say that they don't give a

Care in the world if they don't know exactly

Where the drug is attached or the protein is actually

But I will still say it's important to know

That the drug is right here and the protein just so

And the way to achieve this perfect precision

Just make them under a gene's supervision

Biopolymers born from a plasmid gene template

Are exactly the same in their sequence and weight

Monodisperse, each one the same

You can be sure they will meet their aim

Predictable in their biodistribution

So for the disease they will be your solution

They're each time the same, no if, ands or butt

Made your first year or seventh – seventh, wait what?

Anyways, they're biocompatible to boot

The value of biopolymers you just can't refute

References

1. D. Hanahan, R.A. Weinberg, Hallmarks of cancer: the next generation, Cell 144 (2011) 646-674.

2. A.M. Soto, C. Sonnenschein, The tissue organization field theory of cancer: a testable replacement for the somatic mutation theory, Bioessays 33 (2011) 332-340.

3. American Cancer Society, Cancer Facts and Figures 2014, Atlanta: American Cancer Society (2014).

4. J. Bernier, E.J. Hall, A. Giaccia, Radiation oncology: a century of achievements, Nat Rev Cancer 4 (2004) 737-747.

5. R.G. Bristow, R.P. Hill, Hypoxia and metabolism. Hypoxia, DNA repair and genetic instability, Nat Rev Cancer 8 (2008) 180-192.

6. G.K. Dy, A.A. Adjei, Understanding, recognizing, and managing toxicities of targeted anticancer therapies, CA Cancer J Clin 63 (2013) 249-279.

7. T.J. Vogl, P. Farshid, N.N. Naguib, S. Zangos, Thermal ablation therapies in patients with breast cancer liver metastases: a review, Eur Radiol 23 (2013) 797-804.

8. M.H. Falk, R.D. Issels, Hyperthermia in oncology, Int J Hyperthermia 17 (2001) 1-18.

9. E. Jones, D. Thrall, M.W. Dewhirst, Z. Vujaskovic, Prospective thermal dosimetry: the key to hyperthermia's future, Int J Hyperthermia 22 (2006) 247-253.

10. J.R. James, Y. Gao, V.C. Soon, S.M. Topper, A. Babsky, N. Bansal, Controlled radio-frequency hyperthermia using an MR scanner and simultaneous monitoring of temperature and therapy response by (1)H, (23)Na and (31)P magnetic resonance spectroscopy in subcutaneously implanted 9L-gliosarcoma, Int J Hyperthermia 26 (2010) 79-90.

11. B.E. O'Neill, K.C. Li, Augmentation of targeted delivery with pulsed high intensity focused ultrasound, Int J Hyperthermia 24 (2008) 506-520.

12. M.W. Dewhirst, E. Jones, T. Samulski, Z. Vujaskovic, C. Li, L. Prosnitz, Hyperthermia, in: D. Kufe, R. Pollock, R. Weichselbaum (Eds.) Cancer Medicine, B.C. Decker, Hamilton, Ontaria, Canada, 2003, pp. 623-636.

13. F.K. Storm, D.L. Morton, Localized hyperthermia in the treatment of cancer, CA Cancer J Clin 33 (1983) 44-56.

14. R.B. Roemer, Engineering aspects of hyperthermia therapy, Annu Rev Biomed Eng 1 (1999) 347-376.

15. T. Kobayashi, Y. Kida, T. Tanaka, K. Hattori, M. Matsui, Y. Amemiya, Interstitial hyperthermia of malignant brain tumors by implant heating system: clinical experience, J Neurooncol 10 (1991) 153-163.

16. T. Feyerabend, G.J. Wiedemann, B. Jager, H. Vesely, B. Mahlmann, E. Richter, Local hyperthermia, radiation, and chemotherapy in recurrent breast cancer is feasible and effective except for inflammatory disease, Int J Radiat Oncol Biol Phys 49 (2001) 1317-1325.

17. Y. Harima, K. Nagata, K. Harima, V.V. Ostapenko, Y. Tanaka, S. Sawada, A randomized clinical trial of radiation therapy versus thermoradiotherapy in stage IIIB cervical carcinoma, Int J Hyperthermia 17 (2001) 97-105.

18. T.M. Zagar, J.R. Oleson, Z. Vujaskovic, M.W. Dewhirst, O.I. Craciunescu, K.L. Blackwell, L.R. Prosnitz, E.L. Jones, Hyperthermia combined with radiation therapy for superficial breast cancer and chest wall recurrence: a review of the randomised data, Int J Hyperthermia 26 (2010) 612-617.

19. K. Engin, D.B. Leeper, L. Tupchong, F.M. Waterman, Thermoradiotherapy in the management of superficial malignant tumors, Clin Cancer Res 1 (1995) 139-145.

20. R.D. Issels, L.H. Lindner, J. Verweij, P. Wust, P. Reichardt, B.C. Schem, S. Abdel-Rahman, S. Daugaard, C. Salat, C.M. Wendtner, Z. Vujaskovic, R. Wessalowski, K.W. Jauch, H.R. Durr, F. Ploner, A. Baur-Melnyk, U. Mansmann, W. Hiddemann, J.Y. Blay, P. Hohenberger, Neo-adjuvant chemotherapy alone or with regional hyperthermia for localised high-risk soft-tissue sarcoma: a randomised phase 3 multicentre study, Lancet Oncol 11 (2010) 561-570.

21. J. van der Zee, D. Gonzalez Gonzalez, G.C. van Rhoon, J.D. van Dijk, W.L. van Putten, A.A. Hart, Comparison of radiotherapy alone with radiotherapy plus hyperthermia in locally advanced pelvic tumours: a prospective, randomised, multicentre trial. Dutch Deep Hyperthermia Group, Lancet 355 (2000) 1119-1125.

22. R. Colombo, L.F. Da Pozzo, A. Salonia, P. Rigatti, Z. Leib, J. Baniel, E. Caldarera, M. Pavone-Macaluso, Multicentric study comparing intravesical chemotherapy alone and with local microwave hyperthermia for prophylaxis of recurrence of superficial transitional cell carcinoma, J Clin Oncol 21 (2003) 4270-4276.

23. H.R. Moyer, K.A. Delman, The role of hyperthermia in optimizing tumor response to regional therapy, Int J Hyperthermia 24 (2008) 251-261.

24. M.R. Horsman, Tissue physiology and the response to heat, Int J Hyperthermia 22 (2006) 197-203.

25. Y. Liu, C.W. Cho, X. Yan, T.K. Henthorn, K.O. Lillehei, W.N. Cobb, K.Y. Ng, Ultrasound-Induced hyperthermia increases cellular uptake and cytotoxicity of P-glycoprotein substrates in multi-drug resistant cells, Pharm Res 18 (2001) 1255-1261.

26. J.L. Roti Roti, Heat-induced alterations of nuclear protein associations and their effects on DNA repair and replication, Int J Hyperthermia 23 (2007) 3-15.

27. G. Kong, R.D. Braun, M.W. Dewhirst, Characterization of the effect of hyperthermia on nanoparticle extravasation from tumor vasculature, Cancer Res 61 (2001) 3027-3032.

28. G. Kong, R.D. Braun, M.W. Dewhirst, Hyperthermia enables tumor-specific nanoparticle delivery: effect of particle size, Cancer Res 60 (2000) 4440-4445.

29. L. Li, T.L. ten Hagen, M. Bolkestein, A. Gasselhuber, J. Yatvin, G.C. van Rhoon, A.M. Eggermont, D. Haemmerich, G.A. Koning, Improved intratumoral nanoparticle extravasation and penetration by mild hyperthermia, J Control Release 167 (2013) 130-137.

30. W. Liu, M.R. Dreher, D.Y. Furgeson, K.V. Peixoto, H. Yuan, M.R. Zalutsky, A. Chilkoti, Tumor accumulation, degradation and pharmacokinetics of elastin-like polypeptides in nude mice, J Control Release 116 (2006) 170-178.

31. M.R. Dreher, W. Liu, C.R. Michelich, M.W. Dewhirst, A. Chilkoti, Thermal cycling enhances the accumulation of a temperature-sensitive biopolymer in solid tumors, Cancer Res 67 (2007) 4418-4424.

32. A.A. Manzoor, L.H. Lindner, C.D. Landon, J.Y. Park, A.J. Simnick, M.R. Dreher, S. Das, G. Hanna, W. Park, A. Chilkoti, G.A. Koning, T.L. ten Hagen, D. Needham, M.W. Dewhirst, Overcoming limitations in nanoparticle drug

delivery: triggered, intravascular release to improve drug penetration into tumors, Cancer Res 72 (2012) 5566-5575.

33. A.M. Ponce, B.L. Viglianti, D. Yu, P.S. Yarmolenko, C.R. Michelich, J. Woo, M.B. Bally, M.W. Dewhirst, Magnetic resonance imaging of temperature-sensitive liposome release: drug dose painting and antitumor effects, J Natl Cancer Inst 99 (2007) 53-63.

34. M.L. Hauck, S.M. LaRue, W.P. Petros, J.M. Poulson, D. Yu, I. Spasojevic, A.F. Pruitt, A. Klein, B. Case, D.E. Thrall, D. Needham, M.W. Dewhirst, Phase I trial of doxorubicin-containing low temperature sensitive liposomes in spontaneous canine tumors, Clin Cancer Res 12 (2006) 4004-4010.

35. A.K. Iyer, G. Khaled, J. Fang, H. Maeda, Exploiting the enhanced permeability and retention effect for tumor targeting, Drug Discov Today 11 (2006) 812-818.

36. F. Yuan, M. Dellian, D. Fukumura, M. Leunig, D.A. Berk, V.P. Torchilin, R.K. Jain, Vascular permeability in a human tumor xenograft: molecular size dependence and cutoff size, Cancer Res 55 (1995) 3752-3756.

37. S.K. Hobbs, W.L. Monsky, F. Yuan, W.G. Roberts, L. Griffith, V.P. Torchilin, R.K. Jain, Regulation of transport pathways in tumor vessels: role of tumor type and microenvironment, Proc Natl Acad Sci U S A 95 (1998) 4607-4612.

38. U. Prabhakar, H. Maeda, R.K. Jain, E.M. Sevick-Muraca, W. Zamboni, O.C. Farokhzad, S.T. Barry, A. Gabizon, P. Grodzinski, D.C. Blakey, Challenges and key considerations of the enhanced permeability and retention effect for nanomedicine drug delivery in oncology, Cancer Res 73 (2013) 2412-2417.

39. I.E. Krop, P. LoRusso, K.D. Miller, S. Modi, D. Yardley, G. Rodriguez, E. Guardino, M. Lu, M. Zheng, S. Girish, L. Amler, E.P. Winer, H.S. Rugo, A phase II study of trastuzumab emtansine in patients with human epidermal growth factor receptor 2-positive metastatic breast cancer who were previously treated with trastuzumab, lapatinib, an anthracycline, a taxane, and capecitabine, J Clin Oncol 30 (2012) 3234-3241.

40. N. Senzer, J. Nemunaitis, D. Nemunaitis, C. Bedell, G. Edelman, M. Barve, R. Nunan, K.F. Pirollo, A. Rait, E.H. Chang, Phase I study of a systemically delivered p53 nanoparticle in advanced solid tumors, Mol Ther 21 (2013) 1096-1103.

41. M.E. Davis, The first targeted delivery of siRNA in humans via a self-assembling, cyclodextrin polymer-based nanoparticle: from concept to clinic, Mol Pharm 6 (2009) 659-668.

42. J. Hrkach, D. Von Hoff, M. Mukkaram Ali, E. Andrianova, J. Auer, T. Campbell, D. De Witt, M. Figa, M. Figueiredo, A. Horhota, S. Low, K. McDonnell, E. Peeke, B. Retnarajan, A. Sabnis, E. Schnipper, J.J. Song, Y.H. Song, J. Summa, D. Tompsett, G. Troiano, T. Van Geen Hoven, J. Wright, P. LoRusso, P.W. Kantoff, N.H. Bander, C. Sweeney, O.C. Farokhzad, R. Langer, S. Zale, Preclinical development and clinical translation of a PSMA-targeted docetaxel nanoparticle with a differentiated pharmacological profile, Sci Transl Med 4 (2012) 128ra139.

43. A.M. Mansour, J. Drevs, N. Esser, F.M. Hamada, O.A. Badary, C. Unger, I. Fichtner, F. Kratz, A new approach for the treatment of malignant melanoma: enhanced antitumor efficacy of an albumin-binding doxorubicin prodrug that is cleaved by matrix metalloproteinase 2, Cancer Res 63 (2003) 4062-4066.

44. Y. Chau, R.F. Padera, N.M. Dang, R. Langer, Antitumor efficacy of a novel polymer-peptide-drug conjugate in human tumor xenograft models, Int J Cancer 118 (2006) 1519-1526.

45. E.S. Lee, H.J. Shin, K. Na, Y.H. Bae, Poly(L-histidine)-PEG block copolymer micelles and pH-induced destabilization, J Control Release 90 (2003) 363-374.

46. E.S. Lee, K. Na, Y.H. Bae, Doxorubicin loaded pH-sensitive polymeric micelles for reversal of resistant MCF-7 tumor, J Control Release 103 (2005) 405-418.

47. N.C. Fan, F.Y. Cheng, J.A. Ho, C.S. Yeh, Photocontrolled targeted drug delivery: photocaged biologically active folic acid as a light-responsive tumor-targeting molecule, Angew Chem Int Ed Engl 51 (2012) 8806-8810.

48. J.L. Nelson, B.L. Roeder, J.C. Carmen, F. Roloff, W.G. Pitt, Ultrasonically activated chemotherapeutic drug delivery in a rat model, Cancer Res 62 (2002) 7280-7283.

49. D. Derossi, S. Calvet, A. Trembleau, A. Brunissen, G. Chassaing, A. Prochiantz, Cell internalization of the third helix of the Antennapedia homeodomain is receptor-independent, J Biol Chem 271 (1996) 18188-18193.

50. A. Kerkis, M.A. Hayashi, T. Yamane, I. Kerkis, Properties of cell penetrating peptides (CPPs), IUBMB Life 58 (2006) 7-13.

51. K. Sadler, K.D. Eom, J.L. Yang, Y. Dimitrova, J.P. Tam, Translocating proline-rich peptides from the antimicrobial peptide bactenecin 7, Biochemistry 41 (2002) 14150-14157.

52. I.A. Khalil, K. Kogure, S. Futaki, H. Harashima, Octaarginine-modified liposomes: enhanced cellular uptake and controlled intracellular trafficking, Int J Pharm 354 (2008) 39-48.

53. Y. Nakamura, K. Kogure, S. Futaki, H. Harashima, Octaarginine-modified multifunctional envelope-type nano device for siRNA, J Control Release 119 (2007) 360-367.

54. S. Al-Taei, N.A. Penning, J.C. Simpson, S. Futaki, T. Takeuchi, I. Nakase, A.T. Jones, Intracellular traffic and fate of protein transduction domains HIV-1 TAT peptide and octaarginine. Implications for their utilization as drug delivery vectors, Bioconjug Chem 17 (2006) 90-100.

55. P.A. Wender, D.J. Mitchell, K. Pattabiraman, E.T. Pelkey, L. Steinman, J.B. Rothbard, The design, synthesis, and evaluation of molecules that enable or enhance cellular uptake: peptoid molecular transporters, Proc Natl Acad Sci U S A 97 (2000) 13003-13008.

56. P.A. Wender, J.B. Rothbard, T.C. Jessop, E.L. Kreider, B.L. Wylie, Oligocarbamate molecular transporters: design, synthesis, and biological evaluation of a new class of transporters for drug delivery, J Am Chem Soc 124 (2002) 13382-13383.

57. P.A. Wender, E. Kreider, E.T. Pelkey, J. Rothbard, C.L. Vandeusen, Dendrimeric molecular transporters: synthesis and evaluation of tunable polyguanidino dendrimers that facilitate cellular uptake, Org Lett 7 (2005) 4815-4818.

58. J.B. Rothbard, T.C. Jessop, R.S. Lewis, B.A. Murray, P.A. Wender, Role of membrane potential and hydrogen bonding in the mechanism of translocation of guanidinium-rich peptides into cells, J Am Chem Soc 126 (2004) 9506-9507.

59. I. Nakase, A. Tadokoro, N. Kawabata, T. Takeuchi, H. Katoh, K. Hiramoto, M. Negishi, M. Nomizu, Y. Sugiura, S. Futaki, Interaction of arginine-rich peptides with membrane-associated proteoglycans is crucial for induction of actin organization and macropinocytosis, Biochemistry 46 (2007) 492-501.

60. M. Dathe, T. Wieprecht, Structural features of helical antimicrobial peptides: their potential to modulate activity on model membranes and biological cells, Biochim Biophys Acta 1462 (1999) 71-87.

61. S.T. Henriques, M.N. Melo, M.A. Castanho, Cell-penetrating peptides and antimicrobial peptides: how different are they?, Biochem J 399 (2006) 1-7.

62. S. Kawamoto, M. Takasu, T. Miyakawa, R. Morikawa, T. Oda, S. Futaki, H. Nagao, Inverted micelle formation of cell-penetrating peptide studied by coarse-grained simulation: importance of attractive force between cell-penetrating peptides and lipid head group, J Chem Phys 134 (2011) 095103.

63. A. Fittipaldi, A. Ferrari, M. Zoppe, C. Arcangeli, V. Pellegrini, F. Beltram, M. Giacca, Cell membrane lipid rafts mediate caveolar endocytosis of HIV-1 Tat fusion proteins, J Biol Chem 278 (2003) 34141-34149.

64. J. Mueller, I. Kretzschmar, R. Volkmer, P. Boisguerin, Comparison of cellular uptake using 22 CPPs in 4 different cell lines, Bioconjug Chem 19 (2008) 2363-2374.

65. K.S. Kawamura, M. Sung, E. Bolewska-Pedyczak, J. Gariepy, Probing the impact of valency on the routing of arginine-rich peptides into eukaryotic cells, Biochemistry 45 (2006) 1116-1127.

66. J.B. Rothbard, E. Kreider, C.L. VanDeusen, L. Wright, B.L. Wylie, P.A. Wender, Arginine-rich molecular transporters for drug delivery: role of backbone spacing in cellular uptake, J Med Chem 45 (2002) 3612-3618.

67. J.S. Wadia, S.F. Dowdy, Transmembrane delivery of protein and peptide drugs by TAT-mediated transduction in the treatment of cancer, Adv Drug Deliv Rev 57 (2005) 579-596.

68. Y. Qin, H. Chen, Q. Zhang, X. Wang, W. Yuan, R. Kuai, J. Tang, L. Zhang, Z. Zhang, J. Liu, Q. He, Liposome formulated with TAT-modified cholesterol for improving brain delivery and therapeutic efficacy on brain glioma in animals, Int J Pharm 420 (2011) 304-312.

69. R.R. Sawant, V.P. Torchilin, Enhanced cytotoxicity of TATp-bearing paclitaxel-loaded micelles in vitro and in vivo, Int J Pharm 374 (2009) 114-118.

70. T. Kanazawa, H. Taki, K. Tanaka, Y. Takashima, H. Okada, Cell-penetrating peptide-modified block copolymer micelles promote direct brain delivery via intranasal administration, Pharm Res 28 (2011) 2130-2139.

71. K. Splith, W. Hu, U. Schatzschneider, R. Gust, I. Ott, L.A. Onambele, A. Prokop, I. Neundorf, Protease-activatable organometal-Peptide bioconjugates with enhanced cytotoxicity on cancer cells, Bioconjug Chem 21 (2010) 1288-1296.

72. E. Oh, J.B. Delehanty, K.E. Sapsford, K. Susumu, R. Goswami, J.B. Blanco-Canosa, P.E. Dawson, J. Granek, M. Shoff, Q. Zhang, P.L. Goering, A. Huston, I.L. Medintz, Cellular uptake and fate of PEGylated gold nanoparticles is dependent on both cell-penetration peptides and particle size, ACS Nano 5 (2011) 6434-6448.

73. J.R. Maiolo, M. Ferrer, E.A. Ottinger, Effects of cargo molecules on the cellular uptake of arginine-rich cell-penetrating peptides, Biochim Biophys Acta 1712 (2005) 161-172.

74. I.A. Khalil, K. Kogure, S. Futaki, H. Harashima, High density of octaarginine stimulates macropinocytosis leading to efficient intracellular trafficking for gene expression, J Biol Chem 281 (2006) 3544-3551.

75. I.A. Khalil, K. Kogure, H. Akita, H. Harashima, Uptake pathways and subsequent intracellular trafficking in nonviral gene delivery, Pharmacol Rev 58 (2006) 32-45.

76. T.J. Davidson, S. Harel, V.A. Arboleda, G.F. Prunell, M.L. Shelanski, L.A. Greene, C.M. Troy, Highly efficient small interfering RNA delivery to primary mammalian neurons induces MicroRNA-like effects before mRNA degradation, J Neurosci 24 (2004) 10040-10046.

77. M.C. Morris, J. Depollier, J. Mery, F. Heitz, G. Divita, A peptide carrier for the delivery of biologically active proteins into mammalian cells, Nat Biotechnol 19 (2001) 1173-1176.

78. C.R. Flynn, J. Cheung-Flynn, C.C. Smoke, D. Lowry, R. Roberson, M.R. Sheller, C.M. Brophy, Internalization and intracellular trafficking of a PTD-conjugated anti-fibrotic peptide, AZX100, in human dermal keloid fibroblasts, J Pharm Sci 99 (2010) 3100-3121.

79. F. Brandt, C. O'Connell, A. Cazzaniga, J.M. Waugh, Efficacy and safety evaluation of a novel botulinum toxin topical gel for the treatment of moderate to severe lateral canthal lines, Dermatol Surg 36 Suppl 4 (2010) 2111-2118.

80. J.B. Rothbard, S. Garlington, Q. Lin, T. Kirschberg, E. Kreider, P.L. McGrane, P.A. Wender, P.A. Khavari, Conjugation of arginine oligomers to cyclosporin A

facilitates topical delivery and inhibition of inflammation, Nat Med 6 (2000) 1253-1257.

81. Y. Miyaji, S. Walter, L. Chen, A. Kurihara, T. Ishizuka, M. Saito, K. Kawai, O. Okazaki, Distribution of KAI-9803, a novel delta-protein kinase C inhibitor, after intravenous administration to rats, Drug Metab Dispos 39 (2011) 1946-1953.

82. J.R. Liu, Y. Zhao, A. Patzer, N. Staak, R. Boehm, G. Deuschl, J. Culman, C. Bonny, T. Herdegen, C. Eschenfelder, The c-Jun N-terminal kinase (JNK) inhibitor XG-102 enhances the neuroprotection of hyperbaric oxygen after cerebral ischaemia in adult rats, Neuropathol Appl Neurobiol 36 (2010) 211-224.

83. E. Koren, A. Apte, A. Jani, V.P. Torchilin, Multifunctional PEGylated 2C5-immunoliposomes containing pH-sensitive bonds and TAT peptide for enhanced tumor cell internalization and cytotoxicity, J Control Release 160 (2012) 264-273.

84. L. Zhu, P. Kate, V.P. Torchilin, Matrix metalloprotease 2-responsive multifunctional liposomal nanocarrier for enhanced tumor targeting, ACS Nano 6 (2012) 3491-3498.

85. H. Mok, K.H. Bae, C.H. Ahn, T.G. Park, PEGylated and MMP-2 specifically dePEGylated quantum dots: comparative evaluation of cellular uptake, Langmuir 25 (2009) 1645-1650.

86. T.J. Harris, G. von Maltzahn, M.E. Lord, J.H. Park, A. Agrawal, D.H. Min, M.J. Sailor, S.N. Bhatia, Protease-triggered unveiling of bioactive nanoparticles, Small 4 (2008) 1307-1312.

87. E.S. Lee, Z. Gao, D. Kim, K. Park, I.C. Kwon, Y.H. Bae, Super pH-sensitive multifunctional polymeric micelle for tumor pH(e) specific TAT exposure and multidrug resistance, J Control Release 129 (2008) 228-236.

88. T.A. Aguilera, E.S. Olson, M.M. Timmers, T. Jiang, R.Y. Tsien, Systemic in vivo distribution of activatable cell penetrating peptides is superior to that of cell penetrating peptides, Integr Biol (Camb) 1 (2009) 371-381.

89. T. Jiang, E.S. Olson, Q.T. Nguyen, M. Roy, P.A. Jennings, R.Y. Tsien, Tumor imaging by means of proteolytic activation of cell-penetrating peptides, Proc Natl Acad Sci U S A 101 (2004) 17867-17872.

90. E.S. Olson, T.A. Aguilera, T. Jiang, L.G. Ellies, Q.T. Nguyen, E.H. Wong, L.A. Gross, R.Y. Tsien, In vivo characterization of activatable cell penetrating peptides for targeting protease activity in cancer, Integr Biol (Camb) 1 (2009) 382-393.

91. E.S. Olson, T. Jiang, T.A. Aguilera, Q.T. Nguyen, L.G. Ellies, M. Scadeng, R.Y. Tsien, Activatable cell penetrating peptides linked to nanoparticles as dual probes for in vivo fluorescence and MR imaging of proteases, Proc Natl Acad Sci U S A 107 (2010) 4311-4316.

92. Q.T. Nguyen, E.S. Olson, T.A. Aguilera, T. Jiang, M. Scadeng, L.G. Ellies, R.Y. Tsien, Surgery with molecular fluorescence imaging using activatable cell-penetrating peptides decreases residual cancer and improves survival, Proc Natl Acad Sci U S A 107 (2010) 4317-4322.

93. W. Zhang, J. Song, B. Zhang, L. Liu, K. Wang, R. Wang, Design of acid-activated cell penetrating peptide for delivery of active molecules into cancer cells, Bioconjug Chem 22 (2011) 1410-1415.

94. A.S. Tatham, P.R. Shewry, Elastomeric proteins: biological roles, structures and mechanisms, Trends Biochem Sci 25 (2000) 567-571.

95. D.W. Urry, Physical chemistry of biological free energy transduction as demonstrated by elastic protein-based polymers, Journal of Physical Chemistry B 101 (1997) 11007-11028.

96. D.E. Meyer, A. Chilkoti, Purification of recombinant proteins by fusion with thermally-responsive polypeptides, Nat Biotechnol 17 (1999) 1112-1115.

97. D.E. Meyer, A. Chilkoti, Genetically encoded synthesis of protein-based polymers with precisely specified molecular weight and sequence by recursive directional ligation: examples from the elastin-like polypeptide system, Biomacromolecules 3 (2002) 357-367.

98. J.R. McDaniel, J.A. Mackay, F.G. Quiroz, A. Chilkoti, Recursive directional ligation by plasmid reconstruction allows rapid and seamless cloning of oligomeric genes, Biomacromolecules 11 (2010) 944-952.

99. M. Amiram, F.G. Quiroz, D.J. Callahan, A. Chilkoti, A highly parallel method for synthesizing DNA repeats enables the discovery of 'smart' protein polymers, Nat Mater 10 (2011) 141-148.

100. D.W. Urry, C.H. Luan, T.M. Parker, D.C. Gowda, K.U. Prasad, M.C. Reid, A. Safavy, Temperature of Polypeptide Inverse Temperature Transition Depends on Mean Residue Hydrophobicity, J Am Chem Soc 113 (1991) 4346-4348.

101. D.W. Urry, The change in Gibbs free energy for hydrophobic association - Derivation and evaluation by means of inverse temperature transitions, Chemical Physics Letters 399 (2004) 177-183.

102. D.E. Meyer, A. Chilkoti, Quantification of the effects of chain length and concentration on the thermal behavior of elastin-like polypeptides, Biomacromolecules 5 (2004) 846-851.

103. Y. Cho, Y. Zhang, T. Christensen, L.B. Sagle, A. Chilkoti, P.S. Cremer, Effects of Hofmeister anions on the phase transition temperature of elastin-like polypeptides, J Phys Chem B 112 (2008) 13765-13771.

104. D.W. Urry, T.M. Parker, M.C. Reid, D.C. Gowda, Biocompatibility of the Bioelastic Materials, Poly(Gvgvp) and Its Gamma-Irradiation Cross-Linked Matrix - Summary of Generic Biological Test-Results, Journal of Bioactive and Compatible Polymers 6 (1991) 263-282.

105. D.W. Urry, A. Pattanaik, J. Xu, T.C. Woods, D.T. McPherson, T.M. Parker, Elastic protein-based polymers in soft tissue augmentation and generation, J Biomater Sci Polym Ed 9 (1998) 1015-1048.

106. A.C. Rincon, I.T. Molina-Martinez, B. de Las Heras, M. Alonso, C. Bailez, J.C. Rodriguez-Cabello, R. Herrero-Vanrell, Biocompatibility of elastin-like polymer poly(VPAVG) microparticles: in vitro and in vivo studies, J Biomed Mater Res A 78 (2006) 343-351.

107. M. Shah, P.Y. Hsueh, G. Sun, H.Y. Chang, S.M. Janib, J.A. MacKay, Biodegradation of elastin-like polypeptide nanoparticles, Protein Sci 21 (2012) 743-750.

108. B. Kim, A. Chilkoti, Allosteric actuation of inverse phase transition of a stimulus-responsive fusion polypeptide by ligand binding, J Am Chem Soc 130 (2008) 17867-17873.

109. W. Hassouneh, M.L. Nunalee, M.C. Shelton, A. Chilkoti, Calcium binding peptide motifs from calmodulin confer divalent ion selectivity to elastin-like polypeptides, Biomacromolecules 14 (2013) 2347-2353.

110. D.L. Nettles, A. Chilkoti, L.A. Setton, Applications of elastin-like polypeptides in tissue engineering, Adv Drug Deliv Rev 62 (2010) 1479-1485.

111. S.R. MacEwan, A. Chilkoti, Applications of elastin-like polypeptides in drug delivery, J Control Release 190 (2014) 314-330.

112. J.R. McDaniel, D.J. Callahan, A. Chilkoti, Drug delivery to solid tumors by elastin-like polypeptides, Adv Drug Deliv Rev 62 (2010) 1456-1467.

113. I. Massodi, G.L. Bidwell, 3rd, D. Raucher, Evaluation of cell penetrating peptides fused to elastin-like polypeptide for drug delivery, J Control Release 108 (2005) 396-408.

114. D. Raucher, A. Chilkoti, Enhanced uptake of a thermally responsive polypeptide by tumor cells in response to its hyperthermia-mediated phase transition, Cancer Res 61 (2001) 7163-7170.

115. G.L. Bidwell, 3rd, A.N. Davis, D. Raucher, Targeting a c-Myc inhibitory polypeptide to specific intracellular compartments using cell penetrating peptides, J Control Release 135 (2009) 2-10.

116. I. Massodi, S. Moktan, A. Rawat, G.L. Bidwell, 3rd, D. Raucher, Inhibition of ovarian cancer cell proliferation by a cell cycle inhibitory peptide fused to a thermally responsive polypeptide carrier, Int J Cancer 126 (2010) 533-544.

117. I. Massodi, E. Thomas, D. Raucher, Application of thermally responsive elastin-like polypeptide fused to a lactoferrin-derived peptide for treatment of pancreatic cancer, Molecules 14 (2009) 1999-2015.

118. G.L. Bidwell, 3rd, A.N. Davis, I. Fokt, W. Priebe, D. Raucher, A thermally targeted elastin-like polypeptide-doxorubicin conjugate overcomes drug resistance, Invest New Drugs 25 (2007) 313-326.

119. G.L. Bidwell, 3rd, I. Fokt, W. Priebe, D. Raucher, Development of elastin-like polypeptide for thermally targeted delivery of doxorubicin, Biochem Pharmacol 73 (2007) 620-631.

120. S. Moktan, C. Ryppa, F. Kratz, D. Raucher, A thermally responsive biopolymer conjugated to an acid-sensitive derivative of paclitaxel stabilizes microtubules, arrests cell cycle, and induces apoptosis, Invest New Drugs 30 (2012) 236-248.

121. G.L. Bidwell, 3rd, E. Perkins, J. Hughes, M. Khan, J.R. James, D. Raucher, Thermally targeted delivery of a c-Myc inhibitory polypeptide inhibits tumor progression and extends survival in a rat glioma model, PLoS One 8 (2013) e55104.

122. L. Walker, E. Perkins, F. Kratz, D. Raucher, Cell penetrating peptides fused to a thermally targeted biopolymer drug carrier improve the delivery and antitumor efficacy of an acid-sensitive doxorubicin derivative, Int J Pharm 436 (2012) 825-832.

123. S. Moktan, E. Perkins, F. Kratz, D. Raucher, Thermal targeting of an acid-sensitive doxorubicin conjugate of elastin-like polypeptide enhances the therapeutic efficacy compared with the parent compound in vivo, Mol Cancer Ther 11 (2012) 1547-1556.

124. I. Massodi, D. Raucher, A thermally responsive Tat-elastin-like polypeptide fusion protein induces membrane leakage, apoptosis, and cell death in human breast cancer cells, J Drug Target 15 (2007) 611-622.

125. T.A.T. Lee, A. Cooper, R.P. Apkarian, V.P. Conticello, Thermo-reversible self-assembly of nanoparticles derived from elastin-mimetic polypeptides, Advanced Materials 12 (2000) 1105-+.

126. M.R. Dreher, A.J. Simnick, K. Fischer, R.J. Smith, A. Patel, M. Schmidt, A. Chilkoti, Temperature triggered self-assembly of polypeptides into multivalent spherical micelles, J Am Chem Soc 130 (2008) 687-694.

127. S.M. Janib, M. Pastuszka, S. Aluri, Z. Folchman-Wagner, P.Y. Hsueh, P. Shi, A. Yi, H. Cui, J.A. Mackay, A quantitative recipe for engineering protein polymer nanoparticles, Polym Chem 5 (2014) 1614-1625.

128. A.J. Simnick, C.A. Valencia, R. Liu, A. Chilkoti, Morphing low-affinity ligands into high-avidity nanoparticles by thermally triggered self-assembly of a genetically encoded polymer, ACS Nano 4 (2010) 2217-2227.

129. A.J. Simnick, M. Amiram, W. Liu, G. Hanna, M.W. Dewhirst, C.D. Kontos, A. Chilkoti, In vivo tumor targeting by a NGR-decorated micelle of a recombinant diblock copolypeptide, J Control Release 155 (2011) 144-151.

130. W. Hassouneh, K. Fischer, S.R. MacEwan, R. Branscheid, C.L. Fu, R. Liu, M. Schmidt, A. Chilkoti, Unexpected multivalent display of proteins by temperature

triggered self-assembly of elastin-like polypeptide block copolymers, Biomacromolecules 13 (2012) 1598-1605.

131. P. Shi, S. Aluri, Y.A. Lin, M. Shah, M. Edman, J. Dhandhukia, H. Cui, J.A. MacKay, Elastin-based protein polymer nanoparticles carrying drug at both corona and core suppress tumor growth in vivo, J Control Release 171 (2013) 330-338.

132. M. Shah, M.C. Edman, S.R. Janga, P. Shi, J. Dhandhukia, S. Liu, S.G. Louie, K. Rodgers, J.A. Mackay, S.F. Hamm-Alvarez, A rapamycin-binding protein polymer nanoparticle shows potent therapeutic activity in suppressing autoimmune dacryoadenitis in a mouse model of Sjogren's syndrome, J Control Release 171 (2013) 269-279.

133. N. Parker, M.J. Turk, E. Westrick, J.D. Lewis, P.S. Low, C.P. Leamon, Folate receptor expression in carcinomas and normal tissues determined by a quantitative radioligand binding assay, Anal Biochem 338 (2005) 284-293.

134. H.B. Muss, A.D. Thor, D.A. Berry, T. Kute, E.T. Liu, F. Koerner, C.T. Cirrincione, D.R. Budman, W.C. Wood, M. Barcos, et al., c-erbB-2 expression and response to adjuvant therapy in women with node-positive early breast cancer, N Engl J Med 330 (1994) 1260-1266.

135. A. Fink-Retter, D. Gschwantler-Kaulich, G. Hudelist, R. Mueller, E. Kubista, K. Czerwenka, C.F. Singer, Differential spatial expression and activation pattern of EGFR and HER2 in human breast cancer, Oncol Rep 18 (2007) 299-304.

136. K. Taniguchi, J. Okami, K. Kodama, M. Higashiyama, K. Kato, Intratumor heterogeneity of epidermal growth factor receptor mutations in lung cancer and its correlation to the response to gefitinib, Cancer Sci 99 (2008) 929-935.

137. D.L. Dexter, J.T. Leith, Tumor heterogeneity and drug resistance, J Clin Oncol 4 (1986) 244-257.

138. K. Trabbic-Carlson, D.E. Meyer, L. Liu, R. Piervincenzi, N. Nath, T. LaBean, A. Chilkoti, Effect of protein fusion on the transition temperature of an environmentally responsive elastin-like polypeptide: a role for surface hydrophobicity?, Protein Eng Des Sel 17 (2004) 57-66.

139. W. Hassouneh, S.R. MacEwan, A. Chilkoti, Fusions of elastin-like polypeptides to pharmaceutical proteins, Methods Enzymol 502 (2012) 215-237.

140. S.R. MacEwan, W. Hassouneh, A. Chilkoti, Non-chromatographic purification of recombinant elastin-like polypeptides and their fusions with peptides and proteins from Escherichia coli, J Vis Exp (2014).

141. V.P. Torchilin, R. Rammohan, V. Weissig, T.S. Levchenko, TAT peptide on the surface of liposomes affords their efficient intracellular delivery even at low temperature and in the presence of metabolic inhibitors, Proc Natl Acad Sci U S A 98 (2001) 8786-8791.

142. J.W. Tobias, T.E. Shrader, G. Rocap, A. Varshavsky, The N-end rule in bacteria, Science 254 (1991) 1374-1377.

143. E.S. Lee, Z. Gao, Y.H. Bae, Recent progress in tumor pH targeting nanotechnology, J Control Release 132 (2008) 164-170.

144. D.A. Dougherty, Cation-pi interactions involving aromatic amino acids, J Nutr 137 (2007) 1504S-1508S; discussion 1516S-1517S.

145. C.P. Moon, K.G. Fleming, Side-chain hydrophobicity scale derived from transmembrane protein folding into lipid bilayers, Proc Natl Acad Sci U S A 108 (2011) 10174-10177.

146. F. Baud, S. Karlin, Measures of residue density in protein structures, Proc Natl Acad Sci U S A 96 (1999) 12494-12499.

147. F. Sallusto, M. Cella, C. Danieli, A. Lanzavecchia, Dendritic cells use macropinocytosis and the mannose receptor to concentrate macromolecules in the major histocompatibility complex class II compartment: downregulation by cytokines and bacterial products, J Exp Med 182 (1995) 389-400.

148. A. Cooper, Y. Shaul, Clathrin-mediated endocytosis and lysosomal cleavage of hepatitis B virus capsid-like core particles, J Biol Chem 281 (2006) 16563-16569.

149. S.R. MacEwan, A. Chilkoti, Digital switching of local arginine density in a genetically encoded self-assembled polypeptide nanoparticle controls cellular uptake, Nano Lett 12 (2012) 3322-3328.

150. M. Hallbrink, J. Oehlke, G. Papsdorf, M. Bienert, Uptake of cell-penetrating peptides is dependent on peptide-to-cell ratio rather than on peptide concentration, Biochim Biophys Acta 1667 (2004) 222-228.

151. M.N. Levine, T.T. Hoang, R.T. Raines, Fluorogenic probe for constitutive cellular endocytosis, Chem Biol 20 (2013) 614-618.

152. S.R. MacEwan, A. Chilkoti, Controlled apoptosis by a thermally toggled nanoscale amplifier of cellular uptake, Nano Lett 14 (2014) 2058-2064.

153. J.S. Shin, S.N. Abraham, Cell biology. Caveolae--not just craters in the cellular landscape, Science 293 (2001) 1447-1448.

154. J.A. MacKay, M. Chen, J.R. McDaniel, W. Liu, A.J. Simnick, A. Chilkoti, Self-assembling chimeric polypeptide-doxorubicin conjugate nanoparticles that abolish tumours after a single injection, Nat Mater 8 (2009) 993-999.

155. D.J. Craik, D.P. Fairlie, S. Liras, D. Price, The future of peptide-based drugs, Chem Biol Drug Des 81 (2013) 136-147.

156. J.R. McDaniel, I. Weitzhandler, S. Prevost, K.B. Vargo, M.S. Appavou, D.A. Hammer, M. Gradzielski, A. Chilkoti, Noncanonical Self-Assembly of Highly Asymmetric Genetically Encoded Polypeptide Amphiphiles into Cylindrical Micelles, Nano Lett (2014).

157. J.R. McDaniel, J. Bhattacharyya, K.B. Vargo, W. Hassouneh, D.A. Hammer, A. Chilkoti, Self-assembly of thermally responsive nanoparticles of a genetically encoded peptide polymer by drug conjugation, Angew Chem Int Ed Engl 52 (2013) 1683-1687.

158. P. Guo, J. Ma, S. Li, Z. Guo, A.L. Adams, J.M. Gallo, Targeted delivery of a peripheral benzodiazepine receptor ligand-gemcitabine conjugate to brain tumors in a xenograft model, Cancer Chemother Pharmacol 48 (2001) 169-176.

159. L.J. Draeger, G.P. Mullen, Interaction of the Bhlh-Zip Domain of C-Myc with H1-Type Peptides - Characterization of Helicity in the H1 Peptides by Nmr, Journal of Biological Chemistry 269 (1994) 1785-1793.

160. M. Sattler, H. Liang, D. Nettesheim, R.P. Meadows, J.E. Harlan, M. Eberstadt, H.S. Yoon, S.B. Shuker, B.S. Chang, A.J. Minn, C.B. Thompson, S.W. Fesik, Structure of Bcl-xL-Bak peptide complex: recognition between regulators of apoptosis, Science 275 (1997) 983-986.

161. E.P. Holinger, T. Chittenden, R.J. Lutz, Bak BH3 peptides antagonize Bcl-xL function and induce apoptosis through cytochrome c-independent activation of caspases, J Biol Chem 274 (1999) 13298-13304.

162. J.M. Adams, S. Cory, The Bcl-2 protein family: arbiters of cell survival, Science 281 (1998) 1322-1326.

163. C.L. Duvall, A.J. Convertine, D.S. Benoit, A.S. Hoffman, P.S. Stayton, Intracellular delivery of a proapoptotic peptide via conjugation to a RAFT synthesized endosomolytic polymer, Mol Pharm 7 (2010) 468-476.

164. B. Albarran, A.S. Hoffman, P.S. Stayton, Efficient Intracellular Delivery of a Pro-Apoptotic Peptide With A pH-Responsive Carrier, React Funct Polym 71 (2011) 261-265.

165. E. Mini, S. Nobili, B. Caciagli, I. Landini, T. Mazzei, Cellular pharmacology of gemcitabine, Ann Oncol 17 Suppl 5 (2006) v7-12.

166. H.A. Burris, 3rd, M.J. Moore, J. Andersen, M.R. Green, M.L. Rothenberg, M.R. Modiano, M.C. Cripps, R.K. Portenoy, A.M. Storniolo, P. Tarassoff, R. Nelson, F.A. Dorr, C.D. Stephens, D.D. Von Hoff, Improvements in survival and clinical benefit with gemcitabine as first-line therapy for patients with advanced pancreas cancer: a randomized trial, J Clin Oncol 15 (1997) 2403-2413.

167. H. von der Maase, L. Sengelov, J.T. Roberts, S. Ricci, L. Dogliotti, T. Oliver, M.J. Moore, A. Zimmermann, M. Arning, Long-term survival results of a randomized trial comparing gemcitabine plus cisplatin, with methotrexate, vinblastine, doxorubicin, plus cisplatin in patients with bladder cancer, J Clin Oncol 23 (2005) 4602-4608.

168. M. Blackstein, C.L. Vogel, R. Ambinder, J. Cowan, J. Iglesias, A. Melemed, Gemcitabine as first-line therapy in patients with metastatic breast cancer: a phase II trial, Oncology 62 (2002) 2-8.

169. S. Adachi, S. Kokura, T. Okayama, T. Ishikawa, T. Takagi, O. Handa, Y. Naito, T. Yoshikawa, Effect of hyperthermia combined with gemcitabine on apoptotic cell death in cultured human pancreatic cancer cell lines, Int J Hyperthermia 25 (2009) 210-219.

170. T. Ohguri, H. Imada, K. Yahara, H. Narisada, T. Morioka, K. Nakano, Y. Korogi, Concurrent chemoradiotherapy with gemcitabine plus regional hyperthermia for locally advanced pancreatic carcinoma: initial experience, Radiat Med 26 (2008) 587-596.

171. R. Montano, R. Thompson, I. Chung, H. Hou, N. Khan, A. Eastman, Sensitization of human cancer cells to gemcitabine by the Chk1 inhibitor MK-8776: cell cycle

perturbation and impact of administration schedule in vitro and in vivo, BMC Cancer 13 (2013) 604.

172. X. Pan, T. Arumugam, T. Yamamoto, P.A. Levin, V. Ramachandran, B. Ji, G. Lopez-Berestein, P.E. Vivas-Mejia, A.K. Sood, D.J. McConkey, C.D. Logsdon, Nuclear factor-kappaB p65/relA silencing induces apoptosis and increases gemcitabine effectiveness in a subset of pancreatic cancer cells, Clin Cancer Res 14 (2008) 8143-8151.

173. Y.P. Istomin, E.A. Zhavrid, E.N. Alexandrova, O.P. Sergeyeva, S.V. Petrovich, Dose enhancement effect of anticaner drugs associated with increased temperature in vitro, Exp Oncol 30 (2008) 56-59.

174. F.M. Veronese, O. Schiavon, G. Pasut, R. Mendichi, L. Andersson, A. Tsirk, J. Ford, G. Wu, S. Kneller, J. Davies, R. Duncan, PEG-doxorubicin conjugates: influence of polymer structure on drug release, in vitro cytotoxicity, biodistribution, and antitumor activity, Bioconjug Chem 16 (2005) 775-784.

175. S.O. Doronina, B.E. Toki, M.Y. Torgov, B.A. Mendelsohn, C.G. Cerveny, D.F. Chace, R.L. DeBlanc, R.P. Gearing, T.D. Bovee, C.B. Siegall, J.A. Francisco, A.F. Wahl, D.L. Meyer, P.D. Senter, Development of potent monoclonal antibody auristatin conjugates for cancer therapy, Nat Biotechnol 21 (2003) 778-784.

176. G. Thomas, Furin at the cutting edge: from protein traffic to embryogenesis and disease, Nat Rev Mol Cell Biol 3 (2002) 753-766.

177. M.F. Mustapa, S.M. Grosse, L. Kudsiova, M. Elbs, E.A. Raiber, J.B. Wong, A.P. Brain, H.E. Armer, A. Warley, M. Keppler, T. Ng, M.J. Lawrence, S.L. Hart, H.C. Hailes, A.B. Tabor, Stabilized integrin-targeting ternary LPD (lipopolyplex) vectors for gene delivery designed to disassemble within the target cell, Bioconjug Chem 20 (2009) 518-532.

178. V.M. Gordon, K.R. Klimpel, N. Arora, M.A. Henderson, S.H. Leppla, Proteolytic activation of bacterial toxins by eukaryotic cells is performed by furin and by additional cellular proteases, Infect Immun 63 (1995) 82-87.

179. M. Harada, H. Sakakibara, T. Yano, T. Suzuki, S. Okuno, Determinants for the drug release from T-0128, camptothecin analogue-carboxymethyl dextran conjugate, J Control Release 69 (2000) 399-412.

180. J. Huotari, A. Helenius, Endosome maturation, EMBO J 30 (2011) 3481-3500.

181. S.S. Molloy, L. Thomas, J.K. VanSlyke, P.E. Stenberg, G. Thomas, Intracellular trafficking and activation of the furin proprotein convertase: localization to the TGN and recycling from the cell surface, EMBO J 13 (1994) 18-33.

182. S. Guha, H. Padh, Cathepsins: fundamental effectors of endolysosomal proteolysis, Indian J Biochem Biophys 45 (2008) 75-90.

183. O. Emanuelsson, G. von Heijne, G. Schneider, Analysis and prediction of mitochondrial targeting peptides, Methods Cell Biol 65 (2001) 175-187.

184. E. Frohlich, The role of surface charge in cellular uptake and cytotoxicity of medical nanoparticles, Int J Nanomedicine 7 (2012) 5577-5591.

185. K. Ahmed, Q.L. Zhao, Y. Matsuya, D.Y. Yu, T.L. Salunga, H. Nemoto, T. Kondo, Enhancement of macrosphelide-induced apoptosis by mild hyperthermia, Int J Hyperthermia 23 (2007) 353-361.

186. R. Zukiene, Z. Nauciene, J. Ciapaite, V. Mildaziene, Acute temperature resistance threshold in heart mitochondria: Febrile temperature activates function but exceeding it collapses the membrane barrier, Int J Hyperthermia 26 (2010) 56-66.

187. J.R. McDaniel, D.C. Radford, A. Chilkoti, A unified model for de novo design of elastin-like polypeptides with tunable inverse transition temperatures, Biomacromolecules 14 (2013) 2866-2872.

188. J.R. McDaniel, S.R. MacEwan, X. Li, D.C. Radford, C.D. Landon, M. Dewhirst, A. Chilkoti, Rational design of "heat seeking" drug loaded polypeptide nanoparticles that thermally target solid tumors, Nano Lett 14 (2014) 2890-2895.

189. D. Sarko, B. Beijer, R. Garcia Boy, E.M. Nothelfer, K. Leotta, M. Eisenhut, A. Altmann, U. Haberkorn, W. Mier, The pharmacokinetics of cell-penetrating peptides, Mol Pharm 7 (2010) 2224-2231.

190. W. Kim, J. Thevenot, E. Ibarboure, S. Lecommandoux, E.L. Chaikof, Self-assembly of thermally responsive amphiphilic diblock copolypeptides into spherical micellar nanoparticles, Angew Chem Int Ed Engl 49 (2010) 4257-4260.

191. S. Grijalvo, R. Eritja, Synthesis and in vitro inhibition properties of oligonucleotide conjugates carrying amphipathic proline-rich peptide derivatives of the sweet arrow peptide (SAP), Mol Divers 16 (2012) 307-317.

192. A. del Pozo-Rodriguez, S. Pujals, D. Delgado, M.A. Solinis, A.R. Gascon, E. Giralt, J.L. Pedraz, A proline-rich peptide improves cell transfection of solid lipid nanoparticle-based non-viral vectors, J Control Release 133 (2009) 52-59.

193. S. Pujals, N.G. Bastus, E. Pereiro, C. Lopez-Iglesias, V.F. Puntes, M.J. Kogan, E. Giralt, Shuttling gold nanoparticles into tumoral cells with an amphipathic proline-rich peptide, Chembiochem 10 (2009) 1025-1031.

194. I. Martin, M. Teixido, E. Giralt, Design, synthesis and characterization of a new anionic cell-penetrating peptide: SAP(E), Chembiochem 12 (2011) 896-903.

Biography

Sarah Reagan MacEwan was born in Arlington, Texas in 1984. Sarah attended Case Western Reserve University, from which she earned her BS degree in 2007 in the Department of Biomedical Engineering with a focus on polymeric biomaterials. At CASE Sarah worked in the laboratory of Dr. James Anderson in the Department of Pathology. In Dr. Anderson's lab Sarah worked in collaboration with Dr. Amy McNally, investigating inflammatory macrophage responses to biomedical polymers, and with Dr. Analiz Rodriguez, investigating the primary and secondary host response to implanted biomaterials in rats.

In 2007 Sarah joined the laboratory of Dr. Ashutosh Chilkoti at Duke University in the Department of Biomedical Engineering. Her work at Duke focused on the targeted cellular uptake of drug delivery vehicles and the development of stimulus-responsive biomaterials with novel block copolymer architectures. During her time at Duke Sarah was a James B. Duke fellow (2007-2011), an Integrative Graduate Education and Research Traineeship (IGERT) graduate fellow in the Center for Biologically Inspired Materials and Material Systems (CBIMMS) (2007-2008), a Howard G. Clark III fellow (2008-2009), and a Triangle Materials Research Science and Engineering Center (MRSEC) fellow (2011-2014). Sarah's work at Duke helped produce the following publications:

1. S.R. MacEwan, A. Chilkoti, Applications of elastin-like polypeptides in drug delivery, Journal of Controlled Release 190 (2014) 314-330.

2. J.R. McDaniel, S.R. MacEwan, X. Li, D.C. Radford, C.D. Landon, M. Dewhirst, A. Chilkoti, Rational design of "heat seeking" drug loaded polypeptide nanoparticles that thermally target solid tumors, Nano Letters 14 (2014) 2890-2895.

3. S.R. MacEwan, W. Hassouneh, A. Chilkoti, Non-chromatographic purification of recombinant elastin-like polypeptides and their fusions with peptides and proteins from Escherichia coli, Journal of Visualized Experiments 88 (2014) e51583.

4. S.R. MacEwan, A. Chilkoti, Controlled apoptosis by a thermally toggled nanoscale amplifier of cellular uptake, Nano Letters 14 (2014) 2058-2064.

5. S.R. MacEwan, A. Chilkoti, Harnessing the power of cell-penetrating peptides: Activatable carriers for targeting systemic delivery of cancer therapeutics and imaging agents, WIREs: Nanomedicine and Nanobiotechnology 5 (2012) 31-48.

6. S.R. MacEwan, A. Chilkoti, Digital switching of local arginine density in a genetically encoded self-assembled polypeptide nanoparticle controls cellular uptake, Nano Letters 12 (2012) 3322-3328.

7. J.R. McDaniel, S.R. MacEwan, M. Dewhirst, A. Chilkoti, Doxorubicin-conjugated chimeric polypeptide nanoparticles that respond to mild hyperthermia, Journal of Controlled Release 159 (2012) 362-367.

8. W. Hassouneh, K. Fischer, S.R. MacEwan, R. Branscheid, C.L. Fu, R. Liu, M. Schmidt, A. Chilkoti, Unexpected multivalent display of proteins by temperature triggered self-assembly of elastin-like polypeptide block copolymers, Biomacromolecules 13 (2012) 1598-1605.

9. W. Hassouneh, S.R. MacEwan, A. Chilkoti, Fusions of elastin-like polypeptides to pharmaceutical proteins, Methods in Enzymology 502 (2012) 215-237.

10. S.R. MacEwan, D.J. Callahan, A. Chilkoti, Stimulus-responsive macromolecules and nanoparticles for cancer drug delivery, Nanomedicine 5 (2010) 793-806.

11. S.R. MacEwan, A. Chilkoti, Elastin-like polypeptides: Biomedical applications of tunable biopolymers, Peptide Science 94 (2010) 60-77.